# Role of metabolism and mitochondrial function for stem cell differentiation and stress responses upon genotoxic noxae

Inaugural-Dissertation

zur Erlangung des Doktorgrades
der Mathematisch-Naturwissenschaftlichen Fakultät
der Heinrich-Heine-Universität Düsseldorf

vorgelegt von

**Michelle Westerhoff** 

aus Bensheim

Düsseldorf, April 2025

aus dem Institut für Biochemie und Molekularbiologie I
der Heinrich-Heine-Universität Düsseldorf
Gedruckt mit der Genehmigung der Mathematisch-Naturwissenschaftlichen Fakultät der
Heinrich-Heine-Universität Düsseldorf
Berichterstatter:
1. Prof. Dr. rer. nat. Andreas S. Reichert
2. Prof. Dr. rer. nat. Gerhard Fritz

Tag der mündlichen Prüfung: 21.08.2025

Ich hab' gelernt das Leben zu genießen
Meine Freunde wie Blumen zu gießen
Ich hab' gelernt das Feuer zu schür'n
Den Zauber nicht zu verlieren
Ich hab' gelernt der erste Blick täuscht
Und dass es gut ist, wenn man sich verläuft
Ich hab' gelernt auch wenn's mies ist
Geht die Sonne trotzdem auf

Bosse (2018)<sup>1</sup>

-

<sup>&</sup>lt;sup>1</sup> Bosse, A.(2018). "Alles ist jetzt", Axel Bosse, Jochen Naaf, Vertigo Berlin

## **Table of contents**

Table of contents	I
List of figures	V
List of tables	VII
List of abbreviations	VIII
1. Introduction	1
1.1. Mitochondria	1
1.1.1. Mitochondrial organization	1
1.1.2. Mitochondrial functions	3
1.1.3. Mitochondrial dynamics and quality control	6
1.1.4. Mitochondrial DNA	8
1.1.5. Role of mitochondria in disease	9
1.2. Cardiovascular system	11
1.2.1. Function and anatomy of the heart	11
1.2.2. Cell types within the heart	13
1.2.2.1. Cardiomyocytes	13
1.2.3. Regeneration capacity within the heart	15
1.3. Stem cells	16
1.3.1. Embryonic stem cells	17
1.3.2. Adult stem cells	
1.3.3. Induced-pluripotent stem cells	18
1.3.4. Mitochondria as mediators of stemness, differentiation and reprogramming	20
1.4. Chemotherapeutic treatment	
1.4.1. Doxorubicin	22
1.4.2. Mitochondria as mediators of doxorubicin-induced cardiomyopathies	24
1.5. Objectives and aims	25
2. Material and methods	27
2.1. Material	27
2.1.1. Chemicals, kits and media	27
2.1.2. Consumables	31
2.1.3. Equipment and software	32
2.2. Methods	34
2.2.1. Cell culture methods	34
2.2.1.1. Cell line IMR-90 (clone 4)	34
2.2.1.2. Maintenance, passaging and freezing of cells	34
2.2.1.3. Generation of iPSC-derived cardiomyocytes	35
2.2.2. Doxorubicin treatment regimen	35

2.2.3. Cell viability assays	35
2.2.3.1. MTT assay	35
2.2.3.2. SRB assay	36
2.2.4. SDS PAGE and Western Blot	36
2.2.4.1. Determination of protein concentration with Lowry assay	37
2.2.4.2. SDS PAGE	37
2.2.4.3. Western Blot	38
2.2.5. Blue Native and Clear Native PAGE	40
2.2.5.1. Blue Native PAGE	40
2.2.5.2. Clear Native PAGE	41
2.2.6. Gene expression analysis	42
2.2.6.1. RNA isolation	42
2.2.6.2. Complementary DNA (cDNA) synthesis	42
2.2.6.3. Genomic DNA (gDNA) isolation	43
2.2.6.4. Quantitative real-time PCR (qRT-PCR)	44
2.2.6.5. Measurement of mitochondrial copy number	45
2.2.7. Transfection of iPSCs	45
2.2.8. Immunofluorescence staining	46
2.2.9. Fluorescence microscopy	47
2.2.9.1. Analysis of DNA damage	48
2.2.9.2. Mitochondrial morphology	48
2.2.9.3. Mitochondrial membrane potential ( $\Delta\Psi_{m}$ )	49
2.2.9.4. Mitochondrial nucleoids	49
2.2.9.5. Mitochondrial aging (pMitoTimer)	52
2.2.10. Electron microscopy (EM)	53
2.2.11. Measurement of bioenergetics	54
2.2.11.1. Measurement of mitochondrial respiration	54
2.2.11.2. ATP assay	55
2.2.12. Flow cytometer-based methods	56
2.2.12.1. Cell cycle measurement	56
2.2.13. Beating characterization of iPSC-derived cardiomyocytes	56
2.2.14. Whole genome transcriptome profiling	59
2.3. Recipes	63
2.4. Statistics	65
3. Results	66
3.1. Influence of short pulse-treatment with doxorubicin on human iPSCs	66
3.1.1. Pulse-treatment of iPSCs with doxorubicin is not accompanied with loss of the	22
pluripotent state	66

3.1.2. Pulse-treatment with low concentrations of doxorubicin is insufficient to initiate elevated apoptosis or activate canonical DNA damage response	71
3.1.3. Influence of acute doxorubicin exposure on mitochondrial function in human iPSCs	
3.1.3.1. Pulse-treatment with doxorubicin is accompanied with mitochondrial fragmentation and loss of mitochondrial membrane potential	on
3.1.3.2. Mitochondrial respiration is impaired upon pulse-treatment with doxorubicin	82
3.1.3.3. Doxorubicin treatment of iPSCs is not sufficient to disrupt mitochondrial ultrastruc	
3.1.3.4. Doxorubicin treatment is accompanied with modulation of mitochondrial genome organization	88
3.2. Influence of short pulse-treatment with doxorubicin on human iCMs	93
3.2.1. Establishment of iCMs as robust cardiac model system	93
3.2.2. Stable cardiac differentiation even under exposure to doxorubicin at different stage cardiac differentiation	
3.2.3. Effect of doxorubicin pulse-treatment on mitochondrial function in iCMs	99
3.2.3.1. Fragmentation of mitochondrial network upon pulse-treatment of iCMs with doxorubicin	99
3.2.3.2. Pulse-treatment with doxorubicin is sufficient to reduce mitochondrial content in i	CMs .101
3.3. Whole genome transcriptome profiling of iPSCs and iCMs upon exposure to low concentrations of doxorubicin	.103
3.3.1. Doxorubicin pulse-treatment of iPSCs results in suppression of genes relevant for metabolism and cellular homeostasis	.104
3.3.2. Differentiation of iPSCs into cardiomyocytes is not affected upon doxorubicin treatr throughout cardiac differentiation	nent .106
3.3.3. Major differences in the transcriptional response to doxorubicin pulse-treatment between iPSCs and iCMs	.109
3.3.4. Transcriptional changes induced by pulse-treatment with doxorubicin in iPSC stage results in suppression of genes associated with cardiac muscle regeneration	
3.3.5. Treatment of terminal iCMs is accompanied with increased expression of apoptosis relevant genes	
3.3.6. Pre-conditioning of cells in iPSC stage is accompanied with alterations in genes associated with energy metabolism and muscle contraction	.122
3.3.7. Treatment timepoint independent general dysregulation of genes associated with cardiac muscle formation	.124
3.3.8. Suppression of contractility function of iCMs upon is directly associated with treatment in iPSC stage prior to cardiac differentiation	
3.3.9. Timepoint-independent induction of mitochondrial dysfunction in iCMs pulse-treate with Dox	
4. Discussion	.131
4.1. Successful cardiac differentiation following a chemical defined protocol	.132
4.2. Mitochondria as a major target of mild and transient doxorubicin exposures	.134

	Low concentrations of doxorubicin do not lead to canonical DNA damag C 137	e repair in
	Doxorubicin-mediated perturbations in transcriptional response of iPSC lications for fibrosis and cellular dysfunction	
4.5.	Conclusion and Outlook	144
5.	Summary	145
6.	Zusammenfassung	148
7.	References	XIV

Publications XXXII Acknowledgements XXXIII

Eidesstatliche Erklärung ......XXXIV

List of contribution to this publication ......XXXIV

8.

9.10.

11.

# List of figures

Fig. 1: Overview of mitochondrial function	1
Fig. 2: Mitochondrial organization and functional parameters	2
Fig. 3: Conversion of energy into ATP upon mitochondrial respiration.	
Fig. 4: The dynamic nature of mitochondria	
Fig. 5: Schematic diagram of the anatomy of the heart	
Fig. 6: Functional units within the sarcomere of a cardiomyocyte	
Fig. 7: Symmetric and asymmetric division of stem cells.	
Fig. 8: Biomedical potential of human induced-pluripotent stem cells	
Fig. 9: Categories of mitochondrial morphology.	
Fig. 10: CellProfiler Pipeline for analysis of mitochondrial nucleoids	.51
Fig. 11: Schematic illustration of crista phenotypes in iPSCs	
Fig. 12: Schematic illustration of Seahorse XF Cell Mito Stress Test run.	
Fig. 13: Contraction analysis of iPSCs via CardioVision program	
Fig. 14: Multidimensional scaling of the expression profiles whole genome transcriptome	
	.60
Fig. 15: Viability measurement of iPSCs upon short pulse-treatment with doxorubicin	.67
Fig. 16: Influence of short pulse-treatment of iPSCs with doxorubicin on pluripotency and	
proliferation capacity	.68
Fig. 17: Proliferation capacity of iPSCs short pulse-treated with low concentrations of	
· · · · · · · · · · · · · · · · · · ·	.70
Fig. 18: Apoptotic induction in iPSCs upon exposure to low concentrations of doxorubicin	.72
Fig. 19: Induction of DNA double-strand breaks in iPSCs upon short pulse-treatment with	
	.74
Fig. 20: Mitochondrial morphology in iPSCs upon short pulse-treatment with doxorubicin	.77
Fig. 21: Mitochondrial motility marker in iPSCs upon short pulse-treatment with Dox	.79
Fig. 22: Short pulse-treatment of iPSCs with doxorubicin is accompanied with disruption of	į
mitochondrial membrane potential (ΔΨ <sub>m</sub> ).	.81
Fig. 23: Measurement of live-cell respiration and ATP levels in iPSCs after short-time	
exposure to low concentrations of doxorubicin.	.83
Fig. 24: Time-lapse measurement of doxorubicin induced effects on mitochondrial respirati	on
in iPSCs	.84
Fig. 25: Influence of short pulse-exposure of doxorubicin on mitochondrial ultrastructure in	
iPSCs	.85
Fig. 26: Mitochondrial respiratory complex assembly and activity upon short pulse-treatme	nt
with of iPSCs with doxorubicin	
Fig. 27: Nucleoid content and size in iPSCs after short pulse-treatment with doxorubicin	.89
Fig. 28: Mitochondrial DNA copy number in iPSCs upon short pulse-treatment with	
doxorubicin	
Fig. 29: Measurement of mitochondrial aging in iPSC pulse-treated with doxorubicin	.92
Fig. 30: Scheme for generation of iCMs following a chemical defined protocol	.94
Fig. 31: Morphological changes of cells during cardiac differentiation	.94
Fig. 32: Characterization of iCMs on mRNA level.	.95
Fig. 33: Viability measurement in CPs and iCMs after doxorubicin treatment	.96
Fig. 34: Expression levels of pluripotency and cardiac markers in CPs and iCMs upon short	rt
pulse-treatment with doxorubicin	
Fig. 35: Protein levels of pluripotency and cardiac markers of in iPSCs, CPs and iCMs upo	'n
pulse-treatment with doxorubicin	
Fig. 36: Mitochondrial morphology in iCMs upon short pulse-treatment with doxorubicin1	100

Fig. 37: Relative protein levels of the mitochondrial fusion factor OPA1 in ICNIs pulse-treated
with doxorubicin
Fig. 38: Mitochondrial DNA in iCMs pulse-treated with doxorubicin
Fig. 39: GO-term enrichments of differentially regulated genes in iPSCs influenced upon
pulse-treatment with doxorubicin
Fig. 40: Influence of doxorubicin application on iCMs at different timepoints of cardiac
differentiation
Fig. 41: Comparison between doxorubicin-induced transient response in iPSCs and iCMs.111 Fig. 42: Comparison between doxorubicin-induced transient response in iPSCs and iCMs.
112
Fig. 43: Targeted hierarchical analysis of metabolic processes in iPSCs and iCMs upon
influence of doxorubicin treatment114
Fig. 44: Gene concept network of iCMs pluse-treated in iPSC stage with doxorubicin116
Fig. 45: Gene concept network of iCMs pluse-treated in iPSC stage with doxorubicin117
Fig. 46: Timepoint specific influence on whole genome transcriptome in iCMs pulse-treated
with doxorubicin prior to cardiac differentiation
Fig. 47: Timepoint specific influence on whole genome transcriptome in iCMs pulse-treated
with doxorubicin prior to cardiac differentiation
Fig. 48: Influence of doxorubicin pulse-treatment on whole genome transcriptome of
terminally differentiated iCMs121
Fig. 49: Influence of a second encounter with doxorubicin on the transcriptional response of
pre-conditioned iCMs
Fig. 50: Influence of a second encounter with doxorubicin on the transcriptional response of
pre-conditioned iCMs
Fig. 51: Effect of pulse-treatment with doxorubicin on the overall transcriptional response of
iCMs
Fig. 52: Measurement of cardiac functionality upon exposure of iCMs to doxorubicin128
Fig. 53: Mitochondrial morphology and copy number in iCMs pulse-treated with doxorubicin
at different timepoints throughout cardiac differentiation

## List of tables

Tab. 1: Chemicals, kits and media used in this study	27
Tab. 2: Consumables	
Tab. 3: Equipment and software	
Tab. 4: Primary (1 <sup>st</sup> ) and secondary (2 <sup>nd</sup> ) antibodies for Western blot	
Tab. 5: Primary (1 <sup>st</sup> ) and secondary (2 <sup>nd</sup> ) antibodies for blue native PAGE	
Tab. 6: Reverse transcription mix	42
Tab. 7: Reverse transcription reaction mix	43
Tab. 8: Cyclying protocol for cDNA synthesis	43
Tab. 9: Quantitative real-time PCR master mix	44
Tab. 10: Cycling protocol for qRT-PCR	44
Tab. 11: Primer sequences used for quantitative real-time PCR approaches	
Tab. 12: Transfection master mix preparation	46
Tab. 13: Primary (1st) and secondary (2nd) antibodies for immunofluorescence microscopy	
Tab. 14: Information about the plasmid pMitoTimer	53
Tab. 15: Calculations for Mito Stress Test Seahorse parameters	55
Tab. 16: Number of significantly differential regulated genes resulting from the pairwise	
comparison between doxorubicin-treated iPSCs or iCMs and their respective controls	61
Tab. 17: Number of significantly differential regulated genes resulting from the pairwise	
comparison between the doxorubicin treatment regimens in iPSCs and iCMs	62
Tab. 18: Recipes of solutions utilized in this study	63

#### List of abbreviations

°C Degree celsius µg Mikrogramm µM Micromolar

2D Two-dimensional3D Three-dimensional

53BP1 Tumor Protein P53 Binding Protein 1

Acetyl-CoA Acetyl-coenzyme A *ACTN3* Actinin Alpha 3

ADP Adenosine diphosphate

ALDOA Fructose bisphosphate aldolase A

ANKRD1 Ankyrin Repeat Domain 1

APAF-1 Apoptotic Peptidase Activating Factor 1

APS Ammonium Persulfate

ASC Adult stem cells

ATM Ataxia Telangiectasia Mutated

ATP Adenosine triphosphate

ATP1B1 ATPase Na+/K+ Transporting Subunit Beta 1

ATP5A ATP Synthase F1 Subunit Alpha

AV Aortic valves

Bak BCL2 Antagonist/Killer 1
Bax BCL2 Associated X

BBC3 BCL2 Binding Component 3

BMFZ Genomics & Transcriptomics Laboratory

BNC2 Basonuclin Zinc Finger Protein 2

bp base pairs

BSA Bovine serum albumin

Ca<sup>2+</sup> Calcium

CBM Cardiac differentiation media

CDK1 Cyclin dependent kinase 1

CDKN1A Fas cell surface death receptor

cDNA Complementary DNA CF Cardiac fibroblasts

CFEM Core facility for electron microscopy
CI Complex I / NADH-dehydrogenase
CII Complex II / Succinate-dehydrogenase
CIII Complex III / Cytochrome c reductase
CIV / COX Complex IV / Cytochrome c oxidase

CJs Crista junctions

c-Myc proto oncogene c Myc

CO<sub>2</sub> Carbon dioxide CoQ CoenzymeQ

COX5B Cytochrome C Oxidase Subunit 5B COXIV Cytochrome C Oxidase Subunit 4I1

CP Cardiac progenitors

CSC Cardiac stem cells

cTNT Troponin T2, Cardiac Type

CV Complex V / F1Fo-ATP synthase

Cyt c Cytochrome c

DAB 3,3'-diaminobenzidine

DAPI 4',6-diamidino-2-phenylindole

ddH<sub>2</sub>O double-distilled water

DEG Differential regulated gene

dim Dimension

DMEM/F-12 Dulbecco's Modified Eagle Medium F12

DMSO Dimethyl sulfoxide
DNA Deoxyribonucleic acid

Dox Doxorubicin

Drp1 GTPase dynamin-related protein 1

DSB DNA double-strand breaks

DsRed Discosoma Red Fluorescent Protein

EC Cardiac endothelial cells

ECL Enhanced chemiluminescence

ECM Extracellular matrix

EDTA Ethylenediaminetetraacetic acid

EM Electron microscopy
ER Endoplasmatic reticulum
ESC Embryonic stem cell
ETC Electron transport chain

Eto Etoposide EtOH Ethanol

FAD Flavin adenine dinucleotide

FADH<sub>2</sub> 1,5-dihydro-FAD

FAS Cyclin dependent kinase Inhibitor 1A

FCCP Trifluoromethoxy carbonylcyanide phenylhydrazone

FCS Fetal calf serum
Fe / S cluster Iron-sulfur cluster

FLNA Filamin A g Gramm

GAPDH Glyceraldehyde-3-Phosphate Dehydrogenase

GATA4 GATA Binding Protein 4

gDNA Genomic DNA

GJA5 Gap junction protein alpha 5

GO-term Gene Ontology term H2AX H2A.X Variant Histone

H<sub>2</sub>O Water

H<sub>2</sub>O<sub>2</sub> Hydrogen Peroxide

HCN4 Hyperpolarization activated cyclic nucleotide gated potassium channel 4

HEPES 4-(2-Hydroxyethyl)piperazine-1-ethanesulfonic acid

hESC Human embryonic stem cell
HHU Heinrich-Heine-University

HIF1A Hypoxia inducible factor 1 subunit alpha

HK1 Hexokinase 1

HPRT1 Hypoxanthine Phosphoribosyltransferase 1

HRP Horseradish peroxidase

HSP60 Heat Shock Protein Family D (Hsp60) Member 1

IBM Inner boundary membrane

ICM Inner cell mass

iCM iPSC-derived cardiomyocyte

IMS Inter membrane space

INS Insulin

iPS (IMR90)- iPSC derived from IMR90, clone 4

4

iPSC Induced-pluripotent stem cell

ISI ISL LIM Homeobox 1
ISL 1 ISL LIM Homeobox 1

kb Kilobases kDa Kilodalton

Ki-67 Marker Of Proliferation Ki-67

Kit Proto-oncogene tyrosine-protein kinase Kit

KLf4 Krüppel-Like Factor 4

KV Kilovolt

LDHA Lactate dehydrogenase

Lin28 Lin-28 Homolog logFC Log-fold change mA Milliampere

MCU Mitochondrial Calcium Uniporter

MeOH Methanol Mfn1 Mitofusin 1 Mfn2 Mitofusin 2

Mic60 Inner Membrane Mitochondrial Protein

MICOS Mitochondrial contact site and cristae organizing system

min Minutes
mL Mililiter
mM Milimolar
Mol Molar

mRNA Messenger RNA

MSC Mesenchymal stem cells

Mt Mock-treatment

MT-ATP6 Mitochondrially Encoded ATP Synthase Membrane Subunit 6MT-ATP8 Mitochondrially Encoded ATP Synthase Membrane Subunit 8

MT-CO1 Mitochondrially Encoded Cytochrome C Oxidase I
 MT-CO2 Mitochondrially Encoded Cytochrome C Oxidase II
 MT-CO3 Mitochondrially Encoded Cytochrome C Oxidase III

MT-CYB Mitochondrially Encoded Cytochrome B

mtDNA Mitochondrial DNA

MtND1 Mitochondrially Encoded NADH: Ubiquinone Oxidoreductase Core Subunit

1

MT-ND1 Mitochondrially Encoded NADH: Ubiquinone Oxidoreductase Core Subunit

1

MT-ND2 Mitochondrially Encoded NADH: Ubiquinone Oxidoreductase Core Subunit

2

MT-ND3 Mitochondrially Encoded NADH: Ubiquinone Oxidoreductase Core Subunit

3

MT-ND4 Mitochondrially Encoded NADH: Ubiquinone Oxidoreductase Core Subunit

4

MT-ND4L MT-ND4L Pseudogene 23

MT-ND5 Mitochondrially Encoded NADH: Ubiquinone Oxidoreductase Core Subunit

5

MT-ND6 Mitochondrially Encoded NADH: Ubiquinone Oxidoreductase Core Subunit

6

mtSSB Single-stranded DNA binding protein 1

MTT 3-(4,5-dimethylthiazol-2-yl)-2,5-diphenyl-2H-tetrazolium bromide

MuRF Muscle-specific RING finger

MV Mitral valve

MYH6 Myosin Heavy Chain 6 MYL9 Myosin Light Chain 9

Number of biological replicatesNumber of technical replicates

NaCl Sodium chloride

NADH Nicotinamide adenine dinucleotide phosphate

Nanog Homeobox transcription factor

NANOG Nanog Homeobox

NBT Nitro blue tetrazolium chloride

NDUFB4 NADH: Ubiquinone Oxidoreductase Subunit B4

NDUFS2 NADH: Ubiquinone Oxidoreductase Core Subunit S2

NDUFS8 NADH: Ubiquinone Oxidoreductase Core Subunit S8

NEBL Nebulette
ng Nanogramm

NKX2-5NK2 Homeobox 5NKX2-5NK2 Homeobox 5NKX2-6NK2 Homeobox 6

nM Nanomolar nm Nanometer

NRAP Nebulin related anchoring protein

O<sub>2</sub> Molecular oxygen
O2<sup>--</sup> Superoxide anions

OCR Oxygen consumption rate
Oct4 Octamer binding-protein 4
Oma1 Oma1 zinc metallopeptidase
OMM Outer mitochondrial membrane

Opa1 Optic atrophy protein 1
Opti-MEM Minimum Essential Medium
OXPHOS Oxidative phosphorylation
p53 Tumor suppressor protein p53
PAGE Polyacrylamide gel electrophoresis

PARP Poly(ADP-Ribose) Polymerase
PBS Phosphate Buffered Saline

PDHB Pyruvate dehydrogenase E1 subunit beta

PDK1 Pyruvate dehydrogenase kinase 1

PGC1α Peroxisome Proliferator-Activated Receptor Gamma Coactivator 1-Alpha

PGK1 Phosphoglycerate kinase 1
PGM1 Phosphoglucomutase 1

PI Propidium iodide

POU5F1 Octamer binding-protein 4

PPM1D Wild-Type P53-induced phosphatase 1

PV Pulmonary valves

PVDF Polyvinylidene fluoride membrane

px Pixel

qRT-PCR Quantitative real-time PCR

RG Research group

RGMA Repulsive guidance molecule BMP co-receptor A

RIPA Radioimmunoprecipitation assay buffer

RNR2 MT-RNR2 Like 4 (Pseudogene)

ROCK Rho-Kinase 1
ROI Region of interest

ROS Reactive oxygen species

RPMI1640 Roswell Park Memorial Institute Medium

rRNA Ribosomal RNA
RyR Ryanodine receptor
RYR1 Ryanodine Receptor 1

s Second

SC Supercomplexes
Sca1 Stem cell antigen 1
SDS Sodium lauryl sulfate

Ser Serine

SHF Second heart field

SHH Sonic hedgehog signaling molecule

Sirt1 Sirtuin 1

SIX1 SIX homeobox 1

SNAI2 Snail family transcriptional repressor 2

Sox2 SRY-box transcription factor 2 SOX2 SRY-box transcription factor 2 SOX4 SRY-Box Transcription Factor 4 SOX9 SRY-Box transcription factor 9

SRB Sulforhodamine B

t Time

TBST Tris-buffered saline with Tween 20

TBST Tris-buffered saline

T-Box transcription factor 1

TCA Trichloracetic acid
TCA cycle Tricarboxylic acid cycle
TEMED Tetramethylethylenediamine

TFAM Mitochondrial transcription tactor A TMRM tetramethylrhodamine-methylester

TNNT2 Troponin T2, Cardiac Type

 $\begin{array}{lll} TopolI & Toposiomerase \ II \\ TopolII\alpha & Topoisomerase \ III \ \alpha \\ TopolI\alpha & Topoisomerase \ II \ alpha \\ TopolI\beta & Topoisomerase \ II \ beta \\ Topolmt & Topoisomerase \ Ib \\ \end{array}$ 

TRDN Triadin

TRIS 2-Amino-2-(hydroxymethyl)-1,3-propandiol

tRNA Transfer-RNA TV Tricuspid valve

Twinkle mtDNA helicase

UBR5 Ubiquitin Protein Ligase E3 Component N-Recognin 5

UKD Universitätsklinikum Düsseldorf

UQCR2 Ubiquinol-Cytochrome C Reductase Core Protein 2

UQCRC1 Ubiquinol-Cytochrome C Reductase Core Protein 1

V Volt

VDAC Voltage-dependent anion channel

Wt1 Wilms tumor 1

x g gravitational acceleration, 9.81 m/s<sup>2</sup>

γH2AX H2A.X Variant Histone phosphorylated at Ser139

 $\Delta \Psi_m$  Mitochondrial membrane potential

μm² Square micrometer

#### 1. Introduction

#### 1.1. Mitochondria

Mitochondria are present in most eukaryotic cells since their endosymbiotic uptake as  $\alpha$ -proteobacteria about two billion years ago (Degli Esposti, 2014). During these evolutionary processes, mitochondria transferred most of their genome to the nucleus. Within the cell, mitochondria are versatile organelles playing an integral role in numerous cellular processes, including energy conversion through oxidative phosphorylation (OXPHOS) and the tricarboxylic acid (TCA) cycle. Furthermore, they mediate apoptotic induction, senescence, iron-sulfur (Fe / S) cluster synthesis, heme biosynthesis, redox- and calcium-signaling, thermogenesis, lipid oxidation and synthesis, production of reactive oxygen species (ROS) as well as regulation of immune responses (Friedman & Nunnari, 2014; Tábara et al., 2024; Yien & Perfetto, 2022) (Fig. 1).

In the following chapters, the organization, function and role of mitochondria are examined in more detail.

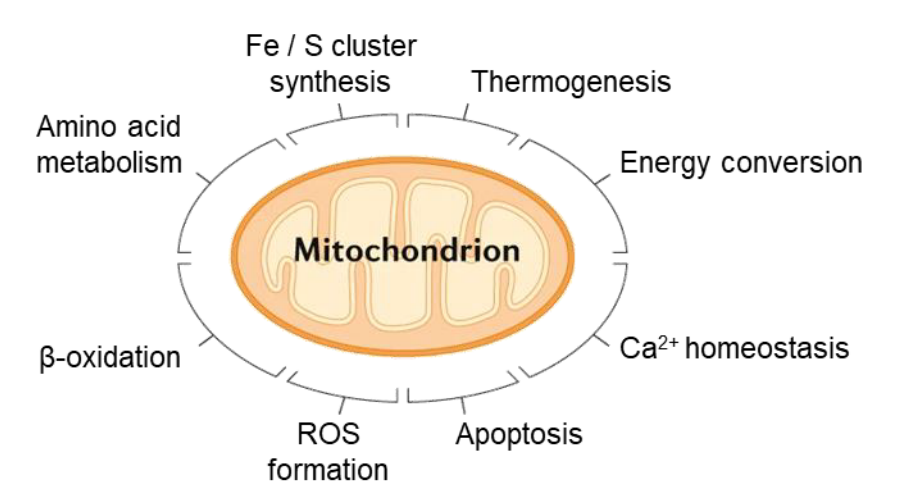


Fig. 1: Overview of mitochondrial function.

This scheme highlights the functions of mitochondria mediating different cellular functions and metabolic processes including energy conversion to ATP. Additionally, they perform other functions including iron-sulfur (Fe / S) cluster synthesis, thermogenesis, or apoptotic induction. Image modified from (Giacomello et al., 2020).

#### 1.1.1. Mitochondrial organization

Mitochondria are double-membrane organelles surrounded by an outer mitochondrial membrane (OMM) and inner boundary membrane (IBM). The remaining inner mitochondrial space enclosed by the IBM is defined as the mitochondrial matrix. Located between OMM and IBM is the inter membrane space (IMS). Through invagination of the IBM into the mitochondrial

matrix space, known as mitochondrial cristae, the surface of mitochondria can be increased. Mitochondrial cristae serve as assembly platform for OXPHOS complexes and sub compartmentalize mitochondria (Mannella, 2006).

The formation of mitochondrial cristae is highly dependent on the mitochondrial contact site and cristae organizing system (MICOS) complex which plays a pivotal role in the formation and stabilization of crista junctions (CJs) (Harner et al., 2011; Hoppins et al., 2011; G. B. John et al., 2005; Rabl et al., 2009; Stephan et al., 2020; von der Malsburg et al., 2011), a defined pore-like structure (ranging between 12 to 40 nm) from which the internal cristae lumen opens into the IMS of mitochondria (Mannella, 2006). Changes in the steady-state level of MICOS proteins have been reported to be associated with a numerous amount of diseases including Parkinson's, epilepsy and hepatic encephalopathy (Benincá et al., 2021; Kishita et al., 2020; Van Laar et al., 2016). The regulation of CJs has been previously reported and plays an important role in the diffusion of substrates, proteins, and lipids between the cristae lumen and the IMS (Frey & Mannella, 2000). Most importantly, cristae formation enables dense occupancy of the membrane complexes of the electron transport chain (ETC) complexes essential for the function of mitochondria as a major energy supplier (Fig. 2).

Taken together, the unique ultrastructure of mitochondria, comprising the delicate orchestration of double membranes, cristae and crista junctions, plays a crucial part in the efficient energy conversion and supports of cellular function. Furthermore, the disruption of these structures is directly linked to several diseases.

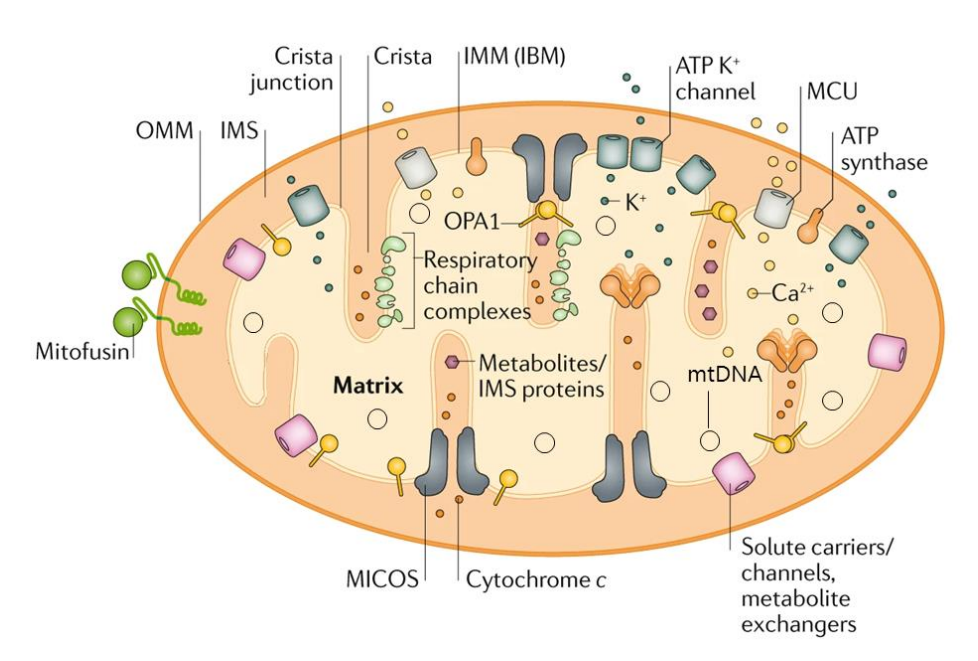


Fig. 2: Mitochondrial organization and functional parameters.

Overview of mitochondrial compartments comprising outer mitochondrial membrane (OMM), inter membrane space (IMS), inner mitochondrial membrane / inner boundary membrane (IMM / IBM), cristae, crista junctions and matrix. Furthermore, proteins involved in diverse mitochondrial functions such as fusion, calcium homeostasis, and respiration are indicated. Additionally, mitochondria contain

their own circular genome (mtDNA) which is distributed throughout mitochondria. Image modified from (Giacomello et al., 2020).

#### 1.1.2. Mitochondrial functions

Mitochondria fulfill diverse functions to support cellular viability and homeostasis. One major function of mitochondria is the conversion of adenosine diphosphate (ADP) to energy in form of adenosine triphosphate (ATP) via OXPHOS (Fig. 3). ETC complexes (CI - CIV) accommodate along the invagination of the IMM, to efficiently produce an electrochemical gradient across the IMM that is used by F<sub>1</sub>F<sub>0</sub>-ATP synthase (ATPase / CV) for generation of ATP. The first complex in the ETC is the NADH-dehydrogenase, also termed as complex I (CI). CI oxidizes NADH derived from the TCA-cycle and transfers electrons from NADH to ubiquinone (CoenzymeQ / CoQ) which is embedded in the IMM (Vinothkumar et al., 2014). During this process, four protons are pumped from the matrix into the IMS (Zickermann et al., 2009). The second complex is succinate-dehydrogenase (SDH) or complex II (CII). During respiration, CII transfers electrons to ubiquinone via oxidation of FADH<sub>2</sub>, while succinate is oxidized to fumarate in the TCA-cycle (Rizwan et al., 2018). However, during this process no protons are transported into the IMS. The middle segment of the respiratory chain comprises complex III (CIII), namely cytochrome c (Cyt c) reductase. Dimerization of CIII (CIII<sub>2</sub>) has been shown to facilitate its function through a slight rotation of one monomer to the ubiquinol-producing site of CI that enhances the oxidation of ubiquinol and simultaneously the reduction of two molecules of Cyt c (Sousa et al., 2016). Throughout this process four protons pass the IMM into the intermembrane space. Cytochrome c oxidase (COX) or complex IV (CIV) transfers four electrons from Cyt c onto molecular oxygen (O2) resulting in the generation of water (H<sub>2</sub>O) via the reaction of molecular oxygen with two protons (Kadenbach, 2021). During this reaction, four protons are carried into the IMS. The last complex, F<sub>1</sub>F<sub>0</sub>-ATP synthase or complex V (CV), consist of the matrix-facing F<sub>1</sub>-part and a membrane-embedded F<sub>0</sub>-part connected with each other over a peripheral stalk (Walker & Dickson, 2006). Assembly of CV and dimerization  $(V_2)$  at the cristae tip supports further membrane curvature (Strauss et al., 2008). During the electron transport between the single complexes, protons are continuously transferred from the mitochondrial matrix into the intermembrane space, thereby generating an electrochemical gradient resulting in a mitochondrial membrane potential ( $\Delta \Psi_m$ ). Following the gradient, protons pass via the F<sub>0</sub>-subunits resulting in the rotation of the F<sub>1</sub>-subunit which then catalyzes the conversion of ADP to ATP.

Within mitochondria, OXPHOS complexes can organize in higher-order, namely supercomplexes (SC), underlying a strictly regulated stoichiometry (Schägger & Pfeiffer, 2000). The multienzyme assembly of complexes I (CI), III (CIII) and IV (CIV) into SC I+III<sub>2</sub>+IV

facilitates the electron transport from NADH to  $O_2$  via electron transfer on ubiquinone between CI and CIII, and Cyt c between CIII and CIV (Althoff et al., 2011). Therefore, SCs containing CI, CIII and CIV are referred to as respirasome. With less abundancy, mammalian cells also inherit SCs consisting of SCI+III<sub>2</sub>, SCIII<sub>2</sub>+IV as well as CIV and CV dimers (Schägger & Pfeiffer, 2000). The organization of respiratory complexes as SCs in mitochondria can minimize the formation of ROS and, therefore, reduce oxidative stress while maximizing ATP production. Mitochondrial energy conversion into ATP is fueling various processes including active transport of molecules, generation of signaling molecules, and biosynthesis. Depending on the energy demand of the cells, mitochondrial mass (and, thus, mitochondrial energy supply), can vary (Fernández-Vizarra et al., 2011). For example, muscle cells have been shown to possess the highest mitochondrial content in order to satisfy their high energetic requirements (Kuznetsov et al., 2009).

Mitochondria also play a multifaceted role in cellular metabolism, converting diverse sources such as carbohydrates, fats, and amino acids into energy and metabolites. Thereby, mitochondria are able to connect different metabolic pathways as seen in the TCA-cycle which represents a mitochondrial-mediated link between glycolysis and OXPHOS. In the mitochondrial matrix, ATP and coenzymes are generated by the stepwise oxidation of various metabolites. Coenzymes, including NADH and FADH<sub>2</sub>, play an important role by acting as reduction equivalents for ETC complexes during OXPHOS (Martínez-Reyes & Chandel, 2020). The TCA-cycle is an integral component within mitochondria, interconnecting other metabolic pathways. For example, metabolites produced during the TCA cycle are also used to generate amino and fatty acids, and vice versa. Conversely, products of the fatty acid oxidation and amino acid synthesis can enter the TCA-cycle (Martínez-Reyes & Chandel, 2020). Thus, mitochondria fulfil an important part in the degradation of fatty acids to acetyl-CoA via β-oxidation (Bartlett & Eaton, 2004). In addition, cells can store fatty acids in fat deposits, allowing the cells to use fatty acids as a source of energy during nutrient deprivation. Furthermore, mitochondria can metabolize amino acids in order to generate ATP and metabolites for biosynthesis. However, degradation of amino acids is also accompanied with the production of the toxic by-product ammonia in human brain, liver, and kidney (Herrgård et al., 2006).

As mentioned above, ATP production is mediated by OXPHOS. During this process, ROS, such as superoxide anions  $(O_2^{\bullet-})$ , are produced as by-product within mitochondria by one-electron reduction of  $O_2$ . ROS production enhances the risk of oxidative damage for macromolecules such as lipids, proteins and deoxyribonucleic acid (DNA). In sum, elevated levels of mitochondrial ROS can play an important role in the induction of apoptosis (Simon et al., 2000). However, in a balanced system ROS serve as crucial signaling molecules

orchestrating intracellular processes, but also intercellular communication (Sies & Jones, 2020).

In addition to the generation of energy in form of ATP, mitochondria function as a major player in cellular calcium homeostasis. This function heavily depends on the high buffering capacity of the mitochondrial matrix which serves on the one hand as a storage for Ca<sup>2+</sup> in the form of calcium phosphate, but also enables the mitochondria to rapidly take up Ca<sup>2+</sup> in the event of a Ca<sup>2+</sup> increase in the cytoplasm (Finkel et al., 2015; Rizzuto et al., 2012). In both cases, Ca<sup>2+</sup> has to pass two mitochondrial membranes: the OMM and IMM. In contrast to the selectively permeable IMM, the transport of small molecules, such as Ca<sup>2+</sup>, across the OMM into the IMS is mainly mediated by the 35 kDa voltage-dependent anion channel (VDAC) (Rosencrans et al., 2021). Further transport of Ca<sup>2+</sup> from the IMS across the IMM into the matrix either follows the electrochemical gradient generated by ETC during OXPHOS or via transport through mitochondrial Ca<sup>2+</sup>-uniporter (MCU) (Santo-Domingo & Demaurex, 2010). Furthermore, a close interaction of mitochondria with the endoplasmic reticulum (ER) has been shown to be essential for Ca<sup>2+</sup> cellular homeostasis and overall survival (Naon & Scorrano, 2014).

Consequently, mitochondria have huge influence on the delicate balance of cell survival and cell death. Induction of apoptosis is mediated via two major pathways: The extrinsic and intrinsic pathway. Upon induction of the intrinsic pathway, BCL2 Associated X (Bax) and BCL2 Antagonist/Killer 1 (Bak) enable the release of cytochrome *c* (Cyt c) through opening of the OMM resulting in a downstream activation of Apoptotic Peptidase Activating Factor 1 (APAF-1) and caspase 9 (Green, 2005). Ultimately, downstream caspases initiate DNA fragmentation, protein degradation and formation of apoptotic bodies (Green & Kroemer, 2004). Induction of apoptosis is essential for cellular homeostasis, embryogenesis, differentiation and development (Knight & Melino, 2011).

Taken together the functionality of mitochondria does not solely comprise the energy conversion, but also the curcial orchestration of other cellular pathways, including cellular signaling and calcium buffering. The delicate management between OXPHOS and ROS generation is essential for maintaining cellular homeostasis and adapting to external and internal stimuli. In addition, mitochondria regulate apoptosis, highlighting their critical influence on cell survival and development.

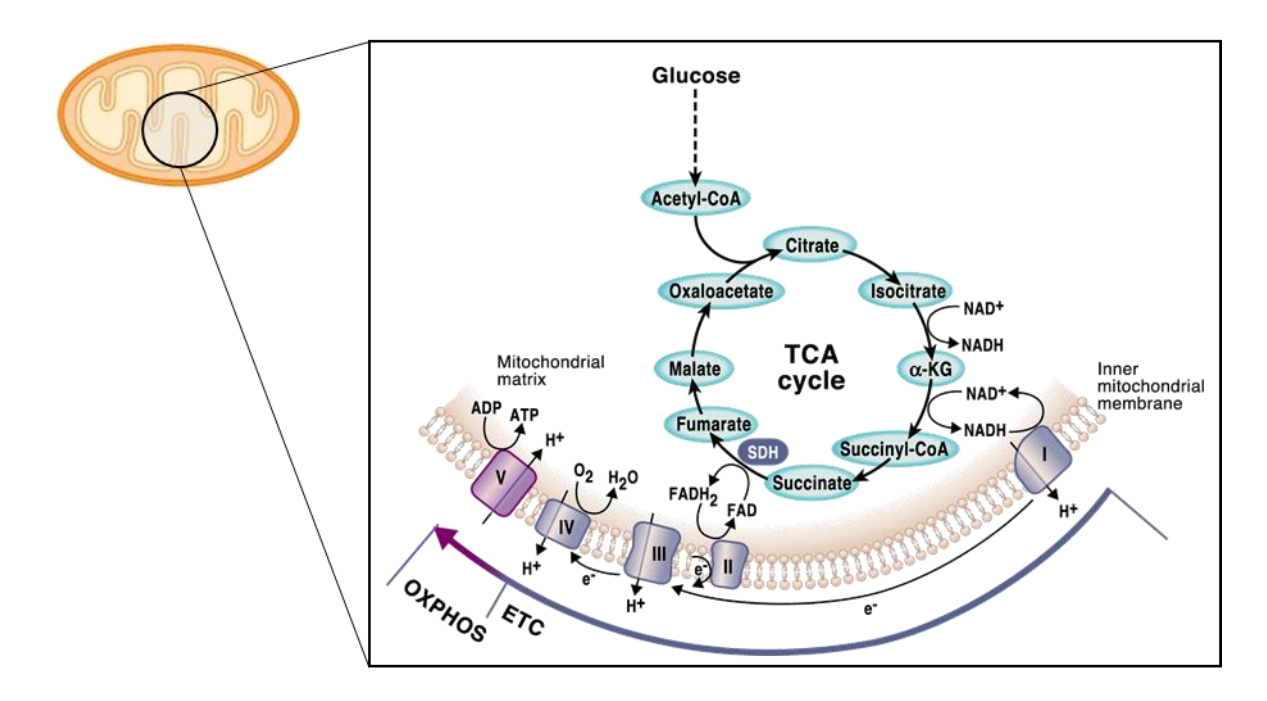


Fig. 3: Conversion of energy into ATP upon mitochondrial respiration.

Shown are the nine subsequent reactions of the tricarboxylic acid (TCA) cycle which starts with acetyl-CoA and ends with oxaloacetate. During this process important coenzyme reduction equivalents are generated (NADH and FADH<sub>2</sub>), which are important for the functionality of oxidative phosphorylation (OXPHOS). Along the electron transport chain, which comprises a total of four complexes, electrons are transported while generating a proton (H<sup>+</sup>)-gradient along the inner mitochondrial membrane. This gradient is then used from complex V to convert ADP to ATP (Images modified from Giacomello et al., 2020 and Vercellino & Sazanov, 2021).

#### 1.1.3. Mitochondrial dynamics and quality control

Mitochondrial morphology and content within the cell is tightly regulated by constant fusion and fission processes within the cell (Fig. 4). The resulting exchange of metabolites, proteins, and solutes is essential for cellular and mitochondrial homeostasis as well as adaptation to external stimuli (H. Chen & Chan, 2005). Furthermore, the ability of targeted isolation of mitochondria from the rest of the network represents an important quality control, ultimately leading in the induction of autophagic or apoptotic processes (H. Chen et al., 2005). Upon fission, one mitochondrion is divided into two or more daughter mitochondria. In mammalian cells, this process is primarily catalyzed by the GTPase dynamin-related protein 1 (Drp1). During fission, Drp1 locates in a ring-like structure around the OMM of mitochondria where it constricts the membrane leading to mitochondrial fragmentation (Smirnova et al., 2001). As shown by a spatiotemporal analysis of mitochondrial fission process, distinct bimodal pattern define the fate of mitochondria (Kleele et al., 2021). Depending on whether mitochondria undergo peripheral (close to the mitochondrial pole) or midzone (the middle of mitochondria) fission, separated mitochondria either undergo mitophagy or mitochondrial biogenesis, respectively.

This strongly highlights the important role of fission in regulating mitochondrial fate. Fission processes help to distribute mitochondria throughout the cell. This can be a crucial aspect of the different energy requirements of subcellular regions as seen, for example, during cell cycle (Martínez-Diez et al., 2006). In contrast, mitochondrial fusion involves the merging of two or more mitochondria, ultimately resulting in the formation of one single mitochondria or interconnections between various mitochondria. The process of fusion is highly dependent on three proteins of the GTPase family: Mitofusin 1 (Mfn1), mitofusin 2 (Mfn2), and optic atrophy protein 1 (Opa1) (Ranieri et al., 2013). Embedded in the OMM, Mfn1 and Mfn2 mediate OMM-OMM fusion. Furthermore, Mfn1 and Mfn2 can form homodimers (Mfn1-Mfn1 or Mfn2-Mfn2) or heterodimers (Mfn1-Mnf2) that initiate the tethering between mitochondria or between mitochondria and ER in close proximity (Koshiba et al., 2004). The fusion process requires the orchestration not only of the OMM, but also of the IMM. The latter, is mainly mediated by Opa1 which tethers the IMM together in a comparable manner as Mfn1 and Mfn2. Thereby, fusion of IMM is highly dependent on the embedding of long-Opa1 isoforms (Mishra et al., 2014), whereas proteolytic cleavage of Opa1 via Oma1 zinc metallopeptidase (Oma1) leads to the loss membrane-anchor promoting fission (Anand et al., 2014; Baker et al., 2014; Duvezin-Caubet et al., 2006). Balancing of fission and fusion processes thus has a significant impact on the internal control of the mitochondrial system and is therefore strictly regulated. Cells missing the ability to undergo fission by silencing Drp1 display hyperfused mitochondria. Consequently, unimpeded fusion processes limit mitochondrial exchange and mitochondrial quality control (Fonseca et al., 2019). Vice versa, knockout of one mitofusin protein results into extensive fragmentation of the mitochondrial system accompanied with disruption of mitochondrial exchange (Alvarez et al., 2016).

Taken together, the delicate balance of fusion and fission processes is essential enabling mitochondria to respond rapidly to both internal and external stimuli. Impairment of these processes ultimately results in altered mitochondrial quality control and energy conversion highlighting the pivotal role of mitochondrial dynamics for cellular function and survival.

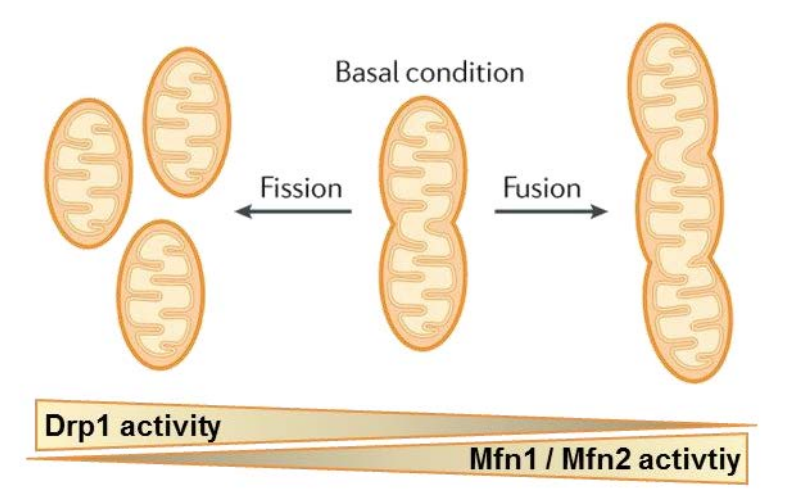


Fig. 4: The dynamic nature of mitochondria.

Mitochondria are highly dynamic organelles undergoing constant merging (fusion) and splitting (fission) events majorly regulated by the GTPases dynamin-related protein 1 (Drp1), mitofusin 1 (Mfn1) and mitofusin 2 (Mfn2). Upon higher activity of Drp1, mitochondria undergo fission and the mitochondrial network undergoes fragmentation (left side). Vice verca, upon higher activity of Mfn1 or Mfn2, mitochondria undergo fusion and the mitochondrial network elongates (right side). The status of the mitochondrial network is directly linked to the energy and homeostatic state of the cell. Image modified from (Giacomello et al., 2020).

#### 1.1.4. Mitochondrial DNA

In mammals, mitochondrial inherit their own circular (DNA)of 16.6 kb in size, namely mitochondrial DNA (mtDNA) (Lang et al., 1997). Within mitochondria, mtDNA is organized in nucleoids, punctae-like dynamic structures harbouring ~1.4 mtDNA molecules per nucleoid (Kukat et al., 2011). Unlike nuclear DNA which is protected by histones, mtDNA is coated with proteins, such as Twinkle mtDNA helicase (Twinkle), single-stranded DNA binding protein 1 (mtSSB), and mitochondrial transcription factor A (TFAM). These play a major role in packaging, transcription, and translation of mtDNA (Bogenhagen et al., 2008). In particular, with confocal microscopy it has been shown that the ratio of TFAM to mtDNA determines whether nucleoids are decondensated and transcriptionally active or condensated, and therefore, transcriptionally repressed (Brüser et al., 2021; Legros et al., 2004).

Of 37 genes encoded, 13 genes encode for proteins, two genes encode for ribosomal-RNA (rRNA), and 22 genes encode for transfer-RNAs (tRNAs) (Anderson et al., 1981). All of these are required for the expression of OXPHOS proteins, which are ultimately essential for mitochondrial energy conversion into ATP. In humans, the inheritance of mtDNA predominantly occurs via uniparental mode, typically within the maternal lineage (Birky, 1995). Nowadays, this inheritance pathway can be utilized in the context of crime solving (Budowle et al., 2003) or genealogical research (Pääbo, 1999). Compared to the nuclear genome, mtDNA is polyploidy and, depending on the cell type, ranges between hundreds to thousands of copies

within one cell (Stewart & Chinnery, 2015). The mitochondrial genome has a roughly 20-times higher mutation rate than nuclear DNA, which might derive from higher levels of oxidative stress, error-prone replication, less efficient repair of occurring mtDNA damage, and higher turnover rates (Árnadóttir et al., 2024; Brown et al., 1982; Ingman et al., 2000; Wallace et al., 1987). With occurrence of mutations on mtDNA, cells inherit a varying amount of healthy and mutated mtDNA copies, a status also known as heteroplasmy (Wallace, 2018). With further proliferation of cells, the ratio between normal and mutated mtDNA can shift to one state resulting in homoplasmy (Wallace, 2018). In healthy cells, a high percentage of mutated mtDNAs can be tolerated before exceeding a biochemical threshold and the respective mutation becomes pathological (Stewart & Chinnery, 2015). In this case, mitochondrial function may be impaired, resulting in clinical symptoms or even developmental disorders. For instance, mutation in the mitochondrial encoded tRNA-Leu (UUA / G) 1 is the major driver of mitochondrial encephalopathy, lactic acidosis and stroke-like episodes (MELAS) (Goto et al., 1990). Also, during aging processes mitochondria have been shown to be major drivers as mtDNA mutations significantly increase with age (Bratic & Larsson, 2013).

To summarize, mitochondrial DNA is a small, maternally inherited molecule encoding for protein subunits essential for energy conversion into ATP and cellular function that makes it a valuable structure within mitochondria with regard to genetics, evolution and disease development. Its importance in both biology and medicine is highlighted by its critical role in understanding human ancestry and diagnosing mitochondrial disorders.

#### 1.1.5. Role of mitochondria in disease

As already described in section 1.1.2, mitochondria have a significant influence on energy metabolism, apoptosis, and the regulation of various pathways. Mitochondrial dysfunction is recognized as major contributor to the development of a numerous amount of diseases, including metabolic disorders (Lowell & Shulman, 2005), neurodegenerative diseases (Knott et al., 2008), cardiovascular diseases (Feng et al., 2021), and cancer (Sainero-Alcolado et al., 2022). Mitochondrial dysfunction is multifaceted and can be accompanied by following characteristics: Reduction in metabolic functions (e.g. OXPHOS,  $\beta$ -oxidation, degradation of amino acids), increased oxidative stress, and imbalance in mitochondrial fission and fusion processes. However, in terms of disease development, loss of mitochondrial mass has been shown to correlate with the development of chronic kidney disease (X. Zhang et al., 2021) or of Alzheimer's disease (Sheng et al., 2012). Furthermore, imbalance of mitochondrial fusion and fission processes due to lack of OPA1 or Mfn2 has been shown to be directly linked to the development of optic atrophy type 1 (Liao et al., 2017) or Charcot-Marie-Tooth disease type 2A (Rocha et al., 2018), respectively. In addition, the rate of people developing metabolic

diseases, such as type-2-diabetes (Kovács et al., 2024), has been shown to increase significantly and is caused by inappropriate dietary behavior. Here, mitochondria are the main drivers, as nutrient overload is associated with diminished mitochondrial content and, therefore, reduced OXPHOS capacity (Szendroedi et al., 2012).

Most importantly, mitochondria are a major contributor to cardiovascular diseases. Compared to other tissues, muscle cells and cardiac muscle cells in particular have the highest mitochondrial content (Fernández-Vizarra et al., 2011). The primary source of energy for the heart is provided by the oxidation of fatty acids and their metabolites are used by mitochondria to carry out the conversion of energy into ATP. In addition, the role of mitochondria as a major Ca<sup>2+</sup> storage plays an important role in the contractility of heart muscle cells (Bers, 2000). For instance, mutations in TFAM of fetal cardiomyocytes are associated with impaired ETC function and an energy deficit, which ultimately results in compromised contraction function (D. Zhang et al., 2018). Moreover, genetically inherited heart diseases such as hypertrophic cardiomyopathy (Ranjbarvaziri et al., 2021) and dilated cardiomyopathy (Govindaraj et al., 2019) are associated with suppression of mitochondrial respiration, accumulation of mtDNA mutations and damaged mitochondria. Furthermore, mitochondria have been shown to play a key role in the development of chemotherapy-induced cardiomyopathies (Varga et al., 2006). Overall, mitochondria are central for energy metabolism, apoptosis regulation and the maintenance of cellular homeostasis. On the other hand, mitochondrial dysfunction contributes to the development of many diseases including neurodegenerative, metabolic, cardiovascular disorders, and cancer. Most importantly, disruption of mitochondrial function is closely linked to inherited cardiac conditions as well as chemotherapy-induced cardiomyopathies resulting in comprised cardiac function.

#### 1.2. Cardiovascular system

The cardiovascular system is a complex system composed of the heart, blood vessels and blood. The function of the cardiovascular system is mainly based on the contraction of the heart enabling the distribution of oxygen and nutrients (e.g. glucose, amino acids, and fatty acids) to the cells in all body tissues. Simultaneously, waste products (e.g. carbon dioxide) are being eliminated upon nutrient supply. In the event of an infection or injury, immune cells are being transported by the blood to their respective destination. Similar is true for systolic distribution of blood throughout the body as it enables the transportation of hormones and, consequently the communication between specific organs. Mammals are homothermic organisms and maintenance of a constant temperature is essential for organ function. Here, the cardiovascular system plays a regulating role, protecting the body from cooling and overheating by increasing blood flow to the skin (González-Alonso, 2012). Thus, the homeostasis of the whole organism is highly dependent on the function of the cardiovascular system. Lifestyle choices including alcohol abuse, smoking, stress, and unhealthy nutrition have been shown to enhance the risk of cardiovascular diseases (Mozaffarian et al., 2008). Also, external factors such as radiotherapy (Lee et al., 2013) or the treatment with chemotherapeutic drugs (Avagimyan et al., 2024), such as doxorubicin, can also have a negative effects on the cardiovascular system.

#### 1.2.1. Function and anatomy of the heart

Anatomically, the heart is a muscular pump consisting of four chambers, which can be divided into a left and a right side. Via the interventricular septum, both chambers are separated from each other. Each of the sides contain an atrium and a ventricle, which majorly consists of heart muscle cells (Fig. 5). One essential part of the heart are the heart valves: semilunar valves and atrio-ventricular valves. The pulmonary (PV) and aortic (AV) valves prevent blood from flowing back into the ventricles when the heart relaxes during diastole. The AVs in particular are the openings that supply the heart muscle with fresh, oxygenated blood. The atrio-ventricular valves consist of tricuspid (TV) and mitral (MV) valves, which prevent reverse blood flow from the ventricle to the atrium during systole, namely the contraction of the heart (Sacks et al., 2009). Briefly, the contraction process can be described as follows: Deoxygenated blood from the body returns to the heart over the *superior* and *inferior venae cavae* and enters in the right atrium. Through the TV, the right ventricle is consecutively filled with blood. Additionally, the atria contracts to increase the speed of blood filling. Upon contraction of the right ventricle, the increased pressure closes the TV and upon further pressure increase, the PV opens into the pulmonary artery, the artery connecting blood

circulation from the heart directly to the lung. Via the PVs, oxygenated blood returns to the empty left atrium in the heart. When the left ventricle fills, blood flows through the MV into the left ventricle. Upon increase in pressure, MV closes and the left ventricular contracts ultimately resulting in the transport of oxygenated blood via the AV and aorta to the rest of the body (Feher, 2012).

The strength of the heart is very much dependent on the wall of the heart. The heart is made up of three layers. The endocardium consists of a thin layer, which lines the inside of the heart wall and plays an important role in the signaling to cardiomyocytes (Harris & Black, 2010). The myocardium is the thickest layer of the heart and is located adjacent to the epicardium. The myocardium is constituted primarily by muscle fibers that are indispensable for the contraction function of the heart. Furthermore, nerve cells of the afferent nervous system extend via the myocardium into the endocardium (Wake & Brack, 2016). The heart is enveloped by an outer sheath of epithelial layer comprising of fat and connective tissue which is in contact with fluids of the pericardial cavity (Männer et al., 2001). This sac-like structure fulfils protective function against injury and infection. Additionally, it maintains the heart's position within the abdominal cavity, namely mediastinum.

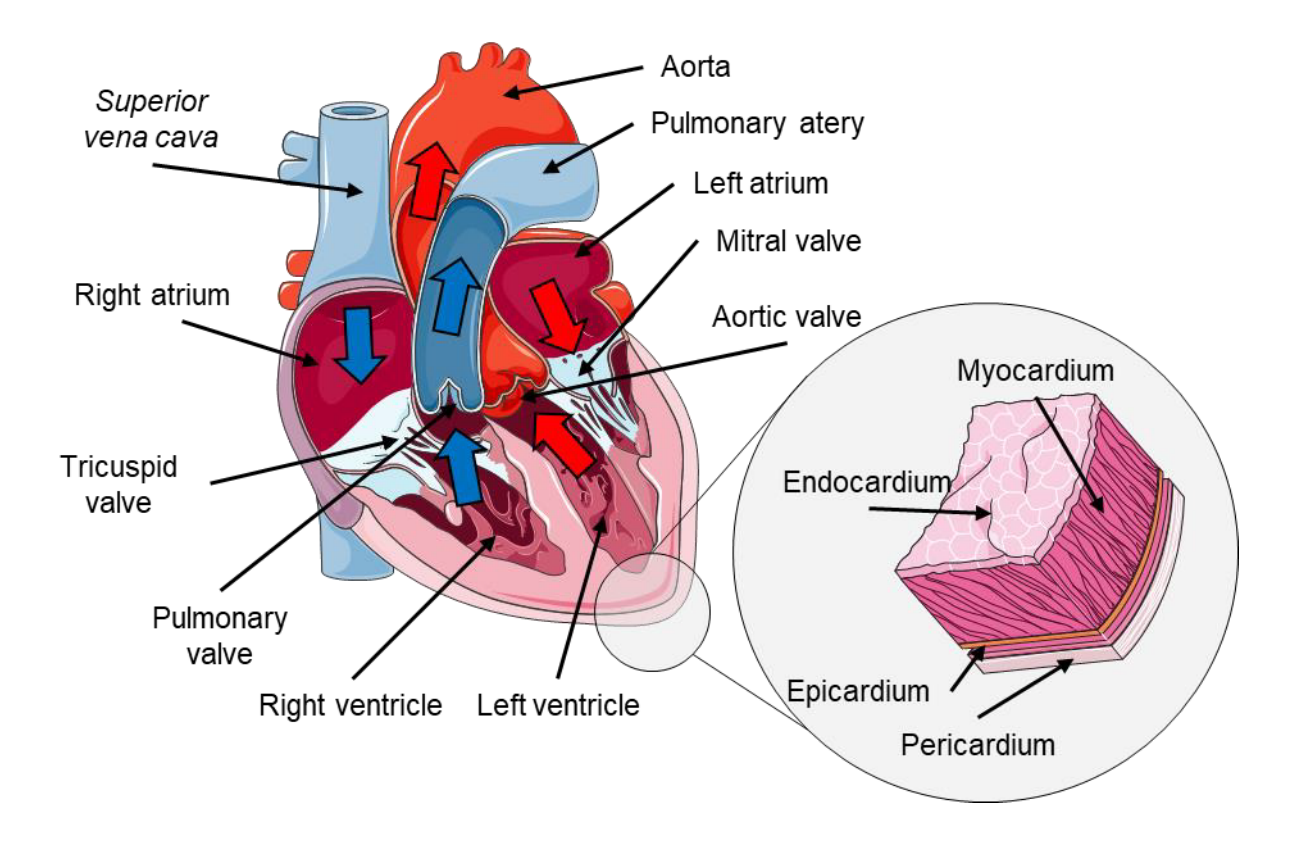


Fig. 5: Schematic diagram of the anatomy of the heart.

This scheme highlights the anatomy of the heart including major compartments, valves, tissues, and blood vessels. The direction of flow of oxygen-poor (blue) and oxygen-rich (red) blood is indicated by arrows in the respective color. This figure was partly generated using Servier Medical Art (https://smart.servier.com), provided by Servier, licensed under a Creative Commons Attribution 4.0 unported license (https://creativecommons.org/licenses/by/4.0/ [Status: 21.01.2025]).

#### 1.2.2. Cell types within the heart

The heart consists of different cell types including cardiomyocytes, fibroblasts, endothelial cells, smooth muscle cells, adipocytes, lymphoids, myeloids, and pericytes (Pinto et al., 2016). Briefly, cardiac fibroblasts (CF) provide structure for the heart, contribute to the extracellular matrix, and are responsible for fibrosis induction within the heart upon injury (Tallquist & Molkentin, 2017). The inner cell layer coating the lumen of blood vessel is comprised of a monolayer of endothelial cells (CE). These represent a mechanical barrier and have an essential function in secretion of interleukins, growth factors or chemokines (Sturtzel, 2017). Furthermore, the heart consists of pace maker cells coordinating the contractions of the heart. These myocytes generating a contraction impulse are located in the sinoatrial as well as in the atrioventricular node and further transfer the signal to a network of Purkinje cells, ultimately resulting in the contraction of cardiomyocytes (Christoffels et al., 2010). In this thesis, the main scope lays on cardiomyocytes, which will be further considered in more detail in the following section.

#### 1.2.2.1. Cardiomyocytes

The contractility force of the heart is majorly driven by cardiomyocytes. Although these cells generate the force required for efficient heart pumping, the percentage of cardiomyocytes ranges between 30 to 49 % among all cell types within the heart (Litviňuková et al., 2020). Within myocytes, actin cytoskeleton is organized into sarcomeres, which represents the major contractile unit. Sarcomeres consist of repetitive units of myosin-containing thick fibers, titin filaments, and actin-containing thin filaments. Thereby, thick filaments are connected to a central M-line and together they resemble the A-band (Hanson & Huxley, 1953). On each site of the M-line, myofilaments organize in a densely interweaved packed pattern. Thin filaments stretch through the I-band towards the Z-disk where their ends anchor and interconnect with α-actinin. Via binding on Ca<sup>2+</sup>, conformational changes on cardiac troponin results in the binding of myosin heads on actin. Upon ATP-consumption, the Z-disk is pulled towards the M-line and the sarcomere contracts (Hinken & Solaro, 2007) (Fig. 6). Cardiac output is thus subject to regulation by a number of factors. For instance, the strength of the heart's contraction is increased by the extent of the stretching of cardiac fibers during diastole, the process of blood filling the heart. This effect ensures that an equal amount of blood is exchanged during one heart cycle, thereby balancing blood input and output within the cardiovascular system. This phenomenon is known as the Frank Starling law (van der Velden & Stienen, 2019). It is important to note that the concentration of Ca<sup>2+</sup> is a pivotal factor in ensuring optimal contracting function. Subsequent to this, further Ca<sup>2+</sup> is released through ryanodine receptor (RyR), resulting in contraction (Bers, 2002).

The contractile force of the heart heavily relies on the precise regulation of sarcomere function within cardiomyocytes. The regulation of intracellular calcium levels plays a crucial role in enabling effective contraction. Additionally, mechanisms like the Frank-Starling law ensure that blood input and output remain balanced, supporting optimal cardiac performance.

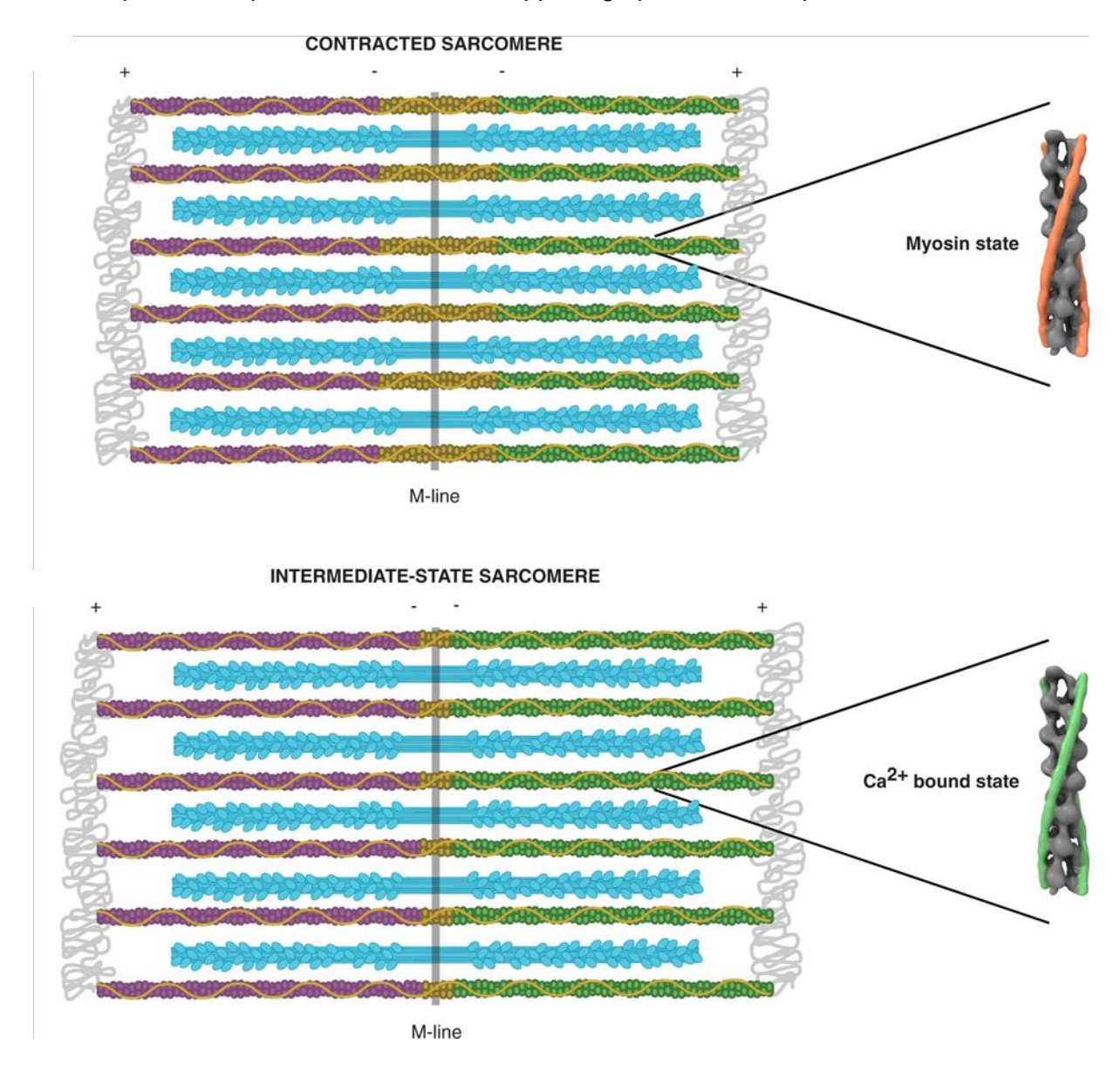


Fig. 6: Functional units within the sarcomere of a cardiomyocyte.

Within cardiomyocytes, the contractile forces are organized in thick myosin and thin actin filaments which are able to contract upon external stimuli, such as calcium. Upon this, conformational changes in titin resulting in the pulling of the Z-disk into the direction of the M-line ultimately resulting in the contraction of the cardiomyocyte. Image modified from (Burbaum et al., 2021).

#### 1.2.3. Regeneration capacity within the heart

As mentioned in section 1.2.2.1, cardiomyocytes represent only 30 to 49 % of the cells within the total heart, yet they make up 75 % of the total heart volume (Litviňuková et al., 2020; Trager et al., 2023). Shortly after birth, cardiomyocytes exit the cell cycle without the completion of cytokinesis resulting in binucleation and ultimately into polyploidization (Bergmann et al., 2015). Yet, with aging of the organism the heart mass increases which is majorly based on an increase in cytoplasmic volume of cardiomyocytes (Bishop et al., 2021; Tracy & Sander, 2011). For many years it has been stated that the heart is an organ with low regeneration capacity (Karsner et al., 1925). Despite some scientific approaches, the regenerative capacity of the heart is still under debate questioning the paradigm within the last 30 years. As shown by a C<sup>12</sup>-based study of Bergmann et al. (2015), the generation of cardiomyocytes never exceeded the original number of cardiomyocytes (Bergmann et al., 2015). Thereby, the annual exchange of cardiomyocytes is estimated to range between 0.5 to 2 %, with up to 50 % during a normal life span (Bergmann et al., 2009; L. He et al., 2020). However, the regenerative capacity has been shown to be strongly age-dependent, with a massive decline with further aging (Bergmann et al., 2009; Mollova et al., 2013). The underlying process of de novo generation of cardiomyocytes is still unclear. It is hypothesized that these pools include mesenchymal stem cells (MSCs) and cardiac stem cells (CSCs). For the latter, multiple proteins including stem cell antigen 1 (Sca1), proto-oncogene tyrosine-protein kinase Kit (Kit), wilms tumor 1 (Wt1) or ISL LIM Homeobox 1 (Isl1), have been described to be adequate markers identifying a residential CSC pool. So far, Sca1 is only expressed in mouse cells and there is no equivalent in humans (Smits et al., 2009). However, tracing in mice revealed the existence of a c-kit<sup>+</sup> pool contributing to the generation of *de novo* cardiomyocyte generation (van Berlo et al., 2014). Yet, the percentage of *de novo* derived cardiomyocytes from c-kit<sup>+</sup> cells remains low, around five times lower (around 0.03 %) than initially predicted by the authors.

Cardiomyocytes constitute the predominant cell type within the heart; however, they cease to proliferate shortly after birth, which limits their capacity for regeneration. This process further diminishes with aging, with a mere 0.5 to 2 % of cells being replaced within one. While stem cell populations, such as c-kit<sup>+</sup> cardiac stem cells, have demonstrated potential for the generation of new cardiomyocytes, their contribution remains negligible, and the precise mechanisms underlying heart cell regeneration remain to be fully elucidated.

#### 1.3. Stem cells

As outlined in section 1.2.3, the regeneration of cells can be achieved through various mechanisms, including dedifferentiation or trans differentiation of somatic and stem cells. The latter comprises a consortium of cells with special attributes supporting embryonic development and tissue homeostasis within the adult organism. The following terms may be used to summarize these attributes, with further elaboration in the subsequent passages: Self-renewal capacity and potency.

The capacity for expansion and maintenance of the stem cell pool is intrinsic to the self-renewal capability of stem cells. To achieve this, stem cells must undergo cell division and give rise to two daughter stem cells (Fig. 7). Symmetric division of stem cells can be enhanced upon regeneration of tissue or during embryonic development (Morrison & Kimble, 2006). However, it is also possible for both daughter cells to become progenitors, which subsequently differentiate into defined cell types. It is noteworthy that both of these processes can be attributed to symmetrical division (Fuchs & Chen, 2013; Morrison & Kimble, 2006). The interplay between self-renewal and differentiation can be observed in the process of asymmetric cell division. During this process, each stem cell divides and gives rise to one daughter stem cell and one daughter cell that further differentiates (Fuchs & Chen, 2013). The occurrence of these events is subject to random processes, yet they can also be induced by extrinsic signaling, as is the case in instances of injury (S. He et al., 2009).

Nonetheless, the capacity to differentiate into specific cell types is contingent on the developmental status of the organism in question. In human subjects, the cell mass between the zygote state and the 8-cell stage exhibits totipotent properties. Between this stages, each single stem cell can differentiated into a complete organism (Johnson et al., 1995). Upon further development stem cells specialize to the inner cell mass (ICM), which later on forms the embryo, while the trophoblast surrounding the ICM develops into the placenta later on (Lu & Zhang, 2015). During this process, cells of the ICM, also known as embryonic stem cells (see section 1.3.1), exit the totipotent state, yet retain their pluripotent characteristics. This status enables the cells to differentiate into cells of the three germ layers that contribute to the developing human organism: mesoderm, ectoderm, and endoderm (Schmidt et al., 2023). In adult organisms, the existence of multipotent and unipotent stem cells (adult stem cells, see section 1.3.2) is restricted to the formation of a defined subset or even specific type of cells, respectively.

Stem cells exhibit the capacity for self-renewal and differentiation, with their potency varying during differentiation progression. These processes, regulated through symmetric and asymmetric divisions influenced by intrinsic and extrinsic factors, are fundamental for tissue regeneration, homeostasis, and embryonic development.

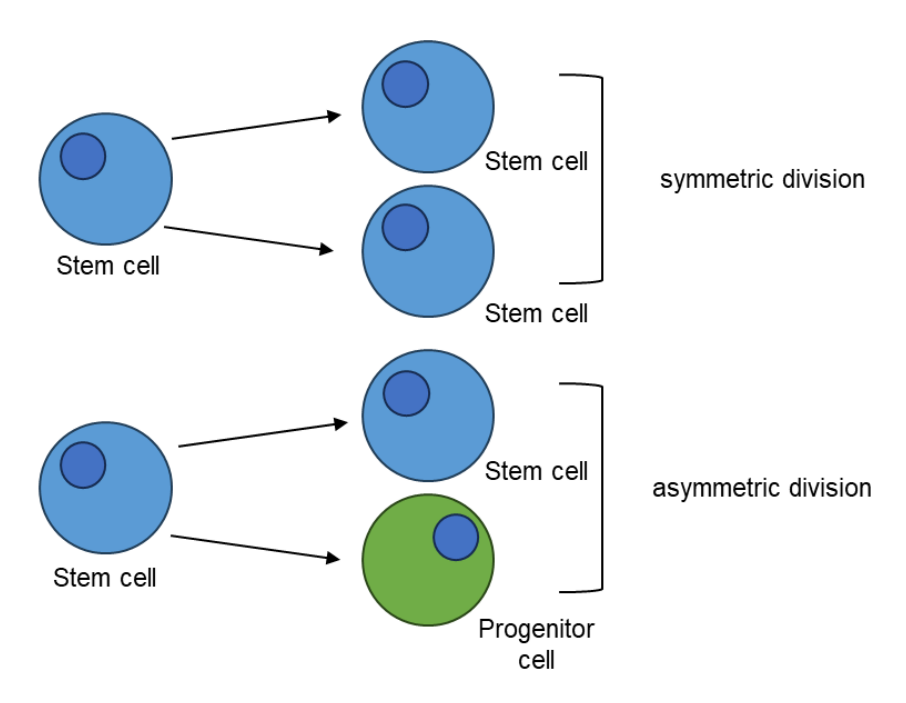


Fig. 7: Symmetric and asymmetric division of stem cells.

Stem cells inherit the capacity to either maintain the stem cell pool or to give rise to differentiating progenitor cells. Upon symmetric division two daughter cells with the same cell fate (in this case two stem cells) are generated. However, asymmetric division is also possible upon external stimuli resulting in the generation of one stem cell and one further differentiating progenitor cell.

#### 1.3.1. Embryonic stem cells

As stated in section 1.3, embryonic stem cells (ESCs) originate from the ICM of the blastocyst. In 1981, the first evidence was presented that pluripotent ESCs could be isolated from the ICM in murine models up to the fourth day of pregnancy, prior to the implantation of the blastocyst (Evans & Kaufman, 1981). Already 17 years later, the first human ESCs were isolated from donated frozen embryos resulting from in vitro fertilizations (Thomson, 1998). The maintenance of the pluripotent state is contingent upon the expression of key transcription factors octamer binding-protein 4 (Oct4), homeobox transcription factor Nanog (Nanog), and SRY-box transcription factor 2 (Sox2) (Chambers & Smith, 2004). However, upon exposure to external stimuli (e.g. growth factors or transplantation into mice), ESCs have been observed to differentiate into all somatic cells except the trophoblast. This phenomenon has been demonstrated through the observation that ESCs isolated from both species have been shown to form teratomas, defined as tumors consisting of cells from all three germ layers (Cunningham et al., 2012), when implanted in immune deficient mice (Evans & Kaufman, 1981; Thomson, 1998). Therefore, the capacity of ESCs to differentiate in vitro into a variety of somatic cells makes them a potent instrument in the domains of developmental biology and drug testing, whilst reducing the necessity for the utilization of animal models. However, the utilization of human ESCs (hESCs) as a research tool in human subjects is accompanied with ethical concerns, as the process entails the sacrifice of an embryo for the isolation of hESCs (King & Perrin, 2014). In Germany, the isolation of hESCs is not permitted by law. However, research involving hESCs lines that can be purchased is permitted (Löser et al., 2010).

The potential for human and murine ESCs to differentiate into all three embryonic germ layers has led to significant advancements in research, particularly in developmental biology and toxicity testing. However, the use of hESCs is accompanied by ethical concerns, which has led to a shift towards alternative cell systems, such as induced-pluripotent stem cells (see section 1.3.3).

#### 1.3.2. Adult stem cells

The human body has a huge capacity for cell renewal. This can be seen, for example, in injuries where skin, hair, and blood can regenerate over time. However, most cells in the body exit the cell cycle and lose their ability to replicate upon further differentiation and specialization (Verfaillie, 2002). In adult organism, regeneration of tissue strongly depends on self-renewal and the differentiation potential of adult stem cells (ASCs). ASCs are located in specific niches including the hematopoietic system (hematopoietic stem cells), the central nervous system (neural stem cells), liver (liver stem cells), as well as adipose tissue and bone marrow (mesenchymal stem cells) (Wagers & Weissman, 2004). These niches protect the ASCs from external stimuli and possible damage (Schofield, 1978). Furthermore, they comprise specific conditions supporting the self-renewal capacity of ASCs and a strictly regulated influence of external stimuli on stem cells fate (Mannino et al., 2022). Most ASCs are quiescent, an alternating period of proliferation / differentiation and dormancy. This process is crucial for the maintenance of ASC pool and alterations are accompanied with depletion of the ASC pool (Ficara et al., 2008).

The capacity for cell renewal within the adult organism relies strongly on the self-renewal and differentiation abilities of adult stem cells, which reside in protective niches across various tissues. These niches regulate ASC activity, thereby alternating between dormancy and proliferation, ensuring long-term tissue regeneration and preventing depletion of the ASC pool.

#### 1.3.3. Induced-pluripotent stem cells

As outlined in the preceding section (see section 1.3.1), research involving hESCs is ethically sensitive (King & Perrin, 2014), and consequently, it is subject to stringent regulations or even prohibitions (Elstner et al., 2009). While isolation of ASCs is accompanied with less concerns, their application to specific research questions is constrained by their limited capacity for

differentiation (Bacakova et al., 2018) and age-dependent influences on the genetic stability of these cells (Burkhalter et al., 2015). The first generation of induced-pluripotent stem cells (iPSCs) from mouse blastocysts (Takahashi & Yamanaka, 2006) paved the way for the generation of iPSCs from human somatic cells (Takahashi et al., 2007), thus circumstancing the major ethical concerns associated with human ESC research. In addition, generated iPSCs possess characteristics highly similar to those found in ESCs (Nishikawa et al., 2008; Takahashi et al., 2007). In the initial approach of Yamanaka in 2006, a pool consistent of 24 genes was reduced to a total of four transcription factors necessary to mediate the reprogramming of somatic cells via retro-viral transduction (Takahashi & Yamanaka, 2006). The so-called 'Yamanaka factors' comprise: Oct4, Sox2, proto-oncogene c-Myc (c-Myc), and Krüppel-Like Factor 4 (Klf4). Until now, different subsets of transcriptional factors, such as Oct4, Sox2, Nanog, and Lin-28 Homolog (Lin28), has been shown to sufficiently induce reprogramming of somatic fibroblasts (Yu et al., 2007). Nevertheless, the retro-viral method is prone to induce mutagenesis by viral genome integration. Nowadays, there is a shift towards non-viral based methods including cDNA, mRNA or protein enhancing the genetic stability of iPSCs (Okita et al., 2008).

Until now, human iPSCs have been a reliable *in vitro* cell model for the investigation of processes throughout embryogenesis and many diseases. Furthermore, the capacity to culture and differentiate iPSCs in 2D or 3D culture, thereby simulating tissues or even organ-like structures, enhances the application of the stem cell model-based system as a standard testing system for wide-ranging applications (Fig. 8). Furthermore, iPSC represent a promising source for tissue engineering and personalized therapy (Rowe & Daley, 2019).

In conclusion, iPSCs represent an ethically favorable alternative, with a broad range of potential applications, including disease modelling, drug testing, and personalized medical approaches. The significant similarity of iPSCs to ESCs, in terms of their ability to differentiate into diverse tissues and organs, emphasizes their significance for developmental and biomedical research. In this study, human iPSCs were used as tool to investigate the influence of low concentrations of the anthracycline doxorubicin on cellular and metabolic function of stem, cardiac progenitor cells and cardiomyocytes.

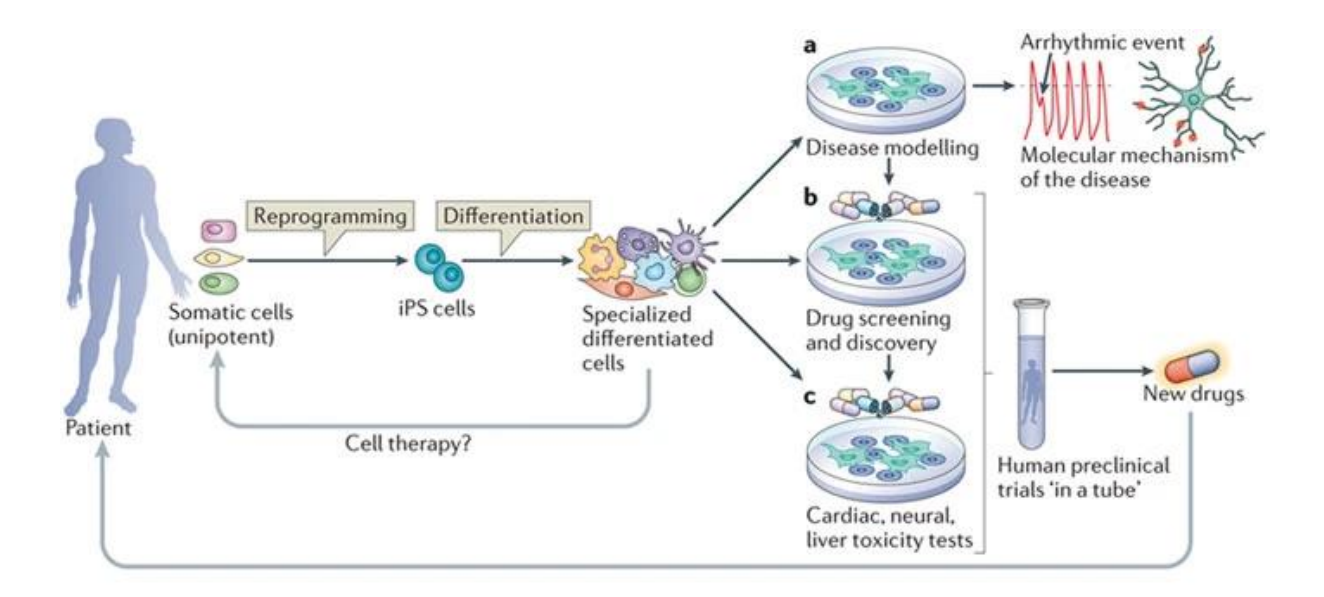


Fig. 8: Biomedical potential of human induced-pluripotent stem cells.

The generation of human induced pluripotent stem cells (iPSCs) from somatic tissue can be achieved through various methodologies. Subsequent differentiation of these cells into one of the three germ layers (endoderm, ectoderm and mesoderm) can be induced, with the resulting cells having applications in disease modelling, drug screening and toxicity testing. This process contributes to the advancement of scientific knowledge and the development of potential treatments. Additionally, the generated somatic cells have the potential to serve as a source for cell therapy. Image modified from an (Bellin et al., 2012).

# 1.3.4. Mitochondria as mediators of stemness, differentiation and reprogramming

In response to external stimuli, stem cells exhibit a high degree of plasticity, which determines whether these cells undergo lineage commitment or contribute to the maintenance of the stem cell pool. This capacity is a crucial element during embryogenesis and tissue homeostasis. Major mediators of these processes are mitochondria as they regulate the delicate balance between stemness and differentiation (Mandal et al., 2011; Pereira et al., 2013). In stem cells, mitochondria locate in prenuclear clusters and exhibit an immature phenotype associated with a low OXPHOS activity and high dependency of stem cells on glycolysis (Varum et al., 2011; J. Zhang et al., 2011). As mentioned in section 1.1.3, motility of this organelle influences most of the central functions of mitochondria including ATP production, Ca<sup>2+</sup> homeostasis, and apoptosis. In neuronal stem cells, fission and fusion processes have been shown to influence stem cell homeostasis and cell fate (Khacho et al., 2016). Mitochondrial-dependent ROS production functions as a second messenger in the modulation of cellular processes in stem cells. Furthermore, ROS have been demonstrated to enhance the induction of spontaneous differentiation and increase during differentiation (Cho et al., 2006). In order reduce ROS-dependent damage, stem cells possess a robust antioxidant defense system. Next,

mitochondria play a pivotal role in preserving stemness, as they function as the predominant hub responsible for the supply of metabolites, such as  $\alpha$ -ketoglutarate, acetyl-CoA, and citrate, which are predominantly produced during the TCA-cycle (Ryall et al., 2015). These have been shown to support enzymes involved in chromatin remodeling and epigenetic regulation of stem cells (Lisowski et al., 2018). In response to external stimuli, this dependency undergoes a shift, as the energy demands of the differentiating cells increase. This phenomenon is concomitant with the maturation of the mitochondria themselves, as well as an augmentation of mitochondrial content (Cho et al., 2006; J. C. S. John et al., 2005; Varum et al., 2011). On the other hand, reprogramming of somatic cells into iPSCs has been shown to result in a decrease in mitochondrial content, which in turn forces a remodeling of the mitochondria back to a stage found in stem cells (Prigione et al., 2010). Nevertheless, it is important to acknowledge the possibility that iPSCs may retain the epigenetic characteristics of their somatic origin influencing metabolism and mitochondrial function.

Mitochondria are responsible for a number of key processes, including energy metabolism, ROS production and epigenetic regulation. These processes have a significant impact on the delicate balance of stemness and differentiation. Due to their plasticity, mitochondria are able to adapt to the respective energy demand, thereby supporting cell homeostasis. Consequently, mitochondria are pivotal regulators of stem cell properties and their plasticity, facilitating differentiation in response to external stimuli.

## 1.4. Chemotherapeutic treatment

Within the last century cancer has become one of the three leading causes of death within modern society (Bray et al., 2021). Among the diverse types of cancer, colorectal, prostate, lung and breast tissue are the most frequently tissues affected in Europe (Ferlay et al., 2013). Treatment option for patients include surgery, ionizing radiation therapy, and chemotherapy (Arruebo et al., 2011; Kashifa Fathima et al., 2022). Compared to the other possibilities, surgery is the most effective treatment, yet solely applicable at an early stage of disease. Since the 1940s, chemotherapeutics have developed as a common therapy of various types of cancer (Falzone et al., 2018). Chemotherapeutic agents can be categorized into four major groups: antimetabolites, alkylating agents, mitotic spindle inhibitors and topoisomerase inhibitors I and II (Nussbaumer et al., 2011). These agents have been shown to promote the death of rapidly proliferating cells, such as cancer cells, through various mechanisms. In order to enhance the efficacy of the treatment, chemotherapeutic agents are primarily administered intravenously, intramuscularly or orally, in defined cycles pending between two and four weeks (Corrie, 2008). Nonetheless, the therapeutic efficacy of chemotherapeutics is constrained by their capacity to not only impact cancerous cells, but also healthy somatic cells. Prolonged treatment with chemotherapeutic agents, such as anthracyclines, is associated with significant adverse effects including nephrotoxicity, cardiotoxicity, hematological toxicity, and gonadal toxicity, limiting the clinical application of chemotherapeutics (van den Boogaard et al., 2022). Cancer remains one of the leading causes of death in humans. Despite other treatments options, chemotherapeutic agents play a pivotal role in anti-cancer treatment. However, the administration of chemotherapeutics is limited by the development of adverse effects, such as cardiotoxicity.

#### 1.4.1. Doxorubicin

The anthracycline antibiotic doxorubicin originally derives from soil bacteria *Streptomyces peucetius* and was first applied as an anti-cancer drug in the 1960s (Arcamone et al., 1969). Among all chemotherapeutic agents, anthracyclines, such as doxorubicin are first line chemotherapeutic agentsdue to the broad application, which encompasses a wide range of solid tumors (e.g. breast, gastrointestinal, and ovary cancer) and hematological malignancies (e.g. lymphatic and myeloid tumors) in adults as well as children (Sritharan & Sivalingam, 2021). During cancer therapy, administration of doxorubicin occurs mostly as fast infusion (Gewirtz, 1999). In patients initial plasma concentrations of doxorubicin range between 0.3 and

 $5 \mu M$ , which rapidly decline to 25 - 250 n M within the first hour after application (Choi et al., 2020; Gewirtz, 1999).

In clinics, application of doxorubicin shows dose-dependent side-effects limiting its application. These comprise, bone-marrow aplasia, neurological disturbances, and most importantly irreversible cardiotoxicity (Carvalho et al., 2009; Henderson & Frei, 1979). Anthracycline-induced cardiotoxicity has been shown to be induced even within hours to weeks after the first application manifesting in electrophysiological changes (Larsen et al., 1992; Steinberg et al., 1987a). Furthermore, up to 9 % of all doxorubicin-treated patients develop side-effects such as, left ventricular fraction reduction and arrhythmias even within one year after the first application (Linders et al., 2024; Mortensen et al., 1986; Mulrooney et al., 2009; Swain et al., 2003).

However, the exact mode of action of doxorubicin is still largely unknown and a wide range of targets are thought to be involved in the development of cardiotoxicity. One important mode of action is genotoxicity. Doxorubicin consists of a tetracyclic ring with quinone-hydroquinone groups, which enables the intercalation into DNA (Jawad et al., 2019). These rings are bound to amino sugar via glycosidic bond, namely daunosamine, which serves as minor groove binding agent. Furthermore, doxorubicin-DNA complex generation is promoted via hydrogen bonds formed by an anthraquinone ring with functional groups such as hydroxyl and methoxy groups (Minotti et al., 2004). These doxorubicin-DNA adducts can inhibit DNA replication and transcription by poisoning topoisomerases II (TopoII), namely topoisomerase II alpha (TopoIIα) and topoisomerase II beta (TopoIIβ). These enzymes are essential manipulators of the DNA structure by the defined induction of double-strand breaks allowing the relaxation of over-coiled DNA (Champoux, 2001). Intercalating Topoll poisons, such as doxorubicin, disrupt the enzyme's ability to re-ligate the double-strand breaks resulting in the generation and accumulation of DNA double-strand breaks (Nitiss, 2009). Furthermore, TopoII-mediated DNA damage is associated with growth arrest and induction of apoptotic pathways (Tewey et al., 1984). In this particular context, mitochondria are of special interest as they inherit their own genome in form of mtDNA representing a further target of doxorubicin for intercalation (Abe et al., 2022; Hu et al., 2000). Simliar to the nuclear genome, mtDNA is under control of a battery of topoisomerases (Das et al., 2021). These comprise topoisomerase III  $\alpha$  (TopoIII $\alpha$ ) and topoisomerase lb (Topolmt). Together with Topollβ, which can also be found within the nucleus, these enroll a powerful machinery reducing the topological stress of mtDNA from bidirectional transcription and replication (Das et al., 2021). Moreover, evidence from animal models indicate that these topoisomerases play a pivotal role in the modulation of doxorubicin-induced cardiotoxicity (Khiati et al., 2014; Nicholls et al., 2018; S. Zhang et al., 2012) emphasizing the role of mitochondrial as major mediators in doxorubicin-induced adversity. Furthermore,

doxorubicin application has been shown to induce further mechanisms increasing its toxicity, such as the formation of ROS (Gewirtz, 1999).

In clinics, doxorubicin has been shown to be a powerful anticancer drug, yet its application is limited due to its small therapeutic window accompanied with the development of long-term side-effects. The mechanisms by which doxorubicin induces apoptosis are diverse, comprising for example DNA damage, ROS induction, and mitochondrial dysfunction, impeding to decipher the one mechanism inducing cardiotoxicity.

# 1.4.2. Mitochondria as mediators of doxorubicin-induced cardiomyopathies

As was stated in the preceding section 1.4.1, besides nuclear DNA mitochondria have been shown to be a major driver of cardiotoxicity, as they perform most of the functions necessary for cellular homeostasis. Mitochondria occupy 30 % of the total cell volume in cardiomyocytes and are the primary source for ATP fueling cardiac function (Cao & Zheng, 2019). As mentioned in section 1.1.2, mitochondria are the main source of ROS due to the ETC activity. With regard to doxorubicin, especially CI has been demonstrated to be the site of doxorubicin reduction resulting in the formation of semiquinone radicals (Davies & Doroshow, 1986). These subsequently react with molecular oxygen to form O2<sup>--</sup> and hydrogen peroxide (H<sub>2</sub>O<sub>2</sub>), inducing oxidative stress within mitochondria and the cell as well as a drop in overall ATP conversion (Minotti et al., 2004). Furthermore, the generation of semiquinone radicals could lead to lipid peroxidation and iron release inducing ferroptosis of cells (Abe et al., 2022). Mitochondria are major hubs for Ca<sup>2+</sup> in cardiomyocytes regulating contractility functions and doxorubicin treatment is accompanied with alterations in Ca<sup>2+</sup>-homeostasis resulting in the release of Ca<sup>2+</sup> (S. Y. Kim et al., 2006).

Although doxorubicin is an effective treatment for a wide range of tumors, its application is limited by severe dose-dependent cardiotoxicity. This is primarily driven by both genotoxic and mitochondrial dysfunction. Understanding the underlying mechanisms of doxorubicin-induced cardiotoxicity and, particularly, its impact on DNA integrity and mitochondrial health, is crucial for developing strategies to mitigate these harmful side effects.

# 1.5. Objectives and aims

The anthracycline antibiotic doxorubicin has been employed as an anti-cancer drug in clinical settings for nearly six decades. Like other chemotherapeutic drugs, doxorubicin exerts a favorable toxic effect on highly proliferative cell types, such as cancer cells. However, it has been observed to have a significant impact on healthy somatic cells. The heart demonstrates a high degree of susceptibility against doxorubicin, exhibiting a dose-dependent responsiveness. Besides other cardiac cell types, the effect of doxorubicin on cardiomyocytes is of special interest. Given that proliferation of cardiomyocytes ceases shortly after birth, the cardiotoxic effect of doxorubicin may not solely depend on the impairment of DNA replication (Gewirtz, 1999).

In addition to the genotoxic effects of doxorubicin, mitochondria have been shown to play a central role in doxorubicin-induced cardiomyopathies by serving as both targets and amplifiers of doxorubicin-induced damage. For cardiomyocytes, doxorubicin treatment has been demonstrated to induce an increase in ROS formation (Lagoa et al., 2014) accompanied with disruption of OXPHOS and mitochondrial dynamics (W. He et al., 2024). This, in turn, has been shown to collectively compromise energy supply, and may subsequently induce apoptosis (Dhingra et al., 2014; Leboucher et al., 2012; Morris et al., 2023). However, most findings on mitochondria were obtained following relatively prolonged exposure times at comparatively high concentrations. Thus, the sensitive role of mitochondria as mediators of cardiotoxicity may be obscured by the effects on various cellular processes, including DNA replication, DNA damage repair, ROS formation, and inhibition of autophagic processes. Consequently, the current perspective of mitochondria as a secondary downstream target of nuclear damage may be inadequate, when considering the relatively high treatment concentrations and exposure times. The underlying role of mitochondria in regulating the sensitivity of cardiomyocytes to doxorubicin exposure is still largely unknown. Furthermore, it remains to be elucidated whether doxorubicin-induced long-term cardiotoxic effects are, at least in part, attributable to the damage of CSCs, as a driving force of cardiac regeneration.

Within the scope of the thesis the general aim was to determine mitochondria as sensitive orchestrator mediating cardiotoxicity. In detail following aims were addressed:

#### Establishment of human iPSC-based cardiac differentiation as as cell model system:

To analyze differentiation-dependent differences and the mediating role of mitochondria, we aimed to establish an iPSC-derived cardiomyocyte (iCM) model system.

#### **Determination of differentiation-dependent sensitivity:**

Building on our previous publication (Jahn et al., 2020), a treatment regimen combining short pulse-exposures and low concentrations of doxorubicin is applied to simulate the plasma concentrations found in patients following chemotherapy sessions. The study aims to assess

the differentiation-dependent differences in the sensitivity of the cells upon exposure to this treatment regimen.

# Deciphering the role of mitochondria under acute low concentration exposures of iPSCs and iCMs:

Given the central role of mitochondria in energy conversion and regulation of cellular homeostasis, this study aims to decipher the metabolic and apoptotic alterations that contribute to doxorubicin-induced toxicity in iPSCs and iCMs. For this, we aimed to apply various techniques to measure mitochondrial function and health.

# Determination of the influence of different doxorubicin treatment regimens during cardiomyocyte differentiation on gene expression profiles and function:

The impact of various doxorubicin treatment regimens throughout cardiac differentiation will be assessed to investigate the influence on the transcriptomic profile in iPSCs and iCMs. Especially, we aimed to understand whether pre-conditioning of iPSC stage is accompanied with changes in the transcriptomic profile and whether this is beneficial upon a second encounter with doxorubicin. With this we aim to delineate the molecular signatures associated with the applied treatment conditions and their implications for doxorubicin-induced cardiotoxicity.

# 2. Material and methods

# 2.1. Material

# 2.1.1. Chemicals, kits and media

Tab. 1: Chemicals, kits and media used in this study

Name	Vendor
Agarose	Carl Roth GmbH + Co. KG, Karlsruhe, Germany
Ammonium peroxodisulfate	Carl Roth GmbH + Co. KG, Karlsruhe, Germany
B-27 Supplement (x50), serum free	ThermoFisher Scientific, Waltham MA, USA
B-27, minus insulin	ThermoFisher Scientific, Waltham MA, USA
Bovine Serum Albumin (BSA), US Origin, Fatty acid free, lyophilized powder	PAN-Biotech, Aidenbach, Germany
Bromphenol blue	AppliChem, Darmstadt, Germany
Carbonylcyanid-m-chlorophenyl hydrazone (CCCP)	Sigma-Aldrich, St. Louis MO, USA
CellTiter-Glo® Luminescent Cell Viability Assay	Promega, Walldorf, Germany
CHIR-99021	MedChemExpress, Monmouth Junction NJ, USA
Compete protease inhibitor EDTA-free	Roche Diagnostics, Indianapolis IN, USA
Coomassie	Abcam, Cambridge, United Kingdom
D (+)-Glucose, anhydrous	Merck KGaA, Darmstadt, Germany
Dimethyl sulfoxide (DMSO)	Sigma-Aldrich, St. Louis MO, USA
DMEM High Glucose (4.5 g/l), without L-Glutamine	Capricorn Scientific, Ebersdorfergrund, Germany
DMEM/Ham's F-12 (DMEM/F-12), with L-Glutamine	Capricorn Scientific, Ebersdorfergrund, Germany
DNeasy Blood & Tissue Kit	QIAGEN, Hilden, Germany
Doxorubicin hydrochloride	Sigma-Aldrich, St. Louis MO, USA
Dulbecco's PBS (10x), without Ca & Mg, without Phenol Red (Phosphate-buffered Saline)	Capricorn Scientific, Ebersdorfergrund, Germany

Ethanol	VWR, Radnor PA, USA
Ethanol absolute	VWR, Radnor PA, USA
Ethylenediaminetetraacetic acid (EDTA)	Merck KGaA, Darmstadt, Germany
FCS	Capricorn Scientific, Ebersdorfergrund, Germany
Geltrex™ LDEV-Free, hESC-Qualified, Reduced Growth Factor Basement Membrane Matrix	ThermoFisher Scientific, Waltham MA, USA
GeneRuler 1 kb DNA Ladder	ThermoFisher Scientific, Waltham MA, USA
Glutaraldehyde	SERVA Electrophoresis GmbH, Heidelberg, Germany
Glycerol	Carl Roth GmbH + Co. KG, Karlsruhe, Germany
Glycin	Carl Roth GmbH + Co. KG, Karlsruhe, Germany
GoScript™ Reverse Transcription Mix, Oligo(dT)	Promega, Walldorf, Germany
GoTaq® qPCR Master Mix	Promega, Walldorf, Germany
Hoechst 33342	ThermoFisher Scientific, Waltham MA, USA
Hydrochloric acid (HCl)	Merck KGaA, Darmstadt, Germany
Hydrogen peroxide solution (H <sub>2</sub> O <sub>2</sub> )	Sigma-Aldrich, St. Louis MO, USA
IWP-4	STEMCELL™Technologies, Vancouver, Canada
L-Ascorbic acid	Sigma-Aldrich, St. Louis MO, USA
Lipofectamine™ Stem Reagent	ThermoFisher Scientific, Waltham MA, USA
Mannitol	Carl Roth GmbH + Co. KG, Karlsruhe, Germany
MitoTracker™ Green FM	ThermoFisher Scientific, Waltham MA, USA
mTeSR™ Plus	STEMCELL™Technologies, Vancouver, Canada
<i>N</i> -2-hydroxyethylpiperazine- <i>N</i> '-2-ethane sulfonic acid (HEPES)	ThermoFisher Scientific, Waltham MA, USA
Na deoxycholate	AppliChem, Darmstadt, Germany
Opti-MEM™, reduced serum medium	ThermoFisher Scientific, Waltham MA, USA
Osmium tetroxide	Sigma-Aldrich, St. Louis MO, USA

PageRuler™ Prestained Protein Ladder, 10 to 180 kDa	ThermoFisher Scientific, Waltham MA, USA
Paraformaldehyde (PFA)	Sigma-Aldrich, St. Louis MO, USA
Penicillin/Streptomycin	Sigma-Aldrich, St. Louis MO, USA
Phosphotunistic acid	Sigma-Aldrich, St. Louis MO, USA
Pierce™ SuperSignal™ West Pico PLUS Chemiluminescent Substrate	ThermoFisher Scientific, Waltham MA, USA
Ponceau S Solution	Sigma-Aldrich, St. Louis MO, USA
Powdered milk	Carl Roth GmbH + Co. KG, Karlsruhe, Germany
Propidium Iodide (PI)	Cayman Chemical, Biomol GmbH; Hamburg, Germany
Protein Assay Reagent A	Bio-Rad, Hercules CA, USA
Protein Assay Reagent B	Bio-Rad, Hercules CA, USA
Protein Assay Reagent S	Bio-Rad, Hercules CA, USA
Proteinase K (from <i>Tritirachium album</i> )	Sigma-Aldrich, St. Louis MO, USA
Quick-Load® 100 bp DNA Ladder	New England Biolabs, Ipswich MA, USA
<b>4</b>	New England Biolabs, Ipswich MA, OOA
ReLeSR™	STEMCELL™Technologies, Vancouver, Canada
·	STEMCELL™Technologies, Vancouver,
ReLeSR™	STEMCELL™Technologies, Vancouver, Canada
ReLeSR™ RNase	STEMCELL™Technologies, Vancouver, Canada Sigma-Aldrich, St. Louis MO, USA
ReLeSR™  RNase  RNeasy Mini Kit	STEMCELL™Technologies, Vancouver, Canada  Sigma-Aldrich, St. Louis MO, USA  QIAGEN, Hilden, Germany  Carl Roth GmbH + Co. KG, Karlsruhe,
ReLeSR™  RNase  RNeasy Mini Kit  ROTI®Mount FluorCare DAPI	STEMCELL™Technologies, Vancouver, Canada  Sigma-Aldrich, St. Louis MO, USA  QIAGEN, Hilden, Germany  Carl Roth GmbH + Co. KG, Karlsruhe, Germany  Carl Roth GmbH + Co. KG, Karlsruhe,
ReLeSR™  RNase  RNeasy Mini Kit  ROTI®Mount FluorCare DAPI  Rotiphorese Gel 40 (37,5:1)	STEMCELL™Technologies, Vancouver, Canada  Sigma-Aldrich, St. Louis MO, USA  QIAGEN, Hilden, Germany  Carl Roth GmbH + Co. KG, Karlsruhe, Germany  Carl Roth GmbH + Co. KG, Karlsruhe, Germany  Carl Roth GmbH + Co. KG, Karlsruhe, Germany
ReLeSR™  RNase  RNeasy Mini Kit  ROTI®Mount FluorCare DAPI  Rotiphorese Gel 40 (37,5:1)  RPMI 1640 Medium, without L-Glutamine	STEMCELL™Technologies, Vancouver, Canada  Sigma-Aldrich, St. Louis MO, USA  QIAGEN, Hilden, Germany  Carl Roth GmbH + Co. KG, Karlsruhe, Germany  Carl Roth GmbH + Co. KG, Karlsruhe, Germany  Capricorn Scientific, Ebersdorfergrund, Germany  Carl Roth GmbH + Co. KG, Karlsruhe,
ReLeSR™  RNase  RNeasy Mini Kit  ROTI®Mount FluorCare DAPI  Rotiphorese Gel 40 (37,5:1)  RPMI 1640 Medium, without L-Glutamine  SDS pellets	STEMCELL™Technologies, Vancouver, Canada  Sigma-Aldrich, St. Louis MO, USA  QIAGEN, Hilden, Germany  Carl Roth GmbH + Co. KG, Karlsruhe, Germany  Carl Roth GmbH + Co. KG, Karlsruhe, Germany  Capricorn Scientific, Ebersdorfergrund, Germany  Carl Roth GmbH + Co. KG, Karlsruhe, Germany
ReLeSR™  RNase  RNeasy Mini Kit  ROTI®Mount FluorCare DAPI  Rotiphorese Gel 40 (37,5:1)  RPMI 1640 Medium, without L-Glutamine  SDS pellets  Seahorse XF Calibrant Solution 500 mL	STEMCELL™Technologies, Vancouver, Canada  Sigma-Aldrich, St. Louis MO, USA  QIAGEN, Hilden, Germany  Carl Roth GmbH + Co. KG, Karlsruhe, Germany  Carl Roth GmbH + Co. KG, Karlsruhe, Germany  Capricorn Scientific, Ebersdorfergrund, Germany  Carl Roth GmbH + Co. KG, Karlsruhe, Germany  Agilent Technologies, Santa Clara CA, USA

Sodium cacodylate	Sigma-Aldrich, St. Louis MO, USA
Sodium chloride (NaCl)	Carl Roth GmbH + Co. KG, Karlsruhe, Germany
Sodium Pyruvate	PAN-Biotech, Aidenbach, Germany
Stable Glutamine (L-Alanyl-L-Glutamine Solution)	Capricorn Scientific, Ebersdorfergrund, Germany
StemPro™ Accutase™ Cell Dissociation Reagent	ThermoFisher Scientific, Waltham MA, USA
Sucrose	Sigma-Aldrich, St. Louis MO, USA
Sulforhodamine B	Sigma-Aldrich, St. Louis MO, USA
Supersignal® West Femto Max Sensitivity Substrate	ThermoFisher Scientific, Waltham MA, USA
Tetramethylethylenediamine (TEMED)	Carl Roth GmbH + Co. KG, Karlsruhe, Germany
Tetramethylrhodamine methyl ester perchlorate (TMRM)	ThermoFisher Scientific, Waltham MA, USA
Thiazolyl blue tetrazolium bromide (MTT)	Sigma-Aldrich, St. Louis MO, USA
Trichloroacetic acid (TCA)	VWR, Radnor PA, USA
Tris(hydroxymethyl)aminomethane (TRIS)	Carl Roth GmbH + Co. KG, Karlsruhe, Germany
Triton™ X-100	Sigma-Aldrich, St. Louis MO, USA
Trypsin-EDTA (0,05%)	Capricorn Scientific, Ebersdorfergrund, Germany
Tween®20	Sigma-Aldrich, St. Louis MO, USA
Uranyl acetate	Sigma-Aldrich, St. Louis MO, USA
Uridine	Sigma-Aldrich, St. Louis MO, USA
Wizard® Genomic DNA Purification Kit	Promega, Walldorf, Germany
Y-27632 2HCl	AdooQ Bioscience, Irvine CA, USA
ZVAD	AdooQ Bioscience, Irvine CA, USA
β-mercaptoethanol	Sigma-Aldrich, St. Louis MO, USA

# 2.1.2. Consumables

Tab. 2: Consumables

Name	Vendor
100 ml reservoir	INTEGRA Biosciences GmbH, Biebertal, Germany
15 ml tubes	Greiner Bio-One GmbH, Frickenhausen, Germany
25 ml reservoir	INTEGRA Biosciences GmbH, Biebertal, Germany
35 mm dish glass bottom	MatTek, Ashland MA, USA
50 ml tubes	Greiner Bio-One GmbH, Frickenhausen, Germany
96 well microplate black bottom	Greiner Bio-One GmbH, Frickenhausen, Germany
Amersham nitrocellulose blotting membrane	VWR, Radnor PA, USA
Amersham™ Hybond® P Membrane, PVDF	Cytiva, Marlborough MA, USA
Amersham™ Protran® Western-Blotting- Membrane, nitrocellulose	Cytiva, Marlborough MA, USA
ClipTip™ pipet tips (200 µL)	ThermoFisher Scientific, Waltham MA, USA
Cryotubes and lids	Greiner Bio-One GmbH, Frickenhausen, Germany
Empty gel cassettes comb mini (10 or 15 wells)	Thermo Fisher Scientific, Carlsbad CA, USA
Extra Thick Blot Filter Paper	Bio-Rad, Hercules CA, USA
FastGene TP Filter Tips (10, 100, 200, 1250 μL)	NIPPON Genetics, Düren, Germany
Inner and outer glass plates for SDS PAGE	Bio-Rad, Hercules CA, USA
Inoculation loop sterile	Carl Roth GmbH + Co. KG, Karlsruhe, Germany
Mini-PROTEAN Tetra Cell Casting Stand & Clamps	Bio-Rad, Hercules CA, USA
Mini-PROTEAN® Comb (10 or 15 wells)	Bio-Rad, Hercules CA, USA
PCR tubes for Rotor-Gene™ Cycler	NIPPON Genetics, Düren, Germany
QIAshredder	QIAGEN, Hilden, Germany
Sapphire pipet tips (10, 100, 200, 1250 μL)	Greiner Bio-One GmbH, Frickenhausen, Germany

Seahorse FluxPaks	Agilent Technologies, Santa Clara CA, USA
PCR SoftTubes, 0.2 ml	Biozym Scientific GmbH, Hessisch Oldendorf, Germany
0.45 μm filter	INTEGRA Biosciences GmbH, Biebertal, Germany
Cell culture plates (6, 12, 24, 48, 96-well)	Greiner Bio-One GmbH, Frickenhausen, Germany
Empty gel cassettes mini 1.5 mm	ThermoFisher Scientific, Waltham MA, USA
Microcentrifuge tubes (1.5 and 2 ml)	Sarstedt, Nümbrecht, Germany

# 2.1.3. Equipment and software

Tab. 3: Equipment and software

Vendor
Beckman Coulter, Brea CA, USA
Beckman Coulter, Brea CA, USA
Carl Zeiss AG, Jena, Germany
Carl Zeiss AG, Jena, Germany
Becton Dickinson GmbH, Heidelberg, Germany
Programmed by Dr. Arif Dönmez
Broad Institute of MIT and Harvard, Cambridge MA, USA
BMG Labtech GmbH, Ortenberg, Germany
Sysmex Deutschland GmbH, Bornbach, Germany
Sysmex Deutschland GmbH, Bornbach, Germany
Nikon. Tokyo, Japan
JEOL, Freising, Germany
Eppendorf, Hamburg, Germany
Eppendorf, Hamburg, Germany

FCS Express™ (7.24.0024)	De Novo Software, Pasadena CA, USA
Fusion SL Gel Documentation System	Vilber, Paris, France
GraphPadPrism 8	GraphPad Software, Boston MA, USA
HERAcell Vios 250i Incubator	ThermoFisher Scientific, Waltham MA, USA
ImageJ 1.53c	Wayne Rasband and contributors, National Insitutes of Health NY, USA
JEM-2100 Plus	JEOL, Freising, Germany
neoBlock-HeizerDuo	neoLab Migge GmbH, Heidelberg, Germany
neoLabLine Rocking Shaker	neoLab Migge GmbH, Heidelberg, Germany
Neubauer counting chamber	Glaswarenfabrik Karl Hecht GmbH & Co KG, Sondheim an der Röhn, Germany
PerkinElmer Spinning Disk Confocal microscope	PerkinElmer, Waltham MA, USA
pH-meter	Hanna Instruments, Vöhringen, Germany
Power Supply EV-Series EV2310	Consort BVBA, Tunrhout, Belgium
Professional TRIO Thermocycler	Analytik Jena, Jena, Germany
Rotor Gene 6000 HRM5Plex	QIAGEN, Hilden, Germany
Rotor-Gene Q Series Software	QIAGEN, Hilden, Germany
Seahorse XFe96 Extracellular Flux Analyzer	Agilent Technologies, Santa Clara CA, USA
Tecan infinite M200 PRO	T M"   CO "
Total Illinia N.200 T T.O	Tecan, Männedorf, Switzerland
Trans-Blot SD Semi-Dry Transfer cell	Bio-Rad, Hercules CA, USA
Trans-Blot SD Semi-Dry Transfer cell	Bio-Rad, Hercules CA, USA
Trans-Blot SD Semi-Dry Transfer cell  UltraVIEW®VoX spinning disc laser system	Bio-Rad, Hercules CA, USA  PerkinElmer, Waltham MA, USA
Trans-Blot SD Semi-Dry Transfer cell  UltraVIEW®VoX spinning disc laser system  Volocity® software 6.3	Bio-Rad, Hercules CA, USA  PerkinElmer, Waltham MA, USA  PerkinElmer, Waltham MA, USA  neoLab Migge GmbH, Heidelberg,
Trans-Blot SD Semi-Dry Transfer cell  UltraVIEW®VoX spinning disc laser system  Volocity® software 6.3  Vortex Mixer	Bio-Rad, Hercules CA, USA  PerkinElmer, Waltham MA, USA  PerkinElmer, Waltham MA, USA  neoLab Migge GmbH, Heidelberg, Germany
Trans-Blot SD Semi-Dry Transfer cell  UltraVIEW®VoX spinning disc laser system  Volocity® software 6.3  Vortex Mixer  Wave software (2.6.3.5)	Bio-Rad, Hercules CA, USA  PerkinElmer, Waltham MA, USA  PerkinElmer, Waltham MA, USA  neoLab Migge GmbH, Heidelberg, Germany  Agilent Technologies, Santa Clara CA, USA

#### 2.2. Methods

### 2.2.1. Cell culture methods

### 2.2.1.1. Cell line IMR-90 (clone 4)

In this thesis, human induced-pluripotent stem cell line iPS (IMR90)-4 cells were cultivated on Geltrex<sup>™</sup>-coated plates under feeder-free conditions. Constant cultivation in mTESR+ media guaranteed the stability of the undifferentiated status of stem cell culture. Human iPSCs were derived from a lung fibroblast line (IMR-90) previously isolated from a fetal female donor of unknown age. For generation of iPSCs, adult cells were reprogrammed via lentiviral transfection with Oct4, Sox2, Nanog and Lin28 (Yu et al., 2007).

For the subsequent parts of the thesis, stem cell line iPS (IMR90)-4 will be referred to as iPSCs.

### 2.2.1.2. Maintenance, passaging and freezing of cells

Human iPSCs were cultured in feeder-free and normoxia conditions. For cell culture, wells were pre-coated with Geltrex<sup>™</sup> to enable attachments of iPSCs. Cell culture media was mTeSR<sup>™</sup> Plus media supplemented with 1 % Penicillin / Streptomycin (see recipe section 2.3). Cells were kept under normoxia conditions (20 %) at 37 °C and 5 % CO<sub>2</sub> with media change every second day. At 80 % confluency, iPSCs were passaged with StemPro<sup>™</sup> Accutase<sup>™</sup> for experiments. Briefly, iPSCs were detached from the cell culture vessel with StemPro<sup>™</sup> Accutase<sup>™</sup> and centrifuged at 300 x g for 5 min. The cell pellet was resuspended in mTeSR<sup>™</sup> Plus media and cells were counted with Neubauer counting chamber. To enhance viability of iPSC after passaging with StemPro<sup>™</sup> Accutase<sup>™</sup>, media was supplemented with 10 μM ROCK inhibitor Y-27632 2HCl for 24 hours. The next day, media was replaced with fresh culture media. For general maintenance of iPSC culture, cells were split with ReLeSR<sup>™</sup> in 1:20 up to 1:25.

For cryo preservation, iPSCs were dissociated with StemPro™ Accutase™ and counted with Neubauer counting chamber. Ideally, at least 1 x 10<sup>6</sup> cells were diluted 1:1 in cell culture media and freezing media consisting of 10 % DMSO, 20 % FCS and freshly added 10 µM ROCK inhibitor Y-27632 2HCl (see recipe section 2.3.). Cryovials were transferred into MR. Frosty boxes for slow cool down at -80 °C overnight before transfer into liquid nitrogen. Cells were thawed by incubating the cryo vial in the water bath in 37 °C until most of the ice was dissolved. Cells suspension was transferred into DMEM / F-12 to dilute DMSO concentration. After centrifugation for 3 min at 300 x g, the supernatant was discarded and cells were resuspended in 1 mL fresh mTeSR™ Plus media. Cells were transferred into wells containing fresh

mTeSR™ Plus media supplemented with 10 µM ROCK inhibitor Y-27632 2HCl to enhance viability of the cells during the thawing procedure. The next day, media was replaced with fresh culture media. Media change was performed every second day until passaging of cells was needed.

### 2.2.1.3. Generation of iPSC-derived cardiomyocytes

Cardiomyocytes were generated using published protocols (Burridge et al., 2014; Lian, Zhang et al., 2012). Briefly, iPSCs were seeded with StemPro™ Accutase™ on Geltrex™-coated plates and 10 µM ROCK inhibitor Y-27632 2HCl for 24 hours. Upon 80 % confluence, cardiac differentiation was initiated by exchanging stem cell media with cardiac media. The basal cardiac differentiation media (CBM) consists of RPMI 1640 media without L-Glutamine supplemented with Penicillin / Streptomycin, stable Glutamine and HEPES buffer. From day 0 to day 2, CBM was supplemented with 1 x B-27 supplement without insulin, ascorbic acid and CHIR99021. On day 3 and of the cardiac differentiation, CBM media was supplemented with 1 x B-27 supplement without insulin, ascorbic acid. From day 4 to day 5, CBM was supplemented with 1 x B-27 supplement without insulin, ascorbic acid and IWP4. From day 5 to day 7 same media composition was used as described for day 3. From day 7, cells received CBM supplemented with 1 x B-27 supplement, ascorbic acid. Expression of cardiac differentiation markers was checked on the respective days of analysis. For a detailed list of the media composition, see recipe section 2.3.

# 2.2.2. Doxorubicin treatment regimen

Treatment regimen of iPSCs and iCMs with the anthracycline chemotherapeutic agent doxorubicin (see section 1.4.1.) was conducted by administration of doxorubicin for 2 hours at defined timepoints. Cells were washed with PBS or DMEM/F-12 after completion of treatment time and were incubated until timepoint of analysis.

# 2.2.3. Cell viability assays

# 2.2.3.1. MTT assay

With 3-(4,5-dimethylthiazol-2-yl)-2,5-diphenyl-2H-tetrazolium bromide (MTT), cell viability was measured after recovery from treatment with doxorubicin. MTT reagent can pass the mitochondrial membrane where it is reduced by the succinate dehydrogenase. The reduction

of the core tetrazole ring of MTT results in the formation of the unsolvable blue formazan (Supino, 1995). For iPSCs, viability was measured 48 hours following treatment with doxorubicin. For iCMs, cells were split on day 4 or day 6 of cardiac differentiation into 96-well plates following doxorubicin treatment the next day. Cell viability was assessed on day 9 of cardiac differentiation. To measure cell viability, cells were incubated for 15 min with MTT at 37 °C and 5 %  $CO_2$  until the cells showed equal distribution of the blue appearing formazan. Cells were washed once with PBS followed by solubilization of formazan with DMSO. The absorbance was measured at 570 nm with Tecan plate reader. For all wells, the average background was subtracted. To calculate the average viability (%), the average absorbance value for all technical replicates was calculated and normalized to the respective control. For this, control was set to 100 %. Cells treated with  $H_2O_2$  were used as positive control and included for background subtraction.

## 2.2.3.2. SRB assay

To measure the cell viability in iPSCs, cells were pulse-treated for 2 hours with doxorubicin prior to recovery for 48 hours. For iCMs, cells were split on day 6 of cardiac differentiation into 96-well plates following doxorubicin treatment the next day. Cell viability was assessed on day 9 of cardiac differentiation. Sulforhodamine B (SRB) colorimetric assay was used. For this, cells were fixed with 10 % trichloracetic acid (TCA) for 1 hour at room temperature. TCA was removed plates were washed thrice with water before the plates were placed inverted on a clean paper sheet to dry overnight. Cells were stained with SRB for 10 min at room temperature under constant shaking. The excess dye was removed by washing five times with 1 % acetic acid and plates were placed inverted on a clean paper sheet to dry overnight. The protein-bound dye was dissolved with 10 mM TRIS base. The absorption was measured at 492 nm and 620 nm as reference at Tecan plate reader. For all wells. The mean background was subtracted. To calculate the average viability (%), the average absorbance value for all technical replicates was calculated and normalized to the respective control. For this, control was set to 100 %. Cells treated with  $H_2O_2$  were used as positive control and included for background subtraction.

#### 2.2.4. SDS PAGE and Western Blot

For protein extraction, cell culture vessel was placed on ice and cells were harvested by scratching the surface of the cell culture vessel. Scratched cells were resuspended in ice-cold

PBS and transferred into a fresh 1.5 mL reaction tube before centrifugation at 1000 x g for 5 min at 4 °C. The supernatant was discarded. At this step, the pellet was either stored at -80 °C until further procedure or directly processed. For cell lysis, 50  $\mu$ L RIPA buffer (see recipe section 2.3) supplemented with protease and phosphatase inhibitor was added to the pellet and incubated for 30 min on ice. Proteins were isolated by centrifugation at 16.000 x g for 30 min at 4 °C. Supernatant was transferred to a fresh reaction tube and either stored at -80 °C or directly further proceeded for the determination of protein concentration.

With respect to iPSC-derived cardiomyocytes, protein extraction was slightly modified. Briefly, right after harvest 90 % of the cell pellet directly frozen away whereas 10 % of the cell pellet was used to determine the protein concentration as mentioned above.

## 2.2.4.1. Determination of protein concentration with Lowry assay

To determine the protein concentration in the RIPA lysates, DC protein assay was performed according to the manufacturer's instructions. Briefly, a microtiter plate was loaded with 2  $\mu$ L of each sample including a BSA-based standard. First, 20  $\mu$ L of reagent S was diluted in 1 mL of reagent A resulting in working reagent A'. To each well, 25  $\mu$ L of working reagent A' was added, followed by 200  $\mu$ L of reagent B. The microtiter plate was incubated for 15 min and absorbance was measured at 750 nm with the Tecan plate reader. The absorption values of the standard were used to determine a regression line for calculation of protein concentration of the samples (in  $\mu$ g /  $\mu$ L). At this point, samples were either stored at -80 °C until further procedure or further processed for SDS-PAGE. For preparation of samples for SDS-PAGE, samples were diluted in 4 x Laemmli buffer (see recipe section 2.3) and water followed by heating the samples to 95 °C for 5 min. At this stage, samples were either stored at -20 °C or directly loaded on SDS-gels.

With respect to iPSC-derived cardiomyocytes, preparation for SDS-PAGE was slightly modified. As mentioned in part 2.4.4, 10 % of the pellet was used for determining of protein concentration with Lowry assay. The remaining 90 % of the pellet were directly resuspended in 1 x Laemmli buffer by vigorously vortexing the sample. The samples were heated to 95 °C for 5 min. At this stage, samples were either stored at -20 °C or directly loaded on SDS-gels.

#### 2.2.4.2. SDS PAGE

For SDS-PAGE, separation and stacking gels were prepared as described in the recipe section of this thesis (see recipe section 2.3.). Separation gel was poured either in mini-gel cassettes

or in glass gel constructions for polymerization. For even distribution, isopropanol was added on top of the gel. After 15 - 30 min, the separation gel was polymerized and isopropanol was discarded. Th prepared stacking gel was poured on top and a comb was inserted. After polymerization of the stacking gel, gels were wrapped in wet sheets and stored in the fridge up to one month. For preparation of SDS-PAGE, prepared gels were clamped in the gel chamber and SDS Running buffer (see recipe section 2.3) was added until the chamber was filled. As a protein size standard, PageRuler™ Prestained Protein Ladder (10 to 180 kDa) was loaded into at least one of the gel pockets. A defined amount of the prepared protein sample (15 µg) was loaded into the gel pockets. For the stacking gel, current was set to 150 V with 20 mA per gel for 20 min, followed by an increase to 150 V and 40 mA per gel with a running time of 60 min for the separation gel.

#### 2.2.4.3. Western Blot

For blotting, the Trans-Blot SD Semi-Dry electrophoretic transfer was used. For this, the SDS gel was stacked between two extra-thick blot papers facing a nitrocellulose membrane. The extra-thick blot paper, nitrocellulose membrane and the gel were soaked in blotting buffer (see recipe section 2.3) prior the construction of the blotting sandwich. Between each layer of the blotting sandwich, air bubbles were carefully removed. Semi-dry blotting was performed at 25 V with 60 mA per gel for 2 hours as standard. For efficient transfer of high kDa proteins (6 % SDS-Gels), the transfer time was extended to 3 hours. To determine the quality of the blotting process, membranes were washed with water and incubated with Ponceau S. Stained membranes were imaged and cut for the respective size of the proteins of interest.

To remove Ponceau S staining, membranes were shortly washed with TBST buffer (see recipe section 2.3) before blocking with 5 % milk / TBST for 1 hour at room temperature. Membranes were incubated in the respective primary antibody solution (see Tab. 4) at 4 °C overnight. For detection of phosphorylated proteins, respective antibodies were diluted in 5 % BSA / TBST. After incubation, membranes were washed thrice with TBST for 10 min. Membranes were incubated in secondary antibody solution for 1 h at room temperature followed by three washing steps with TBST for 10 min. For visualization of protein signal, membranes were decorated with Signal Fire ECL Reagent or Supersignal® West Femto Max Sensitivity Substrate and imaged at Fusion SL Gel Documentation System.

Tab. 4: Primary (1<sup>st</sup>) and secondary (2<sup>nd</sup>) antibodies for Western blot

1 <sup>st</sup> / 2 <sup>nd</sup>	Target	Host	Clonality	Dilution	Vendor	Cat. No.
1 <sup>st</sup>	Actin	mouse	monoclonal	1:5000	ThermoFisher Scientific Waltham MA, USA	MA1-744
1 <sup>st</sup>	ATM	rabbit	monoclonal	1:1000	Cell Signaling Technology, Danvers MA, USA	2873S
1 <sup>st</sup>	Caspase 3	rabbit	monoclonal	1:1000	Abcam, Cambridge, United Kingdom	ab32351
1 <sup>st</sup>	Cleaved Caspase- 3	rabbit	monoclonal	1:1000	Cell Signaling Technology, Danvers MA, USA	9664
1 <sup>st</sup>	cTNT	mouse	monoclonal	1:1000	ThermoFisher Scientific, Waltham MA, USA	MA5-12960
1 <sup>st</sup>	Drp1	rabbit	monoclonal	1:1000	Cell Signaling Technology, Danvers MA, USA	5391S
1 <sup>st</sup>	Mfn1	rabbit	monoclonal	1:1000	Abcam, Cambridge, United Kingdom	ab57602
1 <sup>st</sup>	Mfn2	rabbit	polyclonal	1:1000	Abcam, Cambridge, United Kingdom	ab50838
1 <sup>st</sup>	Oct4	mouse	monoclonal	1:1000	Cell Signaling Technology, Danvers MA, USA	sc-5279
1 <sup>st</sup>	OPA1	rabbit	polyclonal	1:1000	Pineda	custom- made
1 <sup>st</sup>	PARP	rabbit	monoclonal	1:1000	Cell Signaling Technology, Danvers MA, USA	9532S
1 <sup>st</sup>	pDrp1 (Ser616)	rabbit	monoclonal	1:1000	Cell Signaling Technology, Danvers MA, USA	4494S
1 <sup>st</sup>	phopsho- ATM (Ser1981)	mouse	monoclonal	1:1000	ThermoFisher Scientific, Waltham MA, USA	MA1-46069

1 <sup>st</sup>	Vinculin	mouse	monoclonal	1:5000	Sigma-Aldrich, St. Louis MO, USA	V9131- 100UL
1 <sup>st</sup>	γH2AX (Ser139)	rabbit	monoclonal	1:1000	Sigma-Aldrich, St. Louis MO, USA	SAB560003 8-100UG
2 <sup>nd</sup>	Anti- mouse igG (HRP)	goat	polyclonal	1:10.000	Abcam, Cambridge, United Kingdom	ab6789
2 <sup>nd</sup>	Anti-rabbit IgG (HRP)	goat	polyclonal	1:20.000	Dianova, Hamburg, Germany	111-035- 144

#### 2.2.5. Blue Native and Clear Native PAGE

Following doxorubicin treatment, iPSCs were harvested with 1000 x g for 5 min at 4 °C. Supernatant was aspirated and cells were resuspended in 1 mL lysis buffer (see recipe section 2.3) including an incubation for 10 min on ice. With 20G cannula, cells were disrupted followed by sequential centrifugation steps at 1000 x g at 4 °C for 10 min for removal of cell debris and 10.000 x g at 4 °C for 15 min for separation of mitochondria in a pellet. Mitochondrial pellet was resuspended in BSA-free lysis buffer. Protein concentration was determined as described in section 2.2.4.1. Blue natives and clear natives PAGEs were performed by my colleague Yulia Schaumkessel.

#### 2.2.5.1. Blue Native PAGE

For Blue Native PAGE, 100 µg mitochondria were solubilized for 1 hour on ice using 2.5 g / g of digitonin to protein ratio before prior to centrifugation at 20.000 x g at 4 °C for 20 min. Supernatant was supplemented with Blue Native PAGE loading buffer (see recipe section 2.3) and loaded on 3 - 13 % gradient gels. Gel running procedure was performed at 150 V, 15 mA at 4 °C for 16 hours prior to semi-wet blotting onto PVDF membrane and blockage overnight with 5 % milk / TBST. Membranes were incubated overnight with the listed antibodies followed by secondary antibody incubation for 1 hour the next day (Tab. 5). Chemiluminescent signals were acquired using Pierce™ SuperSignal™ West Pico PLUS chemiluminescent substrate reagent and VILBER LOURMAT Fusion SL equipment.

Tab. 5: Primary (1st) and secondary (2nd) antibodies for blue native PAGE

1 <sup>st</sup> / 2 <sup>nd</sup>	Target	Host	Clonality	Dilution	Vendor	Cat. No.
1°	ATP5A	mouse	monoclonal	1:1000	Abcam, Cambridge, United Kingdom	ab14748
1°	COXIV	rabbit	polyclonal	1:1000	Abcam, Cambridge, United Kingdom	ab16056
1°	Mic60	mouse	monoclonal	1:1000	Abcam, Cambridge, United Kingdom	ab110329
1°	NDUFB4	mouse	monoclonal	1:1000	Abcam, Cambridge, United Kingdom	ab110243
<b>1°</b>	OXPHOS cocktail	rabbit	monoclonal	1:2000	Abcam, Cambridge, United Kingdom	ab110412
<b>1°</b>	UQCRC2	mouse	monoclonal	1:1000	Abcam, Cambridge, United Kingdom	ab14745
2°	Anti-mouse IgG (HRP)	goat	polyclonal	1:10.000	Abcam, Cambridge, United Kingdom	ab6789
2°	Anti-rabbit IgG (HRP)	goat	polyclonal	1:20.000	Dianova, Hamburg, Germany	111-035- 144

#### 2.2.5.2. Clear Native PAGE

For Clear Native PAGE, 300  $\mu$ g mitochondria were solubilized with 2.5 g / g digitonin to protein ratio for 1 hour on ice. Cells were centrifuged at 20.000 x g for 20 min at 4 °C prior to resuspension of supernatant with clear native loading buffer and loading on a 3-13 % gradient gel. Complexes were separated upon running the gels at 150 V, 15 mA for 16 h. To acquire complex activity, gel slices were incubated in the respective complex buffers for several hours at room temperature. For complex I, gel was incubated in 5 mM Tris-HCl pH 7.4, 0.1 mg / mL NADH and 2.5 mg / mL nitro blue tetrazolium chloride (NBT). For complex IV activity, the gel was incubated in 50 mM sodium phosphate buffer pH 7.2, 0.05 % 3,3'-diaminobenzidine (DAB) and 50  $\mu$ M horse heart cytochrome c.

### 2.2.6. Gene expression analysis

#### 2.2.6.1. RNA isolation

The isolation of mRNA was performed according to the manufacturer's instructions. Briefly, cells were scratched from the cell culture plates (on ice) and centrifuged at 1000 x g for 5 min at 4 °C. Supernatant was aspirated and at this step cell pellets could be stored at -80 °C. For further procedure, cells were lysed by adding RLT buffer supplemented with  $\beta$ -marcaptoethanol, followed by shredding the cells with QiaShredder at full speed. Lysed cells were resuspended with 70 % EtOH and transferred into Qia Columns. The columns were centrifuged at 8000 x g for 15 s. The flow-through was discarded and RLP buffer was added to the column. The columns were centrifuged at 8000 x g for 15 s. Again, the flow-through was discarded. The columns were washed thrice with washing buffer, each followed with 30 s of centrifugation at 8000 x g. The mRNA was precipitated by adding 30  $\mu$ L of RNase-free water. The RNA concentration of each sample was determined with photometer by measuring the absorption spectra between 260 nm and 280 nm. Only RNA samples showing an absorption maximum at A260 and a quotient of A260 / A280 of approximately 1.8-2 were accepted. RNA samples were stored at -80 °C until further procedure.

# 2.2.6.2. Complementary DNA (cDNA) synthesis

Isolation of mRNA was performed as described above (2.2.6.2). For reverse transcription, GoScript™ Reverse Transcription Mix, Oligo(dT) from Promega was used. Briefly, a mixture consisting of GoScript™ Reaction Buffer with Oligo(dT), GoScript™ Enzyme Mix and nuclease-free water was prepared (see Tab. 6). For each reaction, 1 µg RNA diluted in water was added to the reverse transcription mix (see Tab. 7). The reverse transcription reaction was gently mixed by pipetting and incubated in a programmed thermos cycler (see Tab. 8). cDNA was stored at -20 °C until further procedure.

#### Tab. 6: Reverse transcription mix

Nuclease-free water	4 µL
GoScript™ Reaction Buffer, Oligo(dT)	4 µL
GoScript™ Enzyme Mix	2 µL
Σ	10 µL

#### Tab. 7: Reverse transcription reaction mix

Reverse transcription master mix 10 µL

RNA (1  $\mu$ g) Up to 10  $\mu$ L

Nuclease-free water Up to a final volume of 20 μL

#### Tab. 8: Cyclying protocol for cDNA synthesis

Annealing 5 min at 25 °C
Extension 60 min at 42 °C
Inactivation 15 min at 70 °C

Holding ∞ at 4 °C

### 2.2.6.3. Genomic DNA (gDNA) isolation

Cells were harvested by detaching them with StemPro<sup>™</sup> Accutase<sup>™</sup> or scratching followed by centrifugation at 1000 x g for 5 min at 4 °C. Supernatant was aspirated and at this step cell pellets could be stored at -80 °C until further procedure. For further procedure, gDNA isolation was performed according to the manufacturer's protocol of Wizard® Genomic DNA Purification Kit from Promega. Briefly, cell pellet was washed with 200 µL PBS and centrifuged for 16.000 x g for 10 s. For cell lysis, pellet was resuspended in Nuclei Lysis Solution supplemented with 17.5 µL Proteinnase K (20 mg / mL). RNase digestion was performed by adding 3 µL of RNase Solution to the nuclear lysate and mixing the sample by inverting the tube. The mixture was incubated for 15 min at 37 °C. Before further procedure, the sample was cooled to room temperature. Protein was precipitated by adding Protein Precipitation Solution and vortexing of sample at high speed for 20 s. Samples were incubated on ice for 5 min followed by centrifugation at 16.000 x g for 4 min. The precipitated protein should form a white pellet. The supernatant was transferred into a clean 1.5 mL reaction tube containing 600 µL 100 % isopropanol. The solution was mixed by inversion and centrifuged for 1 min at 16.000 g at room temperature. The supernatant was aspirated and the remaining pellet containing the DNA was washed with 70 % EtOH by gently inverting the tube for multiple times. To remove the EtOH, the solution was centrifuged for 1 min at 16.000 x g. EtOH was carefully aspirated, the reaction tube was inverted and dried on clean absorbent paper for 10 - 15 min. During the drying process, the DNA pellet changed its appearance from transparent to white. For DNA elution, the fully dried DNA pellet was resuspended in 100 µL DNA Rehydration Solution and incubated overnight at 4 °C. DNA concentration was determined with a photometer by measuring the absorption spectra between 230 nm and 320 nm. Only DNA samples showing an absorption maximum at A260 and a quotient of A260 / A280 between 1.8 - 2.0 were used for further procedure. DNA samples were stored at -20 °C.

## 2.2.6.4. Quantitative real-time PCR (qRT-PCR)

Quantitative real-time PCR (qRT-PCR), performed using GoTaq® qPCR Master Mix kit with 20 ng of cDNA or gDNA as described in section 2.2.6.2 or 2.2.6.3, respectively. For this, cDNA or gDNA was added to a qRT-PCR master mix (see Tab. 9) and real-time amplification of the gene of interest was measured in three technical replicates with Corbett Rotorgene RG-6000 (see Tab. 10). Primers used for qRT-PCR are listed in Tab. 11. Receiving qRT-PCR data was analyzed with double ΔCt-analysis. Further analysis was performed in GraphPad Prism 8.

Tab. 9: Quantitative real-time PCR master mix

GoTaq ® qPCR Master Mix, 2X	10 μL
Forward Primer (20X)	0.7 μL (0.7 μM)
Reverse Primer (20X)	0.7 μL (0.7 μM)
cDNA / gDNA	4 μL (20 ng)
Nuclease-free water	4.6 µL

Tab. 10: Cycling protocol for qRT-PCR

PCR initial heat activation	95 °C, 2 min
2- step cycling (40X):	
Denaturation:	95 °C, 5 s
Annealing / extension:	60 °C, 10 s
Melting curve analysis	$65~^{\circ}\text{C}$ to $95~^{\circ}\text{C}$ in 1 $^{\circ}\text{C}$ steps

Tab. 11: Primer sequences used for quantitative real-time PCR approaches

Primer	Forward primer	Reverse primer
GAPDH	CGTAGCTCAGGCCTCAAGAC	GCTGCGGGCTCAATTTATAG
GATA4	GCGGTGCTTCCAGCAACTCCA	GACATCGCACTGACTGAGAACG
HPRT1	CCTGGCGTCGTGATTAGTG	TGAGGAATAAACACCCTTTCCA
ISL1	GCAGAGTGACATAGATCAGCCTG	GCCTCAATAGGACTGGCTACCA
MtND1	CCACCCTTATCACAACACAAGA	GGTTCGGTTGGTCTCTGCTA
МҮН6	GGAAGACAAGGTCAACAGCCTG	TCCAGTTTCCGCTTTGCTCGCT

NANOG	CAGAAGGCCTCAGCACCTAC	ATTGTTCCAGGTCTGGTTGC
NKX2-5	AAGTGTGCGTCTGCCTTTCCCG	TTGTCCGCCTCTGTCTTCTCCA
POU5F1	CAGTGCCCGAAACCCACAC	GGAGACCCAGCAGCCTCAAA
RNR2	AACGATTAAAGTCCTACGTGATC	TCCTTTCGTACAGGGAGGAAT
SOX2	GCCGAGTGGAAACTTTTGTCG	GCAGCGTGTACTTATCCTTCTT
TNNT2	TTCACCAAAGATCTGCTCCTCGCT	AACATAAATACGGGTGGGTGCGTG

### 2.2.6.5. Measurement of mitochondrial copy number

Mitochondrial DNA (mtDNA) content in relation to genomic DNA (gDNA) was determined via qRT-PCR (section 2.2.6.4). For this, the expression of mitochondrial-encoded genes mitochondrially encoded NADH:Ubiquinone oxidoreductase core subunit 1 (*MT-ND1*) and ribosomal 45S cluster 2 (*RNR2*) was determined and normalized to the nuclear encoded gene glyceraldehyde-3-phosphate dehydrogenase (*GAPDH*) (Tab. 11). For each experimental set-up, the relative mtDNA/gDNA ratio of all treatment conditions was normalized to the respective untreated control.

#### 2.2.7. Transfection of iPSCs

For transfection of iPSCs with a plasmid, manufacturer's protocol for Lipofectamine™ Stem Reagent was followed. Briefly, 75.000 cells / well were seeded on Geltrex™-coated coverslips and incubated for 48 hours. On day of transfection, Opti-MEM media and Lipofectamine™ Stem Reagent was combined in tube 1. In parallel, 1 µg of DNA was diluted in Opti-MEM in tube 2. In the next step, both reactions were combined by gently snipping against the tube. The resulting transfection mixture was incubated for 10 min before distribution of 150 µL transfection mix to each well (Tab. 12). Cells were incubated overnight in the incubator. The next day, cells were checked for positive fluorescence signal. If cells showed positive signal, experiment was proceeded with doxorubicin treatment regimen.

Tab. 12: Transfection master mix preparation

Tube 1	Opti-MEM	75 μL
	Lipofectamine Stem reagent	3 µL
Tube 2	Opti-MEM	75 μL
	DNA (1 μg)	Respective amount

### 2.2.8. Immunofluorescence staining

To perform immunostaining, iPSCs were seeded on Geltrex™-coated coverslips and were either directly treated or it was proceeded with cardiac differentiation (section 2.2.1.3). With completion of the doxorubicin treatment regimen, cells were fixed with 4 % paraformaldehyde for 10 min at room temperature prior to washing the coverslips thrice with PBS for 5 min. At this step of the protocol, PBS-covered coverslips can be stored for up to one month at 4°C until further procedure. To proceed with immunofluorescence staining, coverslips were incubated in ice-cold MeOH at -20 °C for ten minutes. Blocking and permeabilization was performed in one step by incubating coverslips with blocking / permeabilization solution containing bovine serum albumin (BSA) and Triton™ X-100 for 30 min at room temperature (section recipe section 2.3). For primary antibody incubation, coverslips were incubated with primary antibody (Tab. 13) in antibody solution overnight at 4 °C (see recipe section 2.3). The next day, coverslips were washed thrice for 5 min with PBS before incubation with secondary antibody (Tab. 13) in antibody solution for 1 hour at room temperature (see recipe section 2.3). Coverslips were mounted with ROTI®Mount FluorCare DAPI on microscopy slides prior to fluorescence imaging. Stained coverslips could be stored for up to one month at 4 °C in the dark.

Tab. 13: Primary (1st) and secondary (2nd) antibodies for immunofluorescence microscopy

1 <sup>st</sup> / 2 <sup>nd</sup>	Target	Host	Clonality	Dilution	Vendor	Cat.No.
1 <sup>st</sup>	53BP1	rabbit	polyclonal	1:500	Cell Signaling Technology, Danvers MA, USA	4937S
<b>1</b> st	anti-DNA	mouse	monoclonal	1:300	PROGEN Biotechnik GmbH, Heidelberg, Germany	AC-30-10

1 <sup>st</sup>	сТПТ	mouse	monoclonal	1:500	ThermoFisher Scientific, Waltham MA, USA	MA5-12960
1 <sup>st</sup>	HSP60	rabbit	monoclonal	1:500	Sigma- Aldrich, St. Louis MO, USA	#SAB4501464- 100UG
1 <sup>st</sup>	Ki-67	mouse	monoclonal	1:500	Cell Signaling Technology, Danvers MA, USA	9449S
1 <sup>st</sup>	Oct4	mouse	monoclonal	1:500	Cell Signaling Technology, Danvers MA, USA	sc-5279
1 <sup>st</sup>	yH2AX (Ser139)	mouse	monoclonal	1:500	Cell Signaling Technology, Danvers MA, USA	80312S
2 <sup>nd</sup>	Mouse IgG (H+L) Alexa Fluor®488	goat	monoclonal	1:500	ThermoFisher Scientific, Waltham MA, USA	A27034
2 <sup>nd</sup>	Rabbit IgG (H) Alexa Fluor®647	goat	monoclonal	1:500	ThermoFisher Scientific, Waltham MA, USA	A27040

# 2.2.9. Fluorescence microscopy

Fluorescence images were acquired at Nikon Ti2 inverted confocal microscope, coupled with an UltraVIEW®VoX spinning disc laser system equipped with a 63 x oil objective (N.A. 1.2). Else with 60 x oil objective at Axio Vert.A1 equipped with AxioCam ICm1. In general, at least 15 Z-stack images comprising of 20 stacks were acquired. For live cell imaging at the confocal microscope, phenol red containing media was exchanged by phenol red-free media Opti-MEM™ supplemented with 10 µM HEPES in order to buffer missing CO₂ supply. Live cell imaging was acquired with confocal microscope using the temperature control system of confocal microscope.

## 2.2.9.1. Analysis of DNA damage

To measure the induction of DNA damage upon moderate pulse-treatment with doxorubicin, DNA damage protein levels of DNA damage surrogate markers histone variant H2A.X phosphorylated at serine 139 (γH2AX) and P53-binding protein 1 (53BP1) were determined via immunofluorescence staining (see section 2.2.8). Briefly, cells were seeded onto Geltrex<sup>TM</sup>-coated coverslips prior to administration of 5 nM and 18 nM doxorubicin (respective to IC<sub>10</sub>-value and IC<sub>30</sub>-value) for 2 hours after 72 hours of recovery from splitting. 10 nM etoposide served as positive control. Cells were fixed 0.5, 4, 8, and 24 hours after treatment and stained for respective targets. For analysis, single γH2AX and 53BP1 foci as well as colocalizing foci per nucleus were counted manually using ImageJ (1.53c). The average number of DNA damage foci per nucleus was determined. Further analysis was performed in GraphPad Prism 8.

## 2.2.9.2. Mitochondrial morphology

In iPSCs, mitochondrial morphology was determined via staining of mitochondria with the fluorescent live cell dye MitoTracker™ Green FM. For this, iPSCs were seeded on Geltrex™-coated glass bottom Matek dishes and followed by a cultivation time of 72 hours before proceeding with the treatment scheme. At the day of analysis, cells were stained with live-cell staining MitoTracker™ Green FM dye (25 nM) for 30 min prior to washing the cells thrice with pre-warmed PBS. Cells were covered with 1 mL Opti-MEM™, reduced serum medium supplemented with 10 µM HEPES buffer solution. Fluorescence imaging of iPSCs was carried out with a Nikon Ti2 inverted confocal microscope, coupled with an UltraVIEW®VoX spinning disc laser system equipped with a 63 x oil objective (N.A. 1.2). Imaging was performed in a chamber at 37 °C.

In iCMs, mitochondrial morphology was assessed via immunofluorescence antibody staining against mitochondrial target protein Heat Shock Protein Family D (Hsp60) Member 1 (HSP60) (Tab. 13). Briefly, doxorubicin treatment was administered at defined timepoints of cardiac differentiation prior to fixation of cells on day 9 of cardiac differentiation. Images were acquired at UltraVIEW®VoX spinning disc laser system equipped with a 63 x oil objective.

For each experiment, at least 15 Z-stack images with 20 stacks were taken. For analysis, images were randomized and mitochondria were categorized into tubular, intermediate or fragmented morphology (Fig. 9). At least 50 images per condition were analyzed and the average distribution of mitochondrial phenotype (%) was determined. Further analysis was performed in GraphPad Prism 8.

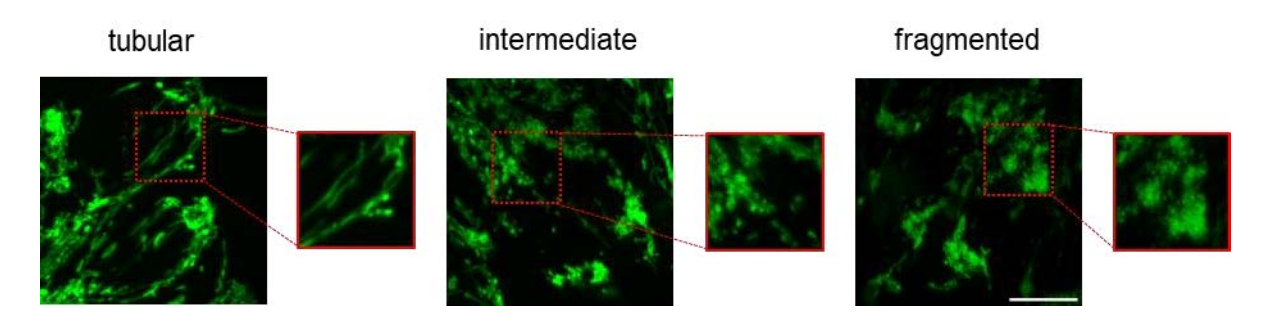


Fig. 9: Categories of mitochondrial morphology.

Representative images of different mitochondrial morphologies in human induced-pluripotent stem cells (iPSCs). Cells were stained with the live-cell dye MitoTracker<sup>TM</sup> Green FM to visualize mitochondria. Tubular (left), intermediate (middle) and fragmented (right) mitochondria are represented. Zoomed-in regions of interest are indicated by the red square. Magnification: x 63, scalebar: 10 µM.

## 2.2.9.3. Mitochondrial membrane potential ( $\Delta \Psi_m$ )

To measure mitochondrial membrane potential in iPSCs, cells were seeded onto Geltrex<sup>TM</sup>-coated glass bottom Matek Dishes. 72 hours after incubation, cells were treated according to the treatment scheme. On the day of analysis, cells were incubated with 20 nM tetramethylrhodamine-methylester (TMRM) diluted in cell culture media for 30 min at 37 °C.  $\Delta\Psi_m$  was measured with a Nikon Ti2 inverted confocal microscope, coupled with an UltraVIEW®VoX spinning disc laser system equipped with a 63 x oil objective (N.A. 1.2). Imaging was performed in a chamber at 37 °C. For each biological replicate, the control sample was used for the set-up of imaging conditions. In general, at least 15 Z-stack images with 20 stacks were acquired. Background correction and TMRM intensity measurement of at least 50 cells per sample was performed using Volocity® software 6.3 for spinning disc microscopy. The average TMRM fluorescence intensity was determined for each experimental set-up outliers were cleaned using outlier test in GraphPad Prism 8, namely ROUT (Q = 1 %). Cleaned data was used for statistical and graphical analysis in GraphPad Prism 8. To decipher the influence of doxorubicin on TMRM intensity, treatments were normalized to the respective control.

#### 2.2.9.4. Mitochondrial nucleoids

Mitochondrial nucleoids were detected via immunofluorescence staining. For this, untreated and treated cells were fixed and immunofluorescence antibody staining against mtDNA and mitochondrial marker HSP60 were performed (Tab. 13). Imaging was carried out at UltraVIEW®VoX spinning disc laser system equipped with a 63 x oil objective (N.A. 1.2). For each condition, at least 15 Z-stack images with 20 stacks were imaged. For analysis, a semi-automated system combined of ImageJ and CellProfiler was used. At first, images were

prepared for CellProfiler (4.2.5) pipeline by using an ImageJ (1.53c) macro. Briefly, images were imported with Bio Formats Importer and instantly split into all three channels (green, red and blue). Each channel was saved renamed and saved as maximum Z-stack projection image. For further analysis, images were impetrated into CellProfiler (Fig. 10). Here, images were sorted by name. Each image containing mtDNA in the image name was categorized as 'nucleoid'. Images containing HSP60 in the name was categorized as 'mitochondria'. In order to ensure comparability between treatment conditions, analysis settings were pre-defined based on control images of each biological replicate. In the beginning of the pipeline, all images were background subtracted and thresholded (1). In the subsequent step, the thresholded nucleoid image was masked by the thresholded mitochondria image to determine nucleoids within mitochondria (2). Here, also nucleoids which were partially masked by mitochondrial signal were included to reduce false-positive release of nucleoids. The resulting image corresponds to nucleoids solely localized within mitochondria. For measurement of nucleoids outside of mitochondria, the image containing all nucleoids was masked by the signal of nucleoids within mitochondria (2) received from the previous step (3). Here, nucleoids which were partially masked were excluded to prevent false-positive signal for released nucleoids. The resulting image corresponds to nucleoids solely found within the cytoplasm of the cell. In the next steps, for each image a parent-child relation was established in order to assign the number and size of nucleoids within or outside of mitochondria to a certain cell. First, cell surroundings were manually determined resulting in the definition of the cells as parent object (4). Nucleoids from previous steps (2 and 3; nucleoids within and outside of mitochondria, respectively) were identified as child objects based on a defined size (3-6 px) in order to reduce signal-to-noise-ratio (5). In the next step, parent and child objects were connected and measurements of interest were defined. Accordingly to step 4 and step 5, all nucleoids within the defined area were related to their respective cell (6). Based on this relation, the cell area occupied by nucleoids (nucleoids / µm² / cell) and the nucleoid size (µm²) of at least 50 cells was measured (step 7). The average cell area occupied by nucleoids and nucleoid size for all three independent experiment was calculated in GraphPad Prism 8.

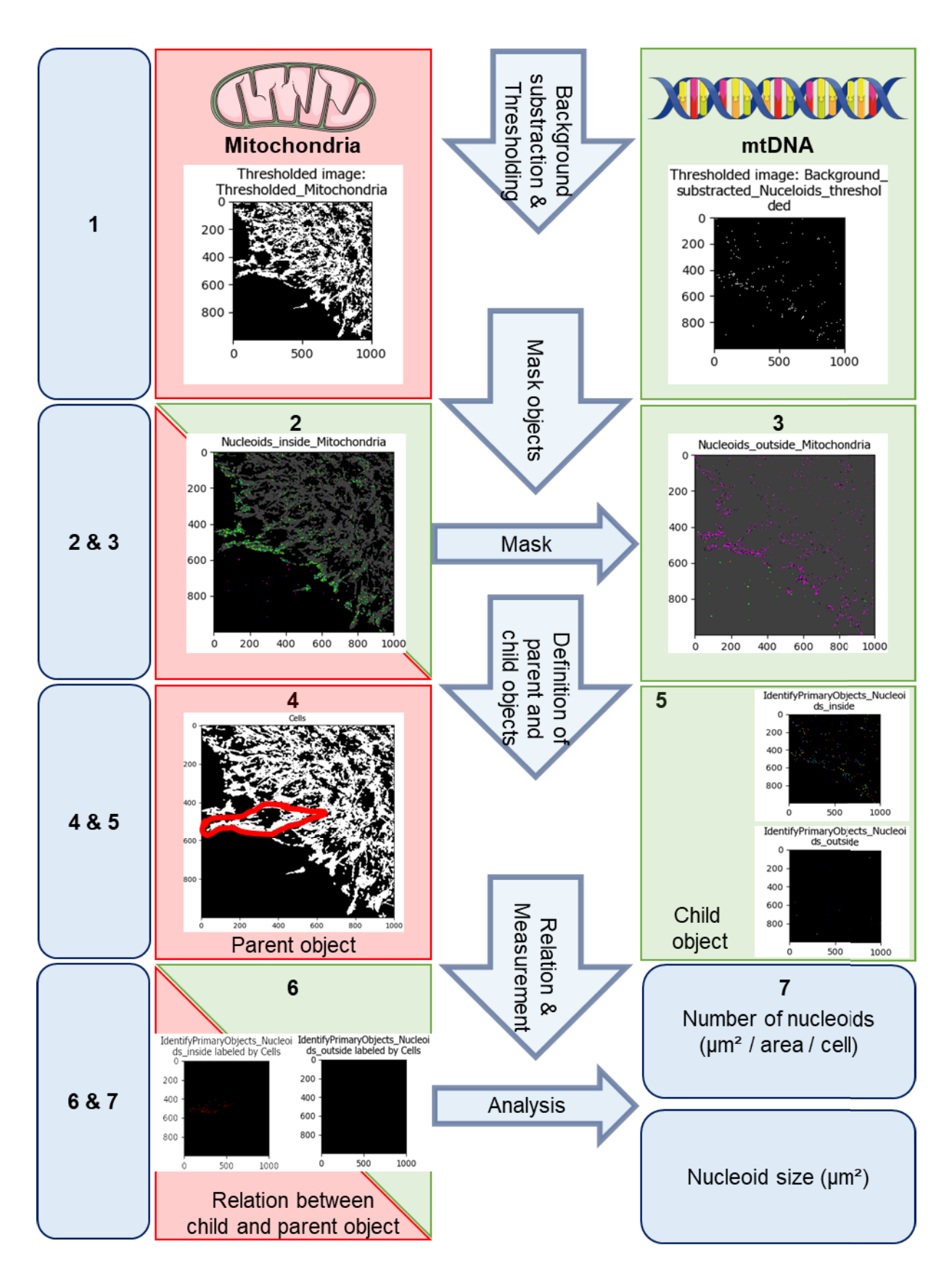


Fig. 10: CellProfiler Pipeline for analysis of mitochondrial nucleoids.

Schematic illustration of semi-automated CellProfiler pipeline applied for analyzing mitochondrial nucleoids within in human-induced pluripotent stem cells (iPSCs). With the first step (1) images containing mitochondrial and mtDNA signal were loaded into the pipeline followed by background

subtraction and thresholding. Since mtDNA is organized in dynamic punctae-like structures, namely nucleoids. For the sake of simplicity all subsequent images were termed as 'nucleoids'. Thresholding conditions for all treatment conditions was defined based on the untreated control of each biological replicate. Resulting thresholded images were used to define the location of nucleoids within the cell. In the subsequent step (2), thresholded nucleoid image was masked by respective mitochondrial signal resulting in an image comprising all nucleoids which are completely or partially located within mitochondria. Next (3), the image containing mtDNA signal (1) was masked by the image containing the information of nucleoids within mitochondria (2) resulting in an image comprising all nucleoids which were located outside of mitochondria/in cytoplasm of the cell. In order to gain the information of each nucleoid within a certain cell, a relation between cells and nucleoids needed to be established. For this, cells were manually defined as parent objects based on thresholded mitochondrial signal (4) and nucleoids within or outside of mitochondria (resulting from (2) and (3), respectively) were defined as child objects (5). In the latter step, nucleoids were also thresholded by size (3-6 px) in order to reduce the signal-to-noise ratio. Based on the definition of parent (cell) and child objects (nucleoids), all child objects were then assigned to their respective parent objects resulting in the information of nucleoids within the manually defined cell (6). In the last step (7), the receiving information can used to measure the number of nucleoids (µm² / area / cell) and their size (µm²). In total, at least 50 cells were defined and the amount and size of all nucleoids within the defined parent cells was analyzed. This figure was partially generated using Servier Medical Art (https://smart.servier.com), provided by Servier, licensed under a Creative Commons Attribution 4.0 unported license (https://creativecommons.org/licenses/by/ 4.0/ [Status: 25.03.2025].

## 2.2.9.5. Mitochondrial aging (pMitoTimer)

The plasmid pMitoTimer (Laker et al., 2014) contains a cytochrome *c* subunit VIII gene at the N-terminus of *Timer*. This region encodes for DsRed1-E5 which results in a green fluorescent protein upon new synthesis (Tab. 14). Upon oxidation of a Tyrosine-67 residue, the signal shifts towards a red fluorescent spectrum (Verkhusha et al., 2004). Thus, pMitoTimer can be used for investigating mitochondrial content and aging.

Following the treatment regimen with doxorubicin, cells were fixed with 4 % paraformaldehyde for 10 min in the dark at room temperature after following timepoints: 0, 8, 16, 24, 30, and 48 hours. Coverslips were washed thrice with PBS thrice for 5 min before either storage at 4 °C until further procedure or images were directly acquired at Nikon Ti2 inverted confocal microscope, coupled with an UltraVIEW®VoX spinning disc laser system equipped with a 63 x oil objective (N.A. 1.2). In general, at least 15 Z-stack images with 20 stacks were acquired. For analysis, the ratio between DsRed / Green-signal using a semi-automated pipeline in Cell Profiler (4.2.5) was performed. Prior to Cell Profiler pipeline application, z-stack images were cropped using Z-stack projection (maximum projection). Cropped images were fed into the Cell Profiler pipeline. Briefly, background subtraction was performed using a block size of 1 followed by ImageMath module dividing the signal of the green channel by the signal of the red channel. Region of interest (ROI) was manually determined based on mitochondrial signal and the intensity within the ROI was measured. Further analysis was performed in GraphPadPrism 8. In general, at least 50 cells were considered for the respective analysis.

Tab. 14: Information about the plasmid pMitoTimer

Name	Internal number	Catalogue Number	Vendor	Reference
pMitoTimer	8	52659	addgene, Watertown MA, USA	Laker et al., 2014

## 2.2.10. Electron microscopy (EM)

To assess mitochondrial ultrastructure, samples were prepared for EM as depicted in the following chapter. The acquisition of images was performed by our technical assistant Andrea Borchardt at the core facility for electron microscopy (CFEM). For acquisition of electron micrographs, iPSCs were seeded onto on Geltrex™-coated 10 cm cell culture vessels and pulse-treated with 5 nM and 18 nM doxorubicin. 48 hours after recovery, cells were washed once and fixed with EM fixation buffer (Tab. 18). Cell pellets were washed with fresh 0.1 M cacodylate buffer (pH 7.2) and embedded in 3 % low melting agarose. Staining procedure was performed by incubation with 1 % osmium tetroxide for 50 min followed by two washing steps with cacodylate buffer and one time 70 % EtOH for 10 min each. Samples were stained further with 1 % uranyl acetate / 1 % phosphotunistic acid in 70 % EtOH for 1 hour. Stained samples were embedded in low viscosity EMS for polymerization prior to incubation at 70 °C for 48 hours. Ultrathin section were cut with a microtome and images were acquired under transmission electron microscope JEM-2100 Plus at 200 KV equipped with an EM-24830 flash CMOS camera system. For each condition mitochondrial ultrastructure was assessed via randomization of the images. Mitochondrial cristae ultrastructure (%) was categorized in tubular, septa, arched and branched (Fig. 11).

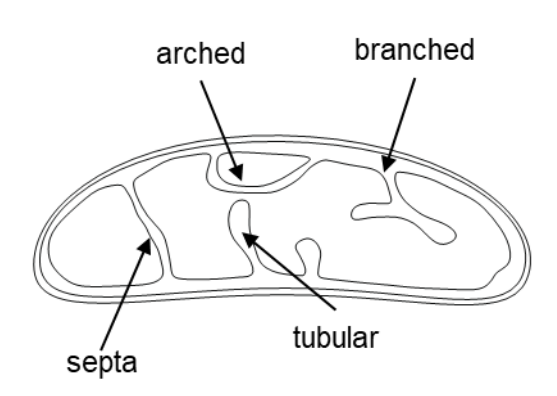


Fig. 11: Schematic illustration of crista phenotypes in iPSCs.

Schematic illustration of tubular, arched, septa and branched cristae morphology detectable in human induced pluripotent stem cells (iPSCs). Based on these categories, crista morphology within each individual mitochondrion was determined and analyzed.

### 2.2.11. Measurement of bioenergetics

## 2.2.11.1. Measurement of mitochondrial respiration

For measurement of mitochondrial respiration, Mito Stress Test kit from Seahorse Agilent was used (Fig. 12). Prior to any Seahorse experiment series, a suitable cell number and FCCP concentration needed to be tested. For the iPSC line used in this thesis, 35.000 cells / well and a FCCP concentration of 0.125 µM was considered as most suitable experimental setup. One day before the run, 35.000 cells / well were seeded in the Geltrex™-coated each of the wells of a Seahorse cell culture plate. For each experiment four empty wells were included for background measurements. Cells were shortly incubated at room temperature to support equal distribution of the cells on the well before further incubation for 24 hours at 37 °C and 5 % CO<sub>2</sub>. Sensor cartridge was hydrated by addition of 200 µL Seahorse Calibrant media in each well and incubation in a CO<sub>2</sub>-free incubator overnight. On the day of the Seahorse run, cell culture media was exchanged by Seahorse media supplemented with glucose, pyruvate and stable glutamine (see recipe section 2.3). Cells were incubated at 37 °C in a CO<sub>2</sub>-free incubator for at least 45 min. Meanwhile, each port of the sensor cartridge was loaded with mitochondrial toxin of the Mito Stress Test and placed in the Seahorse Flux Analyzer for calibration. After the calibration procedure, the calibrant loaded plate was exchanged by the cell culture plate and the run was further proceeded. During the run, the Flux Analyzer injected the mitochondrial toxin according to the Mito Stress Test protocol and OCR values were measured every three minutes. At the beginning of each basal respiration was measured. With the injection of oligomycin, ATP-linked respiration was determined until maximal respiration was determined by injection of the mitochondrial membrane potential uncoupler FCCP. Lastly, rotenone / antimycin A was injected to inhibit complex I and II of the electron transport chain complexes and shut down the complete mitochondrial respiration. With completion of the Seahorse run, media was discarded in toxic waste. The cell number in each well was determined by Hoechst staining. Briefly, cells were incubated for 10 min in 10 µg / mL Hoechst solution and fluorescence signal (451 nm) was measured at Tecan plate reader. For further analysis, OCR values of each well were normalized to the mean cell number determined by Hoechst. Mitochondrial parameters listed in Tab. 15 were determined. For each biological replicate, outliers were identified and removed using ROUT (Q = 1 %) outliers test in GraphPadPrism 8. Mean OCR values were normalized to basal respiration of the control samples.

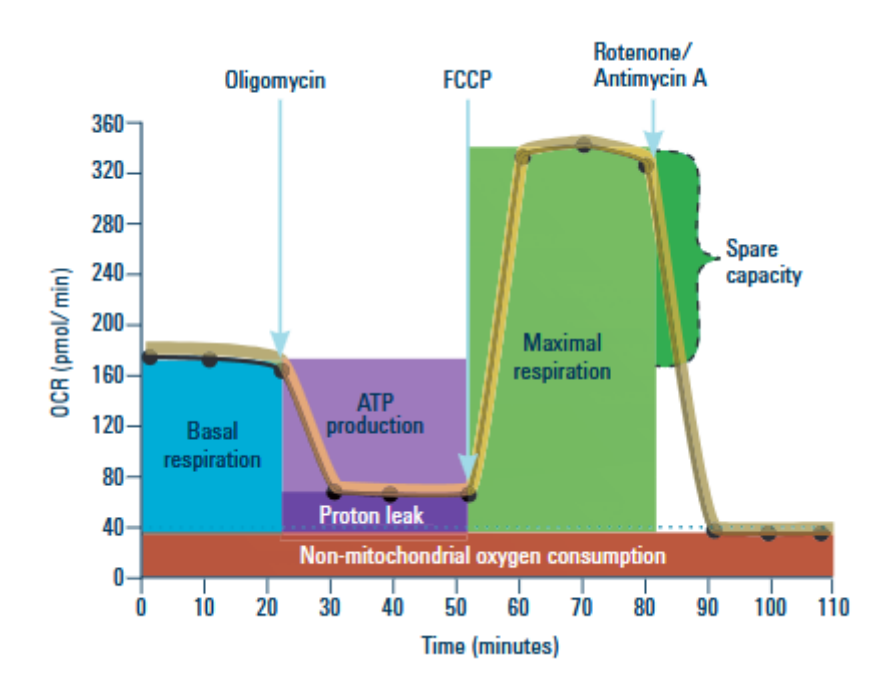


Fig. 12: Schematic illustration of Seahorse XF Cell Mito Stress Test run.

This scheme highlights the different parameters measured via live-cell measurement with Seahorse Flux Analyzer. Shown are the injections of mitochondrial oligomycin (Oligo), Trifluoromethoxy carbonylcyanide phenylhydrazone (FCCP), and rotenone / antimycin A (R / A) at the specific timepoints of the run (image modified from Seahorse XF Cell Mito Stress Kit handbook).

Tab. 15: Calculations for Mito Stress Test Seahorse parameters

Non-mitochondrial respiration	Minimal OCR value after rotenone / antimycin A injection
Basal respiration	(Last OCR value prior to Oligomycin A injection) – (non-mitochondrial respiration)
Maximal respiration	(Maximal OCR value after FCCP injection) – (non-mitochondrial respiration)
Spare respiratory capacity (SRC)	(Maximal respiration) – (Basal respiration)
ATP production	(Last OCR value prior to oligomycin A injection) – (Minimum OCR value after oligomycin A injection)
Proton leak	(Minimum OCR value after oligomycin A injection) – Minimal OCR value after rotenone / antimycin A injection

# 2.2.11.2. ATP assay

For measurement of cellular ATP levels, iPSCs were seeded onto Geltrex<sup>™</sup>-coated black glass bottom plates and 2 hours pulse-treated with doxorubicin 72 hours after seeding. 48 hours after recovery time, luminescence signal was acquired using CellTiter-Glo® 2.0 Cell Viability Assay (Promega). Luminescence was measured in four technical replicates of three

independent using CLARIOStar<sup>Plus</sup> plate reader (RG Stork). Cell number was normalized using Hoechst normalization assay. Relative ATP level of each condition was normalized to the respective control. Further analysis was performed in GraphPad Prism 8.

## 2.2.12. Flow cytometer-based methods

### 2.2.12.1. Cell cycle measurement

For measurement of the cell cycle via measurement of propidium iodide (PI) signal with fluorescence flow cytometry, seeded into Geltrex™-coated 6-well plates. Following doxorubicin treatment scheme, cells were detached with StemPro™ Accutase™ and centrifuged at 500 x g for 5 min at 4 °C (with reduced brake). The samples were placed on ice and supernatant was aspirated. The pellet was resuspended in 200 µL PBS and fixed by dropwise adding 2 mL of ice-cold 80 % EtOH while constantly vortexing the sample. At this step of the protocol, cells were either stored at -20 °C or protocol was directly proceeded after at least 20 min of incubation on ice. The subsequent steps were performed together with Sina Federmann (RG Fritz). For further procedure, cells were centrifuged at 500 x g for 10 min at 4 °C (with reduced brake). The supernatant was discarded and RNA was digested by incubation of the samples with RNAse diluted in PBS (1 mg / mL) for 30 min at room temperature. Samples were stained with PI (50 µg / mL) for 1 h on ice before measurement of the samples with Accuri™ C6 flow cytometer. As positive control, iPSCs were pulse-treated with 10 nM Etoposide respectively following the same treatment scheme as for doxorubicin. For each condition, at least 10.000 events were measured. Cell cycle phases (G1-, S-, G2-, and Sub-G1-phase) were defined based on the control. Analysis was performed in FCS Express™ (7.24.0024). The average distribution of cell cycle populations per samples (%) were calculate and further analyzed in GraphPad Prism 8.

# 2.2.13. Beating characterization of iPSC-derived cardiomyocytes

Prior to analysis, iCMs were generated as previously described in section 2.2.1.3 and pulse-treated at defined timepoints during cardiac differentiation. On day 9, beating parameters of iCMs were analyzed via acquisition of live cell videos of 20 seconds length (60 frames per seconds) using Leica DM IL LED Fluo Cellfactory (Leica) with x 20 magnification. Analysis of beating parameters in iCMs was conducted by Dr. Arif Dönmez (Leibniz Research Institute for Environmental Medicine) using the automated system CardioVision published previously

(Galanjuk et al., 2022) (Fig. 13). Briefly, reference points arranged in a grid with a distance of 20 pixels apart were placed on the video to generate a motion profile. Using the Lukas Kanade method for every reference point in each single frame (Lucas & Kanade, 1981), the motion of each reference point was tracked on frame-by-frame basis. This method is available in the OpenCV library (Bradski, 2000). The movement of every reference point was tracked and saved as distance profiles showing how far each point moved from its initial position in the first frame at time (t). Application of Savitzky-Golay filter to the resulting time-distance curves (motion profiles) ensured the reduction of the signal-to-noise-ratio as it excludes noise caused by floating particles (Savitzky & Golay, 1964). Here, only manually defined region of interest (ROI) set by the experimentator were part of the subsequent analysis. These comprised regions of clearly visible contractions. The endpoint beating frequency was determined by performing signal analysis of the distance profile curved of the reference points. A heat map color coding for the beating frequencies was used to visualize the result. Thereby, the total areas of the beating frequency represent the beating area. The endpoint beating frequency was determined by performing peak analysis on the remaining distance profile curves of the grid points. A schematic distance profiles can be found in Fig. 13. Received raw data was further analyzed in with GraphPad Prism8. Here, the data of all treatment conditions in iCMs was normalized to the respective mock-treated control.

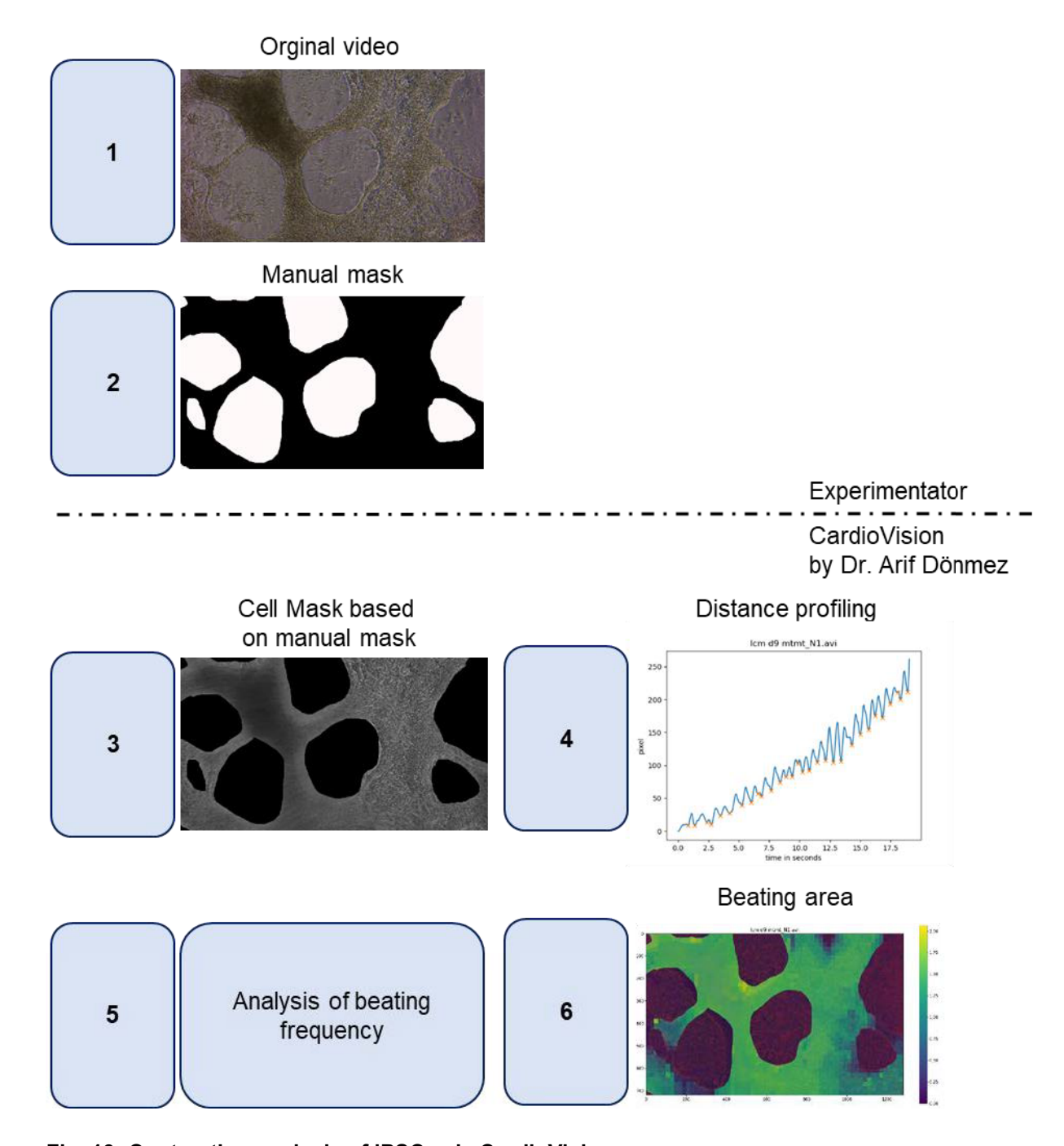


Fig. 13: Contraction analysis of iPSCs via CardioVision program.

Schematic illustration of cardiac beating analysis performed by Dr. Arif Dönmez using the software CardioVision. For this, live-cell videos of human induced-pluripotent stem cells (iPSC)-derived cardiomyocytes (iCMs) of about 20 seconds were acquired using Leica DM IL LED Fluo Cellfactory (Leica) with x 20 magnification (1). Next, regions of prominent beating areas were manually defined by the experimentator and converted into masks (2). The original videos (1) and the defined masks (2) were then further processed by Dr. Arif Dönmez using CardioVision. Briefly, a cell mask based on the one defined in step 2 was generated (3). In the next step (4), reference points were defined in a grid of 20 pixel apart was generated and used for motion profile analysis of each single reference point. An exemplary motion profile of one reference point within the grid of reference points is depicted in step 4. Beats marked with an orange x were counted as a beat. Thresholding was performed in order to reduce the signal-to-noice ratio within the analysis. With the remaining motion profiles, peak analysis was performed based on the motion profiles of each reference point within the defined cell mask (3) resulting in the measurement of the beating frequency (5). This was also represented in a heatmap reflecting the

beats/sec calculated at each reference point via color-coding (6). Sec: second, d: day, mt: mock-treatment

#### 2.2.14. Whole genome transcriptome profiling

Human induced-pluripotent stem cells (iPSCs) were seeded with StemPro™ Accutase™ onto Geltrex™-coated 24-well plates and cultured for 72 hours before starting with Dox treatment schemes (Fig. 15A, Fig. 40A). Following treatment conditions were included: iPSC untreated (iPSC Mt), iPSC treated with doxorubicin (iPSC Dox), iPSC-derived cardiomyocytes (iCMs) treated untreated (iCM Mt Mt), iCMs treated in iPSC stage (iCM Dox Mt), iCMs treated on d7 of cardiac differentiation (iCM\_Mt\_Dox) and iCMs treated in iPSC and iCM stage (iCM Dox Dox). Here, the abbreviation 'Mt'stands for mock-treated at the defined timepoints. Here, doxorubicin was solved in media resulting in the partial exchange of media according to the actual amount of doxorubicin to simulate the comparable conditions. For treatments in iPSC stage, cells were harvested 48 hours after 2 hours pulse-treatment with 18 nM doxorubicin (IC<sub>30</sub>-value) via centrifugation at 1000 x g for 5 min at 4 °C. For iCM conditions, cells were treated with 144 nM (IC<sub>30</sub>-value) for 2 hours followed by a recovery time of 48 hours. On day 9 of cardiac differentiation, cells were harvested and cell pellets were directly stored at -80 °C. For each condition, four biotechnical replicates were harvested. For this, mRNA was isolated with QIAGEN RNeasy kit as described in section 2.2.6.1. Additionally, a DNA digestion step was included during mRNA isolation. The RNA concentration of each sample was determined with photometer by measuring the absorption spectra between 260 nm and 280 nm. Only RNA samples showing an absorption maximum at A260 and a quotient of A260 / A280 of approximately 2 were accepted as sufficient for RNA-seq analysis. RNA samples were stored at -80 °C until further procedure. Prior to submission of samples, the expression pluripotency markers POU Class 5 Homeobox 1 (POU5F1), Nanog Homeobox (NANOG) and cardiac markers Troponin T2 (TNNT2), NK2 Homeobox 5 (NKX2-5), Myosin Heavy Chain 6 (MYH6) and GATA Binding Protein 4 (GATA4) was determined with quantitative real-time PCR before further procedure. For short-read-NGS RNAseq, 20 ng RNA diluted in RNase-free water was sent to the BMFZ core facility Genomics & Transcriptomics Laboratory at the UKD / HHU. All RNA samples were quantified (Qubit RNA HS Assay, Thermo Fisher Scientific, MA, USA) and quality was assessed by capillary electrophoresis using the Fragment Analyzer and the 'Total RNA Standard Sensitivity Assay' (Agilent Technologies, Inc. Santa Clara, CA, USA). Library preparation was performed using manufacturers protocol to 'VAHTS™ Stranded mRNA-Seq Library Prep Kit' for Illumina®. As input for mRNA capturing, fragmentation, cDNA synthesis, adapter ligation and library amplification, 20 ng of RNA was used. The bread purified library was normalized and sequencing was performed on the

NextSeq2000 system (Illumina Inc. San Diego, CA, USA) with a read setup of 1 x 100 bp. Data was converted from bcl files to fastq files using the BCL Convert Tool (version 3.8.4). Additionally, adapter trimming and demultiplexing was performed was performed with this tool. Quality control was done already by sequence unit and submitted together with the read fastq files. Subsequent whole genome transcriptome profiling analysis was performed by Dr. Nahal Brocke-Ahmadinejad. The stranded library of single end mRNA reads was mapped to the human reference genome (ENSEMBL,GRCh38) using the tool HISAT2 (D. Kim et al., 2019). Sorting of alignments was performed with sort options (H. Li et al., 2009) and from applying HTSeq the counts per transcripts were received (Anders et al., 2015). Subsequent analysis was conducted in R (version 4.3.0) using Bioconductor (Huber et al., 2015) packages edgeR (Robinson et al., 2009), and limma/voom (Law et al., 2014; Ritchie et al., 2015) to create a count matrix, so filter with low expression profiles and to identify differentially expressed genes. Relationships between the expression profiles of the samples resulted from multidimensional scaling of the samples (Ritchie et al., 2015). Here, one replicate was excluded to avoid biased results (iPSC\_Dox, Fig. 14).

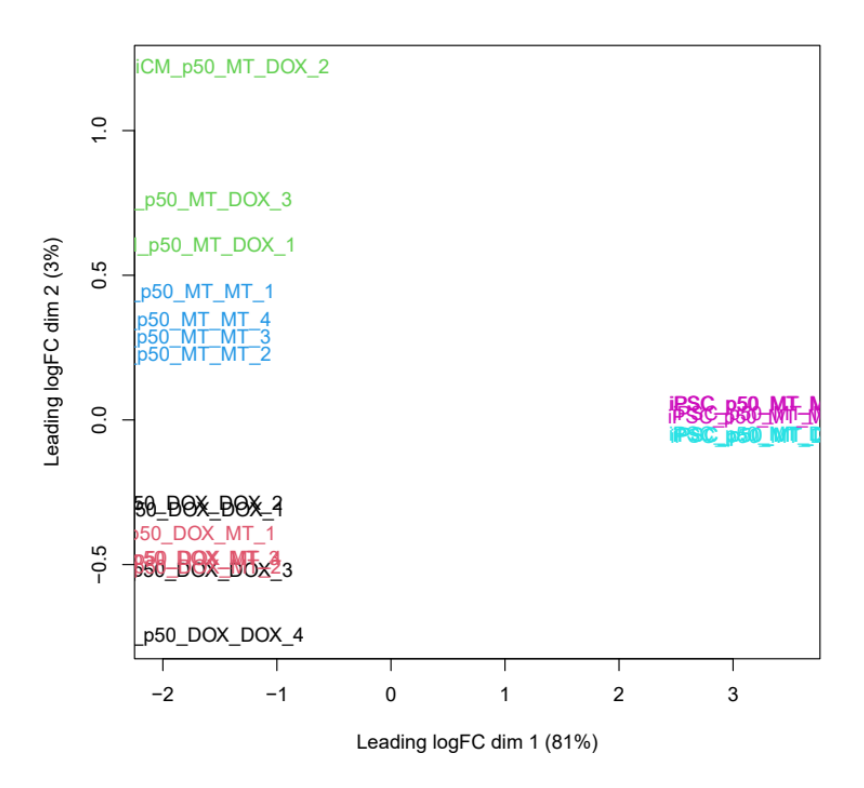


Fig. 14: Multidimensional scaling of the expression profiles whole genome transcriptome profiling samples.

Shown are the results of multidimensional scaling revealing the relationship between expression profiles of the samples. One biotechnical replicate was removed for the further analysis (iPSC\_Mt) to avoid biased results. Shown are the results of multidimensional scaling revealing the relationship between expression profiles of the samples. One biotechnical replicate was removed for the further analysis (iPSC\_Mt) to avoid biased results. logFC: log-fold change, dim: dimension

The expression based on the count data was normalized by trimmed mean of M (TMM) values before testing for differential expression (Robinson & Oshlack, 2010). Counts were then transformed to lcpm (log counts per million reads). Via performance of pairwise comparisons between the treatment conditions, significantly differential expressed genes were determined (Benjamini Hochberg adjusted p-value < 0.05) and further analyzed either by GO-term enrichment and pathway analysis using R packages Cluster Profiler (Wu et al., 2021) and pathview (Luo & Brouwer, 2013), respectively. Heatmaps were generated using the Bioconducter package Complex Heatmaps (Gu, 2022; Gu et al., 2016).

Tab. 16: Number of significantly differential regulated genes resulting from the pairwise comparison between doxorubicin-treated iPSCs or iCMs and their respective controls.

Listed are the upregulated, downregulated and the total sum of significant differential regulated genes (DEGs) of doxorubicin (Dox)-treated induced-pluripotent stem cells (iPSCs) and iPSC-derived cardiomyocytes (iCMs) resulting from the indicated pairwise comparison between the treatment conditions and their respective control. In total, 16198 genes were analyzed via voom (limma) method with an adjusted Benjamini Hochberg of p-value < 0.05. No logFC threshold was applied. logFC: log fold change

Total number of tested genes (16198)	iPSC_Dox vs. iPSC_Mt	iCM_Dox_Mt vs. iCM_Mt_Mt	iCM_Dox_Mt vs. iCM_Mt_Mt	iCM_Dox_Dox vs. iCM_Mt_Mt
Upregulated DEGs	753	97	233	326
Downregulated DEGs	519	89	193	306
Sum of all DEGs	1272	186	426	632

### Tab. 17: Number of significantly differential regulated genes resulting from the pairwise comparison between the doxorubicin treatment regimens in iPSCs and iCMs.

Listed are the upregulated, downregulated and the total sum of significant differential regulated genes (DEGs) of doxorubicin (Dox)-treated induced-pluripotent stem cells (iPSCs) and iPSC-derived cardiomycoytes (iCMs) resulting from the indicated pairwise comparison between the single treatment conditions. Here, solely DEGs resulting from a previous comparison between the treatment regimens and their respective control were included. In total, 16198 genes were analyzed via voom (limma) method with an adjusted Benjamini Hochberg of p-value < 0.05. No logFC threshold was applied. logFC: log fold change

	iPSC_Dox vs. iPSC_Mt vs. iCM_Dox_Mt vs. iCM_Mt_Mt	iCM_Dox_Dox vs. iCM_Mt_Mt vs. iCM_Dox_Mt vs. iCM_Mt_Mt	iCM_Dox_Dox vs. iCM_Mt_Mt vs. iCM_Mt_Dox vs. iCM_Dox_Dox
Upregulated DEGs	842	317	20
Downregulated DEGs	606	305	1
Sum of all DEGs	1448	622	21

### 2.3. Recipes

Tab. 18: Recipes of solutions utilized in this study

Name	Recipe
Antibody solution (Immunofluorescence)	5 % BSA 0.1 % Triton™ X-100 ddH₂O 50 ml
Blocking / permeabilization solution	5 % BSA 0.5 % Triton™ X-100 ddH₂O 50 ml
Blotting buffer	20 mM TRIS 150 mM Glycine 20 % pure ETOH 0.08 % SDS ddH <sub>2</sub> O 1 I pH 8.3
Blue Native PAGE loading buffer	50 % glycerol 8 g/g Comassie to detergent ratio
Clear Native PAGE loading buffer	50 % glycerol 0.01% Ponceau S
EM fixation buffer	6 % glutaraldehyde 0.4 M sodium cacodylate pH 7.2
Freezing buffer for iPSCs	For 10 mL 8 mL mTeSR™ Plus 2 mL DMSO
Laemmli buffer (4x)	250 mM TRIS-HCL 1M, pH 6.8 8 % SDS 40 % Glycerol 8 % β-mercaptoethanol 0.02 % Bromphenol blue
Lysis buffer for crude mitochondrial preparation	210 mM mannitol 70 mM sucrose 1mM EDTA 20 mM HEPES 0.1 % BSA 1 x protease inhibitor
RIPA buffer	50 MM TRIS-HCI 150 mM NaCI 1 % Triton X-100 1 % Sodium deoxycholate 0.1 % SDS 5 mM EDTA ddH <sub>2</sub> O 1 I pH 7.4
SDS Running buffer (10x)	30 g TRIS 144 g Glycine 10 g SDS ddH <sub>2</sub> O 1 l

	200 mM TRIS	
TBS-T (10x)	1.5 M NaCl	
120 1 (10%)	1 % Tween®20	
	ddH₂O 1 I	
mTeSR™ Plus media	400 mL mTeSR™ Plus basal media	
	100 mL mTeSR™ Plus 5 x supplement	
	RPMI 1640 media (without L-Glutamine)	
Cardiac basal media (CBM)	1 % Penicillin / Streptomycin	
Caldiac basai filedia (CDIVI)	2 mM stable glutamine	
	25 mM HEPES	
	CBM	
Cardiac differentiation media	1 x B-27 supplement without insulin	
(CBM-INS1) in 50 mL	50 μg/μL ascorbic acid	
	6 μM CHIR99021	
Cardiac differentiation media	CBM	
(CBM-INS) in 50 mL	1 x B-27 supplement without insulin	
	50 μg/μL ascorbic acid	
0 1: 1:4 1: 1:	CBM	
Cardiac differentiation media	1 x B-27 supplement without insulin	
(CBM-INS2) in 50 mL	50 µg/µL ascorbic acid	
	5 μM IWP4	
Cardiac differentiation media	CBM	
(CBM+INS) in 50 mL	1 x B-27 supplement	
<u> </u>	50 μg/μL ascorbic acid 3.63 mL H₂O	
	0.63 mL Rotiphorese Gel 40 (37,5:1)	
	0.65 mL 1.0 M TRIS (pH 6.8)	
Stacking gel (5 %) 10 mL	50 µL 10 % SDS	
	50 µL 10 % APS	
	5 µL TEMED	
	3.55 mL H <sub>2</sub> O	
	3.75 mL Rotiphorese Gel 40 (37,5:1)	
0 ( 1/45 0/) 40 1	2.5 mL 1.5 M TRIS (pH 6.8)	
Separation gel (15 %) 10 mL	100 μL 10 % SDS ົ້	
	100 µL 10 % APS	
	10 µL TEMED	
	5.29 mL H <sub>2</sub> O	
	2 mL Rotiphorese Gel 40 (37,5:1)	
Separation gel (8 %) 10 mL	2.5 mL 1.5 M TRIS (pH 6.8)	
Coparation got (0 /0) TO THE	100 μL 10 % SDS	
	100 μL 10 % APS	
	10 µL TEMED	
	5.79 mL H <sub>2</sub> O	
	1.5 mL Rotiphorese Gel 40 (37,5:1)	
Separation gel (6%) 10 mL	2.5 mL 1.5 M TRIS (pH 6.8)	
. 5 ( ) -	100 μL 10 % SDS	
	100 μL 10 % APS	
	10 µL TEMED	
	48.5 mL Seahorse XF DMEM	
Seahorse media (50 mL)	0.5 mL pyruvate	
	0.5 mL stable glutamine	
	0.5 mL 1 M glucose	

### 2.4. Statistics

Statistics were performed in GraphPadPrism 8. For multiple comparisons *One*-way ANOVA with Dunnett's or Turkey's *post hoc* test was performed. For statistical comparison between two groups was performed with Student's t-test.

#### 3. Results

## 3.1. Influence of short pulse-treatment with doxorubicin on human iPSCs

For cancer therapy, doxorubicin is a widely used as chemotherapeutic agent due to its efficacy against various types of cancer (Gewirtz, 1999). Yet, the application of doxorubicin is limited since even acute exposure to doxorubicin has been shown to be accompanied with cardiotoxicity. The question of whether doxorubicin-induced cardiotoxicity may partly result from impaired cardiomyocyte regeneration from cardiac stem cells (CSCs) or solely from increased cell death of cardiomyocytes remains unresolved. Together with an iPSC-derived model system, we aimed to simulate the rapid plasma clearance in patients receiving doxorubicin as fast infusion. For this, we implemented a treatment regimen comprising a short pulse-treatment with low concentrations of doxorubicin. In the subsequent part of the thesis, the influence of such moderate doxorubicin treatment on cell viability, stem cell characteristics, differentiation potential, genetic stability, and mitochondrial response was further elucidated.

## 3.1.1. Pulse-treatment of iPSCs with doxorubicin is not accompanied with loss of the pluripotent state

In clinics, initial plasma concentrations of patients receiving fast doxorubicin infusion have been observed to decline within several hours in a concentration range of 25 nM-250 nM (Gewirtz, 1999). Previously, short expositions of cells with doxorubicin followed by a defined recovery time, namely 48 hours, have been shown to be sufficient to simulate the rapid plasma clearance of doxorubicin in patients (Jahn et al., 2020). Here, a similar treatment scheme was applied comprising a transiently exposure in iPSCs (Fig. 15A). To elucidate the toxicity of doxorubicin pulse-exposures, iPSCs were exposed to various doxorubicin concentrations followed by 48 hours of recovery prior to measurement of cell viability using MTT and SRB assay (Fig. 15BC). Here, pulse-treatment of iPSCs with doxorubicin was observed to exert a strong concentrations-dependent effect on the overall viability of iPSCs. As indicated by the dashed line in the graph, the inhibitory concentration of 50 % at which iPSCs undergo cell death (IC<sub>50</sub>-value) was obtained at 35 nM, despite the treatment duration of two hours. Comparable results were obtained using the SRB assay, where IC<sub>50</sub>-value was reached at 64 nM. To preferably induce moderate stress, iPSCs were treated with 5 nM (respective to IC<sub>10</sub>-value) and 18 nM doxorubicin (respective to IC<sub>30</sub>-value) in the subsequent experiments. Overall, a transient pulse-treatment of iPSCs with doxorubicin demonstrated a strong

concentration-dependent reduction of cell viability with an IC<sub>50</sub>-value of 35 nM achieved after 2 hours treatment time, emphasizing the potency of doxorubicin and the sensitivity of stem cells against genotoxic drugs.

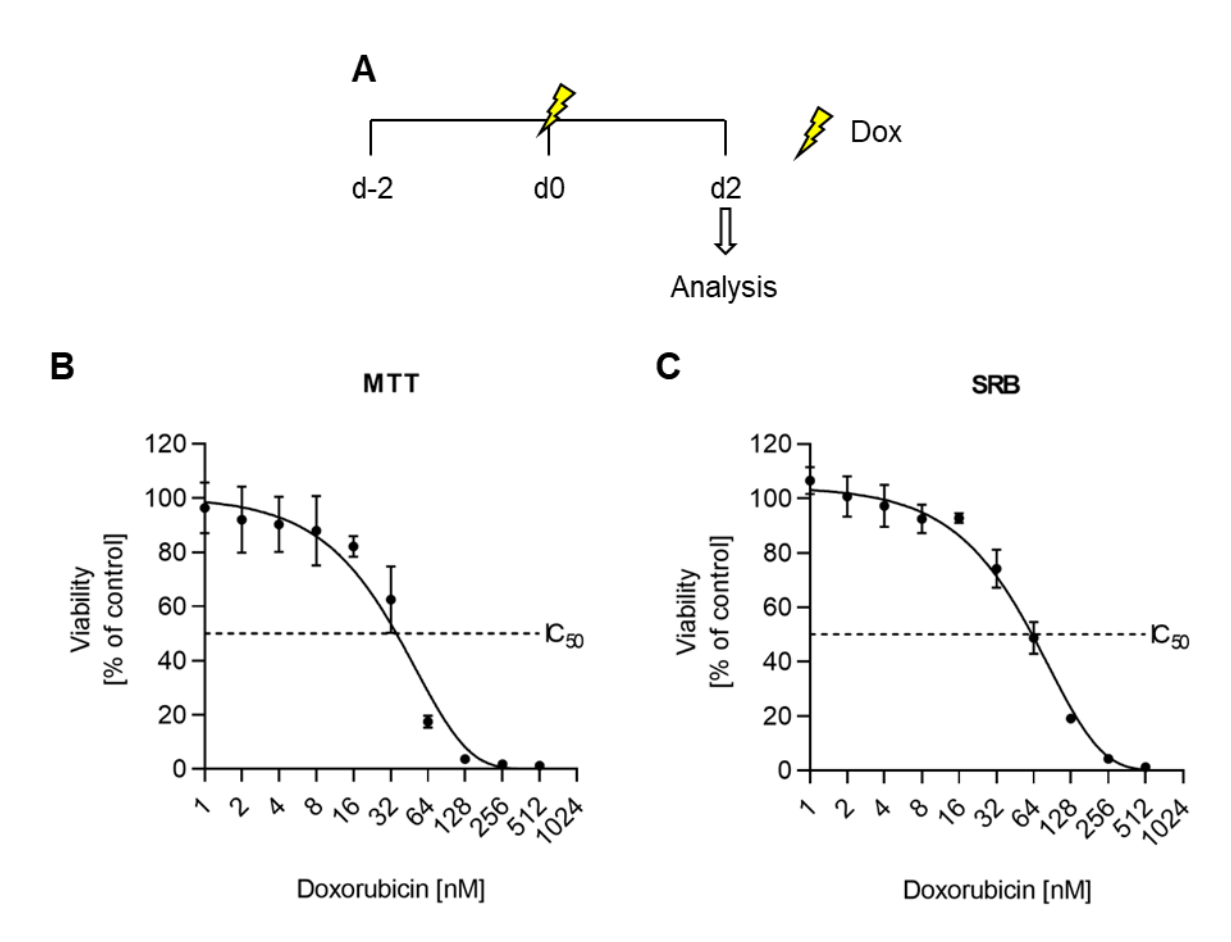


Fig. 15: Viability measurement of iPSCs upon short pulse-treatment with doxorubicin.

**A** Schematic illustration of doxorubicin (Dox) pulse-treatment scheme applied on human induced-pluripotent stem cells (iPSCs). Here, cells were exposed for 2 hours to Dox followed by 48 hours of recovery. Dox pulse-treatment is indicated with lightning symbol. **BC** Viability of iPSCs was measured 48 hours after short pulse-treatment with indicated concentrations of Dox using MTT or SRB assay. Viability data of treatment conditions was normalized to the respective control. Shown is the mean  $\pm$  standard error of mean (SEM) of three independent experiments (n=3; N=8). Inhibitory concentration of 50 % (IC50) was shown by the dashed line. For MTT assay (**B**), IC50-value was reached at around 35 nM and for SRB (**C**) at around 64 nM. MTT: (3-[4,5-dimethylthiazol-2-yl]-2,5 diphenyl tetrazolium bromide, SRB: Sulforhodamine B.

The viability data prompted the investigation of the potential impact of low concentrations of doxorubicin on the pluripotent state of iPSCs, with the hypothesis that it may induce the risk of spontaneous differentiation. Initially, the mRNA expression levels of the pluripotency markers octamer binding-protein 4 (*POU5F1*), homeobox transcription factor Nanog (*NANOG*) and SRY-box transcription factor 2 (*SOX2*) were measured using real-time quantitative PCR. (Fig. 16A). The data was acquired by a former bachelor student, Lluís Enjuanes Ruiz. In this study, the treatment of iPSCs with low concentrations of doxorubicin revealed no significant

alterations in the expression of pluripotency markers. Similar results were found via immunohistochemically detection of the pluripotency marker Oct-4, where acute treatment of iPSCs with doxorubicin did not alter the expression of this pluripotency marker (Fig. 16B). Together, these finding suggests that the pluripotent state of iPSCs remained unaltered following doxorubicin pulse-treatment.

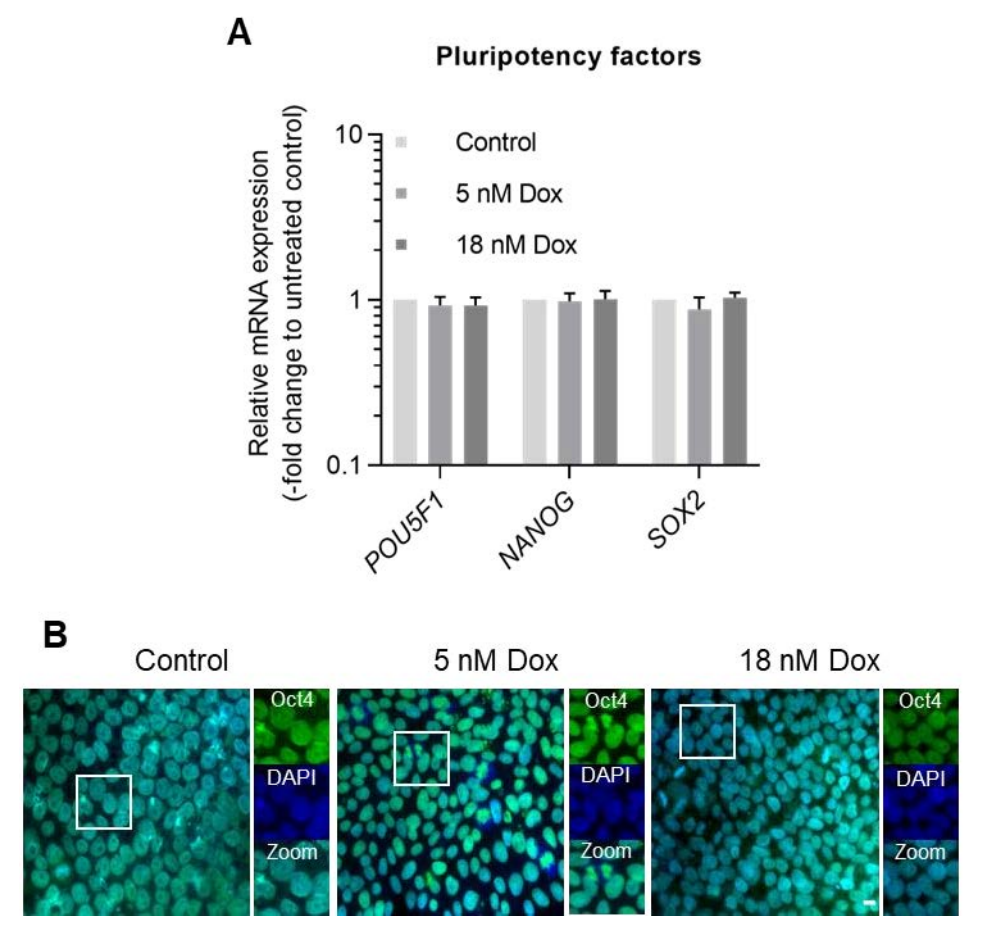


Fig. 16: Influence of short pulse-treatment of iPSCs with doxorubicin on pluripotency and proliferation capacity.

A Measurement of relative expression levels of pluripotency markers octamer binding-protein 4 (POU5F1), homeobox transcription factor Nanog (NANOG) and SRY-box transcription factor 2 (SOX2) in doxorubicin (Dox) pulse-treated human induced-pluripotent stem cells (iPSCs) using quantitative real-time PCR. Relative mRNA expression levels were normalized to the respective control. Shown is the mean ± standard error of mean (SEM) of four independent biological replicates (n=4; N=3). Hypoxanthine phosphoribosyltransferase 1 (HPRT1) was used as reference house-keeping gene. This experiment was performed by the former bachelor student Lluís Enjuanes Ruiz. B Representative images of immunohistochemical detection of octamer binding-protein 4 (OCT4) in Dox-treated iPSCs and their respective control (n=2). DNA was counterstained using DAPI. Magnification: x 20, scale bar: 10 µM. Zoomed regions with in are marked а white square. DAPI: 2-(4-amidinophenyl)-1H-indole-6-carboxamidine.

The retention of the pluripotent state accompanied with a high proliferation capacity is essential for the maintenance of the stem cell pool, and thereof the homeostasis of the organism. First, proliferation capacity in doxorubicin-treated iPSCs was measured via detection of positive

immunofluorescence signal for proliferation marker Ki-67 (Fig. 17A). The analysis of Ki-67 signal remained unaltered following acute exposure to doxorubicin. This finding suggests that the proliferation capacity is not lost upon treatment (Fig. 17B). However, Ki-67 is expressed throughout the cell cycle, with the highest levels of expression observed during the G2-phase or mitosis. (Sobecki et al., 2017). Thus, the question was whether acute exposure with low concentrations of doxorubicin would result alterations of the cell cycle distribution in iPSCs. For this, the incorporation of the DNA-intercalating fluorescent dye PI was measured using a flow cytometer to distinguish the distribution of cell population in G1-, S- and G2-phase as well as sub G1-phase (Fig. 17C). Flow cytometry measurement was acquired with the help of Sina Federmann (RG Fritz). Upon the tested treatment conditions all mentioned cell cycle phases were detectable. Quantification of cell cycle distribution and progression within doxorubicintreated iPSC culture was comparable to mock-treated cells. However, Ki-67 and cell cycle distribution measurements revealed no effect of doxorubicin pulse-treatment on the proliferation capacity of iPSCs. Nevertheless, the growth of iPSCs was determined up to 48 hours following doxorubicin treatment using an SRB assay. (Fig. 17D). The measurement of cells indicated a modest decrease in growth in response to doxorubicin treatment, although this effect was not statistically significant. Together, the results indicate that short pulse-treatment with low concentrations of doxorubicin is not sufficient to interfere with proliferation capacity and cell cycle distribution of iPSC culture within the timeframe of the experimental set-up.

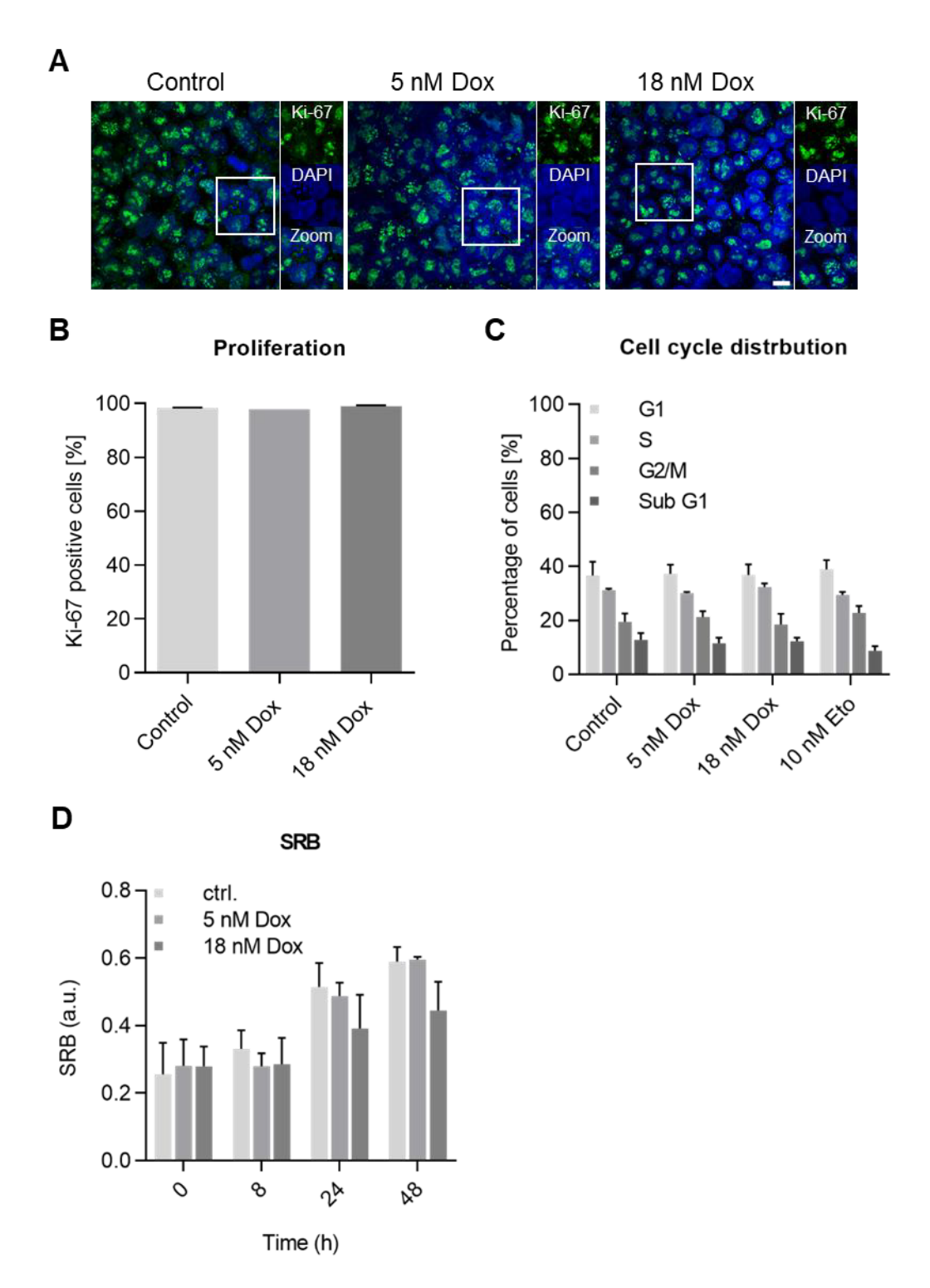


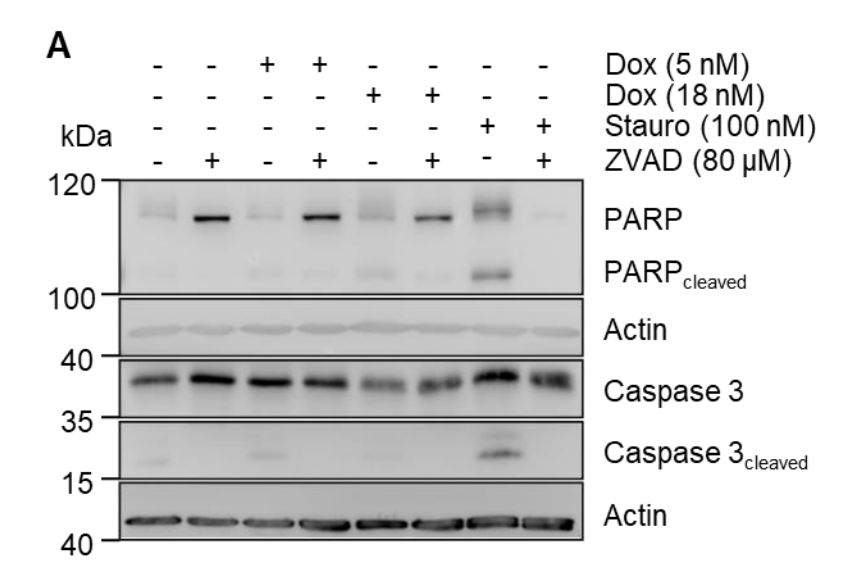
Fig. 17: Proliferation capacity of iPSCs short pulse-treated with low concentrations of doxorubicin.

A Representative immunofluorescence images of KI-67 positive human induced-pluripotent stem cells (iPSCs) conducted 48 hours after 2 hours pulse-treatment with low concentrations of doxorubicin (Dox). DNA was counterstained with DAPI. Scale bar: 10 μm, magnification: x 40. B Quantitative analysis of KI-67 positive cells. Shown is the mean ± standard error of mean (SEM) of two independent biological replicates (n=2; N=257-593 cell nuclei). C Flow cytometry cell cycle measurement of iPSCs pulse-treated for 2 hours with Dox was performed after a recovery of 48h using propidium iodide (PI) staining. As positive control for DNA damage induction, cell received a 2 hours pulse-treatment with etoposide (Eto) prior to cell cycle measurements after 48 hours. Quantitative analysis of the cell cycle distribution of each cell cycle phase is represented by the average percentage ± SEM of three

independent biological replicates (n=2; N=10.000 events). **D** Stem cell proliferation measured up to 96 hours right after 2 hours Dox exposure. Viability of the respective control was set to 100%. Shown is the mean SRB absorption ± SEM of three independent biological replicates (n=3; N=4). DAPI: 2-(4-amidinophenyl)-1H-indole-6-carboxamidine.

# 3.1.2. Pulse-treatment with low concentrations of doxorubicin is insufficient to initiate elevated apoptosis or activate canonical DNA damage response

In section 3.1.1, it was shown that human iPSCs showed high sensitivity against pulse-treatment to doxorubicin (Fig. 15BC). Thus, the aim was the further elucidation of the underlying molecular mechanisms that govern the process of apoptotic induction in iPSCs. To determine the induction of apoptosis in iPSCs, the relative protein levels of Caspase 3 and Poly(ADP-Ribose) Polymerase 1 (PARP) and especially their cleaved forms of both proteins were determined using Western blot technique (Fig. 18AB). These proteins are reliable markers for determination of apoptotic induction (Hengartner, 2000). To show that this process was caspase-dependent, caspase inhibitor carbobenzoxy-valyl-alanyl-aspartyl-[O-methyl]-fluoromethylketone (ZVAD) was included. Furthermore, staurosporine (Stauro) served as positive control for apoptosis induction. As expected, low concentrations of doxorubicin were not sufficient to induce extensive apoptosis in iPSCs, with the strongest induction of apoptosis upon treatment with the positive control Stauro. Consequently, the pulse-treatment of iPSCs with low concentrations of doxorubicin resulted in only mild induction of apoptosis.



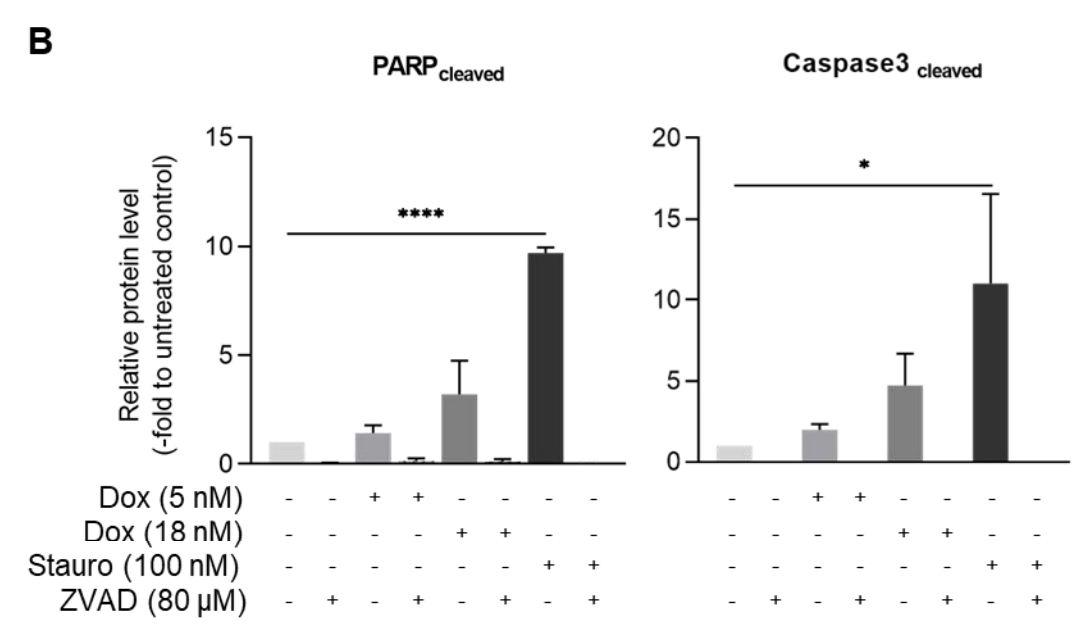


Fig. 18: Apoptotic induction in iPSCs upon exposure to low concentrations of doxorubicin.

A Human induced-pluripotent stem cells (iPSCs) were pulse-treated with 5 nM and 18 nM doxorubicin (Dox) for 2 hours prior to determination of protein level of total and cleaved protein levels of Caspase 3 and PARP after 48 hours of recovery. Actin served as house-keeping protein. 80 µM ZVAD was applied 4 h prior to Dox treatment. Apoptosis induction was induced via application of 100 nM staurosporine (Stauro) overnight. B Quantitative analysis of relative protein levels of cleaved PARP and caspase 3 in pulse-treated and control iPSCs. First, expression levels of each protein were normalized to the house-keeping protein Actin, followed by normalization to the respective control. Shown are the relative protein levels of three independent biological replicates ± standard error of mean (SEM) (n=3). For statistical analysis, *One*-way ANOVA with multiple comparisons was performed. \*\*\*\*P-value ≤ 0.0001, Carbobenzoxy-valyl-alanyl-aspartyl-[O-methyl]-\*P-value ≤ 0.05. kDa: Kilodalton, ZVAD: fluoromethylketone

Exposure of cells to doxorubicin has been shown to correlate with higher induction of DNA damage (Jahn et al., 2020). For cells, DNA damage represents the most harmful damage, thereof sufficient repair of DNA damage is fundamental for cell survival. Upon induction of DNA

damage, cells activate a complex protein pathway important for DNA damage response (DDR) and subsequent recruitment of cells involved in DNA damage repair.. While the DNA-damaging effect of doxorubicin is beneficial in cancer therapy, the strong apoptotic induction also affects somatic cells. Most importantly, rapidly proliferating cells, such as stem cells, may especially be affected increasing the risk of stem cell pool depletion. Thus, efficient DDR is crucial for overall stem cell survival and stem cell pool maintenance. To determine whether DDR is activated in iPSCs exposed to low concentrations of doxorubicin, DDR kinetics were measured. Upstream of the DNA damage repair cascade, histone variant H2A.X gets activated by phosphorylation at serine 139 through the protein kinases ataxia telangiectasia mutated (ATM) (Rogakou et al., 1998). The activation of H2AX via phosphorylation has been shown to be directly linked with double-strand break induced DNA damage (Burma et al., 2001). Besides phosphorylated H2AX (yH2AX), p53-binding protein 1 (53BP1) is another marker for DNA double-strand breaks (DSBs) activated downstream of ATM and H2AX in the DDR signaling cascade. In iPSCs, induction of vH2AX and 53BP1 foci upon moderate short pulse-exposure with doxorubicin was acquired at specific timepoints after treatment using confocal immunofluorescence microscopy (Fig. 19A). As positive control for the induction of DSBs in iPSCs, cells were treated with etoposide (Eto), a compound known to induce DSBs via poisoning of TopoIIB (Sunter et al., 2010). Overall, mock-treated cells revealed stable basal level of yH2AX and 53BP1 foci, while inheriting low levels of colocalization. With respect to our experimental approach upon pulse-treatment, no significant induction of DSB induction was detectable. As seen by the reduction of DSB foci as well as their colocalization, iPSCs appear to have the ability to repair the occurring DSBs within the observed time frame. However, this was not the case for the positive control Eto. Here, compared to doxorubicin-treated cells the average number of DSB foci and their colocalization was strongly elevated indicating an induction of the DDR to transduce the signal of Eto-induced DSBs for subsequent DNA damage repair.

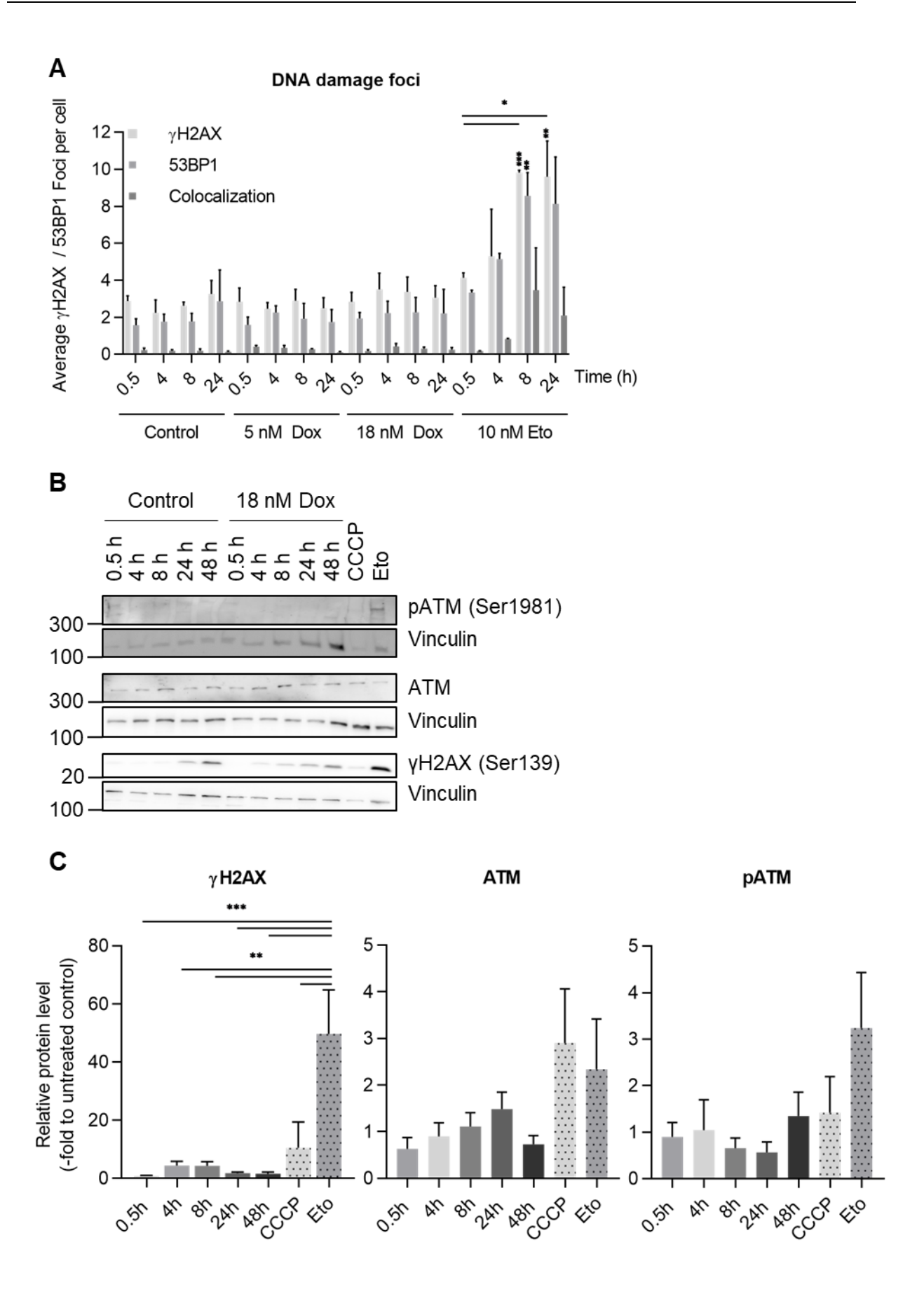


Fig. 19: Induction of DNA double-strand breaks in iPSCs upon short pulse-treatment with doxorubicin.

Human induced-pluripotent stem cells (iPSCs) were pulse-treated for 2 hours with 5 nM and 18 nM doxorubicin (Dox) and cells were fixed to indicated timepoints followed by immunohistochemical staining for at serine139 phosphorylated histone variant H2A.X (yH2AX), p53-binding protein 1 (53BP1). As positive control, cells were pulse-treated with 10 nM etoposide (Eto) and treated according to other conditions. A Shown is the quantification of DNA damage marker and colocalizing foci. Respective timepoints of analysis are indicated. Shown is the mean ± standard error of mean (SEM) of three independent experiments (n=3; N=100). For the positive control Eto, the mean ± SEM of two independent experiments is shown (n=2; N=45-100). B Representative Western blot images of different biological replicates showing phosphorylated vH2AX (Ser139), protein kinases ataxia telangiectasia mutated (ATM) and its activated, phosphorylated (Serine 1981) form. Respective timepoints of treatment are indicated. Vinculin served as house-keeping protein. Additionally, cells were exposed for 4 h to 10 μM CCCP and 10 nM etoposide (Eto) and served as mitochondrial and genomic stress control, respectively. C Quantitative analysis of relative protein levels from yH2AX, ATM and pATM (Ser1981) were first normalized to house-keeping protein Vinculin before normalization to the control of the respective timepoint. CCCP and Eto were normalized to the respective 4 h timepoint of the control. The relative protein levels of γH2AX is shown ± SEM for four biological replicates (n=4). For ATM and pATM the relative protein levels of three independent biological replicates are shown ± SEM (n=3). For statistical analysis, One-way ANOVA with multiple comparisons was performed. \*\*P-value ≤ 0.01, \*P-value ≤ 0.05. CCCP: Carbonyl cyanide m-chlorophenyl hydrazine

Furthermore, signaling cascades upstream of H2AX activation was elucidated. This comprised the kinase ATM including its activated form. The latter comprises phosphorylation of ATM at serine 1981 which is necessary for activation of ATM (Bakkenist & Kastan, 2003). Expression levels of ATM, phosphorylated ATM and yH2AX was followed in comparable time scales as considered for DNA damage foci formation using Western blot technique (Fig. 19BC). As positive control for mitochondrial and genotoxic stress, cells were exposed for 4 h to Carbonyl cyanide m-chlorophenyl hydrazine (CCCP) and 10 nM Eto, respectively. Following exposure of cells to doxorubicin, relative protein levels of yH2AX increased within eight hours of doxorubicin pulse-treatment, subsequently decreasing to basal levels within the observed time frame. However, this trend did not reach statistical significance following doxorubicin treatment. Also, no significant trends were observed for ATM and pATM. Notably, for the positive control Eto, yH2AX and ATM activation increased, resulting in a significant increase in the relative expression of yH2AX. These results show that DNA damage induced by low concentrations of doxorubicin is accompanied with comparably low induction of DNA damage and DDR capacity is not affected as seen by reduction of DDR signaling within the observed time frame. Together with the measurement of apoptosis, these results suggest apoptotic induction independent of the induction of genotoxic stress.

### 3.1.3. Influence of acute doxorubicin exposure on mitochondrial function in human iPSCs

As shown in previous sections, short pulse-treatment of iPSCs with low concentrations of doxorubicin had no influence on stem cell properties (see Fig. 16) and DNA damage repair capacity (Fig. 19), we aimed to further understand the sensitive phenotype of iPSCs. As shown in previous studies, mitochondria play a pivotal role in modulating the sensitivity of cells against chemotherapeutic, including as doxorubicin (Gogvadze et al., 2009; Sarosiek et al., 2013). However, most findings were acquired under chronic exposure or high doxorubicin concentrations. This led to the question whether even pulse-treatment with low concentrations of doxorubicin is accompanied with mitochondrial dysfunction in iPSCs. Thus, in the following sections the influence of doxorubicin pulse-treatment on mitochondrial function will be further elucidated in the following sections.

# 3.1.3.1. Pulse-treatment with doxorubicin is accompanied with mitochondrial fragmentation and loss of mitochondrial membrane potential

Mitochondria are highly dynamic organelles undergoing constant fusion and fission events depending on the metabolic demand. Morphological changes in the mitochondrial network are directly related to mitochondrial health and the cellular energy demand (H. Chen et al., 2005; Ishihara et al., 2006).

In order to understand whether pulse-treatment of iPSCs with doxorubicin is accompanied with changes in mitochondrial network morphology, Z-stack images of MitoTracker-stained mitochondria were acquired using confocal microscopy. Mitochondrial morphology was categorized into tubular, intermediate and fragmented morphology (Fig. 20A). It is noteworthy that iPSC cell line IMR-90 (clone 4) showed mitochondria with mostly tubular morphology and global distribution within the cell. Upon short pulse-treatment of iPSCs with doxorubicin, mitochondrial network shifted significantly from a majorly tubular network towards a more fragmented system (Fig. 20B). This finding suggests that even short pulse-treatment of iPSCs doxorubicin can have a significant impact on mitochondrial morphology.

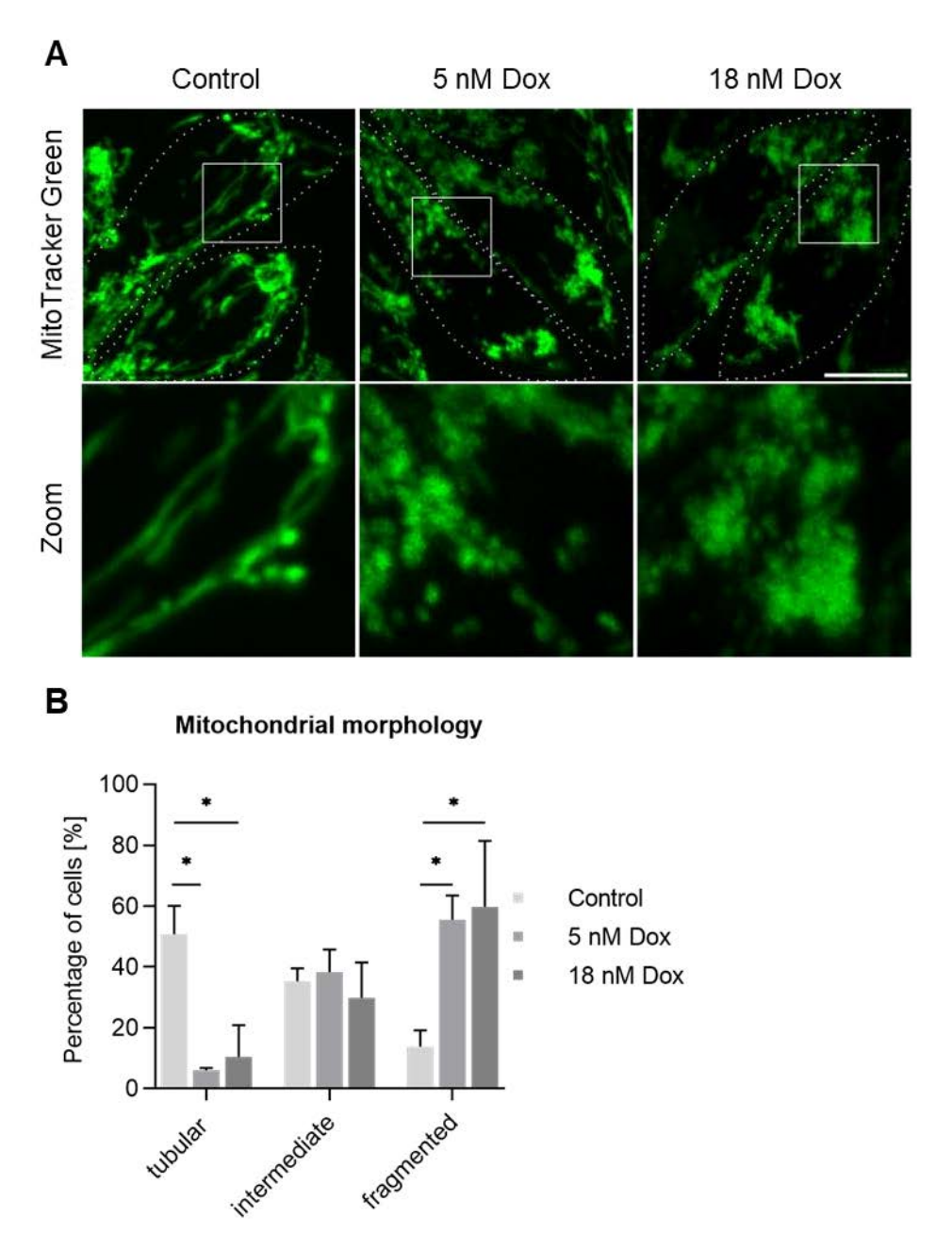


Fig. 20: Mitochondrial morphology in iPSCs upon short pulse-treatment with doxorubicin. Mitochondrial morphology in human induced-pluripotent stem cells (iPSCs) was assessed 48 hours after 2 hours pulse-treatment with doxorubicin (Dox) via live-cell confocal microscopy of MitoTrackerGreen signal. A Shown are representative confocal images of mitochondria in control and pulse-treated iPSCs. Zoomed-in regions are indicated by a white box. Magnification: x 63, scale bar: 10  $\mu$ m. B Quantification of mitochondrial morphology categorized in tubular, intermediate, or fragmented morphology 48 hours after pulse-treatment with Dox. Data show mean  $\pm$  standard error of mean (SEM) from three independent experiments (n=3; N=50 cells). 2-way ANOVA was performed. \*P-value  $\leq$  0.05.

Mitochondrial morphology is highly dependent on the delicate balance between fusion and fission (see section 1.1.3). Since iPSC showed drastic changes on mitochondrial morphology level, the expression levels of proteins involved in fusion (Mfn1, Mfn2, OPA1) and fission processes (Drp1, pDRP1) were further elucidated using Western blot technique (Fig. 21A).

Here, carbonyl cyanide m-chlorophenyl hydrazine (CCCP) served as positive control for fission induction. The fission activity of Drp1 is strongly dependent on its phosphorylation at different serine sites (Gao et al., 2022). Here, the activation of Drp1 at serine 616 was further elucidated (pDrp1). Furthermore, the ratio between phosphorylated pDrp1 and its unphosphorylated form serves as indicator of mitochondrial fission. However, pulse-treatment of iPSCs with low concentrations of doxorubicin was accompanied with no changes on relative protein levels (Fig. 21AB). In contrast, mitochondrial fusion factors Mfn1 and Mfn2 showed tendency of downregulation upon treatment with doxorubicin (Fig. 21AC). Interestingly, Mfn2 was slightly upregulated upon treatment with the lowest concentration of doxorubicin possibly indicating towards a compensatory mechanism. The proteolytic processing of OPA1 is associated with dysregulation in mitochondrial function, thereby linking mitochondrial fragmentation with processing of OPA1 (Duvezin-Caubet et al., 2006). Within iPSCs, all five isoforms of OPA1 were detectable comprising of the two long-OPA1 (I-OPA1) isoforms and the three short-OPA1 isoforms (s-OPA1, Fig. 21A). Upon pulse-treatment of iPSC with doxorubicin, no significant trend of OPA1 processing was detected as the ratio between s-OPA1 and I-OPA1 remained unchanged (Fig. 21D). As expected, highest processing of OPA1 was detected with the positive control CCCP.

Taken together, observed fragmentation of mitochondrial network might be caused by doxorubicin-induced changes in the balance of mitochondrial motility proteins, namely downregulation in fusion factors Mfn1 and Mfn2.

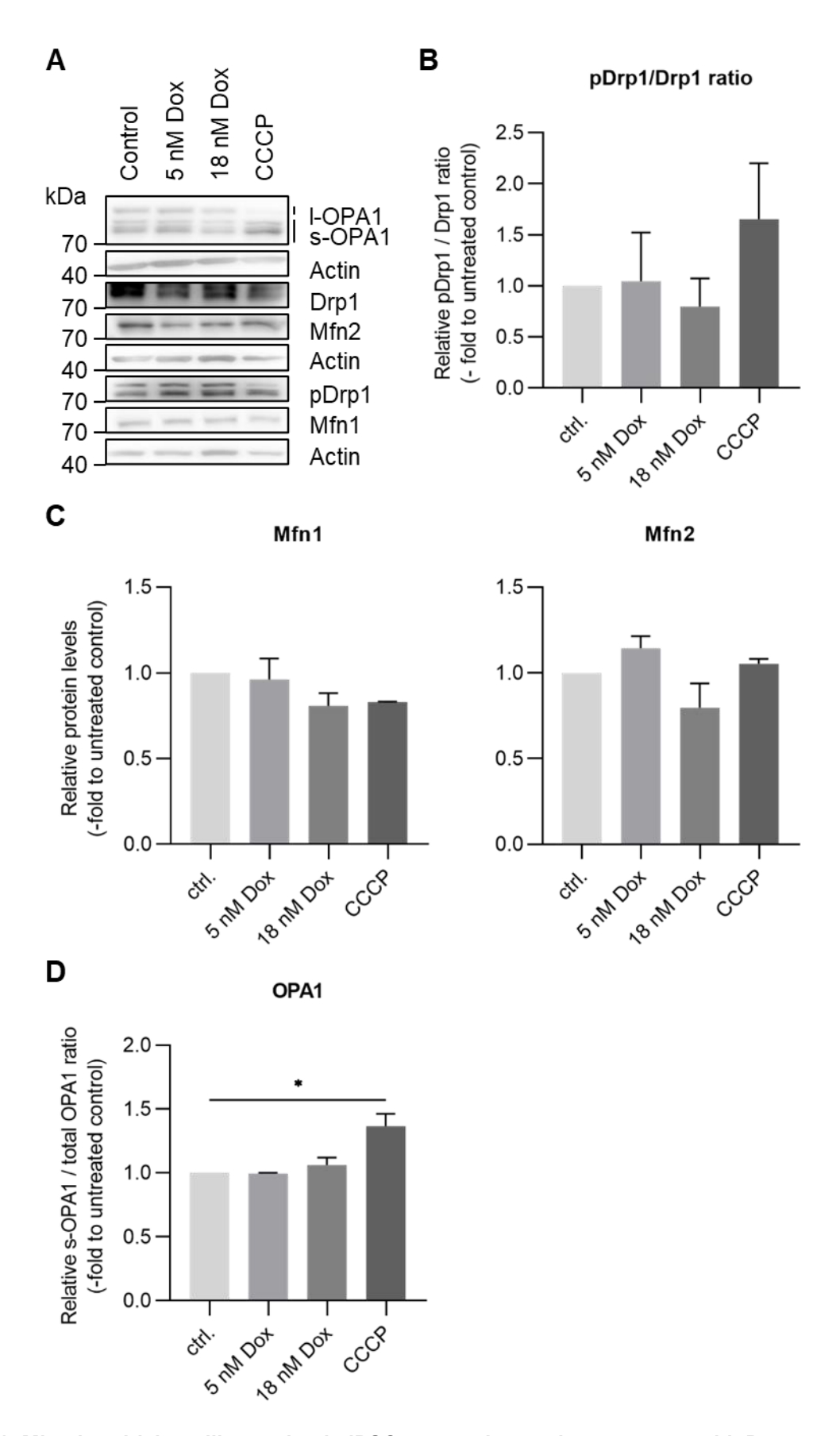


Fig. 21: Mitochondrial motility marker in iPSCs upon short pulse-treatment with Dox. Human induced pluripotent stem cells (iPSCs) were pulse-treated for 2 hours with 5 nM and 18 nM doxorubicin (Dox) prior to harvest and loading on Western blot 48 hours after treatment. Motility markers mitofusin 1(Mfn1) and mitofusin 2 (Mfn2), dynamin-1-like protein (Drp1) and its activate form

phosphorylated at serine616 (pDrp1 Ser616). Furthermore, expression level of optic atrophy 1 (OPA1) as marker for mitochondrial inner membrane processing was assessed. As positive control for mitochondrial fragmentation, cells were treated with CCCP for 2 hours prior to harvest. **A** Representative Western blot of one biological replicate. Treatment conditions and proteins are indicated. **BCD** Shown is the quantification of motility proteins Drp1 (**B**), Mfn1 and Mfn2 (**C**), and OPA1 ratios (**D**). For Drp1, the ratio between the phosphorylated form at serine site 616 and the unphosphorylated form was calculated. For the OPA1, ratios between total short-OPA1 and total OPA1 levels were calculated. Shown are the relative protein levels ± standard error of mean (SEM) of independent experiments (pDrp1/Drp1: n=3, Mfn1/Mfn2: n=5, OPA1, n=2, CCCP=n2), normalized to the respective control. CCCP: Carbonyl cyanide m-chlorophenyl hydrazine.

Disruption of mitochondrial morphology is strongly associated with mitochondrial membrane potential ( $\Delta\Psi_m$ ) and are the first indicator for mitochondrial dysfunction (Frank et al., 2001). To gain further insight whether doxorubicin-induced mitochondrial fragmentation is accompanied with changes on  $\Delta\Psi_m$ , live-cell confocal imaging with the  $\Delta\Psi_m$  -dependent dye tetramethylrhodamine methyl ester (TMRM) was performed (Fig. 22A). Quantification of the relative TMRM signal revealed a significant decrease in  $\Delta\Psi_m$  with increase in doxorubicin concentration (Fig. 22B). Overall, even moderate short pulse-treatment iPSCs to low concentrations of doxorubicin is sufficient to disrupt  $\Delta\Psi_m$ , thereof hinting, together with overserved changes in mitochondrial morphology, towards mitochondrial dysfunction in iPSCs.

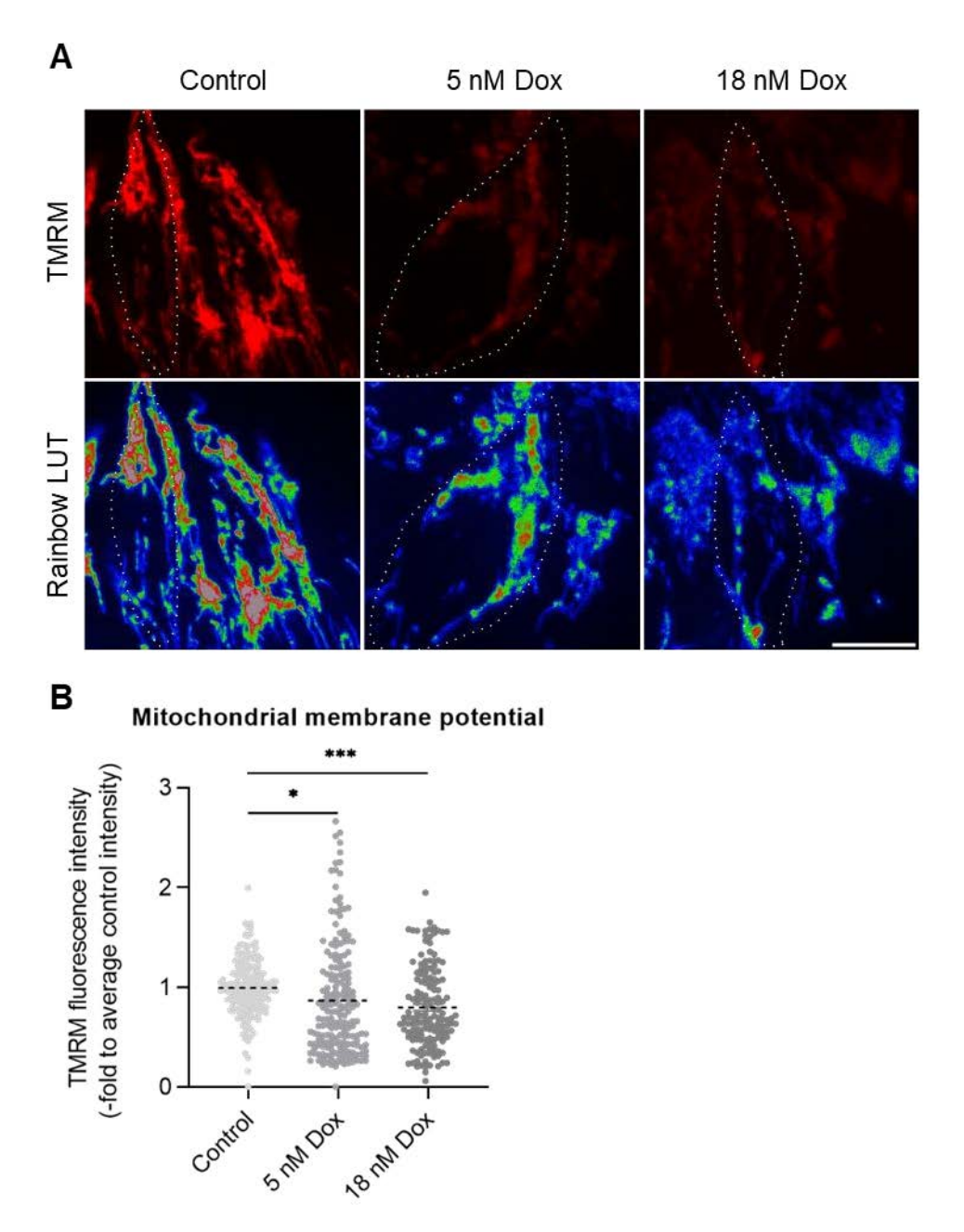


Fig. 22: Short pulse-treatment of iPSCs with doxorubicin is accompanied with disruption of mitochondrial membrane potential ( $\Delta\Psi_m$ ).

A Representative confocal image of  $\Delta\Psi_m$  in iPSCs 48 hours after 2 hours pulse-treatment with low concentrations of doxorubicin (Dox). For this, cells were stained with tetramethylrhodamine methyl ester (TMRM) and images were acquired with confocal microscope (upper row). Intensity of each condition is represented by pseudocolour rainbow LUT (lower row). Magnification: x 63, scale bar: 10 μm. B Quantification of relative TMRM fluorescence intensity normalized to mock-treated iPSCs. Data represent the median plus whiskers of three independent experiments (n=3; N=35-50 cells). For statistical analysis, *One*-way ANOVA with multiple comparisons was performed. \*\*\*P-value ≤ 0.001, \*P-value ≤ 0.05.

## 3.1.3.2. Mitochondrial respiration is impaired upon pulse-treatment with doxorubicin

Generation of mitochondrial membrane potential ( $\Delta\Psi_m$ ) is an essential parameter for mitochondrial respiratory function favoring the transport of protons (H+) across the inner mitochondrial membrane (IMM). This is, in turn, necessary for the ETC-dependent synthesis of ATP (Zorova et al., 2018). To further elucidate whether doxorubicin-dependent disruption of  $\Delta\Psi_m$  in iPSCs is represented by changes in respiratory function of mitochondria, oxidation consumption rate (OCR) was measured using Seahorse live-cell respirometer (Fig. 23A). Overall, measurement of mitochondrial respiration was suppressed upon pulse-treatment with doxorubicin, with the strongest reduction upon 18 nM doxorubicin (Fig. 23A). Further determination of relative Seahorse parameters (basal respiration, maximal respiration, proton leak and ATP production) revealed a trend towards reduction in nearly all measured parameters upon treatment with doxorubicin (Fig. 23B). However, this trend was only significant for 18 nM. In sum, even 48 hours after pulse-treatment of iPSCs with doxorubicin respiration of mitochondria was impaired indicating a prolonged effect of doxorubicin treatment on mitochondrial function.

Since pulse-treatment with low concentrations of doxorubicin was accompanied with reduction in mitochondrial respiration, total cellular ATP concentration was determined to elucidate the influence of doxorubicin pulse-treatment on mitochondrial energy conversion into ATP (Fig. 23C). Short pulse-treatment with 5 nM of doxorubicin was accompanied solely with a slight reduction of the relative cellular ATP level (Fig. 23C). In contrast, cells pulse-treated with the highest doxorubicin concentration showed a significant decrease in relative ATP level, namely around 20 %. In accordance with the live-cell respirometry findings, even short pulse-treatment with low concentrations of doxorubicin is accompanied with disturbance in mitochondrial metabolism hinting towards mitochondrial-dependent metabolic crisis in iPSCs.

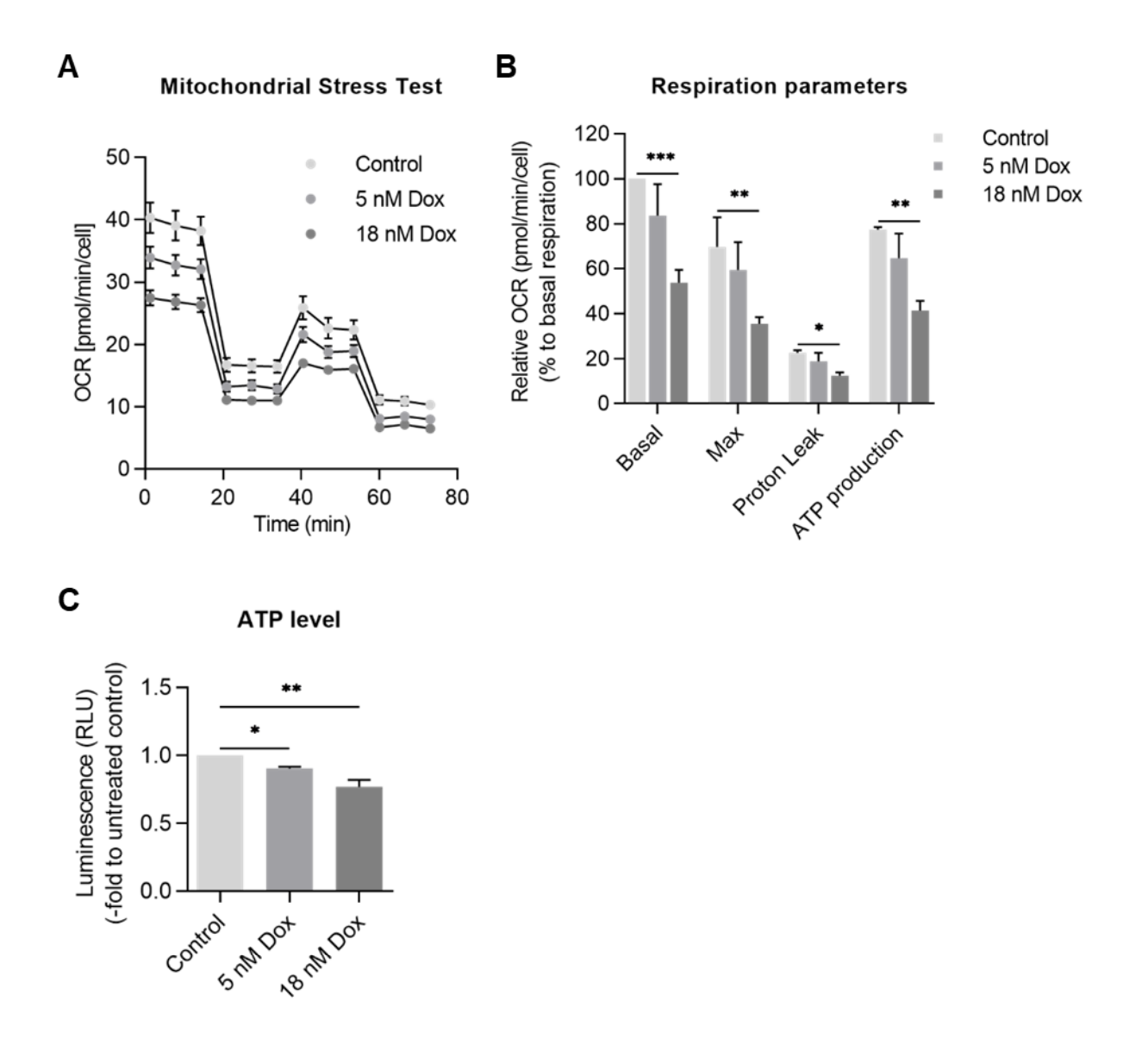


Fig. 23: Measurement of live-cell respiration and ATP levels in iPSCs after short-time exposure to low concentrations of doxorubicin.

A Human induced-pluripotent stem cells (iPSCs) were pulse-treated with low concentrations of doxorubicin (Dox) prior to live-cell respiratory measurement with Seahorse FluxAnalyzer 48 hours after treatment. Representative Seahorse run of one biological replicate. Oxygen consumption rate (pmol/min/cell) was normalized to the respective cell number using Hoechst staining assay. B Quantitative analysis of relative values of basal respiration (basal), maximal respiration (Max, after FCCP injection), proton leak and ATP production is shown for iPSCs 48 hours after 2 hours pulsetreatment with low concentrations of Dox. Data represent the mean ± standard error of mean (SEM) of three independent experiments normalized to basal respiration of the untreated iPSC control (n=3; N=30-32). For statistical analysis, One-way ANOVA with multiple comparisons was performed. \*\*P-value ≤ 0.01, \*\*\*P-value ≤ 0.001. **C** Quantification of relative ATP levels 48 hours after 2 hours pulse-treatment with Dox using CellTiter-Glo® 2.0 Cell Viability Assa. Data shown is the mean ± SEM of three independent experiments (n=3, N=4), normalized to the respective control. One-way ANOVA \*\*P-value comparisons was performed. ≤ 0.01. \*P-value FCCP: Carbonyl cyanide 4-(trifluoromethoxy)phenylhydrazone, ATP: Adenosine triphosphate

The question of the time frame in which doxorubicin -induced suppression of mitochondrial respiration is first measurable has emerged from live-cell respirometry data. For this,

mitochondrial respiration in iPSCs was determined 4 hours and 24 hours after pulse-treatment with the highest doxorubicin concentration, namely 18 nM. Here, live-cell respirometry data showed strong reduction from 24 hours after pulse-treatment (Fig. 24A). This was supported by quantification of respiratory parameters, as these were significantly reduced upon 24 hours after pulse-treatment with 18 nM doxorubicin (Fig. 24B). However, this was not detectable from 4 h after pulse-treatment. Overall, respiration data revealed that treatment of iPSCs with the highest concentration, namely 18 nM doxorubicin, was accompanied by lower mitochondrial respiration and thereof possible reduction in ATP production as early as 24 hours after doxorubicin exposure indicating a persisting effect of doxorubicin on mitochondrial respiration as reduction in OCR was still detectable 48 hours after the treatment.

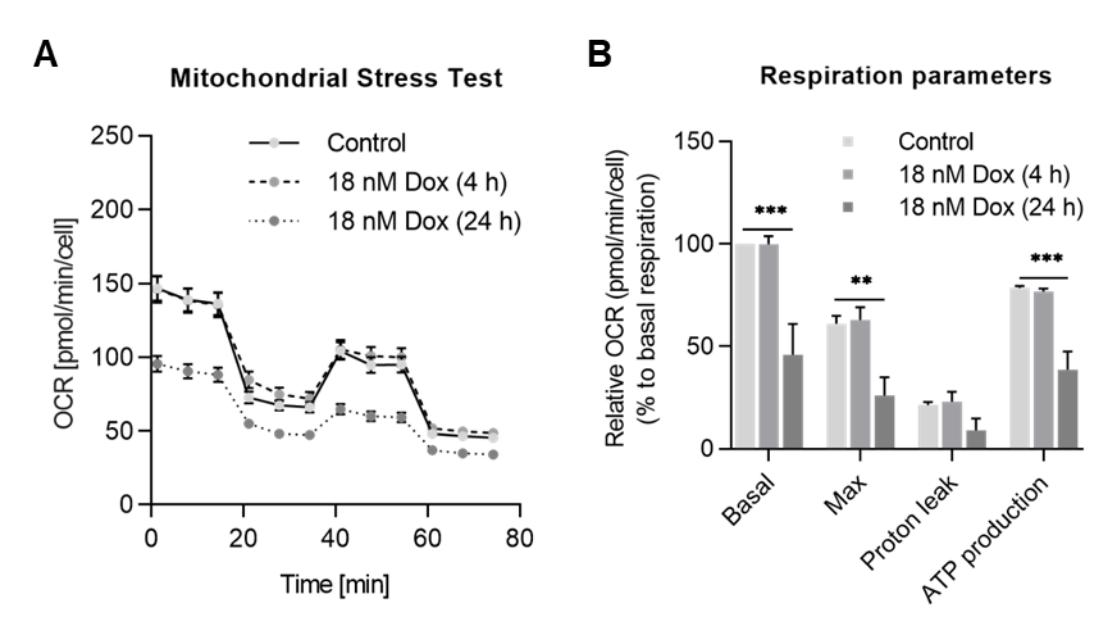


Fig. 24: Time-lapse measurement of doxorubicin induced effects on mitochondrial respiration in iPSCs.

A Representative Seahorse run of one biological replicate 4 h and 24 hours after exposure to 18 nM doxorubicin (Dox) in human induced-pluripotent stem cells (iPSCs). Oxygen consumption rates (pmol/min/cell) were normalized to the cell number using Hoechst staining. **B** Quantitative analysis of relative values of basal respiration (basal), maximal respiration (Max, after FCCP injection), proton leak and ATP production is shown for iPSCs 4 h and 24 hours after 2 hours pulse-treatment with moderate concentrations of Dox. Data represent the mean ± standard error of mean (SEM) of two independent experiments normalized to basal respiration of the untreated iPSC control (n=2; N=30-32). For statistical analysis, *One*-way ANOVA with multiple comparisons was performed. \*\*P-value ≤ 0.01, \*\*\*P-value ≤ 0.001. FCCP: Carbonyl cyanide 4-(trifluoromethoxy)phenylhydrazone, ATP: Adenosine triphosphate

## 3.1.3.3. Doxorubicin treatment of iPSCs is not sufficient to disrupt mitochondrial ultrastructure

As mentioned in section 1.1.2, cristae formation is a crucial parameter for assembly of ETCs. Since previously described data showed that exposure of iPSCs towards low concentrations of doxorubicin was accompanied with reduction in mitochondrial respiration and downstream energy conversion into ATP conversion, we questioned whether pulse-treatment with doxorubicin is sufficient to induce alteration on mitochondrial ultrastructural level and thereof directly affect ETC assembly and activity.

First, mitochondrial ultrastructure and cristae formation were acquired by our technical assistant Andrea Borchardt at the CFEM using standard transmission electron microscopy. Mitochondrial cristae types were categorized into 'tubular', 'septa', 'arched' and 'branched'. In general, electro micrographs of iPSC line used in this study revealed mitochondria with low cristae density and mostly tubular morphology. (Fig. 25A) Quantification of the average distribution of cristae phenotypes revealed that exposure of iPSCs with low concentrations of doxorubicin had no direct effect on mitochondrial ultrastructure (Fig. 25B).

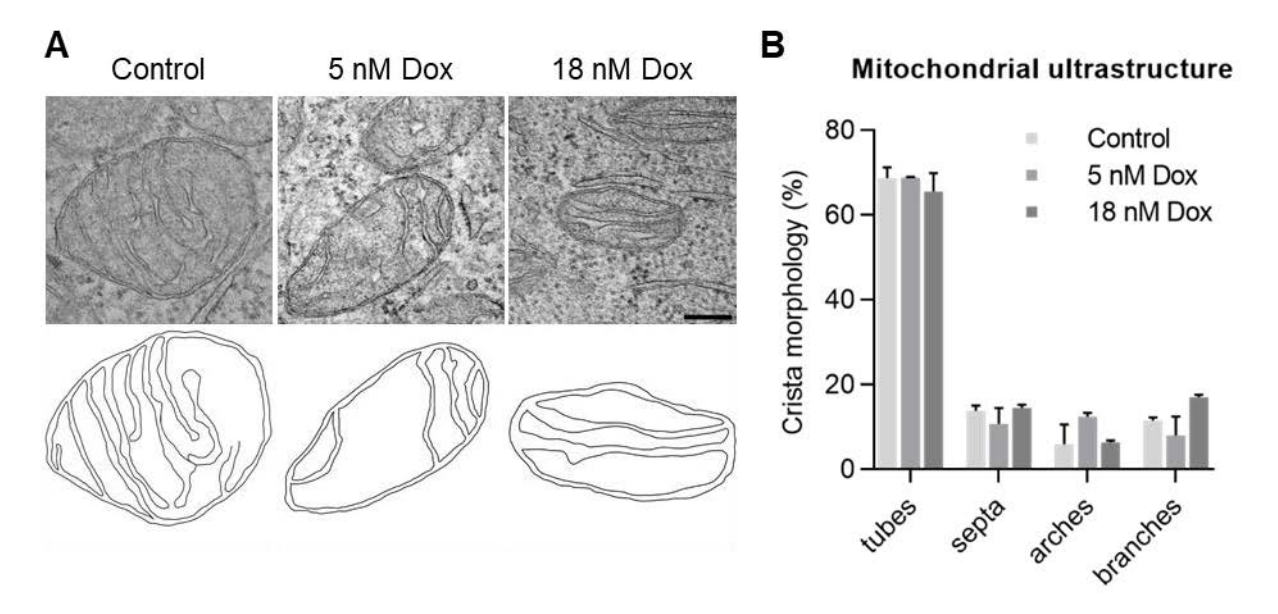


Fig. 25: Influence of short pulse-exposure of doxorubicin on mitochondrial ultrastructure in iPSCs.

**A** Electron micrographs of iPSCs 48 hours after pulse-treatment with low concentrations of doxorubicin (Dox). Images were acquired at transmission electron microscope JEM-2100 Plus by our technical assistant Andrea Borchardt at the CFEM. Scalebar: 0.1  $\mu$ m. Drawn surroundings of respective mitochondria are shown in the second row. **C** Percentage of cristae ultrastructure phenotype categorized in tubes, septa, arches and branches in iPSCs after Dox pulse-treatment. Data show mean  $\pm$  standard error of mean (SEM) from two independent experiments (n=2; N=38-50 mitochondria). CFEM: Core facility electron microscopy

In previous publications, doxorubicin has been previously shown to interfere with the expression and assembly level of ETCs. Especially the activity of ETCs, mainly complex I, has been described to be directly affected upon treatment of doxorubicin due to the quinone-like structure (Jawad et al., 2019). This raised the question whether treatment with low concentrations of doxorubicin is accompanied by effects on assembly and activity level of ETCs. Most importantly, complex I and complex IV were closer examined. The following blue native and clear native PAGEs were performed by Yulia Schaumkessel. First, crude mitochondrial preparations of each condition were loaded on Blue Native or Clear Native gels to elucidate the assembly and activity level of complex I and complex IV, respectively (Fig. 26A). As seen on both membranes of native gels, the assembly level as well as in gel-activity of the respective complexes was largely unaffected upon treatment of iPSCs doxorubicin. To determine whether the remaining complexes were affected upon exposure to doxorubicin, the assembly of the total ETCs (OXPHOS cocktail) as well as remaining ETC complexes comprising complex II and III were determined via blue Native PAGE. Additionally, MICOS protein MIC60 was detected as marker for cristae formation (Fig. 26B). Neither total OXPHOS cocktail samples, nor the single respiratory subunits showed a doxorubicin treatment dependent effect on the assembly level.

Taken together, respiratory defects measured with Seahorse could neither be explained by demolition of mitochondrial ultrastructure nor alterations in ETC complex assembly and activity in iPSCs.

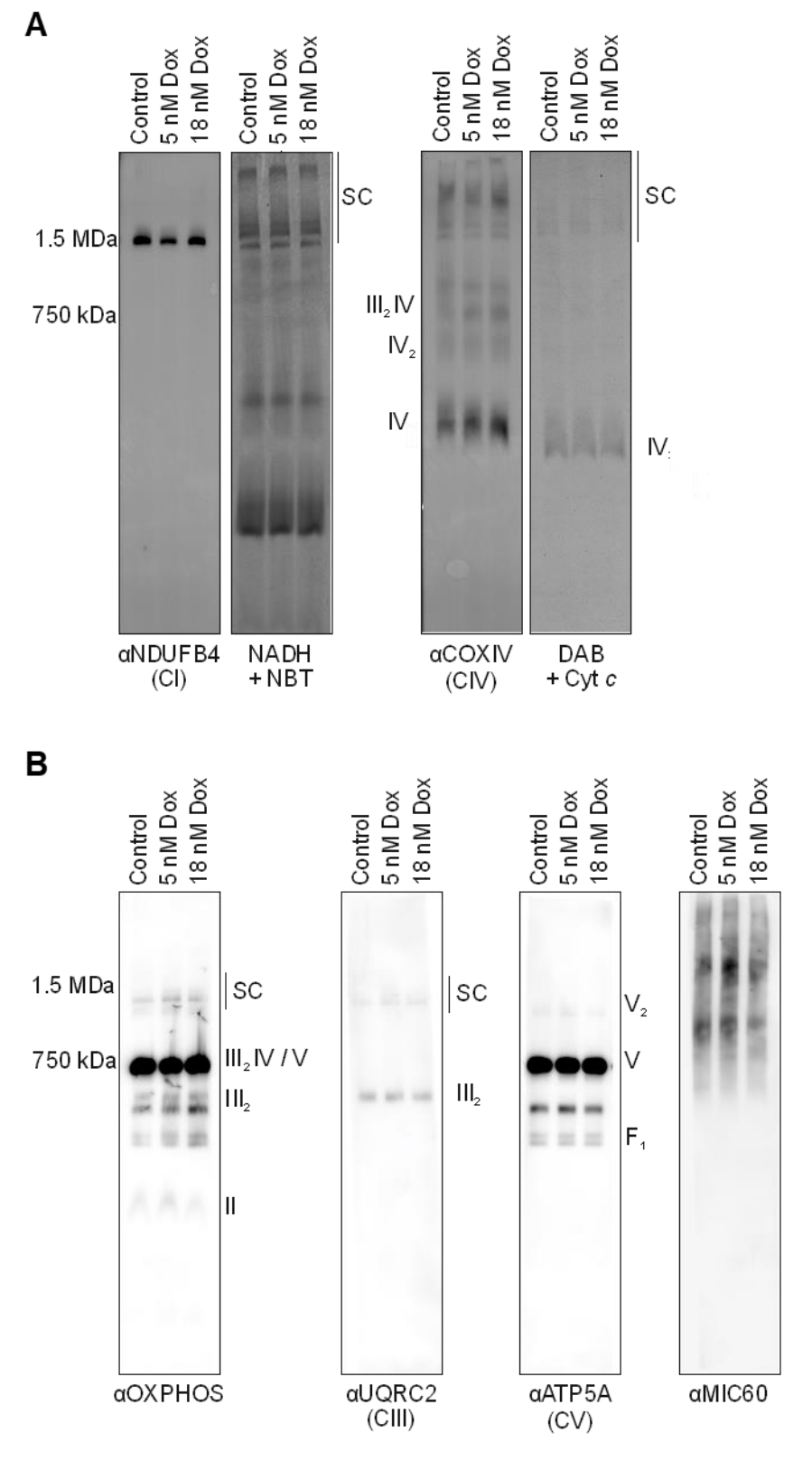


Fig. 26: Mitochondrial respiratory complex assembly and activity upon short pulse-treatment with of iPSCs with doxorubicin.

Shown are clear native PAGEs and blue native PAGEs from human-induced pluripotent stem cells pulse-treated with doxorubicin (Dox). These PAGEs were performed by our colleague Yulia Schaumkessel. **A** Shown are representative images of blue and clear native PAGEs of complex I and IV (CI and CIV) of crude mitochondrial preparations performed 48 hours after 2 hours pulse-treatment of iPSCs with indicated concentrations of Dox (blue native PAGE: n=4; clear native PAGE: n=2). **B** OXPHOS complex,

complex IV (CIV) complex V/ATP5A (CV) and MIC60 assembly in crude mitochondrial preparations 48h after pulse-treatment with Dox in iPSCs. Shown are representative images of blue and clear native PAGEs (blue native PAGE: n=4). NDUFB4: NADH:Ubiquinone Oxidoreductase Subunit B4, NADH: Adenosine 5'-(trihydrogen diphosphate), NBT: nitro blue tetrazolium chloride, DAB: 3,3'-diaminobenzidine, OXPHOS: Oxidative phosphorylation cocktail, SC: Supercomplex

## 3.1.3.4. Doxorubicin treatment is accompanied with modulation of mitochondrial genome organization

As elucidated in section 1.1.4, mitochondria inherit their own 16.5 kb sized genome encoding for 13 subunits crucial for the function of respiratory complexes. Within mitochondria, several thousand copies are organized punctate-like structures, namely nucleoids. Dox penetrates the mitochondrial membranes, where it intercalates into the double-stranded mitochondrial DNA leading to the induction of DNA damage and thereof enhances the formation of DSBs and mtDNA mutations. To this date, it is not known whether pulse-treatment of cells with low concentrations is accompanied with changes in the distribution, amount and size of nucleoids within the cell. The effect of short pulse-treatment with low concentration of Dox on mitochondrial nucleoid size and distribution was determined via detection of mitochondrial double-stranded DNA with confocal immunofluorescence imaging (Fig. 27A). With help of a semi-automated pipeline in CellProfiler (4.2.5), the average number of nucleoids per cell (per μm² per cell area) and the average size of nucleoids (per μm² of cell) within mitochondria was determined. Simultaneously, the same parameters were measured for released mtDNA in the cytoplasm. Upon pulse-treatment of iPSCs with low concentrations of Dox, the average number of nucleoids per area of cells counted within mitochondria was significantly reduced with increase in doxorubicin concentration (Fig. 27B). Besides reduction in the number of nucleoids, the average size of nucleoids per cell (µm²) inside mitochondria was affected, showing a significant reduction in nucleoid size of 5 nM doxorubicin treated cells (Fig. 27C). Since the number of mitochondrial nucleoids was significantly reduced in a least one sample, the question was whether mtDNA release was induced. Semi-automated analysis revealed that the number of nucleoids per area of cell (µm²) which were released in the cytoplasm was not elevated upon short pulse-treatment with doxorubicin. (Fig. 27D). In sum, exposure of iPSCs to low concentrations of doxorubicin was accompanied with reduction in nucleoid size and number, yet mitochondrial mtDNA release was not elevated indicating a possible doxorubicin-induced stress mechanism to protect mtDNA integrity.

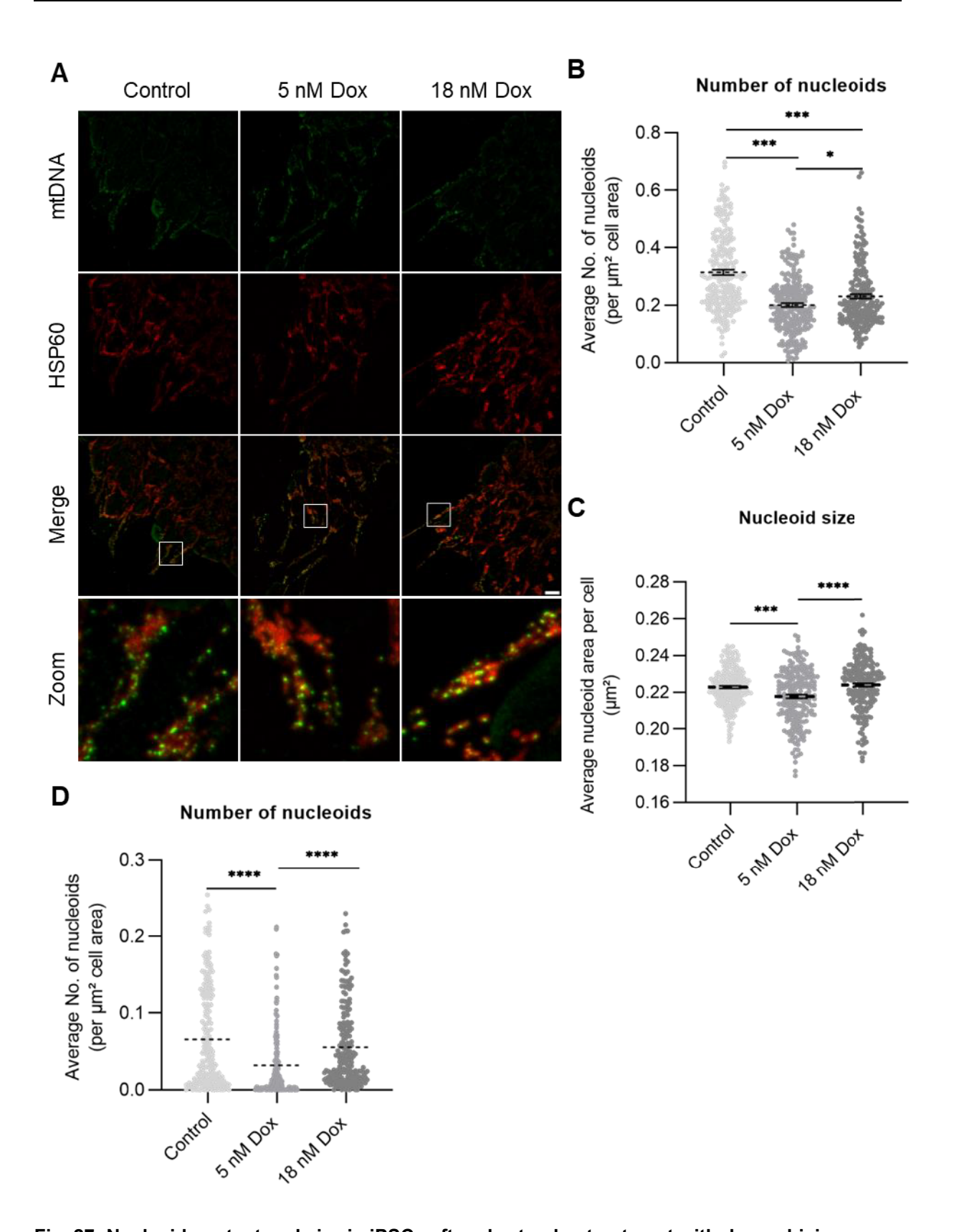
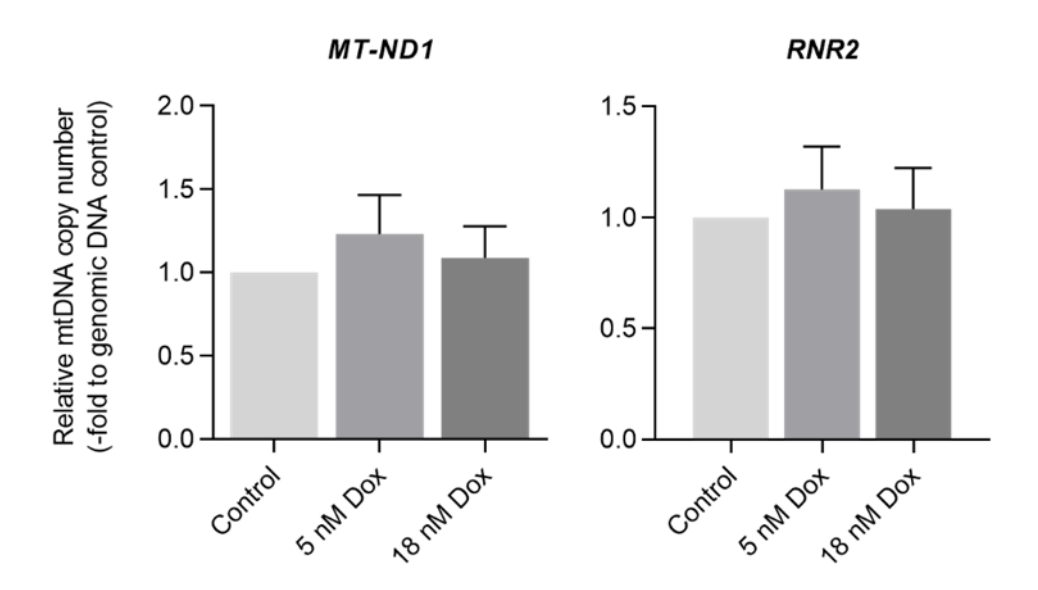


Fig. 27: Nucleoid content and size in iPSCs after short pulse-treatment with doxorubicin. A Representative confocal image of mitochondrial nucleoids ( $\alpha$ -DNA) in human induced-pluripotent

stem cell (iPSC) 48 hours after 2 hours pulse-treatment with 5 nM and 18 nM doxorubicin (Dox). Magnification: x 63, scale bar: 10  $\mu$ M. Zoomed-in regions are marked with a white square. **BC** Quantification of nucleoid distribution within mitochondria ( $\mu$ m² per cell per area, **B**) and size (per  $\mu$ m² of cell, **C**) after Dox treatment was performed using semi-automated system in CellProfiler (4.2.5). Data show mean ± standard error of mean (SEM) from three independent experiments (n=3; N=50 cells). **D** 

Quantification of released mitochondrial mtDNA (nucleoids/ $\mu$ m²/cell after Dox treatment was performed using automated system in CellProfiler (4.2.5). Data show mean  $\pm$  SEM from three independent experiments (n=3; N=50 cells). *One*-way ANOVA was performed. \*P-value  $\leq$  0.05, \*\*\*P-value  $\leq$  0.001, \*\*\*\*P-value  $\leq$  0.0001.

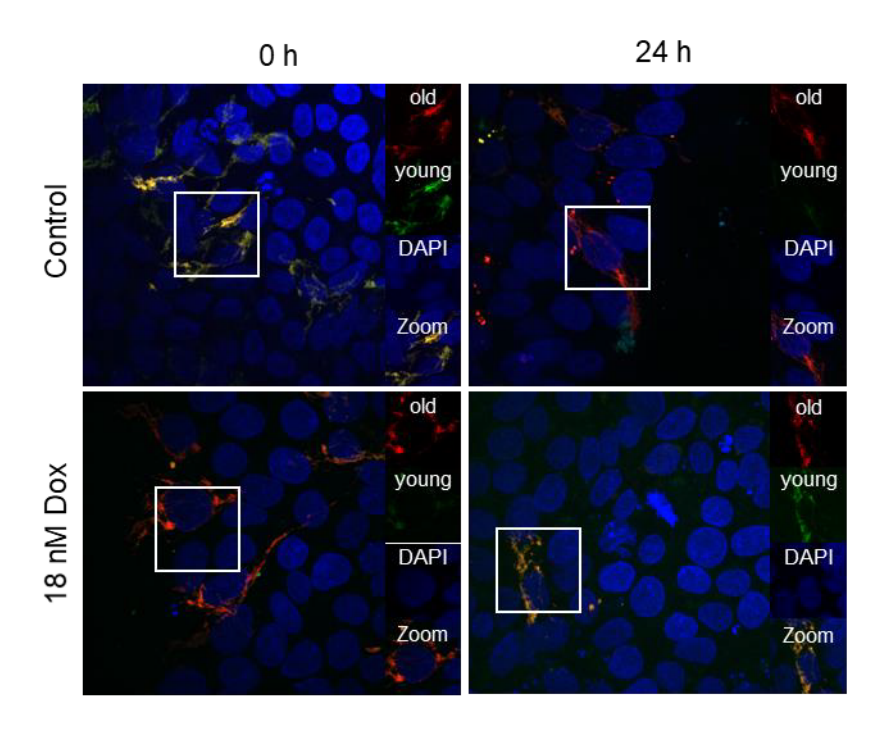
Since pulse-treatment with doxorubicin significantly influenced the number and size of mitochondrial nucleoids, the influence of this treatment on mitochondrial biogenesis was further elucidated. For this, mitochondrial mtDNA copy number was determined via measurement of the ratio between mtDNA-encoded genes, in this case mitochondrial encoded 16S rRNA (RNR2) and NADH-ubiquinone oxidoreductase chain 1 (MTND1), and genomic DNA (gDNA) using quantitative real-time PCR (Fig. 28). Upon treatment of iPSCs with low concentrations of doxorubicin, a present, but not significant tendency, towards an increase in mtDNA copy number was measured. Overall, short pulse-treatment of iPSCs with doxorubicin resulted in remodeling of mitochondrial nucleoids showing a tendency towards nucleoid swelling, yet without influence on mtDNA content.



**Fig. 28: Mitochondrial DNA copy number in iPSCs upon short pulse-treatment with doxorubicin.** Mitochondrial copy number was determined via measuring the expression of mitochondrial-encoded genes mitochondrial encoded 16S rRNA (*RNR2*) and NADH-ubiquinone oxidoreductase chain 1 (*MTND1*) using quantitative real-time PCR 48 hours after 2 hours pulse-treatment of human induced-pluripotent stem cells (iPSCs) with doxorubicin (Dox). Hypoxanthine phosphoribosyltransferase 1 (HPRT1) was used as housekeeping gene. Data as normalized to the respective control. Data shown represents the relative mean ± standard error of mean (SEM) from four independent experiments (n=4; N=3).

Besides its DNA damaging properties, treatment of cells with doxorubicin has been shown to be associated with elevated ROS production (D. Zhang et al., 2018). Increase in mtDNA mutation load due to enhanced production of ROS because of, for an instance, treatment with

chemotherapeutic drugs enhancing the production of ROS, is one of the drivers of mitochondrial aging in cells. To further elucidate whether observed mitochondrial defects might be in direct correlation with mitochondrial aging, aging process of mitochondria in iPSCs was monitored over time via transfection of iPSCs with pMitoTimer (Laker et al., 2014). In more detail, DsRed fluorescence signal representing older mitochondria, while green fluorescence sign representing younger mitochondria (Fig. 29). To determine the aging of mitochondria a ratio between DsRed:Green was determined at defined timepoints after short pulse-treatment with doxorubicin using confocal microscopy using semi-automated pipeline in CellProfiler (4.2.5), mitochondrial aging was determined by measuring the DsRed:Green ratio of the immunofluorescence signal. In contrast to the control group, which exhibited a gradual rise in the DsRed:Green ratio, the doxorubicin treatment group demonstrated a more precipitous and pronounced increase in DsRed signal eight hours after administration indicating an accumulation of older mitochondria. Overall, there was no significant effect on mitochondrial aging detectable which is in line with the low toxicity observed with the treatment conditions applied.



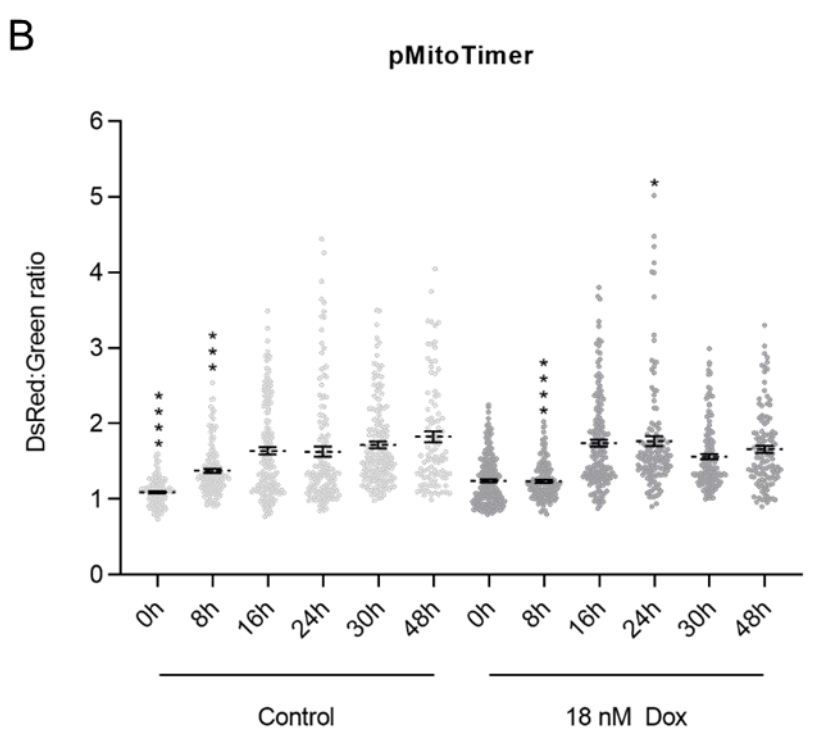


Fig. 29: Measurement of mitochondrial aging in iPSC pulse-treated with doxorubicin.

The aging of mitochondria in short pulse-treated human induced-pluripotent stem cells (iPSCs) with 18 nM doxorubicin (Dox) was measured at defined timepoints via measuring the DsRed-Green fluorescent shift using confocal microscopy. **A** Representative confocal microscopic image of one biological replicate comprising two selected timepoints after treatment with Dox. DsRed-positive mitochondria are marked as "old". Green fluorescent mitochondria are marked as "young". Zoomed-in regions are marked with a white square. **B** Shown is the average DsRed:green ratio of three independent biological replicates of pMitoTimer-transfected iPSCs  $\pm$  standard error of mean (SEM) from three independent experiments (n=3; n=50 cells). *One*-way ANOVA was performed. \*p-value  $\leq$  0.001, \*\*\*\*P-value  $\leq$  0.0001. Significances refer to the comparison to next timepoint.

#### 3.2. Influence of short pulse-treatment with doxorubicin on human iCMs

As seen in the previous result sections (see section 3.1), even short-term exposure of iPSCs to low concentrations of doxorubicin revealed a high sensitivity of these cells against the chemotherapeutic drug. These results indicate that mitochondrial dysfunction plays a major role in the development of this phenotype (see section 3.1.3). Together with previous findings describing cardiomyocytes as major somatic cell types negatively affected by doxorubicin treatment *in vivo* and *in vitro*, we aimed to further understand how moderate pulse-treatment at defined timepoints is affecting the viability and function of cardiac progenitor cells (CPs) and iPSC-derived cardiomyocytes (iCMs). With the establishment of iPSC differentiation into cardiomyocytes the differences between iPSCs, CPs and iCMs in their sensitivity against low concentrations of doxorubicin was further elucidated in a comparable manner. For this, each differentiation stage was treated with doxorubicin concentrations according to their IC<sub>30</sub>-value. Furthermore, mitochondrial morphology was further corroborated in order to understand the influence doxorubicin treatment mitochondria in iCMs.

#### 3.2.1. Establishment of iCMs as robust cardiac model system

For generation of iPSC-derived cardiomyocytes, differentiation of iPSCs into iCMs was based on adaptations of published protocols inducing cardiac differentiation via modulation of Wnt /  $\beta$ -catenine pathway (Balafkan et al., 2020; L. Li et al., 2022; Lian et al., 2012). To initiate cardiac differentiation, stem cell culture media was removed and exchanged by serum-free cardiac basal medium (CBM) supplemented with defined growth factors to initiate cellular commitment into cardiac axis (Fig. 30). At the initial stage of differentiation, differentiation of iPSCs into the mesodermal line was induced by supplementation of CBM without insulin (-INS) and addition of GSK3i (CHIR99021) for two days (CBM-INS1). From day 3 of differentiation, CBM-INS2 was supplemented with IWP4 to induce further differentiation into cardiac mesodermal progenitor cells. From day 5, media was exchanged by CBM containing insulin (+INS) and in addition B-27 supplement to complete cardiac differentiation (CBM+INS). Media was changed every second day. First contracting areas were identified from d7 of differentiation.

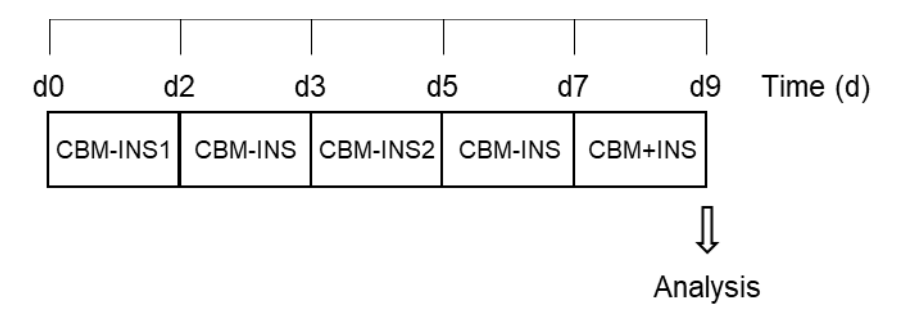


Fig. 30: Scheme for generation of iCMs following a chemical defined protocol.

Schematic illustration differentiation of induced-pluripotent stem cells (iPSCs) into iPSC-derived cardiomyocytes (iCMs) using a chemically defined protocol starting from 'd0' as timepoint of initiation of cardiac differentiation. More detail description of media composition can be found in section 2.2.1.3. d: day, CBM: Cardiac basal medium, -INS: without insulin, +INS: with insulin, CBM-INS1: Mesodermal induction media without insulin containing GSK3i inhibitor CHIR99021, CBM-INS2: Cardiac mesodermal progenitor induction media containing Wnt-inhibitor IWP4, CBM+INS: Cardiomyocyte induction media with insulin, GSK3: Glycogen synthase kinase 3

Differentiation of iPSCs into iCMs was accompanied with morphological changes of cells (Fig. 31). Thereby, in colonies growing iPSCs switched towards a densely growing single cell monolayer within two days after initiation of mesodermal differentiation. During this time, the amount and size of cells increased in size accompanied with a morphological switch towards a triangular shape. With further commitment into cardiac mesodermal line and thereof cardiac progenitor cells (CPs), condensation of cells and resulting formation of cardiac sheets was visible as early as on day 5 of cardiac differentiation protocol (CP d5). On the last day of cardiac differentiation (day 7; iCM d7) of cardiac differentiation, further development of cardiac sheets was visible accompanied with the first visual observation of spontaneously pulsing areas within these sheets. With further progress in differentiation the number of contracting areas within the well increased (day 9; iCM d9).

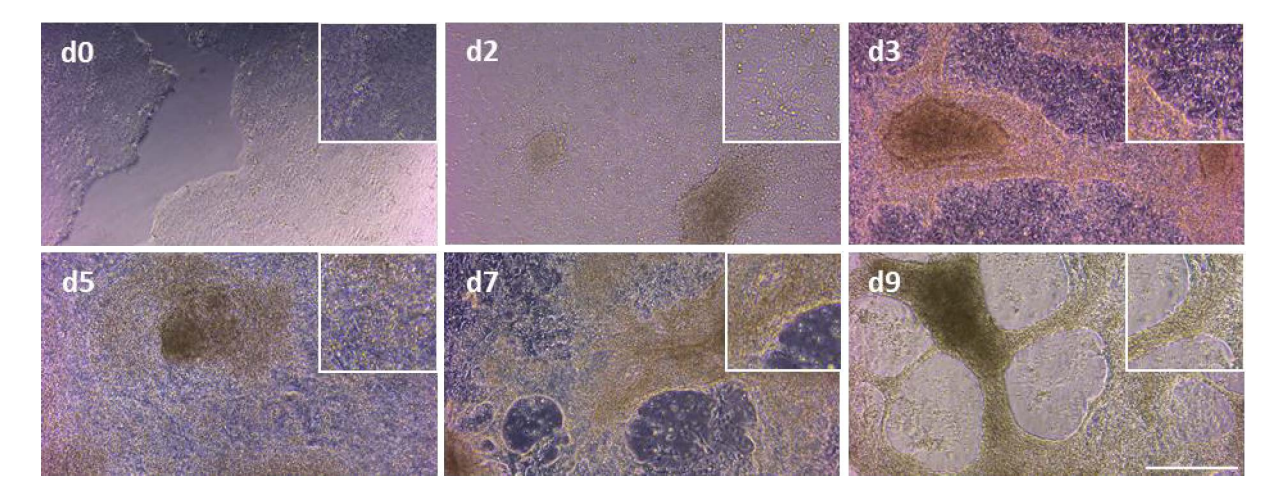


Fig. 31: Morphological changes of cells during cardiac differentiation.

Morphological changes of human induced-pluripotent stem cells (iPSCs) upon cardiac lineage commitment into cardiomyocytes (iCMs). iPSCs growing in colonies are shown in image d0. With initiation of mesodermal induction (d2), images show the changes upon commitment of cells into the

cardiac mesodermal lineage (d2-d5). With completion of cardiac differentiation protocol on day7 (d7), pulsing areas in the cardiac sheets were visible which increased with further progression of cardiac differentiation day9 (d9). Zoomed-in regions are marked with white box. Shown are representative images of one cardiac differentiation. Images were taken with x 40 magnification. Scale bar: 100  $\mu$ M. d: day

Besides described morphological changes, successful differentiation of iPSCs into iCMs was corroborated via measurement of the relative mRNA expression levels of pluripotency markers POU Class 5 Homeobox 1 (*POU5F1*), as well as cardiac-related markers Troponin T2 (*TNNT2*), NK2 Homeobox 5 (*NKX2-5*), Myosin Heavy Chain 6 (*MYH6*) and GATA Binding Protein 4 (*GATA4*). The expression of the mentioned genes was measured in iPSC stage (d0), in cardiac progenitor stage on day 5 (CP d5), and in iCM stage (iCM d7) of cardiac differentiation (Fig. 32). Quantitative analysis revealed suppression of pluripotency genes while relative expression of cardiac markers was enhanced with further progression of cardiac differentiation indicating successful differentiation of iPSCs into iCMs.

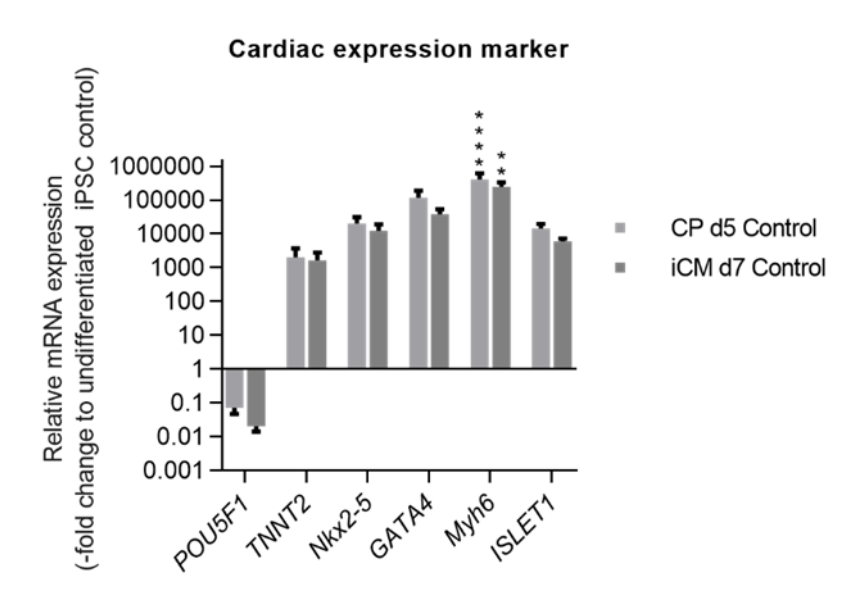


Fig. 32: Characterization of iCMs on mRNA level.

Measurement of mRNA expression of stem cell marker POU Class 5 Homeobox 1 (*POU5F1*) as well as cardiac-related markers Troponin T2 (*TNNT2*), NK2 Homeobox 5 (*NKX2-5*), Myosin Heavy Chain 6 (*MYH6*) and GATA Binding Protein 4 (*GATA4*) in human induced-pluripotent stem cells (iPSCs d0), cardiac progenitor cells (CP d5), and iPSC-derived cardiomyocytes (iCM d7). Relative mRNA expression of undifferentiated iPSCs was set to 1.0. Data shown is the mean ± standard error of mean (SEM) of three independent experiments (n=3; N=3). Unpaired t-test comparing 2 conditions. \*\*P < 0.01 d: day

## 3.2.2. Stable cardiac differentiation even under exposure to doxorubicin at different stages of cardiac differentiation

To determine the sensitivity of iPSC-derived CPs and iCMs, an analogous treatment scheme administered for iPSCs (see section 3.1.1) was applied at defined stages of cardiac differentiation (Fig. 33A). Viability of CPs and iCMs was measured 48 hours after the exposure to various concentrations of doxorubicin using MTT assay (Fig. 33BC). The measurement of susceptibility of CPs and iCMs revealed an overall reduction in the viability of cells in a concentration-dependent manner. Here, with further differentiation of cells, CPs (IC50-value: 80 nM) and iCMs (IC50-value: 512 nM) displayed higher resistance against doxorubicin exposure as compared to their undifferentiated counterparts, where IC50-value was reached with 35 nM Dox (Fig. 15B). Consistent to the treatment scheme applied in iPSCs, CPs and iCMs were treated with a doxorubicin concentration equivalent to IC30-value (namely 27 nM and 144 nM, respectively) in all subsequent experiments. Overall, measurement of viability revealed a higher resistance of CPs and iCMs against pulse-treatment with doxorubicin as compared to their undifferentiated counterparts.

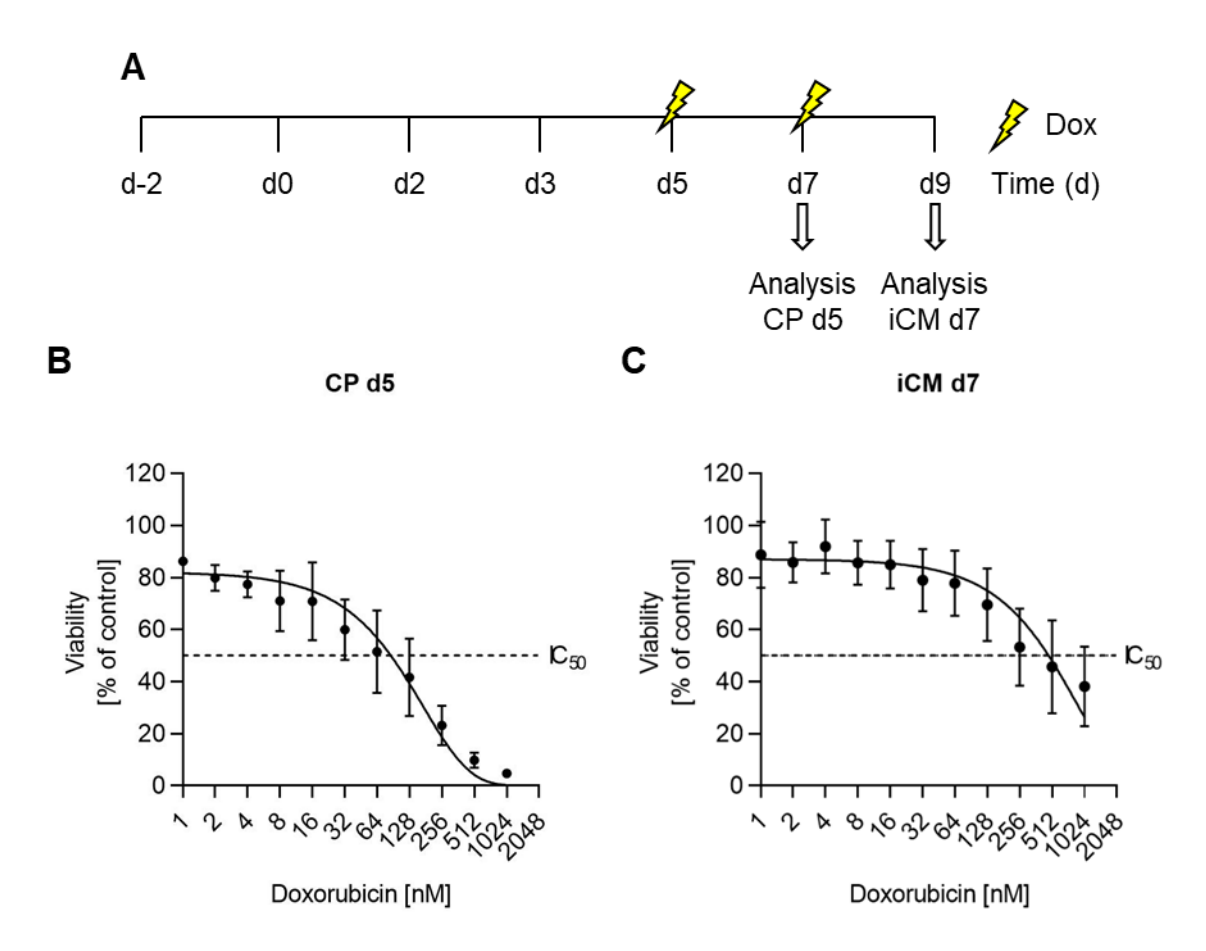


Fig. 33: Viability measurement in CPs and iCMs after doxorubicin treatment.

A Schematic illustration of pulse-treatment with doxorubicin (Dox) at defined timepoints of cardiac differentiation including cardiac progenitor cells (CP d5) and iPSC-derived cardiomyocytes (iCM d7).

Dox pulse-treatment is represented by the lightning symbol. **BC** Quantitative cell viability measurement of cardiac progenitor (CP d5) and iPSC-derived cardiomyocytes on day7 (iCM d7) of cardiac differentiation using MTT assay. The average viability (%) was normalized to the respective control. Shown is the relative viability (%)  $\pm$  standard error of mean (SEM) of three independent experiments (n=3; N=8). Inhibitory concentration of 50 % (IC50) was shown by the dotted line. MTT: (3-[4,5-dimethylthiazol-2-yl]-2,5 diphenyl tetrazolium bromide, d: day

Based on viability measurements, the question was whether exposure of CPs and iCMs towards doxorubicin might be associated with problems in cardiac differentiation progression. Therefore, the relative mRNA expression of cardiac differentiation markers in CPs and iCMs 48 hours after short pulse-treatment with doxorubicin was determined using qRT-PCR. As shown in Fig. 34, relative mRNA expression levels of pluripotency markers were downregulated, while cardiac markers were elevated independent of the timepoint of treatment. Thus, moderate pulse-treatment throughout cardiac differentiation had no influence on the progression of cardiac differentiation.

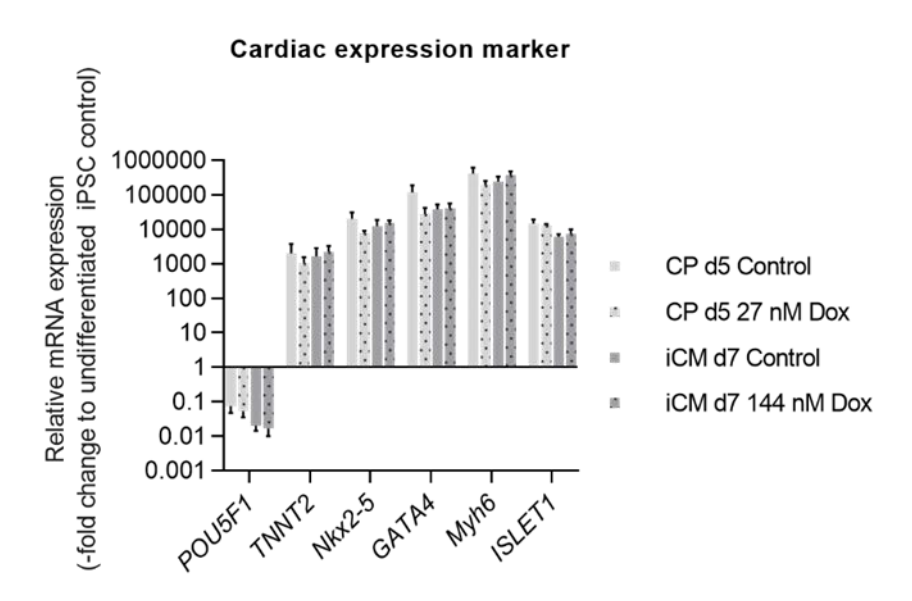


Fig. 34: Expression levels of pluripotency and cardiac markers in CPs and iCMs upon short pulse-treatment with doxorubicin.

Cardiac progenitor cells (CP) and iPSC-derived cardiomyocytes (iCM d7) were pulse-treated with 27 nM and 144 nM doxorubicin (Dox) prior to measurement of relative mRNA expression of pluripotency and cardiac markers. These comprised POU Class 5 Homeobox 1 (*POU5F1*) as well as cardiac-related markers Troponin T2 (*TNNT2*), NK2 Homeobox 5 (*NKX2-5*), Myosin Heavy Chain 6 (*MYH6*), GATA Binding Protein 4 (*GATA4*) and ISL LIM Homeobox 1 (*ISLET1*). All treatment conditions were normalized to untreated human induced-pluripotent stem (iPSC) cell control. Data shown is the mean ± standard error of mean (SEM) of three independent differentiations (n=3, N=4). d: day

In order to corroborate the observations made on mRNA level (Fig. 34), the protein levels of the pluripotency marker Octamer binding-protein 4 (Oct4) and the cardiac marker cardiac-related markers Troponin T2 (cTNT) were determined following short pulse-exposure

to doxorubicin. This was achieved by means of immunohistochemically and Western blot determinations (Fig. 35A-C). In accordance with the previous findings on mRNA expression level, pulse-treatment of CPs and iCMs had no influence on the expression cardiac differentiation marker. Solely for iCMs treatment with doxorubicin resulted in an increase in cTNT expression. However, only untreated iCMs showed initial formation of sarcomeres, which was not visible in doxorubicin-treated iCMs. In the context of the administered concentrations examined in this study, the collective findings suggest that no discernible impact on cardiac differentiation has been observed. However, doxorubicin treatment showed to selectively influence the expression levels of specific cardiac markers with changes in their cellular organization.

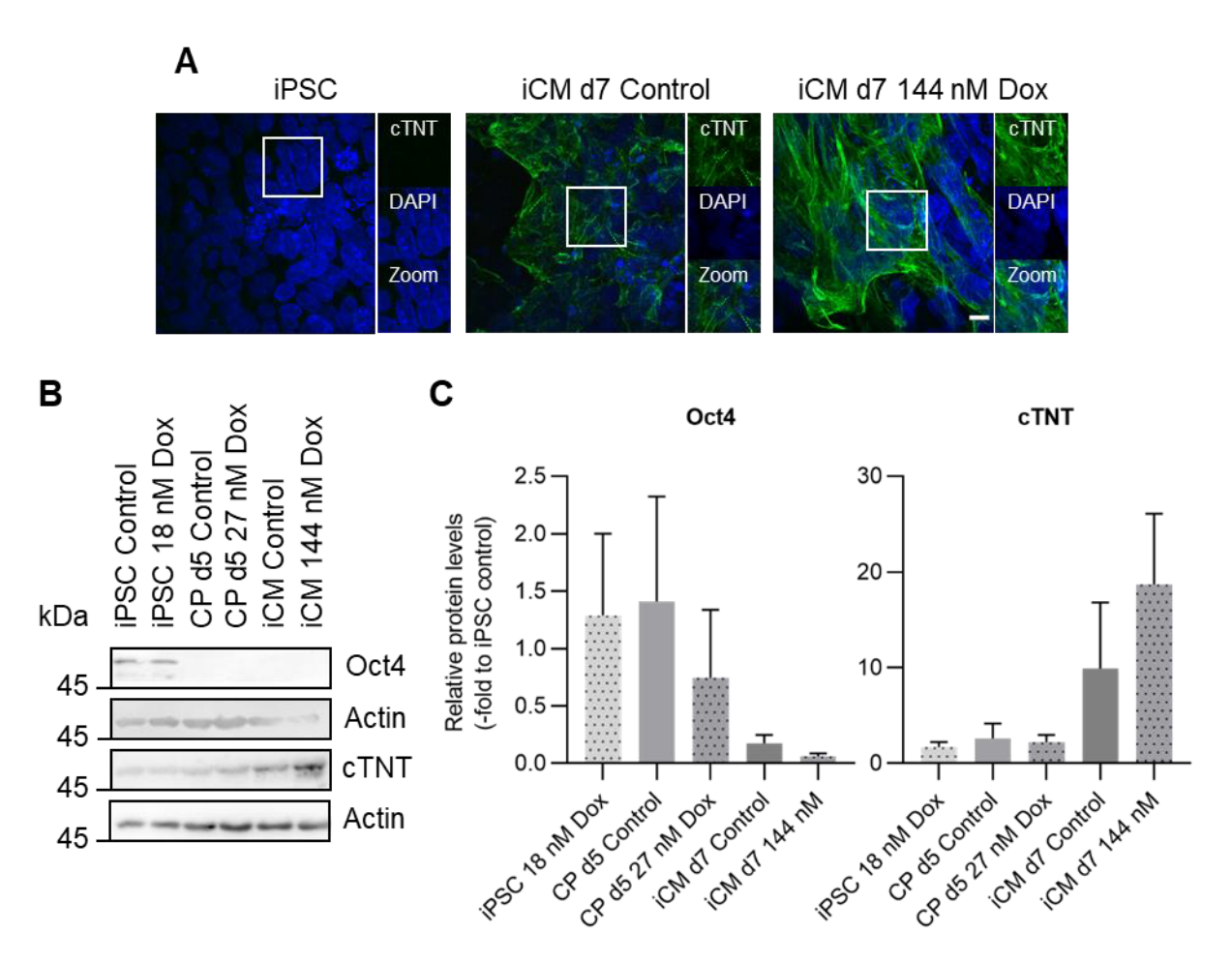


Fig. 35: Protein levels of pluripotency and cardiac markers of in iPSCs, CPs and iCMs upon pulse-treatment with doxorubicin.

Human induced pluripotent stem cells (iPSCs), cardiac progenitor (CPs), and iPSC-derived cardiomyocytes were pulse-treated with the indicated concentrations (respective to IC $_{30}$ -value) prior to determination of protein levels of pluripotency marker POU Class 5 Homeobox 4 (Oct4) and the cardiac marker cardiac-related markers Troponin T2 (cTNT) using immunohistochemical staining and Western blot technique. A Representative image of immunohistochemical detection of cTNT in Dox-treated iCMs and their respective control (n=3). iPSCs served as negative control. DNA was counterstained using DAPI. Magnification: x 20, scalebar: 10  $\mu$ M. Zoomed in regions are marked with a white square. B Representative Western blot of one biological replicate. Treatment conditions and proteins are indicated. C Shown is the quantification of motility proteins. Shown are the relative protein levels  $\pm$  standard error

of mean (SEM) of three independent experiments (n=3) normalized to the respective control. DAPI: 2 (4 amidinophenyl) 1H indole 6 carboxamidine, d: day

#### 3.2.3. Effect of doxorubicin pulse-treatment on mitochondrial function in iCMs

As mentioned in section 1.4.1, mitochondria play a pivotal role as mediators of doxorubicin-induced cardiotoxicity. Thus, the effect of moderate pulse-treatment of iCMs (d7) was further elucidated. For this, cells were pulse-treated with 144 nM doxorubicin (respective to  $IC_{30}$ -value), followed by 48 hours recovery prior to analysis of mitochondrial parameters (see treatment scheme: Fig. 33A).

### 3.2.3.1. Fragmentation of mitochondrial network upon pulse-treatment of iCMs with doxorubicin

In order to understand whether short pulse-treatment with doxorubicin under comparable treatment conditions as iPSCs has an influence on mitochondrial network, mitochondrial morphology in iCMs was assessed. Due to the spontaneous contractility of iCMs, mitochondrial morphology was assessed using immunohistochemical staining against the mitochondrial marker HSP60 (Fig. 36A). Undifferentiated iPSCs served as an undifferentiated counterpart. In general, iCMs showed elevated levels of intermediate and fragmented mitochondria as compared to their undifferentiated counterparts indicating differentiation specific differences in the distribution of mitochondrial network. Upon transient exposure of iCMs towards low concentrations of doxorubicin, mitochondrial morphology shifted significantly towards fragmentation. Thus, even short pulse exposures of iCMs to doxorubicin resulted in strong fragmentation of mitochondrial network, which was still measurable 48 hours after exposure indicating a long persistent effect of the applied treatment conditions on mitochondrial morphology.

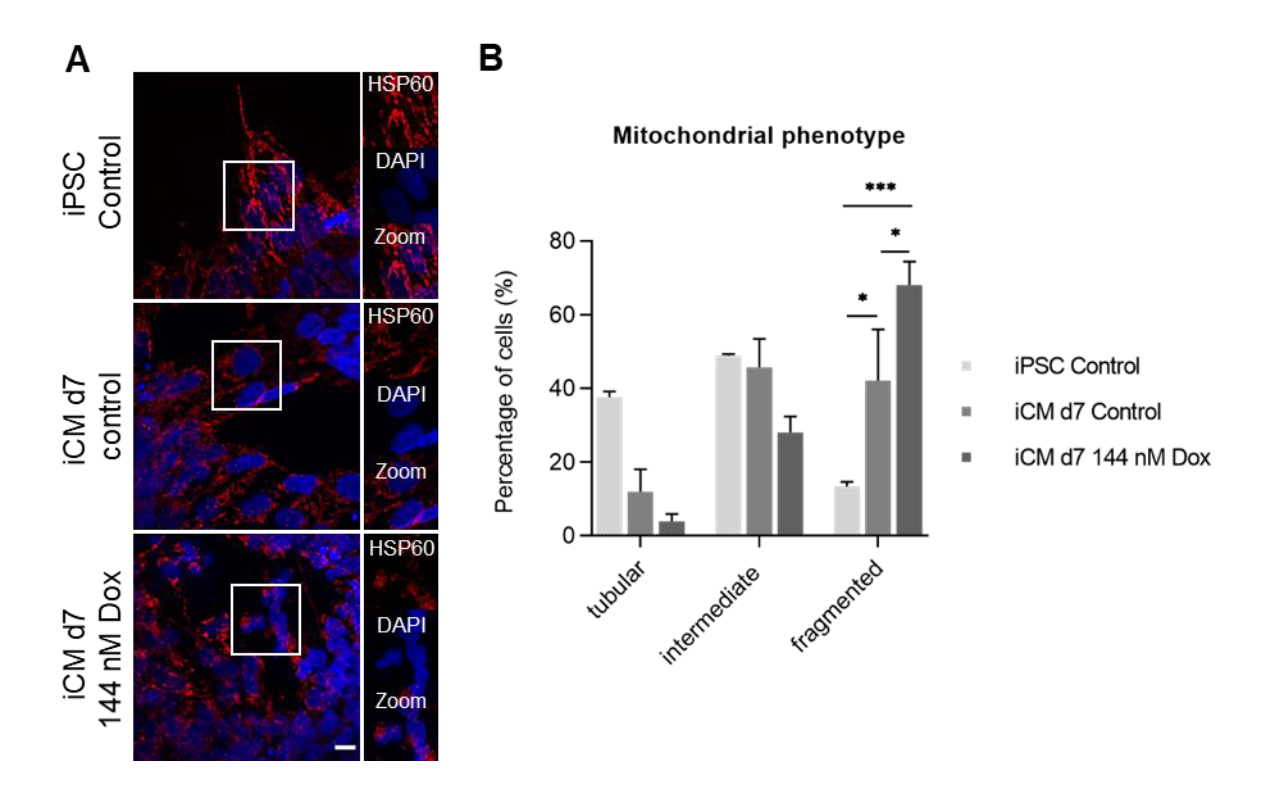


Fig. 36: Mitochondrial morphology in iCMs upon short pulse-treatment with doxorubicin. Mitochondrial morphology in iPSC-derived cardiomyocytes (iCMs d7) was assessed 48 hours after 2 hours pulse-treatment with doxorubicin (Dox) via immunohistochemical staining of mitochondrial marker heat-shock protein 60 (HSP60). A Shown are representative confocal images of mitochondria in control and pulse-treated iCMs. Zoomed-in regions are indicated by a white box. Magnification: x 63, scale bar: 10  $\mu$ m. B Quantification of mitochondrial morphology categorized in tubular, intermediate, or fragmented morphology 48 hours after pulse-treatment with Dox. Data show mean  $\pm$  standard error of mean (SEM) from three independent experiments (n=3; N=75 cells). 2-way ANOVA was performed. \* P-value  $\leq$  0.005, \*\*\* P-value  $\leq$  0.0001. d: day

OPA1 processing is a strong indicator for mitochondrial dynamics and health. Since moderate pulse-treatment of iCMs (iCM d7) with doxorubicin resulted in fragmentation of mitochondrial network, the question was whether this is accompanied with enhanced OPA1 processing. Thus, the ratio between short (s-OPA1) and long OPA1 (I-OPA1) isoforms upon doxorubicin treatment was determined throughout different stages of cardiac differentiation comprising iPSC stage, CP (CP d5) stage and iCM (iCM d7) stage (Fig. 37A). Overall, pulse-treatment with doxorubicin had no influence on the ratio between s-OPA1 and I-OPA1. However, it is noteworthy that solely in CP stage the s-OPA1:I-OPA1 ratio was higher than compared to their undifferentiated and differentiated counterparts. Together this shows that in all stages of cardiac differentiation there was no processing of OPA1 visible even 48 hours after treatment. However, it cannot be excluded that 48 hours of recovery could be sufficient to replenish I-OPA1 isoforms indicating that OPA1 processing might be detectable at an earlier timepoint after treatment. Although doxorubicin treatment did not result in enhanced OPA1 processing, the increased s-OPA1:I-OPA1 ratio in CPs might hint towards an important role of OPA1 during

early timepoints of cardiac differentiation. Thus, in progenitor stage the delicate balance between fusion and fission processes of mitochondria might play an important role in cell homeostasis and progression of cardiac differentiation.

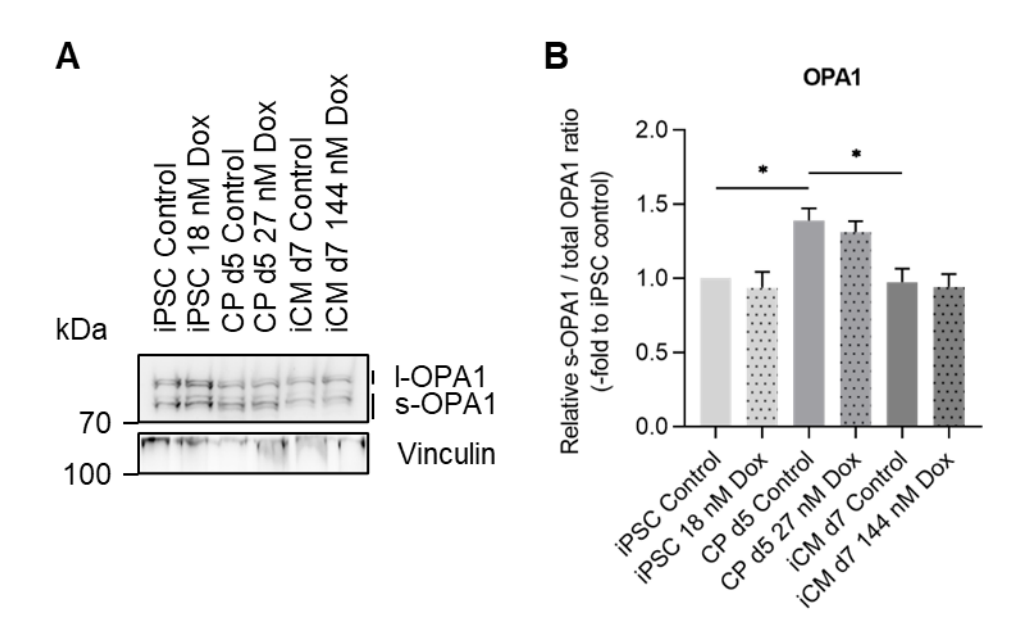


Fig. 37: Relative protein levels of the mitochondrial fusion factor OPA1 in iCMs pulse-treated with doxorubicin.

OPA1 protein levels in induced-pluripotent stem cells (iPSCs d0), cardiac progenitors (CP d5), and iPSC-derived cardiomyocytes (iCM d7) was determined after 2 hours pulse-treatment with doxorubicin (Dox). A Representative blot showing OPA1 protein levels from one biological replicate. B Quantitative analysis of the ratio between short-OPA1 isoforms (s-OPA1) and total OPA1 isoforms. Data shown are the relative protein levels of three independent experiments  $\pm$  standard error of mean (SEM) which were normalized to the respective iPSC control (n=3). *One*-way ANOVA was performed. \* P-value  $\leq$  0.05. d: day

#### 3.2.3.2. Pulse-treatment with doxorubicin is sufficient to reduce mitochondrial content in iCMs

As previously seen in iPSCs, disturbance of mitochondrial network has been shown to be directly connected to mitochondrial dysfunction composed of loss in mitochondrial membrane potential (Fig. 20), changes in mitochondrial dynamic proteins (Fig. 21) and reduction in mitochondrial respiration (Fig. 23), as well as architectural changes of mtDNA. In iCMs, it became visible that mitochondrial content seemed to be affected even upon exposure of low concentrations of doxorubicin (Fig. 36). To further elucidate whether mtDNA copy number was affected upon treatment of iCMs to doxorubicin, mitochondrial copy number was determined via qRT-PCR of mtDNA-encoded genes *RNR2* and *MTND1* (Fig. 38). In accordance to the observed fragmentation of mitochondria upon-treatment with doxorubicin, mtDNA copy number significantly reduced. This indicates that even 48 hours after doxorubicin treatment,

mitochondrial morphology is drastically altered indicating a persistent effect of doxorubicin on mitochondrial content and function in iCMs.

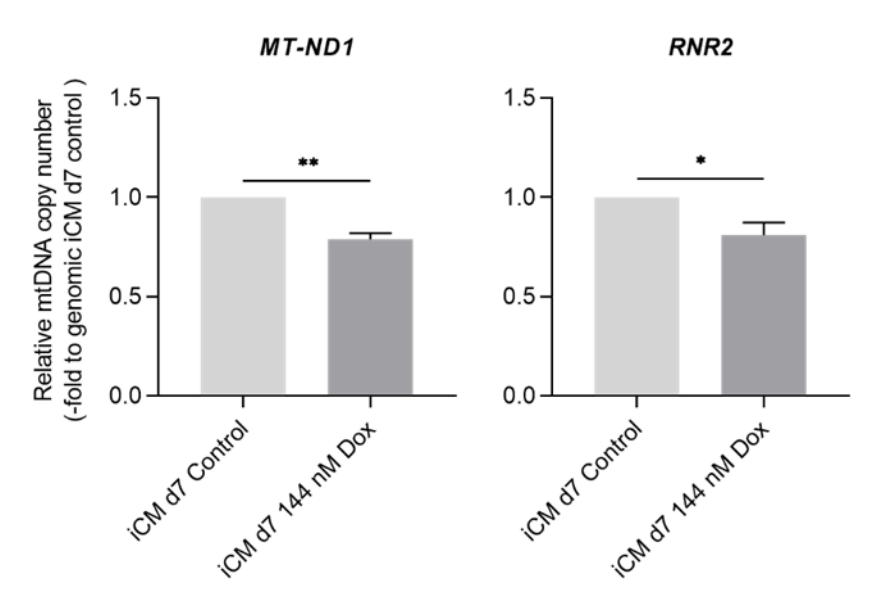


Fig. 38: Mitochondrial DNA in iCMs pulse-treated with doxorubicin.

Mitochondrial copy number was determined via measuring the expression of mitochondrial-encoded genes mitochondrial encoded 16S rRNA (*RNR2*) and NADH-ubiquinone oxidoreductase chain 1 (*MTND1*) using qRT-PCR 48 hours after 2 hours pulse-treatment of iPSC-derived cardiomyocytes (iCMs d7) with doxorubicin (Dox). Hypoxanthine Phosphoribosyltransferase 1 (*HPRT1*) was used as housekeeping gene. Data as normalized to the respective control. Data shown represents the relative mean ± standard error of mean (SEM) from three independent experiments (n=3; N=3).

### 3.3. Whole genome transcriptome profiling of iPSCs and iCMs upon exposure to low concentrations of doxorubicin

The present study has demonstrated that treatment of both iPSCs and iCMs is linked to cellular dysfunction, particularly mitochondrial dysfunction, despite a brief exposure duration. In the subsequent section, the objective is to illuminate the impact of doxorubicin on the transcriptional response of the cells, with the aim to gain further insight into the underlying differential response of iPSCs and iCMs. In accordance with this concept, in addition to the prevailing treatment regimen for iPSCs and iCMs, further treatment regimens were introduced to investigate the influence of doxorubicin-treatment during the early development of the mesodermal lineage and its impact on the resulting cardiomyocytes. Furthermore, the concept of a putative 'hormesis' or 'pre-conditioning' effect was introduced. The latter comprises the idea that doxorubicin treatment in iPSC stage prior to cardiac differentiation could possibly lead to an activation of stress responses, which possibly lead to an advantage (or disadvantage) with regard to a second encounter of iCMs towards doxorubicin.

### 3.3.1. Doxorubicin pulse-treatment of iPSCs results in suppression of genes relevant for metabolism and cellular homeostasis

Based on the previously described findings, mitochondrial function is strongly impaired by the exposure of iPSCs towards doxorubicin (Fig. 23). Therefore, the question was which transient transcriptional response is activated and whether genes associated with metabolic processes directly linked to mitochondria might be modulated upon this treatment. According to the treatment scheme, iPSCs were pulse-treated for 2 hours with a doxorubicin concentration equivalent to IC<sub>30</sub>-value (18 nM) followed by whole genome transcriptome profiling 48 hours after recovery (Fig. 39A). Here, mock-treated iPSCs served as a control. Within the respective replicates a high homogeneity was revealed by multidimensional scaling (Fig. 14). From the short read-NGS RNAseq dataset, the expression levels of 16198 genes were detected. To elucidate the influence doxorubicin pulse-treatment on the transient transcriptional response of iPSCs, a pairwise comparison between pulse-treated iPSCs (iPSC Dox) and mock-treated iPSCs (iPSC Mt) was conducted. This comparison resulted in significant upregulation of 753 and downregulation of 519 genes (see Tab. 16). Upon doxorubicin treatment of iPSCs no significant genes were elevated as shown by GO-term enrichment analysis of biological processes (BP). However, analysis of significantly downregulated genes revealed enrichment in genes associated with various biological processes, such as negative regulation of protein modification, cytoplasmic translation, response to interleukin-7, and pyruvate metabolic process (Fig. 39B). Genes including several ribosomal genes and eukaryotic initiation factors involved in cytoplasmic translation were significantly downregulated. Likewise Lin-28 Homolog A (LIN28A), a major modulator of metabolism and essential player in transcriptional regulation of pluripotency genes, was downregulated (Peng et al., 2011; J. Zhang et al., 2016). Among the list of genes associated with negative regulation of protein modification, Ubiquitin Protein Ligase E3 Component N-Recognin 5 (UBR5) and Sirtuin 1 (Sirt1) were found to be downregulated. Additionally, treatment with doxorubicin in iPSCs was also accompanied with suppression in genes crucial during processes in embryogenesis, such as SRY-Box Transcription Factor 4 (SOX4). Overall, suppression of genes within the described processes hint towards dysregulation of cellular protein homeostasis and cell fate. Furthermore, exposure to doxorubicin was accompanied with downregulation of genes encoding for major metabolic regulators, such as hexokinase 1 (HK1), pyruvate dehydrogenase kinase 1 (PDK1), phosphoglucomutase 1 (PGM1), pyruvate dehydrogenase E1 subunit beta (PDHB), and hypoxia inducible factor 1 subunit alpha (HIF1A). Accordingly, pairwise comparison revealed a clear doxorubicin -induced trend towards metabolic alteration in iPSCs, especially glycolysis and downstream pathways within mitochondria. In sum, even short pulse-treatment with low

concentrations of doxorubicin is sufficient to induce transient downregulation in genes playing a pivotal role in regulation of cell homeostasis and major metabolic pathways in iPSCs.

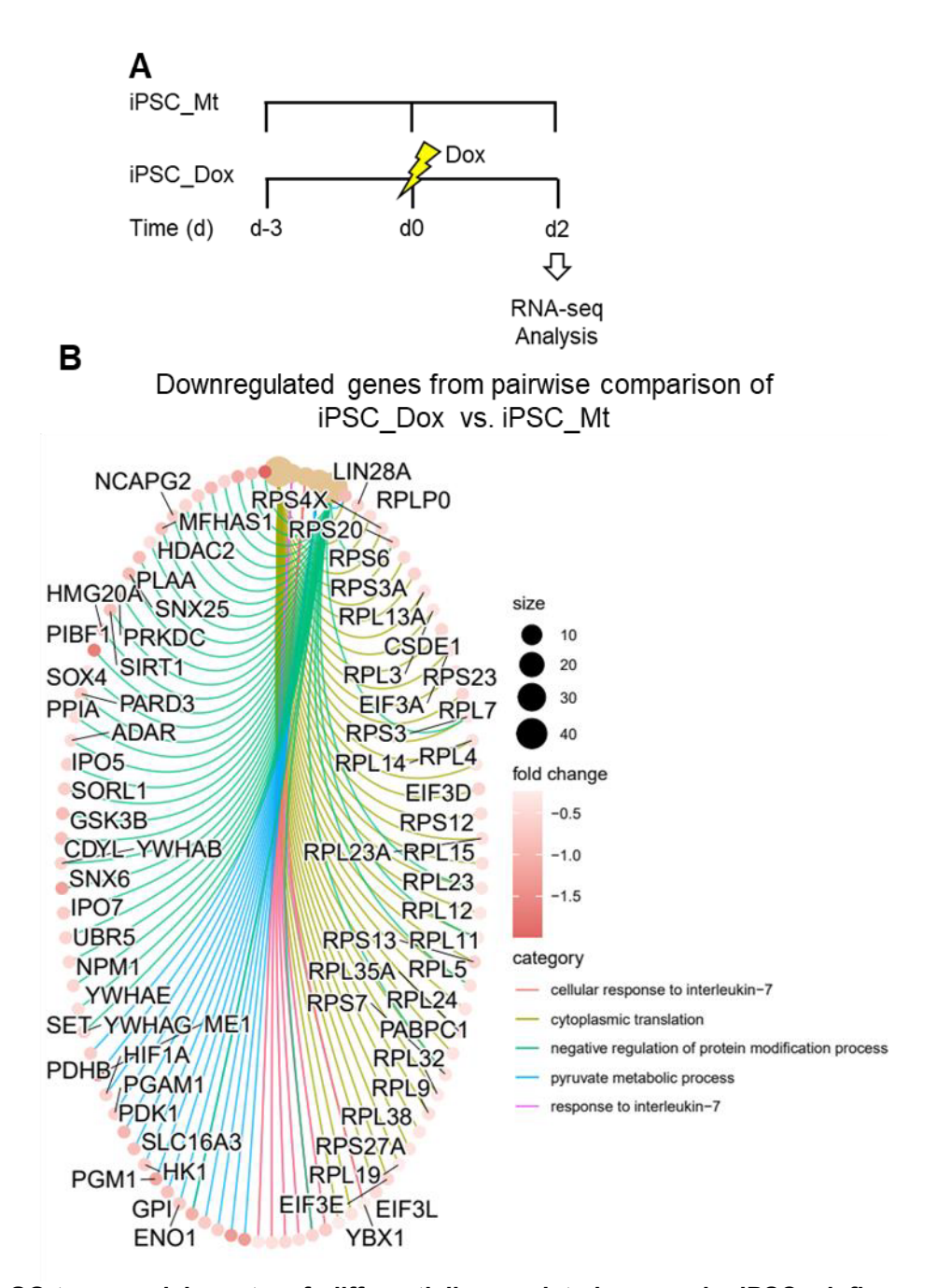


Fig. 39: GO-term enrichments of differentially regulated genes in iPSCs influenced upon pulse-treatment with doxorubicin.

**A** Schematic illustration of the treatment scheme in induced-pluripotent stem cells (iPSCs) prior to short-read-NGS RNAseq analysis 48 hours after pulse-treatment (d2). Timepoint of 2 hours pulse-treatment with 18 nM doxorubicin (Dox) and timepoint of RNA-seq analysis is indicated by a lightning symbol. **B** Gene concept network of GO-term enrichments and associated downregulated genes of pairwise comparison between Dox-treated iPSCs and the respective control. Number of genes, logFC-value, and GO-terms are listed in the respective legend. Mt: Mock-treatment, d: day

### 3.3.2. Differentiation of iPSCs into cardiomyocytes is not affected upon doxorubicin treatment throughout cardiac differentiation

Administration of doxorubicin as chemotherapeutic agent during cancer treatment has been described to be accompanied with long-term cardiotoxicity manifesting even years after the treatment. Until today it is rather unclear whether the cardiotoxicity is mainly induced by toxic effects on terminally differentiated cardiomyocytes or whether the regeneration capacity and thereof tissue regeneration via cardiac stem cell differentiation (CSCs) is altered upon the treatment with doxorubicin. In the following part, four different treatment regimens of iCMs with doxorubicin were established in order to perform short read-NGS RNAseq (Fig. 40A). Treatment conditions described for iPSCs were simultaneously performed and included in the analysis (Fig. 39). To further elucidate whether damage already induced by treatment in iPSCs stage has an influence on the differentiation and function of iCMs, iPSCs were pulse-treated with doxorubicin concentrations respective to IC<sub>30</sub>-value in iPSCs (18nM) prior to initiation of cardiac differentiation (iCM Dox Mt). To determine the effect of doxorubicin pulse-treatment on terminally differentiated cardiomyocytes, generated iCMs were pulse-treated with 144 nM (respective to IC<sub>30</sub>-value) for 2 hours followed by 48 hours recovery before further analysis (iCM Mt Dox). Furthermore, to understand the influence of pre-conditioning of iCMs on transcriptome level, cells were treated in iPSC stage prior to cardiac differentiation and on day 7 of cardiac differentiation with the respective IC<sub>30</sub>-values of Dox (iCM\_Dox\_Dox). Here, all described treatment conditions (iCM Dox Mt, iCM Mt Dox, iCM Dox Dox) were compared to a mock-treated control cardiac differentiation (iCM Mt Mt). Pulse-treatment with concentrations of doxorubicin resulted in a high number of significantly differential regulated genes (DEGs), which were detected upon analysis of genes received from whole genome transcriptome profiling (Tab. 16, Tab. 17). The ensuing changes on transient expression are systematically discussed in the following sections.

First, to ensure that differentiation iPSCs into iCMs is not affected upon application of mentioned treatment schemes, cardiac differentiation was examined in more detail. Independent of the timepoint of treatment with doxorubicin, cardiac differentiation was not impaired as cellular morphology and the autonomous beating of iCMs appeared to be normal. In line with these observations, no significant effect on the relative mRNA expression levels of pluripotency markers POU class 5 homeobox 1 (*POU5F1*), Nanog homeobox (*NANOG*) and cardiac-related markers Troponin T2 (*TNNT2*), NK2 homeobox 5 (*NKX2-5*), Myosin Heavy Chain 6 (*MYH6*) and GATA binding protein 4 (*GATA4*) was observable (Fig. 40B). Furthermore, multidimensional scaling of whole genome transcriptome profiling revealed a clear segregation between all six groups with high homogeneity within the replicates (Fig. 14). By analysis of the RNA-seq 16198 were found to be significantly differential regulated. Upon performance of

hierarchical clustering of all treatment conditions, a strong separation between gene clusters of iPSCs and iCMs was revealed indicating changes in transient expression induced by the differentiation process itself (Fig. 40C). In sum, successful differentiation of iPSCs into iCMs was confirmed as the expression of cardiac markers was also reflected within the set of analyzed DEGs thereof revealing that cardiac lineage commitment is possible independent of the timepoint of doxorubicin application.

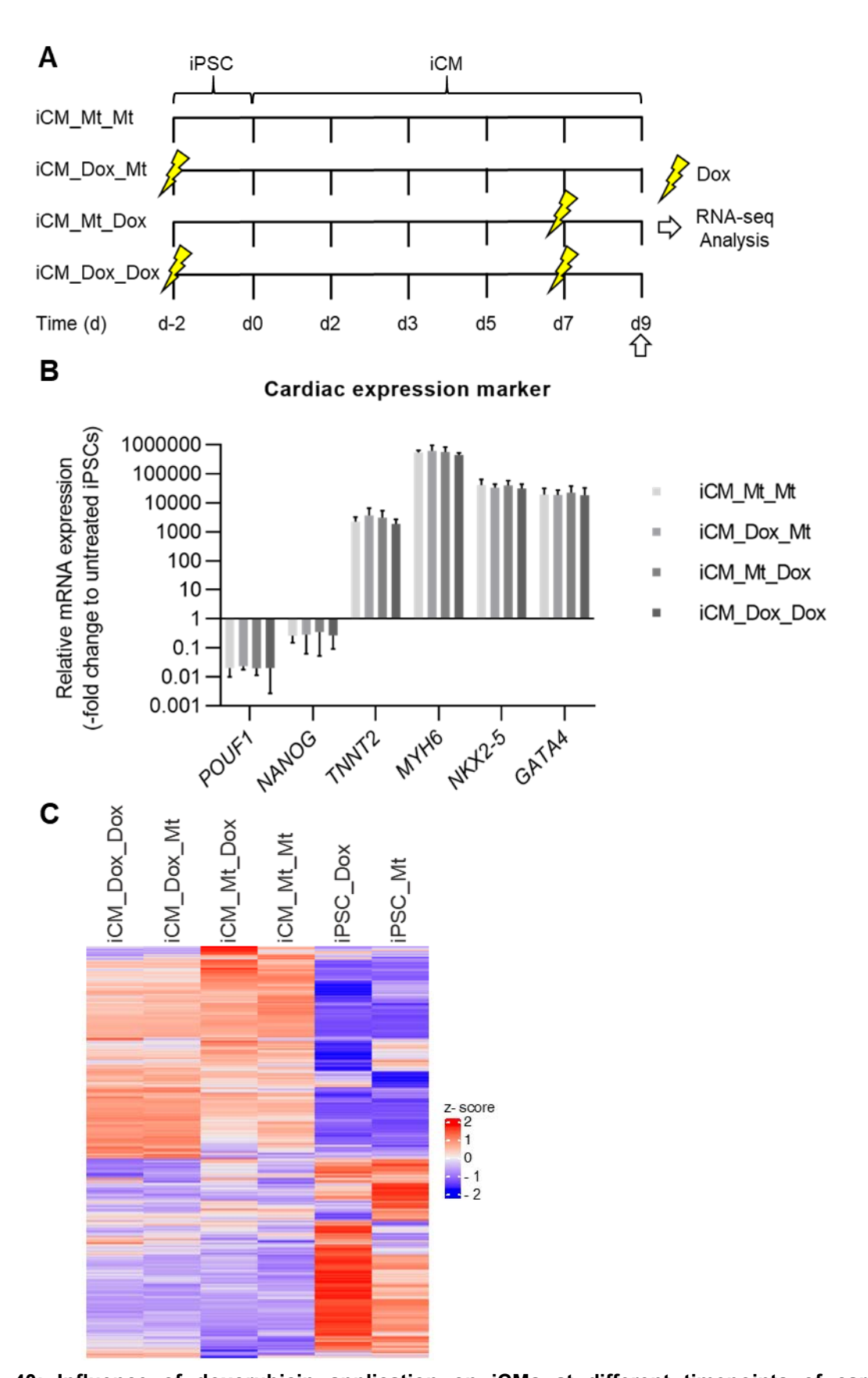


Fig. 40: Influence of doxorubicin application on iCMs at different timepoints of cardiac differentiation.

 $\bf A$  Schematic illustration of doxorubicin (Dox) pulse-treatment scheme for iPSC-derived cardiomyocytes (iCMs) prior to whole genome transcriptome profiling. Briefly, all samples were pulse-treated for 2 hours with respective IC<sub>30</sub>-values of Dox before RNA-seq analysis on day 9 of cardiac differentiation. Following

samples were investigated: Cells treated in iPSC stage (iCM\_Dox\_Mt), on day 7 of cardiac differentiation (iCM\_Mt\_Dox), and pre-treated in iPSC stage prior to a second pulse-treatment on day 7 of cardiac differentiation (iCM\_Dox\_Dox). All conditions were compared to mock-treated cardiac differentiation (iCM\_Mt\_Mt). Dox pulse-treatment is represented by the lightning symbol. **B** Analysis of relative mRNA expression levels of pluripotency markers POU Class 5 Homeobox 1 (*POU5F1*), Nanog Homeobox (*NANOG*) and cardiac-related markers Troponin T2 (*TNNT2*), NK2 Homeobox 5 (*NKX2-5*), Myosin Heavy Chain 6 (*MYH6*) and GATA Binding Protein 4 (*GATA4*) using quantitative real-time PCR. All expression levels were normalized to a mock-treated iPSC control. Shown is the mean relative expression ± standard error of mean (SEM) of three independent experiments (n=3; N=4). **C** Heatmap of all 16198 genes detected in the indicated treatment conditions. The average z-score is given of all four technical replicates in all conditions scaled per gene. Mt: Mock-treatment

### 3.3.3. Major differences in the transcriptional response to doxorubicin pulse-treatment between iPSCs and iCMs

As seen with the relative mRNA expression data of iCMs (Fig. 40B), cardiac differentiation is largely unaffected upon exposure doxorubicin. Therefore, the question was how the transcriptional response of iCMs is affected by pulse-treatment with doxorubicin and differs to their undifferentiated counterparts. By performance of pairwise comparison between doxorubicin-treated iPSCs (iPSC Dox) and iCMs treated on day 7 (iCM Mt Dox) to their respective mock-treated control (iPSC Mt Mt and iCM Mt Mt), DEGs significantly affected by doxorubicin treatment were determined and a pairwise comparison between the determined DEGs was performed to elucidate the similarities and differences in the transient response of iPSCs and iCMs towards doxorubicin pulse-treatment (Fig. 41, Fig. 42) This comparison resulted in the significant upregulation of 842 genes, while 606 genes were significantly downregulated (Fig 41B, Fig. 42B; Tab. 17). Solely 10 significant DEGs were shared by both treatment conditions, whereas the number of significantly DEGs was elevated for the specific transcriptional response of each treated cell type. Interestingly, cell specific transient response was accompanied by a higher number of significant DEGs in iPSCs (1262) than compared to their differentiated counterparts (176). GO-term enrichment of biological processes (BP) resulted in similar gene enrichments as previously described for pulse-treated iPSCs (Fig. 39B). In direct comparison, the number of significant DEGs was much lower in iCMs as pulse-treatment of these cells was accompanied with upregulation of 89 genes, while 87 were downregulated. Here, GO-term enrichment of biological processes (BP) of significant upregulated DEGs was associated with embryonic morphogenesis and kidney development (Fig. 41C). Among these functional terms, T-Box transcription factor 1 (TBX1), SIX homeobox 1 (SIX1), sonic hedgehog signaling molecule (SHH), and repulsive guidance molecule BMP co-receptor A (RGMA) were found to be elevated hinting towards the upregulation of processes directly linked to embryogenesis when cells were treated with doxorubicin. Analysis of significantly downregulated DEGs by GO-term enrichment revealed the suppression of genes playing a role in cardiac muscle development, heart contraction, muscle cell development, muscle tissue development, and striated muscle tissue development (Fig. 42C). Repressed genes associated with these terms, were gap junction protein alpha 5 (*GJA5*), nebulin related anchoring protein (*NRAP*), and hyperpolarization activated cyclic nucleotide gated potassium channel 4 (*HCN4*). Here, suppression of these genes hints towards alteration in establishment of an electrochemical gradient and cell-cell contacts necessary for cardiac function. Comprehensively, iPSCs and iCMs showed distinct differences in their transcriptional response towards doxorubicin pulse-treatment. Interestingly, doxorubicin-induced effects observed on GO-terms associated with metabolic processes in iPSCs were not seen in iCMs hinting towards cell-type specific effects transcriptional responses upon doxorubicin treatment.

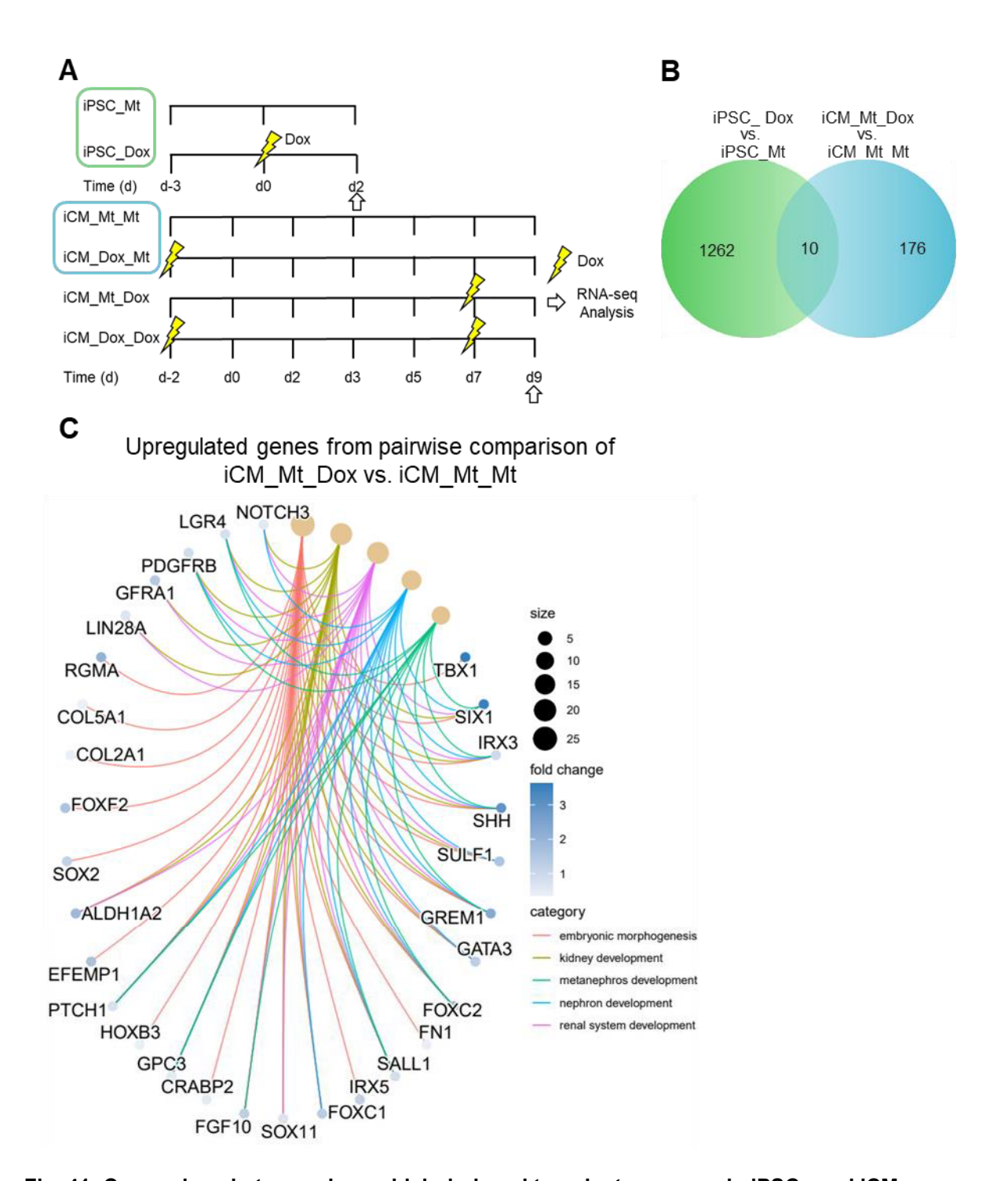


Fig. 41: Comparison between doxorubicin-induced transient response in iPSCs and iCMs.

A Schematic illustration of doxorubicin (Dox) pulse-treatment scheme for human induced-pluripotent stem cells (iPSCs) and iPSC-derived cardiomyocytes (iCMs) prior to whole genome transcriptome profiling. Briefly, all samples were pulse-treated for 2 hours with respective IC<sub>30</sub>-values of Dox before RNA-seq analysis 48 hours after treatment or on day 9 of cardiac differentiation. Following samples were investigated: iPSCs treated with doxorubicin (iPSC\_Dox), cells treated in iPSC stage (iCM\_Dox\_Mt), on day 7 of cardiac differentiation (iCM\_Mt\_Dox), and pre-treated in iPSC stage prior to a second pulse-treatment on day 7 of cardiac differentiation (iCM\_Dox\_Dox). All conditions were compared to mock-treated cardiac differentiation (iCM\_Mt\_Mt). Dox pulse-treatment is represented by the lightning symbol. B Venn diagram of pairwise comparison of significantly upregulated differential regulated genes (DEGs) between human pluripotent-induced stem cells (iPSCs) and iPSC-derived cardiomyocytes (iCMs) pulse-treated on in iPSC stage (iPSC\_Mt) and on day 7 of cardiac differentiation (iCM\_Mt\_Dox), respectively. C Gene concept network of GO-term enrichment of biological processes

(BP) comprising genes found to be specifically upregulated for pulse-treated iCMs (iCM\_Mt\_Dox). Number of genes, logFC-value, and GO-terms are indicated. logFC: log-fold change, Mt: Mock-treatment

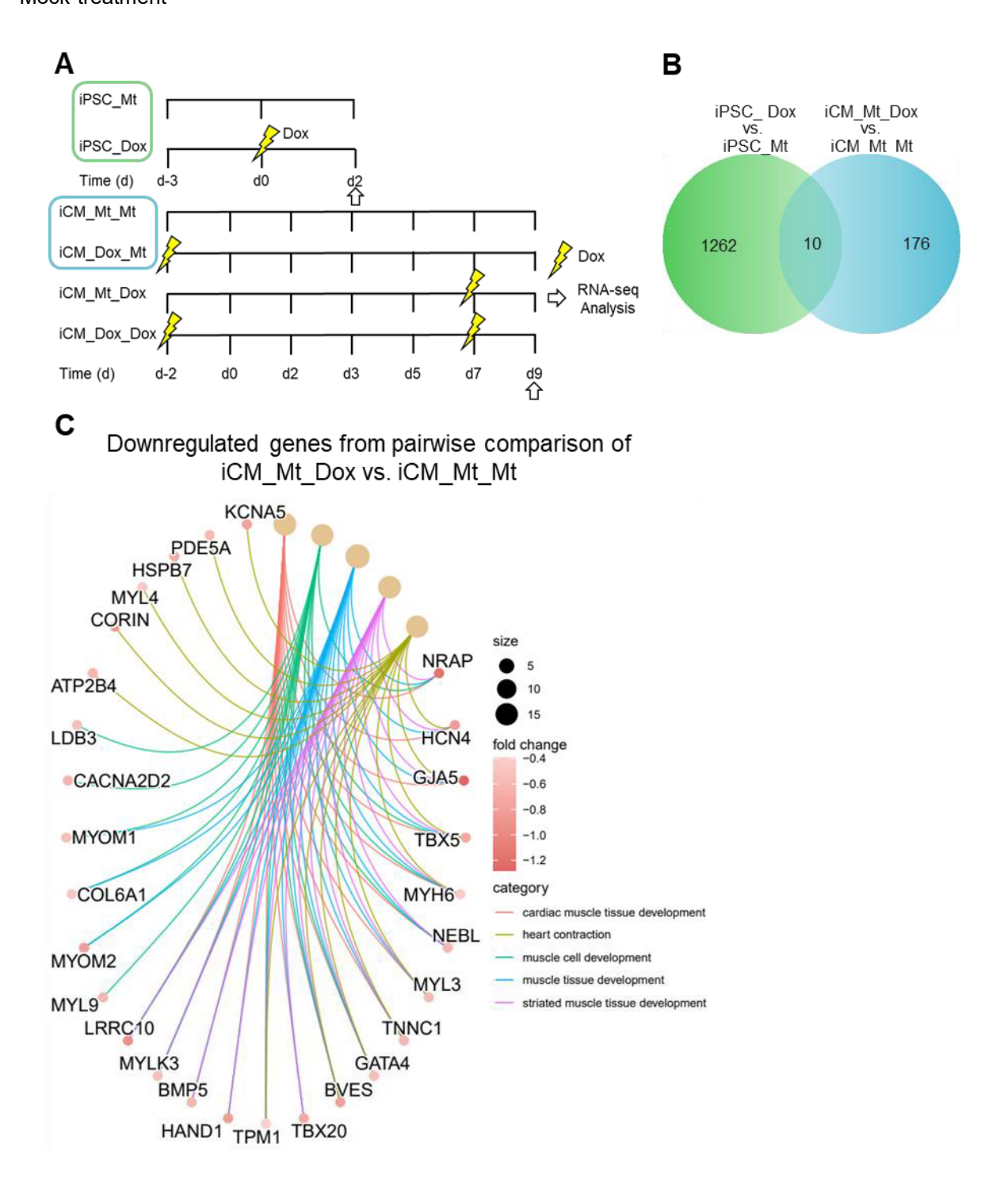


Fig. 42: Comparison between doxorubicin-induced transient response in iPSCs and iCMs.

A Schematic illustration of doxorubicin (Dox) pulse-treatment scheme for human induced-pluripotent stem cells (iPSCs) and iPSC-derived cardiomyocytes (iCMs) prior to whole genome transcriptome profiling. Briefly, all samples were pulse-treated for 2 hours with respective IC<sub>30</sub>-values of Dox before RNA-seq analysis 48 hours after treatment or on day 9 of cardiac differentiation. Following samples were investigated: iPSCs treated with doxorubicin (iPSC\_Dox), cells treated in iPSC stage (iCM\_Dox\_Mt), on day 7 of cardiac differentiation (iCM\_Mt\_Dox), and pre-treated in iPSC stage prior to

a second pulse-treatment on day 7 of cardiac differentiation (iCM\_Dox\_Dox). All conditions were compared to mock-treated cardiac differentiation (iCM\_Mt\_Mt). Dox pulse-treatment is represented by the lightning symbol. **B** Venn diagram of pairwise comparison of significantly upregulated differential regulated genes (DEGs) between human pluripotent-induced stem cells (iPSCs) and iPSC-derived cardiomyocytes (iCMs) pulse-treated on in iPSC stage (iPSC\_Mt) and on day 7 of cardiac differentiation (iCM\_Mt\_Dox), respectively. **C** Gene concept network of GO-term enrichment of biological processes (BP) comprising genes found to be specifically downregulated for pulse-treated iCMs (iCM\_Mt\_Dox). Number of genes, logFC-value, and GO-terms are indicated. logFC: log-fold change, Mt: Mock-treatment

Since previous data revealed alteration of metabolic function in iPSCs by pulse-treatment with doxorubicin, a target-oriented analysis of our transcriptional data was performed. For this, based on a defined gene set for glycolysis and gluconeogenesis from Harmonizome 3.0 hierarchical clustering of all transcriptome condition was performed (Rouillard et al., 2016). Here, a reciprocal effect in the transcriptional regulation of essential genes of glycolysis between iPSCs and iCMs could be seen independent of the time point of treatment (Fig. 43A). Thereby, within this cluster of genes reciprocal regulated genes were Hexokinase 1 (*HK1*), Glyceraldehyde-3-phophatase dehydrogenase (*GAPDH*), fructose bisphosphate aldolase A (*ALDOA*), fructose bisphosphate aldolase C (*ALDOC*), lactate dehydrogenase (*LDHA*), and phosphoglycerate kinase 1 (*PGK1*). Similar effects were observable upon targeted analysis with a Harmonizome3.0 derived list of genes associated with oxidative phosphorylation (OXPHOS; Fig. 43B). Interestingly, solely in iPSCs all mitochondrial encoded genes (*MT-ATP6*, *MT-ATP8*, *MT-CO1*, *MT-CO2*, *MT-CO3*, *MT-CYB*, *MT-ND1*, *MT-ND2*, *MT-ND3*, *MT-ND4*, *MT-ND5*, and *MT-ND6*) were robustly upregulated.

In sum, major differences in the transcriptional response of iPSCs and iCMs were observable when cells were pulse-treated with doxorubicin. While in iCMs transcriptional response was accompanied with downregulation of genes essential for cardiac function, in iPSCs majorly metabolic processes such as glycolysis and OXPHOS were negatively affected. Especially the latter effect seemed to be regulated in a reciprocal manner as this effect was not observable in iCMs.

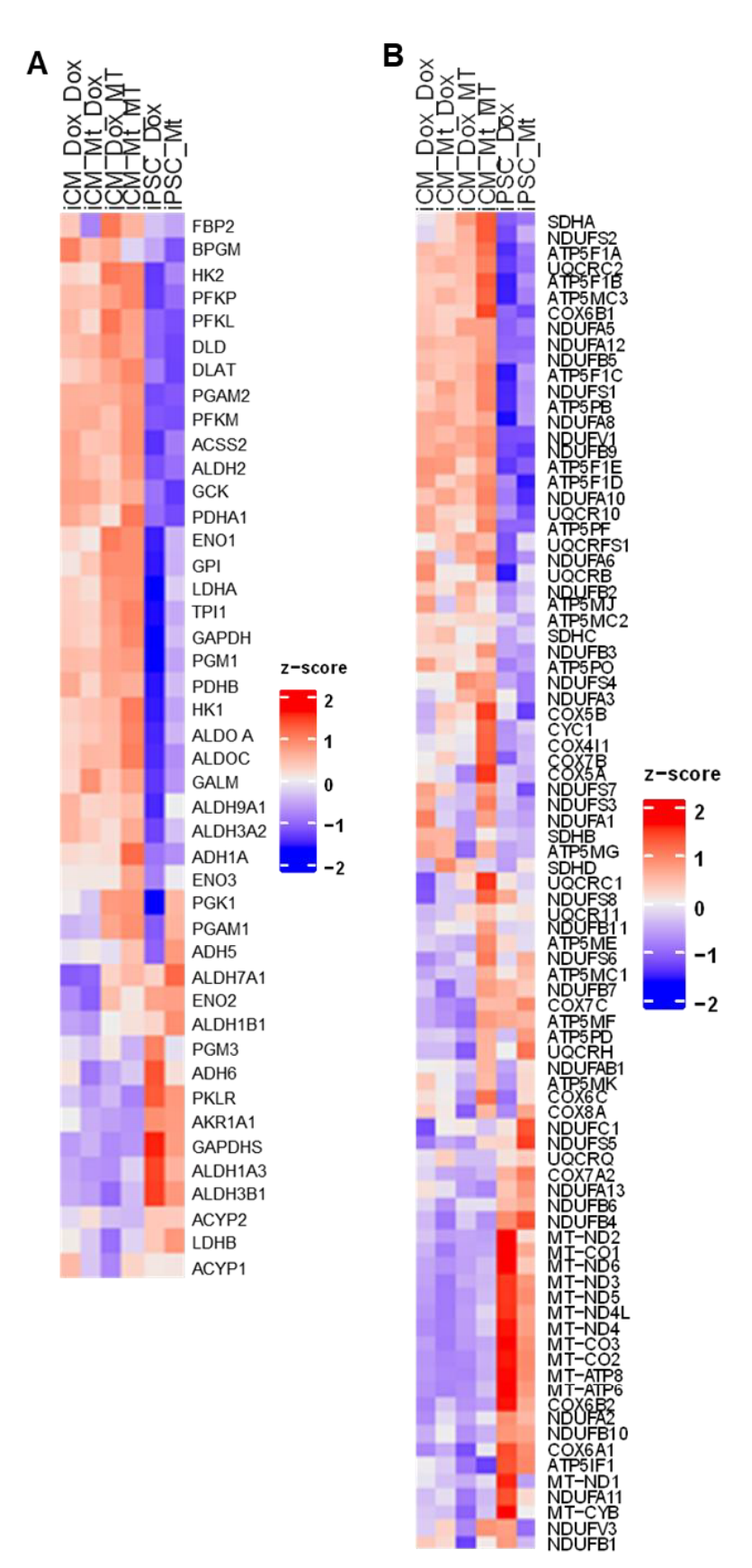


Fig. 43: Targeted hierarchical analysis of metabolic processes in iPSCs and iCMs upon influence of doxorubicin treatment.

Heatmap of targeted analysis of genes involved in glycolysis and gluconeogenesis ( $\bf A$ ) and oxidative phosphorylation (OXPHOS,  $\bf B$ ) of doxorubicin (Dox)-treated human induced-pluripotent (iPSCs) and

iPSC-derived cardiomyocytes with a defined gene list from Harmonizome 3.0 (Rouillard et al., 2016). Shown is the average z-score for all conditions. Coloring for adjusted z-scores is indicated.

# 3.3.4. Transcriptional changes induced by pulse-treatment with doxorubicin in iPSC stage results in suppression of genes associated with cardiac muscle regeneration

Since pulse-treatment of iPSCs with doxorubicin resulted in major transcriptional changes (Fig. 39), the question was whether these transcriptional changes are still measurable after commitment of iPSCs to the cardiac lineage. First, pairwise comparison between iCMs receiving doxorubicin as pulse-treatment prior to cardiac differentiation and the respective control was performed (iCM Dox Mt vs. iCM Mt Mt; Fig. 44, Fig. 45). Upon pulse-treatment prior to cardiac differentiation 233 genes were significantly upregulated and 193 downregulated (Tab. 17). To elucidate the effect of early treatment with doxorubicin, GO-term enrichment analysis of biological processes (BP) was conducted revealing significant enrichment in processes such as angiogenesis, blood vessel morphogenesis, positive regulation of cell migration, and positive regulation of cell motility (Fig. 44B). These included the enrichment of genes associated with the collagen production regulation and thereof fibrosis promotion via enhanced collagen synthesis. Along with enhanced collagen synthesis, genes associated with the GO-terms cardiac muscle tissue development, heart development, and muscle tissue development were shown to be suppressed (Fig. 45B). In sum, moderate doxorubicin pulse-treatment of iPSCs prior to cardiac differentiation seemed to be associated with suppression of genes essential for cardiac function while enhancement of collagen production hinting towards possible timepoint-specific influences of early doxorubicin treatment.

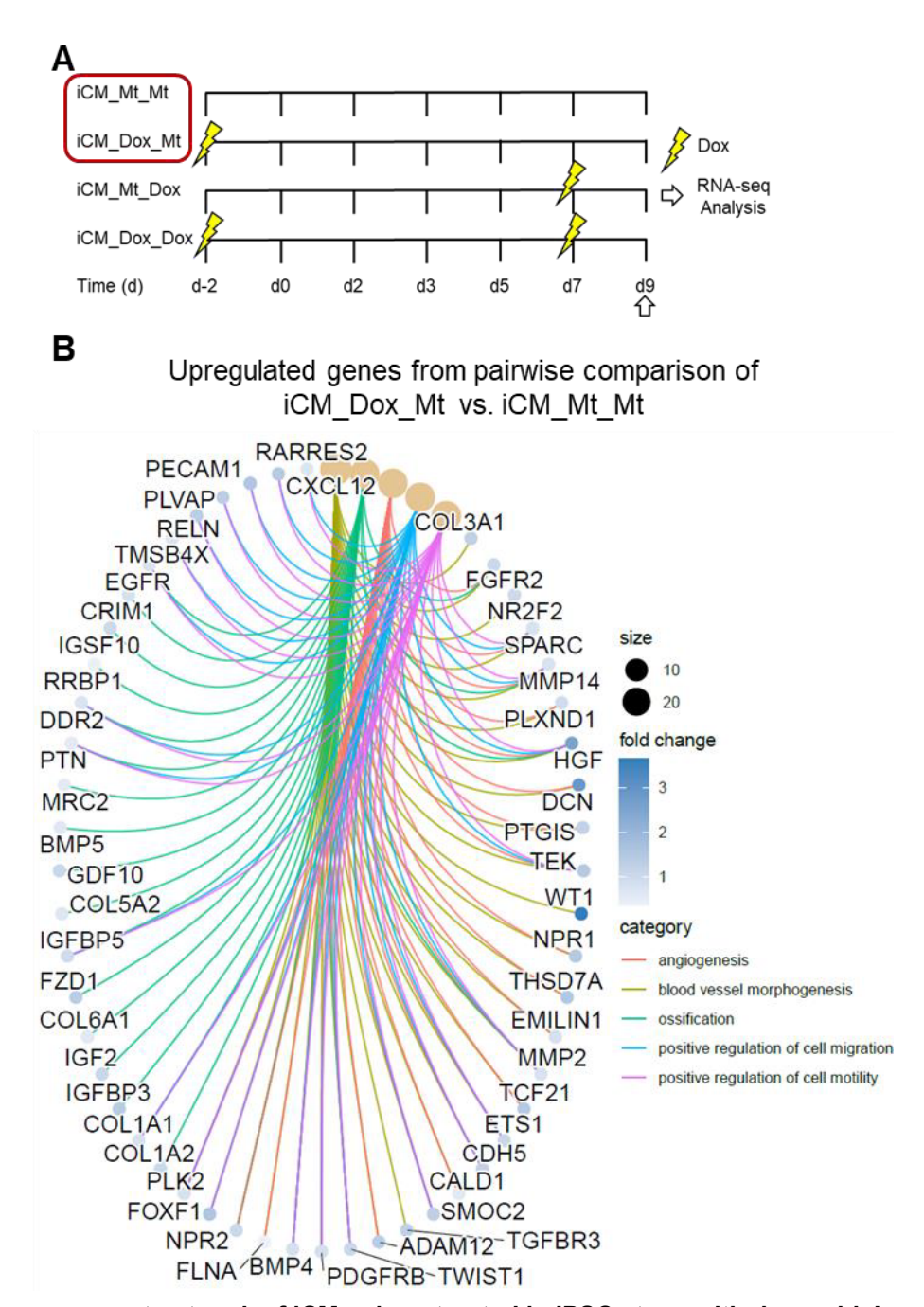


Fig. 44: Gene concept network of iCMs pluse-treated in iPSC stage with doxorubicin.

A Schematic illustration of doxorubicin (Dox) pulse-treatment scheme for induced-pluripotent stem cell (iPSC)-derived cardiomyocytes (iCMs) prior to whole genome transcriptome profiling. Briefly, all samples were pulse-treated for 2 hours with respective IC<sub>30</sub>-values of Dox before RNA-seq analysis on day 9 of cardiac differentiation. Dox pulse-treatment is represented by the lightning symbol. Current pairwise comparison is indicated by the red square **B** Gene concept network of significant upregulated differentially genes (DEGs) resulting from the pairwise comparison between iCMs pulse-treated with Dox in iPSC stage prior to cardiac differentiation (iCM\_Dox\_Mt) and their respective mock-treated control (iCM\_Mt\_Mt). DEGs listed are the result of GO-term functional analysis of biological processes (BP). GO-terms of associated genes, number of genes, and logFCs are indicated. Mt: Mock-treatment

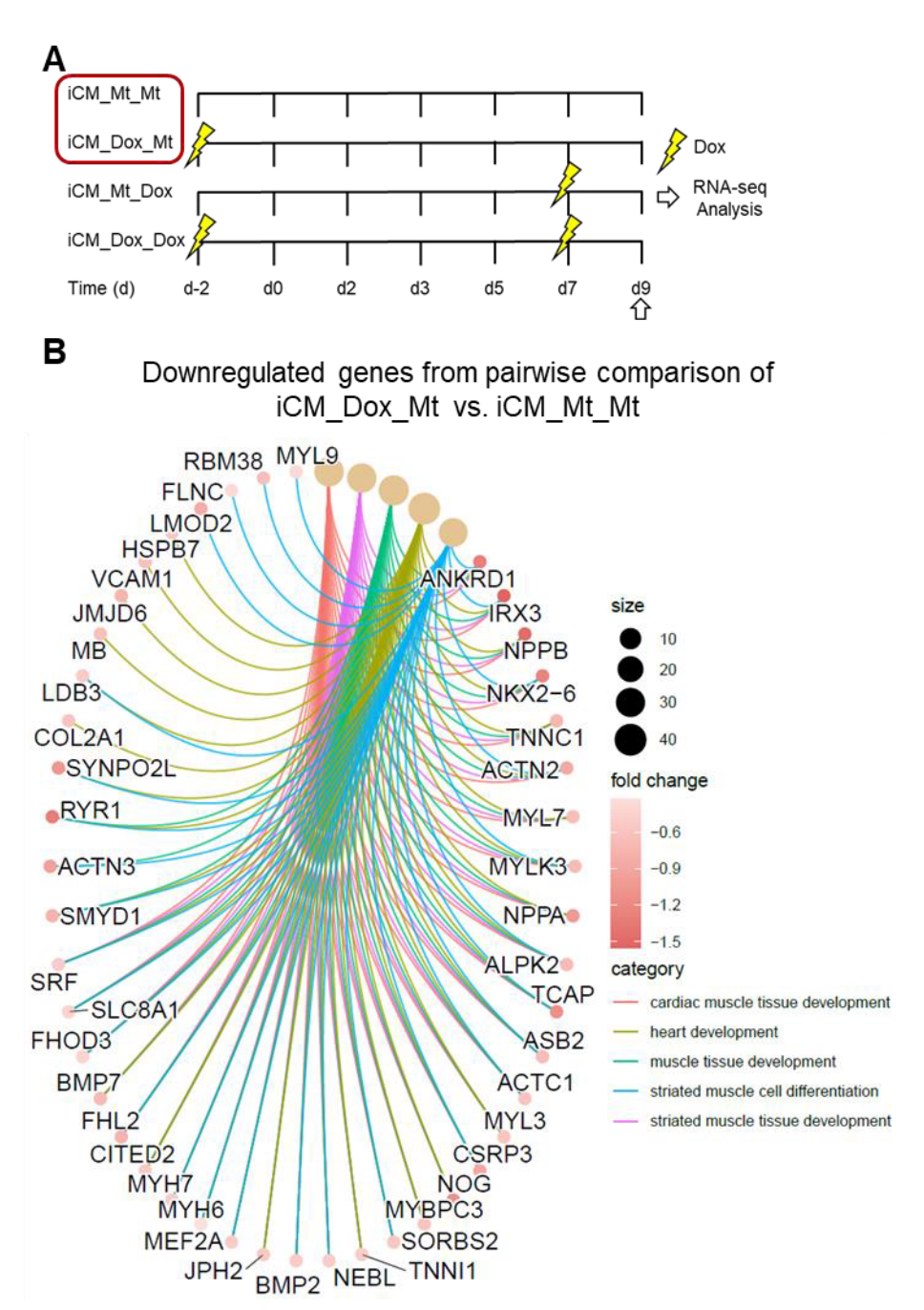


Fig. 45: Gene concept network of iCMs pluse-treated in iPSC stage with doxorubicin.

A Schematic illustration of doxorubicin (Dox) pulse-treatment scheme for induced-pluripotent stem cell (iPSC)-derived cardiomyocytes (iCMs) prior to whole genome transcriptome profiling. Briefly, all samples were pulse-treated for 2 hours with respective IC<sub>30</sub>-values of Dox before RNA-seq analysis on day 9 of cardiac differentiation. Dox pulse-treatment is represented by the lightning symbol. Current pairwise comparison is indicated by the red square **B** Gene concept network of significant downregulated differentially genes (DEGs) resulting from the pairwise comparison between iCMs pulse-treated with Dox in iPSC stage prior to cardiac differentiation (iCM\_Dox\_Mt) and their respective mock-treated control (iCM\_Mt\_Mt). DEGs listed are the result of GO-term functional analysis of biological processes (BP). GO-terms of associated genes, number of genes, and logFCs are indicated. Mt: Mock-treatment

To gain further insights into the relevance of the treatment timepoint of doxorubicin, various pairwise comparisons of significant DEGs received from the direct comparison to the mock-

treated control (iCM Mt Mt) were accomplished (iCM Dox Mt, iCM Mt Dox, and iCM Dox Dox; Fig. 46). Within the scope of the previous question, the aim was to elucidate the influence of early doxorubicin pulse-treatment. For this, comparison of all treatment conditions was performed to receive shared genes of iCMs influenced by early doxorubicin treatment (iCM Dox Mt vs. iCM Dox Dox). Here, early treatment of cells was accompanied by 139 upregulated and 133 downregulated genes (Fig. 46B). GO-term enrichment analysis of biological processes (BP) genes associated with blood vessel morphogenesis, ossification, extracellular matrix organization, and extracellular structure organization were upregulated (Fig. 46C). Since this effect is observable solely upon early treatment, these findings indicate a transcriptional response caused before induction of cardiac differentiation. Within the upregulated GO-terms, Decorin (DCN), WT1 Transcription Factor (WT1), Filamin A (FLNA), and Basonuclin Zinc Finger Protein 2 (BNC2) have been shown to be highly upregulated upon Dox pulse-treatment prior to cardiac differentiation. Thereby, genes associated with these terms have been reported to play pivotal roles in regulation of cardiac regeneration and fibrosis. Concurrently, doxorubicin pulse-treatment in iPSCs stage prior to cardiac differentiation revealed downregulation of genes involved in cardiac muscle tissue development, striated muscle cell differentiation, muscle tissue development, and muscle cell development (Fig. 47B). Among these functional GO-terms, genes responsible for cardiac function such as NK2 Homeobox 6 (NKX2-6), Ryanodine Receptor 1 (RYR1), Ankyrin Repeat Domain 1 (ANKRD1), and Actinin Alpha 3 (ACTN3), were the highly suppressed. Based on these findings, it can be concluded that even pulse-treatment of iPSCs with doxorubicin prior to cardiac differentiation is sufficiently inducing transcriptional reprogramming still measurable in terminally differentiated cells, as seen by promotion of fibrosis factors and suppression of essential genes required for cardiac regeneration. It is therefore reasonable to assume that these findings may indicate a reduced regeneration capacity of iPSCs even upon pulse-treatment with doxorubicin.

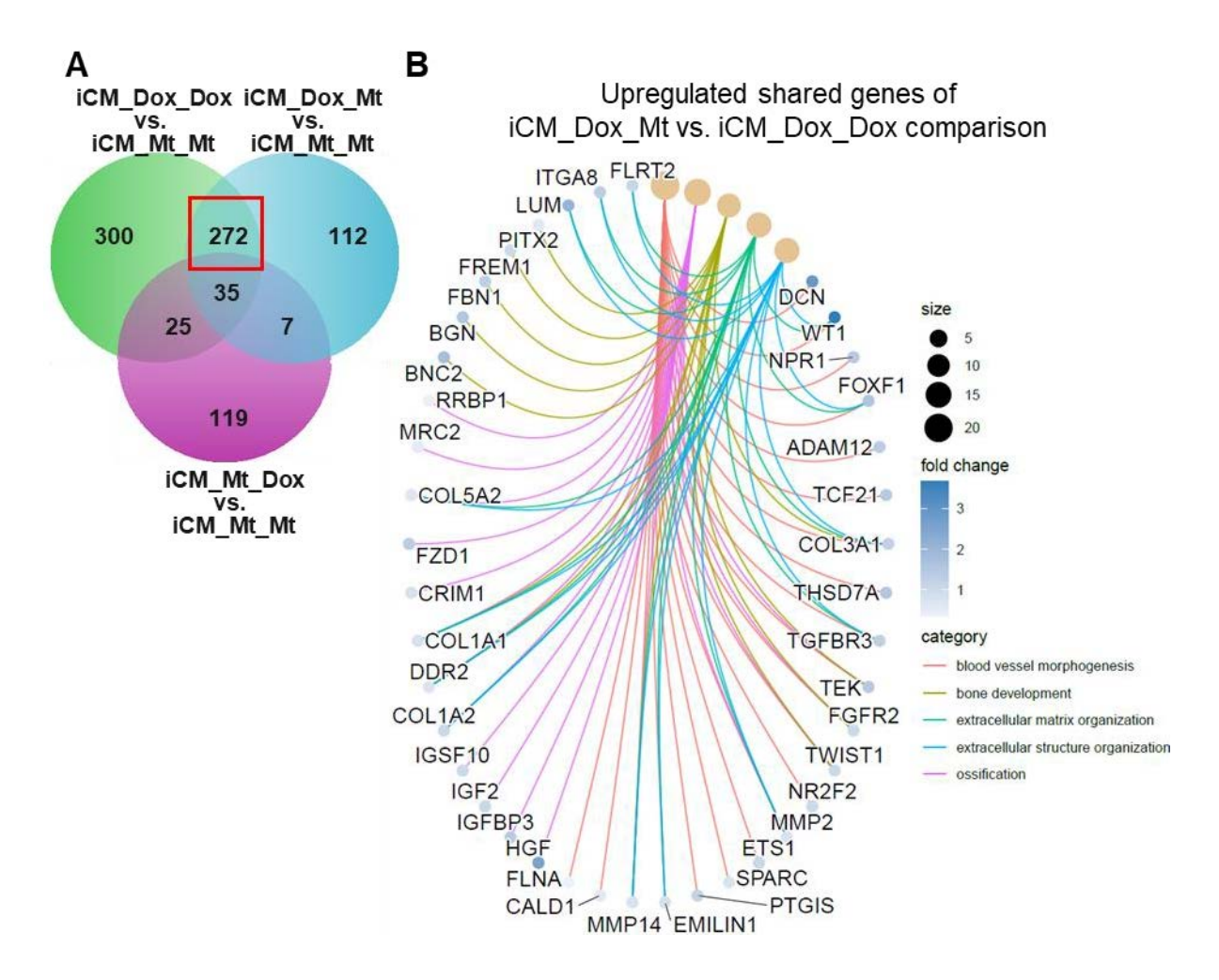


Fig. 46: Timepoint specific influence on whole genome transcriptome in iCMs pulse-treated with doxorubicin prior to cardiac differentiation.

A Venn diagram of pairwise comparison between all treatment conditions in iPSC-derived iCMs pulse-treated with doxorubicin (Dox) at different timepoints of cardiac differentiation iCM\_Dox\_Mt, iCM\_Mt\_Dox, and iCM\_Dox\_Dox). All significantly differential regulated genes resulting from indicated pairwise comparisons in which mock-treated iCMs (iCM\_Mt\_Mt) were always used as control. **BC** Gene concept network of GO-term enrichment of biological processes (BP) and associated shared genes upregulated (**B**) and downregulated (**C**) genes upon Dox pulse-treatment prior to cardiac differentiation (iCM\_Dox\_Mt and iCM\_Dox\_Dox). Respective comparison is marked with a red square. Number of genes, GO-terms, and logFCs are shown. logFC: log-fold change, Mt: Mock-treatment

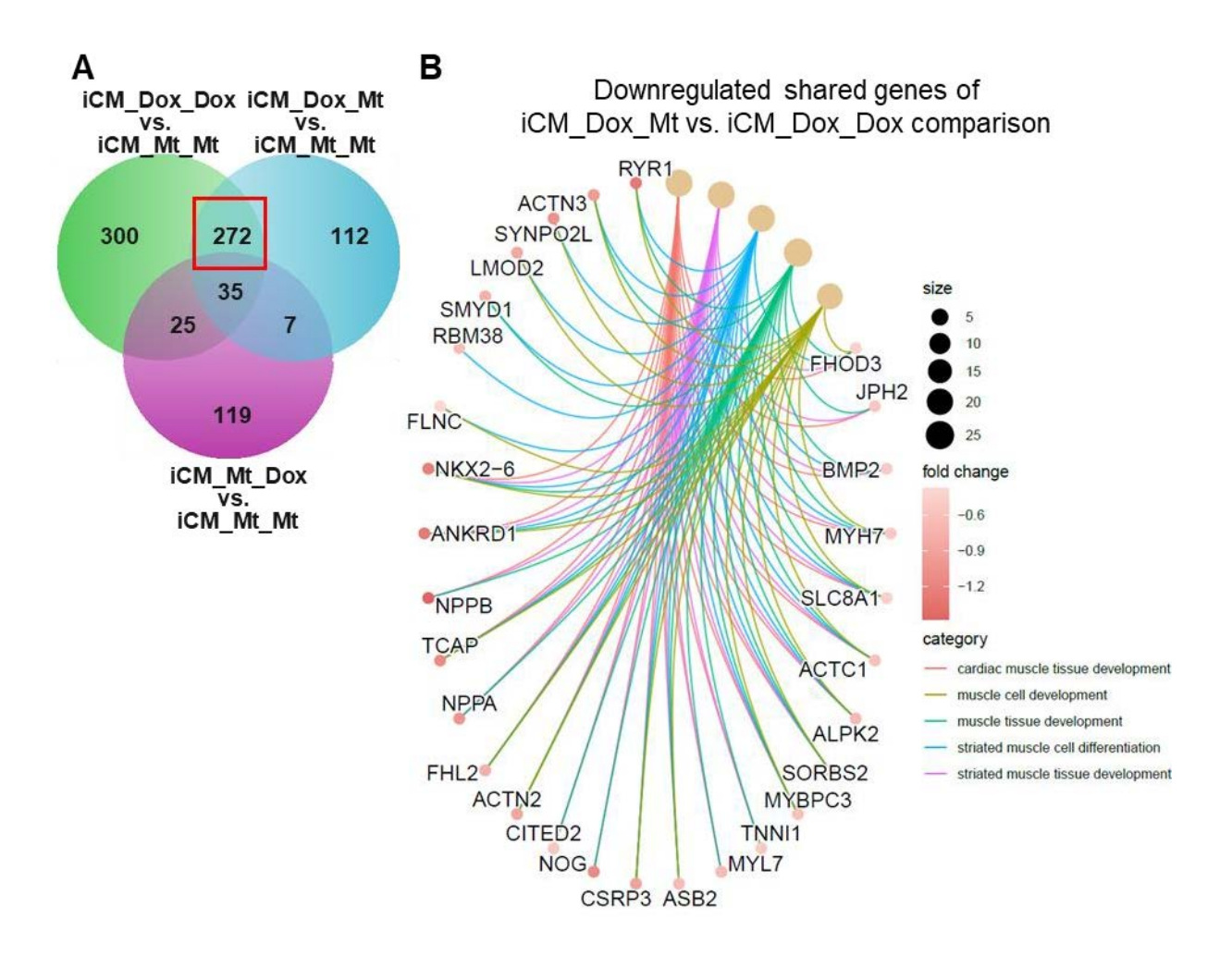


Fig. 47: Timepoint specific influence on whole genome transcriptome in iCMs pulse-treated with doxorubicin prior to cardiac differentiation.

A Venn diagram of pairwise comparison between all treatment conditions in iPSC-derived iCMs pulse-treated with doxorubicin (Dox) at different timepoints of cardiac differentiation iCM\_Dox\_Mt, iCM\_Mt\_Dox, and iCM\_Dox\_Dox). All significantly differential regulated genes resulting from indicated pairwise comparisons in which mock-treated iCMs (iCM\_Mt\_Mt) were always used as control. **BC** Gene concept network of GO-term enrichment of biological processes (BP) and associated shared genes upregulated (**B**) and downregulated (**C**) genes upon Dox pulse-treatment prior to cardiac differentiation (iCM\_Dox\_Mt and iCM\_Dox\_Dox). Respective comparison is marked with a red square. Number of genes, GO-terms, and logFCs are shown. logFC: log-fold change, Mt: Mock-treatment

#### 3.3.5. Treatment of terminal iCMs is accompanied with increased expression of apoptosis-relevant genes

As pulse-treatment of iPSCs with doxorubicin prior to cardiac differentiation has been shown to be associated with major impacts seen on transient expression profiles, the influence of doxorubicin pulse-treatment on the transcriptional response of terminally differentiated iCMs was further elucidated. For this, comparison of all treatment conditions was performed to receive shared genes of iCMs influenced by late doxorubicin treatment (Fig. 48A). Interestingly,

the number of shared significantly DEGs was much lower compared to the number of DEGs received upon early-treatment with doxorubicin (Fig. 48A). Within the total number of significant DEGs only 25 genes were solely shared by both treatment conditions, with 12 upregulated and 13 downregulated genes. Upon late treatment positive regulation of programmed cell death, positive regulation of apoptotic process and apoptotic signaling pathway was enhanced as revealed by GO-term enrichment analysis of biological processes (Fig. 48B). Top candidates associated with the previous terms were Fas cell surface death receptor (FAS), cyclin dependent kinase Inhibitor 1A (CDKN1A), and BCL2 Binding Component 3 (BBC3). Thereby, the mentioned genes have been described to be involved in apoptotic pathway induction and regulation of cell cycle processes. Within the intersection of shared downregulated DEGs upon late doxorubicin pulse-treatment, GO-term analysis revealed no significant term enrichment. Altogether, pulse-treatment at a late stage of cardiac differentiation is accompanied with upregulation in apoptotic pathways and thereof is most likely in accordance with the previously described direct toxicity of doxorubicin on cardiomyocytes.

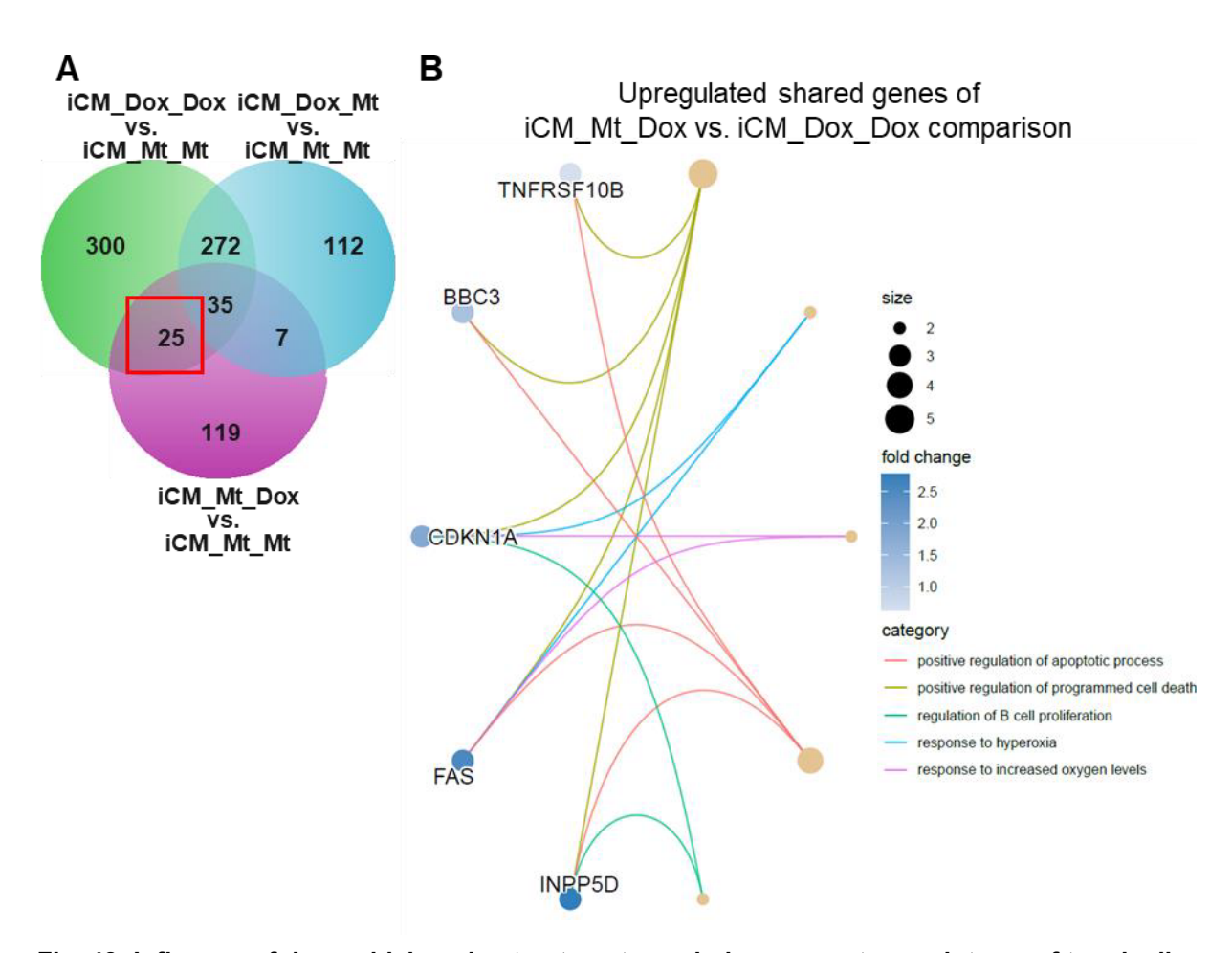


Fig. 48: Influence of doxorubicin pulse-treatment on whole genome transcriptome of terminally differentiated iCMs.

A Venn diagram of pairwise comparison between all treatment conditions in iPSC-derived iCMs pulse-treated with doxorubicin (Dox) at different timepoints of cardiac differentiation iCM\_Dox\_Mt, iCM\_Mt\_Dox, and iCM\_Dox\_Dox). All significantly differential regulated genes resulting from indicated

pairwise comparisons in which mock-treated iCMs (iCM\_Mt\_Mt) were always used as control. **B** Gene concept network of GO-term enrichments of biological processes (BP) of differentially upregulated genes exclusively shared by late-treatment of terminally differentiated iCMs (iCM\_Mt\_Dox and iCM\_Dox\_Dox, all compared to iCM\_Mt\_Mt). GO-terms of associated genes, number of genes, and logFCs are indicated. logFC: log-fold change, Mt: Mock-treatment

# 3.3.6. Pre-conditioning of cells in iPSC stage is accompanied with alterations in genes associated with energy metabolism and muscle contraction

As seen in section 3.3.4, exposure of iCMs in iPSC stage prior to cardiac differentiation was accompanied with strong changes in transcriptional response. Thus, the question was whether the early encounter of iPSCs with doxorubicin manifests in transcriptional changes upon the second encounter with doxorubicin in iCM stage. In order to follow this, a double-treatment scheme including mild and transient doxorubicin treatment in iPSC and iCM stage was introduced (iCM Dox Dox). Within the group of DEGs specific for double-treatment condition resulted in a number of 300 DEGs, of which 164 genes were upregulated and 136 genes were downregulated (Fig. 49A). It is worth to mention that compared specific DEGs solely affected upon late treatment of cells solely comprised 119 DEGs indicating that the transcriptional response upon early treatment has a recognizable impact on the subsequent response of iCMs upon second encounter with doxorubicin. This is also in accordance to the findings, that solely 25 significant DEGs were specifically shared by double-treated iCMs and late-treated iCMs. Within the group of upregulated DEGs in pre-conditioned iCMs (iCM Dox Dox), GO-term enrichment of BP resulted in the enrichment of genes associated with ERK1 and ERK2 cascade, positive regulation of cell motility, signal transduction by p53 class mediator, and gland development (Fig. 49B). Among the list of genes found with GO-term enrichment analysis were SRY-Box transcription factor 9 (SOX9), cyclin dependent kinase 1 (CDK1), Wild-Type P53-induced phosphatase 1 (PPM1D), and snail family transcriptional repressor 2 (SNAI2). These have been shown to play critical regulatory functions regarding cell fate and transcription. Yet, pre-conditioning cells with doxorubicin was accompanied with downregulation of DEGs involved in energy metabolism, muscle system process and muscle contraction (Fig. 50B). Downregulated genes associated with these GO-term functions were, hexokinase 1 (HK1), several respiratory chain complex subunits (COX5B, UQCRC1, NDUFS2, NDUFS8), NK2 homeobox 5 (NKX2-5), ATPase Na+/K+ transporting subunit beta 1 (ATP1B1), and triadin (TRDN). Downregulation of these genes hinting towards a possible doxorubicin-induced dysregulation of cellular metabolism and electrochemical gradients, which represent a major part of cardiac function.

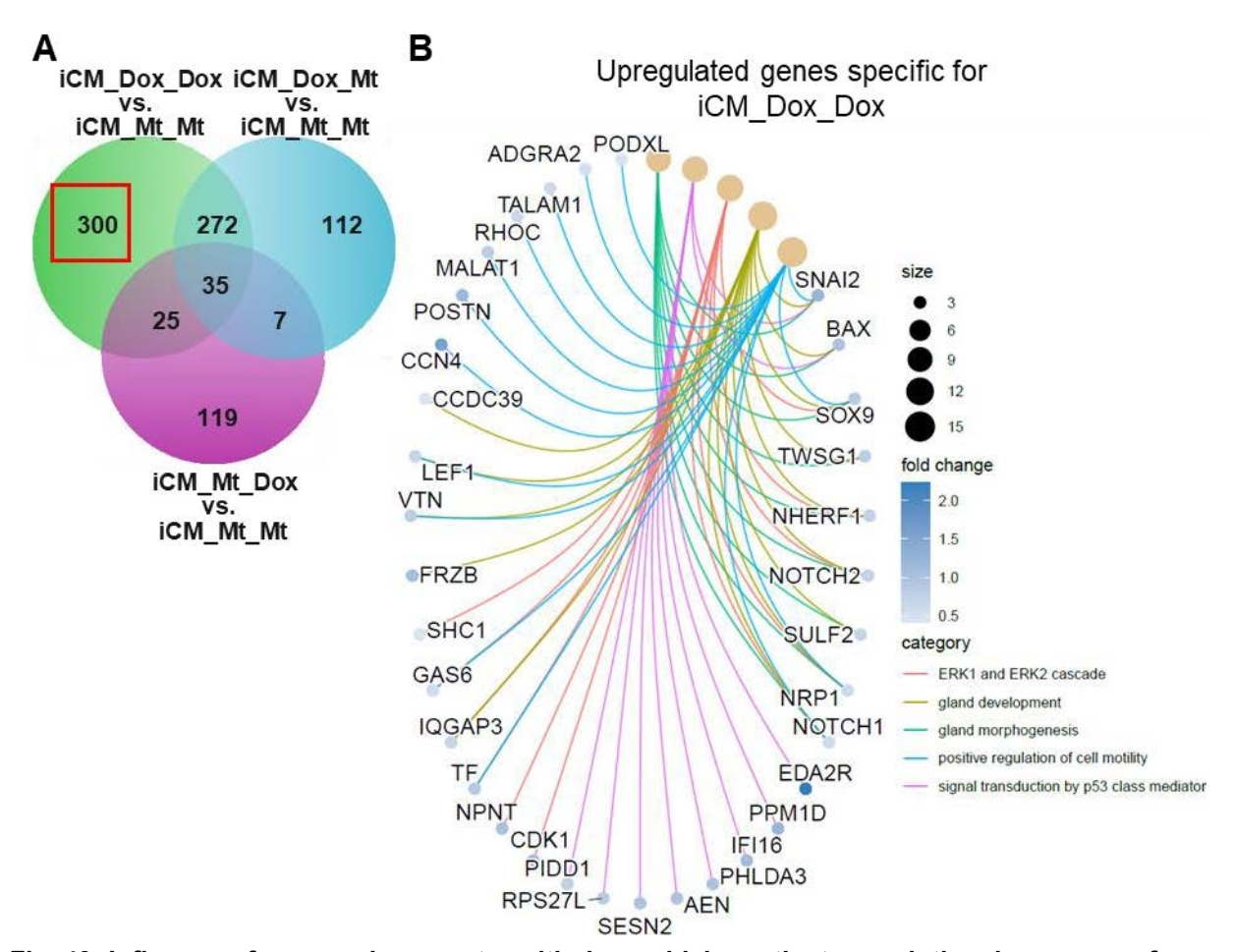


Fig. 49: Influence of a second encounter with doxorubicin on the transcriptional response of pre-conditioned iCMs.

A Venn diagram of pairwise comparison between all treatment conditions in iPSC-derived iCMs pulse-treated with doxorubicin (Dox) at different timepoints of cardiac differentiation iCM\_Dox\_Mt, iCM\_Mt\_Dox, and iCM\_Dox\_Dox). All significantly, differential regulated genes resulting from indicated pairwise comparisons in which mock-treated iCMs (iCM\_Mt\_Mt) were always used as control. **BC** Gene concept network of GO-term enrichments of differentially upregulated (B) and downregulated (C) genes unique for double-treated iCMs (iCM\_Dox\_Dox). GO-terms of associated genes, number of genes, and logFCs are indicated.

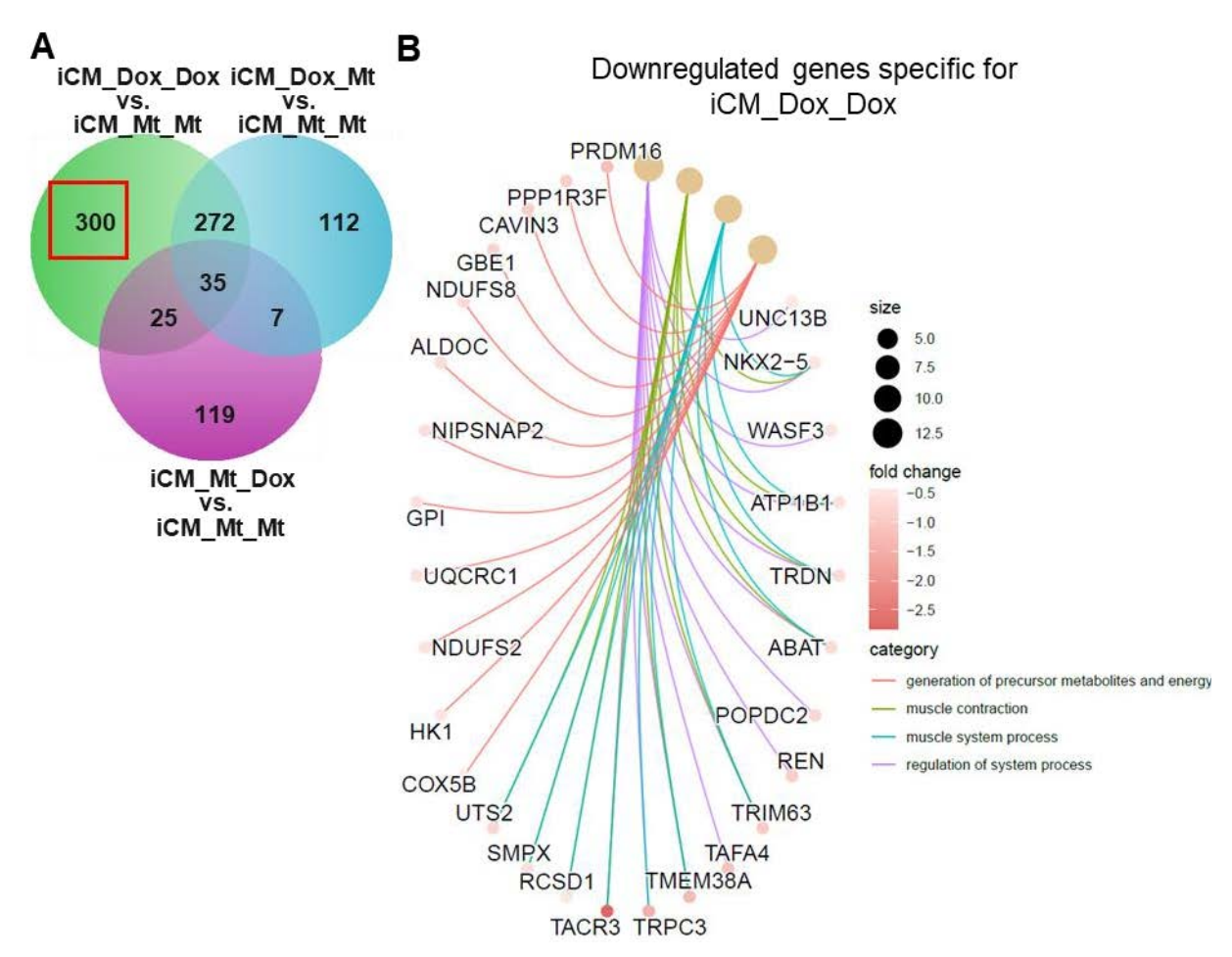


Fig. 50: Influence of a second encounter with doxorubicin on the transcriptional response of pre-conditioned iCMs.

A Venn diagram of pairwise comparison between all treatment conditions in iPSC-derived iCMs pulse-treated with doxorubicin (Dox) at different timepoints of cardiac differentiation iCM\_Dox\_Mt, iCM\_Mt\_Dox, and iCM\_Dox\_Dox). All significantly differential regulated genes resulting from indicated pairwise comparisons in which mock-treated iCMs (iCM\_Mt\_Mt) were always used as control. **BC** Gene concept network of GO-term enrichments of differentially upregulated (B) and downregulated (C) genes unique for double-treated iCMs (iCM\_Dox\_Dox). GO-terms of associated genes, number of genes, and logFCs are indicated.

### 3.3.7. Treatment timepoint independent general dysregulation of genes associated with cardiac muscle formation

Since timepoint-dependent effects were found upon whole genome transcriptome profiling of iCMs, the question was whether doxorubicin pulse-treatment is inducing a time-independent effect on the transcriptome level, in other words, is there a doxorubicin -induced transcriptomic "fingerprint" irrespective of the timepoint of application. Overall, upon treatment of iCMs at diverse timepoints of cardiac differentiation over 870 genes were significantly differential regulated (Fig. 51A). However, only 35 genes were specifically shared by all treatment conditions, indicating a relatively small timepoint-independent effect of doxorubicin

pulse-treatment. Among these 35 genes, some genes were contrary antagonistically as revealed by hierarchical clustering of the average z-scores (Fig. 51B). Enrichment analysis of GO-terms of biological processes (BP) showed no significant term enrichment in the number of significantly upregulated genes. Yet, downregulation of GO-terms such as myofibril assembly, striated muscle cell development, heart contraction, and heart process were downregulated (Fig. 51C). Associated with these terms, pulse-treatment with doxorubicin induced the downregulation of Myosin Heavy Chain 6 (*MYH6*), Nebulette (*NEBL*) and Myosin Light Chain 9 (*MYL9*) hinting towards a time-independent adverse effect of doxorubicin on cardiac function. Taken together, pulse-treatment with doxorubicin is accompanied by suppression of genes involved in support of cardiac function indicating a transcriptional adaptation of iCMs towards treatment independent of application timepoint.

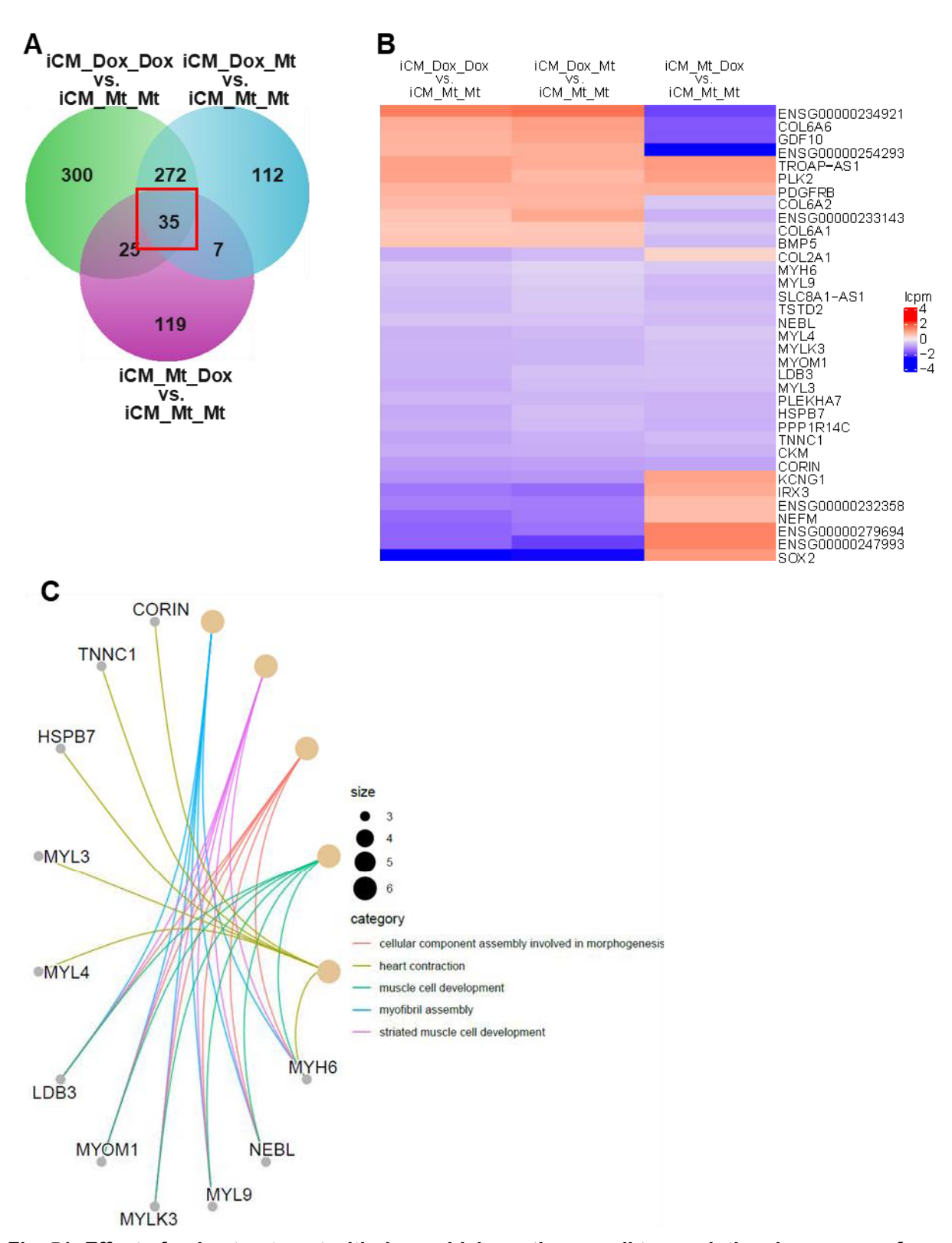


Fig. 51: Effect of pulse-treatment with doxorubicin on the overall transcriptional response of iCMs.

A Venn diagram of pairwise comparison between all treatment conditions in iPSC-derived iCMs pulse-treated with doxorubicin (Dox) at different timepoints of cardiac differentiation iCM\_Dox\_Mt, iCM\_Mt\_Dox, and iCM\_Dox\_Dox). All significantly differential regulated genes resulting from indicated pairwise comparisons in which mock-treated iCMs (iCM\_Mt\_Mt) were always used as control. B Heatmap of time-independent transcriptional response within the selective intersection of early treated iCMs (iCM\_Dox\_Mt), late treated iCMs (iCM\_Mt\_Dox) and double-treated iCMs (iCM\_Dox\_Dox). Shown are the significantly differential regulated genes resulting from pairwise comparison of the

mentioned conditions (all previously compared to mock-treated control iCM\_Mt\_Mt). Shown is the average z-score for all conditions. Coloring for adjusted z-scores is indicated. **C** Gene concept network of GO-term enrichments of biological processes (BP) of differentially downregulated genes exclusively shared all treatment conditions of iCMs (iCM\_Mt\_Dox and iCM\_Dox\_Dox, all compared to iCM\_Mt\_Mt). Respective comparison is marked with a red square. GO-terms of associated genes, number of genes are indicated. Mt: Mock-treatment

# 3.3.8. Suppression of contractility function of iCMs upon is directly associated with treatment in iPSC stage prior to cardiac differentiation

In the present study found whole genome transcriptome profiling in iCMs revealed that even low concentrations of doxorubicin were accompanied by significant downregulation of genes that are crucial for cardiac function, specifically the contraction parameters of iCMs. To validate these findings, contraction parameters of transcriptome conditions were assessed via automated analysis of live-cell videos of all treatment conditions in iCMs (Fig. 52A). Quantitative analysis of all contraction parameters revealed a negative trend in all tested cardiac parameters independent of the application time. However, solely for the double-treated iCMs this observation was significant indicating an additional adverse effect of double-treatment with regards to cardiac function. To elucidate whether the sensitivity in iCMs received via doxorubicin treatment prior to cardiac differentiation was enhanced, the viability of mock-treated iCMs and pre-conditioned iCMs with 18 nM doxorubicin prior to cardiac differentiation was further analyzed using SRB assay (Fig. 52B). Indeed, pulse-treatment of iPSCs prior to cardiac differentiation was accompanied by higher susceptibility of iCMs upon further exposure towards various concentrations of doxorubicin compared to mock-treated control. Yet, this effect was not significant.

In line with the data received from whole genome transcriptome profiling, independent of the timepoint of administration, even transient exposure to low concentrations of doxorubicin has been accompanied by dysregulation in contractility parameters. However, solely double-treated iCMs were most affected as indicated by viability data. This indicates that an early encounter with doxorubicin and the resulting early transcriptional reprogramming in iPSCs strongly enhances the sensitivity of iCMs towards a second encounter with doxorubicin is accompanied with increased dysregulation of cardiac contraction parameters.

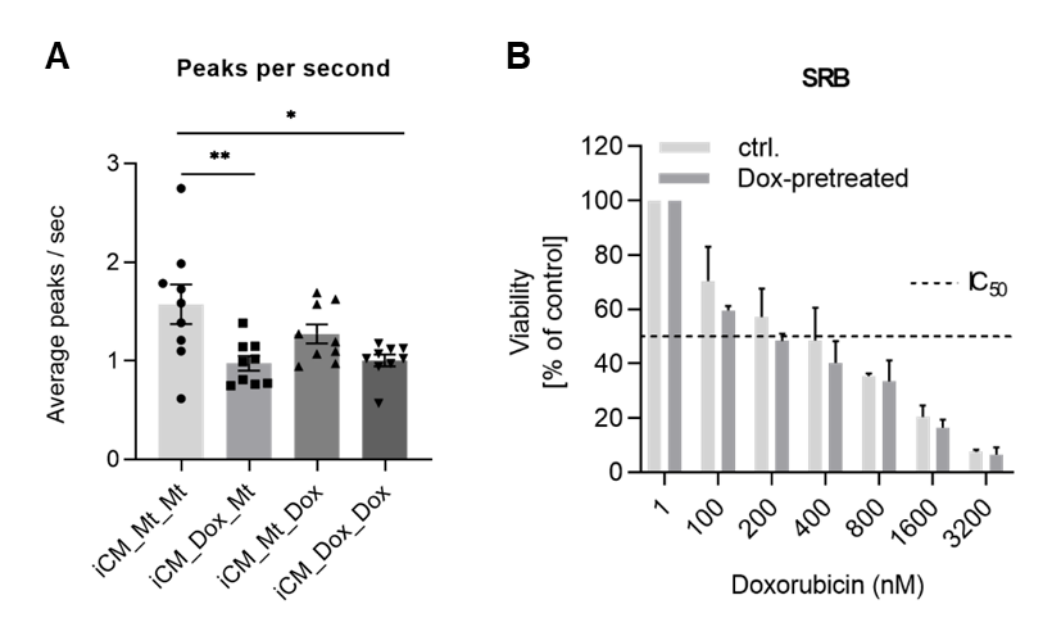


Fig. 52: Measurement of cardiac functionality upon exposure of iCMs to doxorubicin.

A Quantitative analysis of contraction parameters measured in iCMs pulse-treated with doxorubicin (Dox) in induced-pluripotent stem cell (iPSC) stage (iCM\_Dox\_Mt), on day7 of cardiac differentiation (iCM\_Mt\_Dox) or in iPSC stage and iPSC-derived cardiomyocyte (iCM) stage (iCM\_Dox\_Dox). Average contraction parameters were normalized to mock-treated iCM control (iCM\_Mt\_Mt). Prior to analysis procedure, live-cell videos of 20 seconds length with 60 frames per second of all conditions were acquired using Leica DM IL LED Fluo Cellfactory microscope. Analysis of the videos was conducted by using an automated analyzing system. Data shown represents the mean ± standard error of mean (SEM) of six independent experiments (n=6, N=3). *One*-way ANOVA with multiple comparisons was performed. \* P-value ≤0.05; \*\* P-value ≤ 0.01. **B** Viability measurement between iCMs pre-treated with 18 nM Dox prior to cardiac differentiation and mock-treated iCMs. Viability was measured 48 hours after 2 hours pulse-exposure to indicated concentrations of Dox using SRB assay. Viability (%) was normalized to respective control. Shown is the average viability (%) ± SEM (n=3; N=8).

### 3.3.9. Timepoint-independent induction of mitochondrial dysfunction in iCMs pulse-treated with Dox

In order to understand whether the applied treatment schemes for whole transcriptome profiling result in comparable mitochondrial changes as observed earlier in iCMs treated with doxorubicin on day 7 of cardiac differentiation (Fig. 36), mitochondrial morphology and copy number was further elucidated upon the introduced treatment conditions. In accordance with the previous findings in iPSCs, also doxorubicin-treated iCMs showed a more prominent shift of mitochondrial morphology towards fragmentation as compared to their mock-treated control, yet this trend was not significant (Fig. 53AB). Interestingly, the most affected cells were these either receiving doxorubicin on day 7 of cardiac differentiation (iCM\_Mt\_Dox) or cells pre-treated in iPSC stage following by a second encounter on day 7 of cardiac differentiation (iCM\_Dox\_Dox). Similar effects were visible when investigating the mitochondrial copy number (Fig. 53C). Here, a comparable trend was observed showing that iCMs received doxorubicin

as treatment on day 7 of cardiac differentiation (iCM\_Mt\_Dox) and double-treated iCMs (iCM\_Dox\_Dox) resulted in a decrease of mitochondrial copy number. However, the observed trend was not significant. Taken together, independent of the application timepoint of doxorubicin during cardiac differentiation, iCMs displayed a shift of mitochondrial network towards fragmentation and a decrease in mtDNA content, with late-treated (iCM\_Mt\_Dox) and double-treated (iCM\_Dox\_Dox) iCMs showing a stronger tendency towards mitochondrial fragmentation and mtDNA copy number reduction.

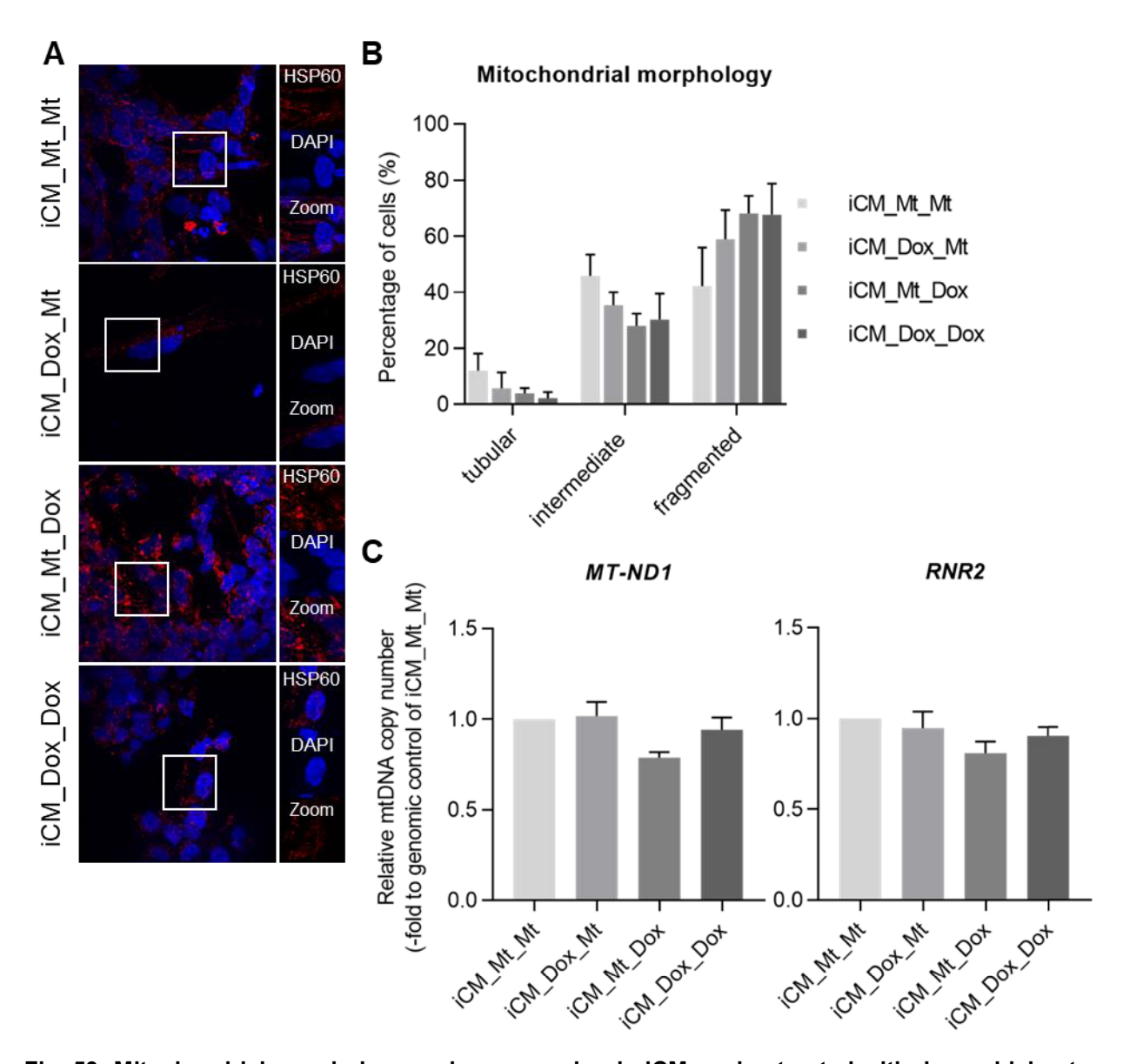


Fig. 53: Mitochondrial morphology and copy number in iCMs pulse-treated with doxorubicin at different timepoints throughout cardiac differentiation.

Mitochondrial parameters in cardiomyocytes (iCMs) derived from human induced-pluripotent stem cells (iPSC)-derived was assessed after application of a defined treatment scheme with doxorubicin (Dox). Here, iCMs were pulse-treated with Dox in iPSC stage (iCM\_Dox\_Mt), on day7 of cardiac differentiation (iCM\_Mt\_Dox) or in iPSC stage and iCM stage (iCM\_Dox\_Dox). A Mitochondrial morphology was assessed via confocal microscopy of the immunohistochemical staining of mitochondrial marker heat-shock protein 60 (HSP60). Shown are representative confocal images of mitochondria in control and pulse-treated iCMs of one biological replicate. Zoomed-in regions are indicated by a white box.

Magnification: x 63, scale bar: 10  $\mu$ m. **B** Quantification of mitochondrial morphology categorized in tubular, intermediate, or fragmented morphology in the different treatment conditions with Dox. Data show mean  $\pm$  standard error of mean (SEM) from three independent experiments (n=3; N=75 cells). **C** Mitochondrial copy number was determined via measuring the expression of mitochondrial encoded genes mitochondrial encoded 16S rRNA (*RNR2*) and NADH-ubiquinone oxidoreductase chain 1 (*MT-ND1*) using quantitative real-time PCR 48 hours after 2 hours pulse-treatment of iPSC derived cardiomyocytes (iCMs d7) with doxorubicin (Dox). Hypoxanthine Phosphoribosyltransferase 1 (HPRT1) was used as housekeeping gene. Data as normalized to the respective control. Data shown represents the relative mean  $\pm$  standard error of mean (SEM) from three independent experiments (n=3; N=3).d: day

#### 4. Discussion

The aim of this dissertation was to provide further insights into the role of mitochondria in mediating the susceptibility of stem, cardiac progenitor cells and cardiomyocytes towards treatment with doxorubicin. Previous publications described the disruption of mitochondrial function at comparably elevated treatment doses and administration times, which greatly exceed the actual plasma concentrations observed in cancer patients undergoing treatment with doxorubicin. Here, we implemented a previously published treatment scheme comprising the exposure of cells to short time pulses and low concentrations of doxorubicin (Jahn et al., 2020). The establishment of an iPSC-derived cardiac model system was the foundation of our research, which sought to elucidate the differentiation-specific differences between iPSCs and iCMs regarding susceptibility, differentiation capacity, and cellular function. A primary objective was to gain insights into the potential role of mitochondria as major mediators of doxorubicin-induced cardiotoxicity. To this end, a combination of mitochondrial-based assays was employed, revealing high susceptibility of these organelles even to transient and moderate exposures to doxorubicin. Utilizing a whole genome transcriptome approach, we sought to elucidate the transcriptional alterations that accompanied the application of doxorubicin pulsetreatment regimens throughout cardiac differentiation, incorporating the introduction of a hormesis approach. In this study, we demonstrated metabolic dysfunction in iPSCs and doxorubicin-induced transcriptional alterations of cardiac-relevant genes in iCMs. For the hormesis approach, we observed the increased sensitivity of iCMs to a second encounter with doxorubicin accompanied with downregulation of mitochondrial genes, highlighting the partial involvement of this organelle in the possible development of doxorubicin-induced cardiotoxicity.

# 4.1. Successful cardiac differentiation following a chemical defined protocol

In this work, human iPS (IMR90)-4 cells served as a model for undifferentiated progeny and iCMs as model for terminal differentiated cardiomyocytes. Human iPSCs (IMR90-4 line) were maintained under feeder-free conditions using proprietary media designed to preserve pluripotency and prevent spontaneous differentiation (Yamamoto et al., 2022). Consistent monitoring of morphology and pluripotency markers ensured culture quality prior to differentiation.

In this study, in vitro differentiation of iPSCs into cardiomyocytes was induced on monolayer cell culture. Cardiac differentiation protocol involved the temporal modulation of the Wnt signaling pathway through the controlled application of activators and inhibitors, as previously established (Burridge et al., 2012; Lian et al., 2013) (Fig. 30). The first step towards cardiac lineage commitment involved the replacement of iPSC maintenance media with cardiac basal media supplemented with glycogen synthase kinase (GSK) 3 inhibitor CHIR99021 (d0-d2), simulating the early embryonic development where Wnt signaling is required for primitive streak formation and mesodermal specification (Burridge et al., 2012; Kelly et al., 2004; Liu et al., 1999). Embryonic stem cells lacking Wnt signaling failed to generate cardiac mesoderm. To promote mesodermal transition into cardiac progenitors, Wnt signaling was inhibited between day 3 and day 5 using IWP-4, a small molecule that blocks Wnt ligand secretion by inhibiting the acetyltransferase Porcupine (Chen et al., 2009). This finding is consistent with the results of the *in vivo* studies, demonstrating that Wnt signaling pathway inhibition is a determining factor in the cellular fate that leads to heart development (Marvin et al., 2001; Nakamura et al., 2003). From day 7 onwards (d7 - d9), cells were cultured in basal media containing insulin to support further cardiac differentiation. A primary indicator of effective differentiation was the emergence of spontaneously contracting areas as early as day 7, which was in agreement with earlier observations (Burridge et al., 2014; Lian et al., 2013; Prondzynski et al., 2024).

In this study, the differentiation process was validated through the analysis of pluripotency and cardiac marker expression at both the mRNA and protein levels (Fig. 32, Fig. 40). Pluripotency markers such as *POU5F1*, *NANOG*, and *SOX2* were downregulated, while expression of cardiac-specific genes increased from day 5 of cardiac differentiation. This included transcription factors such as ISL1, which identifies secondary heart field progenitors involved in early cardiac development (Bu et al., 2009). Interestingly, ISL1 expressing cells have also been associated with positive regulation of cardiac regeneration processes (Cai et al., 2003). The cardiac transcription factor GATA4 was also upregulated. Interestingly, mutations in this gene are linked to congenital heart defects (Ang et al., 2016). Additionally, *NKX2-5*, a

hallmark of early cardiac progenitors, showed increased expression (de Sena-Tomás et al., 2022). The contractility of the heart is majorly dependent on the sarcomere function. The ATP dependent conformational change of myosin heavy chains results in the pulling of titin filaments towards the z-disc and thereof to the contraction of the cardiomyocyte (Wang et al., 2022). Cardiomyocyte contractility depends on the structural organization and function of the sarcomere. Key sarcomere genes, including *MYH6* (encoding myosin heavy chain 6), were highly expressed during early cardiac development and are known to be associated with congenital heart defects when mutated (Ching et al., 2005; Mahdavi et al., 1984). The expression of cardiac troponin T (cTnT), encoded by *TNNT2*, was also elevated. This protein plays a crucial role in mediating cardiomyocyte contraction of actin-myosin in response to Ca <sup>2+</sup> (Ahmad et al., 2008).

Despite the expression of cardiac markers on mRNA and protein level, iCMs at day 7 or 9 exhibited features characteristic of fetal cardiomyocytes, such as disorganized sarcomere structure, and spontaneous beating (Gherghiceanu et al., 2011; Goversen et al., 2018; Vučković et al., 2022). These immature features are particularly relevant when analyzing mitochondrial function, as the metabolic state is closely associated with mitochondrial morphology and function (Seo et al., 2018). Morphological analysis revealed a tubular mitochondrial network in iPSCs, in contrast to a more fragmented network in iCMs. Notably, iPSCs exhibited a more developed, tubular mitochondrial network compared to the sparse, perinuclear distribution of mitochondria previously described in other iPSC lines, which is closely attributed to their glycolytic metabolism (Cho et al., 2006; Krantz et al., 2021; Mandal et al., 2011). These findings suggest cell line-specific differences in mitochondrial structure, potentially influenced by the genetic background of the donor somatic cells (Harvey et al., 2016). The representation of fragmented mitochondria in iCMs is in contradiction with previous studies reporting elongation of mitochondrial network as cardiac differentiation progresses (Hoque et al., 2018; Morris et al., 2023; Xu et al., 2022). However, those studies focused on mature iCMs, limiting the comparability to the current findings Thus, observed tendency of mitochondrial fragmentation in iCMs may therefore reflect their fetal-like stage.

Taken together, iPSCs were successfully differentiated into terminally cardiomyocytes using a chemically defined protocol. However, generated iCMs exhibited fetal-like characteristics including spontaneous beating and premature sarcomere development. This is of particular interest as the risk of late-onset cardiotoxicity is increased in childhood cancer survivors treated with doxorubicin (Nysom et al., 1998). Given the immature state of the iCMs, further maturation would enhance the physiological relevance of this model system. Several approaches have been shown to promote iCM maturation, including fatty acid supplementation, long-term *in vivo* culture, and biomaterial-based techniques (Lundy et al., 2013; Pedron et al., 2011; X. Yang et al., 2019). Thus, investigating doxorubicin-induced cardiotoxic effects across different

maturation stages could offer deeper insights into age- and development-dependent susceptibilities towards doxorubicin. Applying such methods could significantly improve the application of iPSC-derived cardiomyocytes for simulation of late-stage cardiac physiology and drug responses. As stated in section 1.2.2, cardiomyocytes constitute 35 to 49% of the total cell mass within the heart. The current model does not consider the impact of other significant heart cell types (e.g. cardiac fibroblasts, cardiac endothelial cells, etc.) on the response to doxorubicin-cardiotoxicity. Incorporating these populations would enable more accurate modeling of cardiac microenvironments and cell-cell interactions, particularly under cardiotoxic stress. Future efforts should focus on building multicellular, organ-like cardiac systems to enhance the biological relevance and translational potential of iPSC-based platforms.

# 4.2. Mitochondria as a major target of mild and transient doxorubicin exposures

The interplay between mitochondrial morphology, dynamics, membrane potential and energy conversion mediate the maintenance of cellular health. Mitochondrial dysfunction has been shown in a range of pathological conditions and is particularly relevant in the context of doxorubicin-induced cardiotoxicity. Doxorubicin disrupts mitochondrial function and structure, as firstly reported in the 1990s (Gewirtz, 1999; Zhao & Zhang, 2017). While many studies reported the dysfunction of mitochondria on different levels, most of these findings were assessed under comparatively high treatment concentrations and chronic exposures. This raises the question of whether acute treatments with low concentrations of doxorubicin (IC<sub>10</sub>- and IC<sub>30</sub>-value) cause comparable mitochondrial dysfunction in stem cell progeny and terminally differentiated cardiomyocytes.

Mitochondrial morphology offers valuable insights into organelle integrity and cellular health. Following the acute exposure of iPSCs and iCMs to doxorubicin, cells exhibited a clear shift of the mitochondrial network towards fragmentation (Fig. 20, Fig. 36, Fig. 52), highlighting the sensitivity of the mitochondrial network to even low concentrations of doxorubicin. The morphological shift towards fragmentation was accompanied with the reduction of mitochondrial fusion proteins Mfn1 and Mfn2 in iPSCs (Fig. 21), aligning with previous findings demonstrating the reduction in Mfn2 protein levels in doxorubicin-treated cardiomyocytes (Tang et al., 2017). However, activation of fission protein Drp1 via phosphorylation at Ser616 was not detected (Fig. 21). While this suggests that Drp1 is not activated though this site under current conditions, the involvement of alternative phosphorylation sites, such as Ser579 and Ser600, cannot be excluded and should be further investigated in future approaches (Valera-Alberni et al., 2021). In addition, also processing of OPA1 as an indicator of mitochondrial

dysfunction and key driver of mitochondrial fission (Duvezin-Caubet et al., 2006; Ishihara et al., 2006), was not detected. Given that OPA1 cleavage can occur within 20 minutes of CCCP exposure, it is possible that under the current conditions the observation of this process was missed due to the timepoint of analysis (Duvezin-Caubet et al., 2006). Finally, the shift of mitochondrial network towards fragmentation and reduced fusion protein levels indicate an imbalance of fusion and fission processes, favoring fragmentation of the mitochondrial network. To strengthen this finding, future experiments should check earlier timepoints for OPA1 assessment and expand the analysis of Drp1 activation to additional phosphorylation sites in both iPSCs and iCMs.

The observed imbalance in mitochondrial dynamics may derive from disruption of the mitochondrial membrane potential and malfunction of respiration following doxorubicin treatment. Even under acute and low concentration treatment conditions, doxorubicin caused depolarization of mitochondrial membrane potential ( $\Delta \Psi_m$ ) in iPSCs (Fig. 22). The loss of  $\Delta \Psi_m$ indicates an imbalance in the proton gradient essential for ATP synthesis and overall mitochondrial function (Dimroth et al., 2000). While  $\Delta \Psi_m$  naturally fluctuates throughout the course of physiological activity in cells, the lasting decrease of  $\Delta \Psi_m$  still observable after 48 hours in this study suggests a persistent impairment rather than a transient fluctuation. Previous studies described the loss of  $\Delta\Psi_m$  in mesenchymal stem cells (MSCs), H9C2 cells and iPSC-derived cardiomyocytes, but under chronic treatment conditions and high concentrations (Burridge et al., 2016; Helal et al., 2021; Maillet et al., 2016; Yang et al., 2013). The fact that we observed such effects at much lower concentration and shorter exposure times emphasizes the sensitivity of the mitochondrial membrane potential to even minimal concentrations of doxorubicin, while the potency of doxorubicin is highlighted. The loss of  $\Delta \Psi_m$ in iPSCs was accompanied by a significant reduction in mitochondrial oxygen consumption rate and ATP production (Fig. 23). Although iPSCs primarily rely on glycolysis, mitochondrial respiration in iPSCs could be evaluated using live-cell respirometry with the Seahorse Flux Analyzer device (Folmes et al., 2011; Prigione et al., 2011). As expected, iPSCs exhibited relative low levels of mitochondrial respiration, consistent with their dependency on glycolysis (Mathieu et al., 2014). Here, live-cell respirometry revealed reduction in mitochondrial respiration as early as 24 hour after doxorubicin treatment (Fig. 24). The alignment of  $\Delta \Psi_m$  and respiration disruption suggests that mitochondrial dysfunction develops rapidly and furthermore persists even 48 hours after recovery. Furthermore, these findings highlight  $\Delta \Psi_m$ and mitochondrial respiration, together with mitochondrial morphology, as sensitive indicators of mitochondrial dysfunction under acute exposure to low concentrations of doxorubicin. To further define the timepoint of mitochondrial malfunction, future approaches should focus on earlier timepoints (e.g.: 4 to 12 hours post-treatment) and investigate whether there are indications of partial recovery with prolongation of the recovery time. Within the timeframe of this study, it was not possible to investigate the effect of doxorubicin on mitochondrial respiration in iCMs. Especially in the context of the cardiotoxicity of doxorubicin, the extension of the studies to iCMs would be of great interest.

Despite the functional impairment of mitochondria shown by fragmentation of mitochondrial network, loss of  $\Delta \Psi_m$ , and reduced respiration, doxorubicin treatment was not accompanied with disruption of mitochondrial ultrastructure in iPSCs (Fig. 25). Electron microscopy revealed mitochondria with relative round shape and sparse cristae, characteristics of the immature mitochondrial phenotype previously described in other iPSC cell lines (Prigione et al., 2010; Suhr et al., 2010). This phenotype of mitochondria in iPSCs remained unaltered following the acute exposure to low concentrations of doxorubicin. This suggests that alterations on the ultrastructural level may require higher concentrations or longer treatment durations, as reported in previous studies applying chronic doxorubicin exposures (Sardão et al., 2009; Yin et al., 2018). Furthermore, the assembly of OXPHOS supercomplexes was unaffected upon doxorubicin treatment, with no visible effect on in-gel activity (Fig. 26). Notably, this finding indicates that mitochondrial energy metabolism is impaired without changes in the assembly of the OXPHOS machinery. To the best of our knowledge, this is the first demonstration of OXPHOS supercomplex assembly in iPSCs. Given the advantageous role of OXPHOS supercomplex formation in efficient ATP conversion and electron transport, this finding may be evaluated as a part of iPSC plasticity, which was previously reported for mouse embryonic stem cells (Carbognin et al., 2016). Further, these results indicate that mitochondrial dysfunction is disconnected from the structural assembly in the context of acute doxorubicin exposure. To assess potential structural alterations, future experiments could apply higher treatment concentrations or longer exposures, and include iCMs, which may lack the immature ultrastructure of iPSCs.

While the assembly of OXPHOS complexes remained unaffected, doxorubicin exposure resulted in changes of the nucleoid number without a corresponding increase in nucleoid size (Fig. 27). This contrasts with previous studies showing the condensation of nucleoids upon chronic exposure to doxorubicin as a response towards stress (Ashley & Poulton, 2009; Q. Chen et al., 2023; Feric et al., 2021). Given the role of TFAM in influencing nucleoid accumulation and condensation, the absence of nucleoid swelling under current conditions either suggests that TFAM-dependent condensation is not induced or that the protein levels of TFAM may be reduced following doxorubicin exposure. To support this finding, future approaches should assess TFAM protein levels and the TFAM:mtDNA ratio within nucleoids. The observed reduction in nucleoid number may alternatively reflect an increased turnover. In iCMs, where doxorubicin was applied at the terminally differentiation stage (iCM\_Mt\_Dox) or iPSC and iCM stage (iCM\_Dox\_Dox), the mtDNA copy number was strongly reduced (Fig. 53C), highlighting the need to examine nucleoids in these cells as well. Given the estimated

turnover rate of mitochondrial proteins in the heart (16–18 days), doxorubicin induced changes may persist rather than being rapidly cleared (Abdullah et al., 2019; Menzies & Golds, 1971). This aligns with previous findings showing that even doxorubicin pulse-treatment can lead to long-term mtDNA damage, potentially playing a role in the development of doxorubicin-induced cardiomyopathies (Lebrecht et al., 2003). To better understand the influence of doxorubicin on mitochondrial nucleoids, future experiments should aim to investigate mtDNA turnover, dynamics, replication efficacy, and mutation rates following acute doxorubicin exposure with low concentrations. These insights could reveal interesting mechanisms that link mitochondrial genome stability to cell fate and the development of long-term cardiotoxic risk.

In conclusion, this study demonstrated that even acute exposure of cells with concentrations of doxorubicin induced significant mitochondrial dysfunction in both iPSCs and iCMs. These findings highlight the role of mitochondria as early and sensitive targets of doxorubicin, even in the absence of ultrastructural defects, and emphasize the need for a more detailed investigation of mitochondrial integrity in cardiotoxicity risk assessment.

## 4.3. Low concentrations of doxorubicin do not lead to canonical DNA damage repair in iPSC

Doxorubicin damages various macromolecules, including the DNA, ultimately resulting in the induction of DNA lesions and activation of programmed cell death (Lin et al., 2018; Zhao & Zhang, 2017). Thereby, the highest potency of doxorubicin is observed in fast proliferating cells like cancer cells or stem cells (van der Zanden et al., 2021). However, terminally differentiated cells (e.g. cardiomyocytes) are also affected by the DNA damaging effects of doxorubicin, albeit to a lesser extend (Bremer & Hartung, 2005; Jahn et al., 2020). Consistent with these observations, our data showed progressive increase in resistance to doxorubicin as cells further progress from iPSC stage to terminally differentiated cardiomyocytes (Fig. 15, Fig. 33). This finding aligns with previous studies demonstrating the decrease of susceptibility to genotoxic insults with differentiation (Bremer & Hartung, 2005; Jahn et al., 2020; Laschinski et al., 1991), which is closely linked to differentiation-dependent changes in DDR signaling and the downstream threshold of apoptotic induction. Right after birth, terminally differentiated cardiomyocytes lose their proliferation capacity, whilst stem cells and their progenies still exhibit high proliferation capacity (Porrello et al., 2011). In accordance with this, iPSCs used in this study exhibited a high proliferation capacity, which was largely unaffected upon treatment with low concentrations of doxorubicin (Fig. 16). In agreement with their high proliferation capacity, treatment of iPSCs with low concentrations of doxorubicin (IC<sub>30</sub>-value) was accompanied with a moderate induction of programmed cell death (Fig. 18), which is

concordant with the low threshold of apoptotic pathway induction found in human stem cells. The susceptibility of iPSCs may be based on the presence of an efficient DNA replication machinery, which also comprises topoisomerase II alpha (TopolIα) and topoisomerase II beta (Topollβ), with both identified as major mediators of doxorubicin-induced DSBs (Tewey et al., 1984). In addition to DNA replication, other enzymes have been observed to interact with the covalent Topoll-DNA complex, resulting in the induction of DSBs. These enzymes include DNA helicases and RNA polymerases. Furthermore, the obstruction of the replication fork contributes to DNA double-strand break formation and, consequently, the induction of apoptosis of fast proliferative cells (J. V. Walker & Nitiss, 2002). The rapid induction of programmed cell death in stem cells has been proposed as a protective mechanism, to maintain the integrity of the stem cell pool by elimination of genetically damaged cells, thereby contributing to the homeostasis of the total organism (Fan et al., 2011). To support this, stem cells possess a strictly orchestrated DDR signaling and DNA damage repair machinery to encounter possible DSBs. Here, low concentrations of doxorubicin were not sufficient to induce DSBs in iPSCs with respect to the measured timepoints (Fig. 19A). Nevertheless, iPSCs used in this study showed a higher number of basal yH2AX foci per cell as compared to other iPSC cell lines (Liedtke et al., 2015) suggesting a strong influence of the somatic origin on DDR signaling in iPSCs, and a possible iPSC cell line-dependent influence on the thresholds of DSB induction. As described in section 3.1.2, yH2AX and 53BP1 activation is highly dependent on the activation of upstream kinases Ataxia Telangiectasia Mutated (ATM) by auto phosphorylation at DNA damage sites. Therefore, the aim was to elucidate the expression of these proteins in iPSCs upon moderate doxorubicin pulse-treatment (Fig. 19B). However, with respect to the applied concentrations, no activation of DDR signaling surrogate markers ATM and yH2AX was observed. In contrast, the positive control Eto did result in increased protein levels, which demonstrates that DNA damage signaling transduction in iPSCs can be activated in general. However, currently applied treatment conditions were insufficient to induce massive DDR signaling (Cruet-Hennequart et al., 2012; Huelsenbeck et al., 2012; Lin et al., 2018). Although our analysis of DNA damage was limited to iPSCs, with transcriptome data available for iCMs, we could not observe increased expression of genes involved in DNA damage response or repair genes at current treatment conditions applied. Furthermore, pairwise comparison between mock-treated iCMs (iCM Mt Mt) and iPSCs (iPSC Mt Mt) revealed suppression of genes associated with homologous recombination (HR), cell cycle and proliferation (data not shown), both shown to be downregulated upon differentiation of cells (Iyama & Wilson, 2013; Mujoo et al., 2017).

Together, these findings suggest that under the current doxorubicin treatment regimen apoptotic induction of iPSCs is not induced by massive induction of DNA double-strand breaks. Yet, the influence of DDR signaling transduction to effectors, such as the activation of tumor

suppressor protein p53 (p53), in the apoptotic induction cannot be excluded. To strengthen this finding, future experiments should entail the incorporation of downstream targets of DDR. Additionally, future experimental approaches should address DBS induction and DDR in iCMs under comparable conditions. Nevertheless, the current findings hint towards alternative targets of doxorubicin, which enhance the sensitivity of iPSCs to doxorubicin. Indeed, we observed persistent mitochondrial dysfunction as consequence of treatment with doxorubicin. Together, this emphasizes that under acute treatment regimens with low concentrations of doxorubicin and missing induction of DSBs, mitochondria may be primary targets of doxorubicin in both proliferative and terminally differentiated cells. Yet, genotoxic effects of doxorubicin on the mitochondrial genome cannot be excluded. Since mtDNA lacks the protection of histones which shield the nuclear DNA from potential damage, it is not clear whether mitochondrial dysfunction is induced via direct damage of mtDNA or through other mechanisms (e.g. ROS formation, ferroptosis, lipid peroxidation, etc.). Further investigations are needed to delineate the underlying mechanism of mitochondrial dysfunction under acute doxorubicin exposures.

# 4.4. Doxorubicin-mediated perturbations in transcriptional response of iPSCs and iCMs: Implications for fibrosis and cellular dysfunction

The investigation of moderate pulse-treatment of doxorubicin on the transcriptional response of iPSCs and iCMs was a strategical approach to investigate (i) the induction of differentiation-specific transcriptional differences, (ii) possible similarities in the stress responses upon Dox treatment, and (iii) the influence of diverse treatment timepoints on the response of iCMs towards doxorubicin, particularly the influence of a double-treatment.

Among the most prominent findings in iPSCs, expression of genes that are essential for the glycolytic process of energy conversion into ATP were found to be decreased indicating metabolic impairment following doxorubicin treatment (Fig. 39). This observation is consistent with previous findings in HepG2 cells (hepatocellar carcinoma) treated with doxorubicin for 24 hours, which also resulted in the suppression of glycolysis-related genes (Korga et al., 2019). Given the strong dependency of cancer cells on glycolysis, namely Warburg effect (Warburg et al., 1927), this suggests that even low concentrations of doxorubicin can impair the expression of metabolic central genes in highly proliferative and glycolysis-dependent cell types. Notably, targeted analysis of the RNA-seq dataset for OXPHOS genes revealed a reciprocal effect between iPSCs and iCMs, most notably the upregulation of mtDNA-encoded OXPHOS subunits (*MT-ATP6*, *MT-ATP8*, *MT-CO1*, *MT-CO2*, *MT-CO3*, *MT-CYB*, *MT-ND1*,

MT-ND2, MT-ND3, MT-ND4, MT-ND4L, MT-ND5, MT-ND6) in iPSCs (Fig. 43). Similar effects have previously been described in the human cardiac cell line AC16 showing upregulation of the mitochondrial complex subunit COX-1 upon chronic exposure to doxorubicin concentrations up to 125 nM (Yuan et al., 2016). These results indicate a compensatory mitochondrial response in iPSCs, possibly induced in order to counteract metabolic stress induced by the doxorubicin-induced suppression of essential genes of glycolysis. To support this hypothesis, future experiments should implement examination of mRNA levels of mtDNA-encoded OXPHOS subunits or OXPHOS activity (e.g. live-cell respirometry) at later timepoints of recovery.

As indicated by the number of DEGs, iPSCs and iCMs exhibit transcriptional profiles that suggest a specific differentiation-dependent response to the doxorubicin treatment (Fig. 41B, Fig. 42B). Notably, iPSCs showed a higher extent of DEGs of transcriptional remodeling compared to iCMs, reflected by the number of DEGs. This aligns with the generally higher transcriptional rate of stem cells compared to terminally differentiated cells (Natarajan et al., 2017). Furthermore, our data exhibited a downregulation of major genes in ribosomal architecture in iPSCs. This finding suggests a substantial impact on the translation in these cells, which was still measurable 48 hours after treatment and is consistent with previous findings showing the reduction in general protein translation upon doxorubicin treatment (Halim et al., 2018).

In contrast, transcriptional response of iCMs primarily revealed downregulation of genes necessary for cardiac myogenesis and thereof cardiac function (Fig. 41). Interestingly, we observed upregulation of developmental markers, TBX1, SHH, and SIX1, which are key regulators of second heart field (SHF) during early cardiac development (Rochais et al., 2009; H. Xu et al., 2004). These progenitor cells contribute to the development of the linear heart tube and persists in the adult heart, however, their function in cardiac repair and remodeling is still under debate (Rochais et al., 2009). Both, the expression of SIX1 and its downstream target TBX1 are essential for the development of SHF, as loss of TBX1 has been linked to congenital cardiac abnormalities (Guo et al., 2011). Consequently, the observed increase in transcription of the genes may be a compensatory mechanism that enhances cellular survival upon exposure to doxorubicin. Only ten DEGs were shared between iPSCs and iCMs under doxorubicin treatment conditions, none of which were linked to mitochondrial function or DNA damage signaling pathways (Fig. 41, Fig. 42). These results emphasize the cell stage-specific difference of the transcriptional response to doxorubicin. While iPSCs displayed a pronounced transcriptional remodeling and suppression of metabolic relevant genes, iCMs showed a more specialized shift in genes related to cardiac function and regeneration. Together, distinct changes in gene expression underscore the cell state-specific impact of doxorubicin and may have implications for understanding lineage-specific susceptibility to doxorubicin-induced toxicity.

To obtain a more comprehensive understanding of the temporal influence of doxorubicin, a systematic transcriptional approach was implemented to decipher how treatment times influences the transcriptional response of iCMs. For this, cells were either exposed to doxorubicin at the iPSC stage, at the late stage of cardiac differentiation or in both stages (Fig. 46). In all conditions, treatment with doxorubicin included the upregulation of genes associated with structural changes (e.g. contractile apparatus), particularly in iCMs, where these changes are shown to be linked to cardiomyopathy-related pathways (Belger et al., 2024). Furthermore, analysis of DEGs shared by all treatment conditions revealed a time-independent downregulation of genes critical for cardiac function, including those involved in contractility and calcium homeostasis (Fig. 51). This aligns with findings from a previous multi-omics study on chronic exposure of iCMs with low concentrations of doxorubicin (Holmgren et al., 2018). The heart exhibits a limited capacity for regeneration rapidly surpassed by exposure to doxorubicin the induction of cardiac fibrosis (Steinberg et al., 1987). Extracellular matrix remodeling (ECM) contributes to an increase in cardiac stiffness and long-term structural dysfunction (Tanaka et al., 2020). Notably, even acute exposures of cells to low concentrations of doxorubicin prior to cardiac differentiation resulted in the upregulation of genes associated with ECM (Fig. 46, Fig. 47). Among these, BNC2, a transcription factor belonging to the zincfinger family mainly expressed in myofibroblasts and implicated role in ECM (Bobowski-Gerard et al., 2022). Previous studies identified BNC2 as reliable marker for cardiac dysfunction showing increased expression in survivors of heart failure when compared to healthy individuals. Moreover, a multi-omics approach identified the increase of BCN2 as a major driver of myofibroblast activation and fibrosis (Bobowski-Gerard et al., 2022). Another gene of interest is WT1, which plays a pivotal role in the regeneration of adult hearts (Wagner et al., 2021). Supporting this, deletion of WT1 in cardiomyocytes was shown to enhance fibrosis following the exposure of mice to doxorubicin (Díaz del Moral et al., 2023), while its upregulation promotes tissue regeneration upon myocardial infarction emphasizing its cardioprotective role (Wagner et al., 2021). Together with BCN2, more detailed examination is needed to gain more insights in the role of both genes in mediating cardiac damage and regeneration. In our study, doxorubicin treatment resulted in the upregulation of several collagen genes, supporting the potency of doxorubicin inducing ECM, even with acute exposure to low concentrations. Particularly in iCMs receiving doxorubicin treatment prior to cardiac differentiation, sustained transcriptional alterations were observed in genes critical for contractile function and calcium homeostasis (Fig. 47). Together, these findings emphasize the potency of doxorubicin as already short exposures initiate ECM and functional remodeling on the transcriptome level in iCMs treated at the iPSC stage. Furthermore, doxorubicin treatment at the stem cell stage

resulted in transcriptional remodeling that remained detectable in differentiated iCMs, suggesting persistent transcriptional regulation initiated during early development. This highlights stem cells not only as highly sensitive targets of doxorubicin-induced stress, but also are potential mediators of impaired cardiac regeneration. To support this hypothesis, future approaches should follow ECM throughout cardiac differentiation via time-course analysis of collagen and of ECM-related gene or protein expression.

Whole-genome transcriptome profiling of iCMs treated on day 7 of cardiac differentiation revealed an upregulation of genes associated with programmed cell death pathways, including increased expression of death receptor pathways (Fig. 48) This aligns with previous findings showing increased death receptor expression in iCMs following doxorubicin exposure (Zhao & Zhang, 2017). Our results indicated that treatment with low concentrations of doxorubicin at a late stage of cardiac differentiation enhances death receptor expression, potentially lowering the threshold for apoptosis in terminally differentiated iCMs. Consistent with this, iCMs pre-conditioned by doxorubicin treatment in iPSC stage exhibited an increased, yet not significant, susceptibility to a second doxorubicin exposure (Fig. 52). To validate the upregulation of death receptors induced by doxorubicin, immunohistochemistry or immunoblotting analysis should be performed in future experiments. Moreover, the characterization of death receptor expression could bring more insights into the effect of repeated doxorubicin exposure on the long-term susceptibility of cardiomyocytes.

Finally, we introduced a novel double-treatment strategy to explore potential hormesis-like effects. This approach involved preconditioning iCMs by exposing iPSCs to low doxorubicin concentrations prior to differentiation. While previous studies have demonstrated that mild ischemic pre-conditioning can enhance cardiac resilience to subsequent ischemic insults (Yellon & Downey, 2003), our results revealed the opposite: Pre-conditioning at the iPSC stage increased the susceptibility of iCMs to a second encounter to doxorubicin, as revealed by cell viability measurements (Fig. 52). As discussed earlier, upregulation of death receptors during late-stage treatment may contribute to the increased susceptibility (Fig. 48). However, transcriptomic data suggest that mitochondrial dysfunction also plays a significant role. Specifically, genes encoding subunits of mitochondrial complex I and III (NDUFS2, NDUFS8, and UQCRC1) were uniquely downregulated in double-treated iCMs, indicating enhanced OXPHOS impairment following a second encounter with doxorubicin. This effect was further supported by reduced expression of COX5B, a nuclear-encoded subunit of cytochrome c oxidase which plays an important part in mitochondrial respiration (Mansilla et al., 2018). Notably, COX5B protein levels have been identified as a reliable biomarker for sudden cardiac death (Tan et al., 2011). This raises the question whether reduction of COX5B proteins are also observed in double-treatment conditions and whether this protein remains a reliable

biomarker under treatment regimens comprising acute and low concentrations of doxorubicin. Together with the observed mitochondrial fragmentation and mtDNA depletion in double-treated iCMs, these finding point to a central role of mitochondrial dysfunction, along with death receptor signaling in mediating doxorubicin-induced cardiotoxicity. This has critical implications for clinical regimens that normally involve the periodical application of doxorubicin during cancer treatment, emphasizing the need of further investigation of mitochondria as mediators of cardiotoxic effects.

In addition to mitochondrial dysfunction, we found alterations in transcript levels of the muscle-specific RING finger (MuRF) protein family members. MuRFs, particularly MURF1, MURF1, MURF2, and MURF3 are RING type E3 ligases orchestrating protein degradation and cardiac homeostasis (Hoshijima, 2006; Peris-Moreno et al., 2020). While MURF1 (encoded by TRIM63) is upregulated in models of muscle atrophy, including high concentrations of doxorubicin (Kumarapeli et al., 2005; Sakai et al., 2014), we observed a reduction of TRIM63 expression in double-treated iCMs (Fig. 50). This hints towards a concentration-dependent regulation of MURF1. Supporting this, previous reports observed downregulation of MURF1 after application of low doses of doxorubicin in mice (Peris-Moreno et al., 2020). This raises the question whether MuRF proteins, beyond their role in muscle atrophy, may also contribute to mitochondrial regulation and cardiac contractility under current treatment conditions. In particular, recent evidence shows that mice lacking MURF1 and MURF3 exhibit reduced levels of mitochondrial biogenesis factor Peroxisome Proliferator-Activated Receptor Gamma Coactivator 1-Alpha (PGC1α), reinforcing their potential role in mitochondrial homeostasis (Elisa Martin, 2024). Overall, these findings reveal that pre-conditioning of stem cells with doxorubicin sensitizes differentiated cardiomyocytes to subsequent treatment by promoting mitochondrial dysfunction, impairing oxidative metabolism, and altering key regulatory pathways involved in contractility and survival. Future studies should investigate whether modulation of mitochondrial biogenesis or stabilization of MuRF protein function could mitigate the cumulative cardiotoxic effects observed under repeated applications of low concentrations of doxorubicin.

### 4.5. Conclusion and Outlook

This study established mitochondria as sensitive mediators of doxorubicin-induced cardiotoxicity, independent of the induction of canonical DNA damage signaling. Our findings point to a strong differentiation- and time-dependent cellular response, with iPSCs showing induction of mitochondrial stress and transcriptional remodeling even under low and acute doxorubicin exposure. Importantly, the data suggest that cardiac progenitors and stem cells should be considered as critical targets in cardiotoxicity as damage of these cells may induce defect healing. Therefore, enhancement of the overall survival and homeostasis of CSCs could potentially minimize doxorubicin-induced cardiotoxic effects seen in former pediatric cancer survivors and serve as future approach for cardiac regeneration.

To strengthen the indication of missing DSB induction under the current treatment conditions, targeted inhibition or knockout of the DNA damage repair proteins as ATM or ATR will help confirm the absence of DSB-driven DDR signaling. Further examination of mitochondrial mtDNA, including TFAM:mtDNA ratio analysis, detection of mtDNA oxidation or deletions, will help to examine the influence of doxorubicin on mtDNA and to define the role of mtDNA alterations as mitochondrial stress marker. The implementation of stimulated emission depletion (STED) microscopy provides higher resolution for further investigation of mitochondrial nucleoid composition in iPSCs and iCMs under doxorubicin treatment.

Furthermore, transcriptomic changes observed in iCMs suggest specific pathways including fibrosis, and cardiac contractility as targets for possible therapeutic modulation. Future studies should explore genetic or chemical interventions in these pathways and evaluate known cardioprotective agents (e.g. dexrazoxane) in this model. The use of 3D engineered heart tissues and iCM maturation protocols will provide more physiological relevance. Furthermore, the implementation of other cardiac cell types into the current model would enable the investigation of doxorubicin treatment on intercellular communication, structural remodeling and contractile dysfunction. Lastly, patient-derived iPSCs could enable personalized screening platforms to identify patient-specific susceptibilities to doxorubicin and optimize protective strategies. Together, this work serves as a start for future approaches that combine mitochondrial protection, transcriptional modulation, and cell-type-specific targeting to reduce the long-term cardiac side effects of doxorubicin therapy.

## 5. Summary

The anthracycline antibiotic doxorubicin is widely used as chemotherapeutic agent for treatment of solid tumors and hematological malignancies in both adults and children. Despite its clinical efficacy, its application is limited by adverse effects on somatic tissue, particularly in the heart. Doxorubicin treatment can lead to irreversible cardiotoxicity, including arrhythmias, long-term cardiovascular complications or congestive heart failure. Several mechanisms have been implicated in the development of cardiotoxicity, such as induction of DNA damage, involvement in the formation of oxidative stress and damage of organelles, especially reflected in mitochondrial dysfunction. Importantly, mitochondrial malfunction has previously been described under comparatively high and prolonged exposure to doxorubicin, raising the question whether observed effects on mitochondria are downstream events of genotoxic effects on nuclear DNA. In order to decipher the influence of mitochondria in mediating doxorubicin toxicity, a treatment regimen mindful to the clinical situation was applied. An additional challenge in studying these processes was the availability of a human based cardiomyocyte model. For this, a human-induced pluripotent stem cells (iPSCs) were established in order to generate cardiac progenitors (CPs) and iPSC-derived cardiomyocytes (iCMs) to provide an experimental platform to study cell type- or differentiation-specific responses to doxorubicin treatment in a clinical relevant set-up. The present study aimed to investigate how acute exposure to low concentrations of doxorubicin affects iPSCs and iCMs, with a focus on DNA damage response, mitochondrial function, transcriptional expression and cellular function. With comparison of the response of iPSCs and iCMs upon doxorubicin treatment regimens in iPSCs and iCMs, we sought to gain further insights into stage-dependent susceptibility to doxorubicin and the induction of transcriptional programs that may be involved in the development of cardiotoxic effects. Furthermore, we aimed to understand whether preconditioning of iPSCs prior to initiation of cardiac differentiation alters iCM susceptibility towards a second exposure to doxorubicin, thereby testing the hypothesis of a hormesis-like protective effect involving the upregulation of genes involved in stress response pathways. Several insights into the cellular effects of doxorubicin at clinically relevant concentrations and exposure times were revealed. The results indicate that even short exposures to low concentrations of doxorubicin induced substantial mitochondrial dysfunction and metabolic disturbances, accompanied with transcriptional alterations, which could contribute to long-term cardiotoxicity.

Firstly, the present study demonstrated that iPSCs are highly sensitive towards acute exposure to low concentrations of doxorubicin with a significant reduction in cell viability. Furthermore, mitochondria exhibited altered morphology, characterized by increased fragmentation, loss of membrane potential, and reduction in mitochondrial content. It is important to note that these effects occurred independently of DSB formation and doxorubicin-induced DDR activation,

suggesting that mitochondrial impairment is a direct and primary target of doxorubicin rather than a secondary consequence of nuclear genotoxicity. The present findings emphasize that the disruption of mitochondrial dynamics and function may play a critical role in the progression of doxorubicin-induced cardiotoxicity, albeit further approaches are needed to validate the observed effects. Secondly, there was evidence of differentiation-dependent variations in the susceptibility of iPSCs and iCMs to doxorubicin. In contrast to terminally differentiated cardiomyocytes, iPSCs predominantly activate apoptosis as a protective mechanism against genomic instability. Indeed, iPSCs displayed a higher sensitivity to doxorubicin-induced apoptosis compared to differentiated iCMs, a finding that correlates with the high proliferative capacity of iPSCs and the generally lower threshold of iPSCs to undergo apoptosis. The increased susceptibility of iPSCs may be attributed to mitochondrial stress comprising of mitochondrial membrane potential loss, metabolic disruption, and alterations in the mitochondrial genome. The latter being consistent with the known genotoxic role of Dox via the inhibition of mitochondrial located topoisomerase IIB. Furthermore, transcriptomic analysis revealed profound effects of doxorubicin treatment on cellular metabolism and cardiac function. In iPSCs, doxorubicin exposure led to downregulation of glycolytic pathway genes, suggesting impaired energy metabolism. Interestingly, we could observe compensatory mechanisms in form of increased mtDNA-encoded OXPHOS genes in iPSCs upon doxorubicin treatment. In contrast, iCMs majorly exhibited a suppression in genes associated with cardiac function (e.g. contractility, calcium homeostasis, and sarcomere organization), highlighting potency of doxorubicin to impair cardiac function even at low concentrations. Furthermore, the activation of extracellular matrix modifying genes in iCMs suggests the promotion of fibrosis under doxorubicin treatment regimens.

The present data demonstrates that pre-conditioning of cells in pluripotent state is accompanied with transcriptional reprogramming in a way that cardiac differentiation is not adversely affected *per se*, yet with alterations of cardiac function. Furthermore, we aimed to understand whether a double-treatment approach, where iPSCs were pre-conditioned with doxorubicin prior to cardiac differentiation followed by a second encounter with doxorubicin in iCM stage, induces protective adaptations of these cells. Contrary to the expectations, this approach exacerbated mitochondrial dysfunction and increased susceptibility to subsequent doxorubicin exposure. Here, double-treated iCMs exhibited a stronger downregulation of genes associated with mitochondrial and cardiac function, along with an increased expression of cell death markers, highlighting has cumulative and persistent adverse effects even with the application of low concentrations, which might explain the increased sensitivity of these cells. Overall, the present results emphasize the potency of doxorubicin, even with acute exposures and low concentrations, resulting in mitochondrial dysfunction, metabolic dysregulation, and transcriptional remodeling possibly mediating cardiotoxic effects. More experimental

approaches are needed to understand the relationship of cardiac malfunction and cardiac stem cell pool contribution to the manifestation of cardiotoxicity observed in patients treated with doxorubicin. However, with the iPSC-based model, we could reproduce the most common side-effects of doxorubicin comprising fibrosis induction and contractile dysfunction of iCMs at comparably low concentrations highlighting the susceptibility of stem cells towards doxorubicin. Thus, future experimental approaches should comprise the application of low concentrations of doxorubicin to examine the underlying mechanisms in doxorubicin-induced damage response as well as to determine the possible role of cardiac stem cells in the manifestation of cardiotoxicity.

Furthermore, future approaches should implement the modulation of mitochondrial function which subsequently improves cellular resistance to metabolic stress. Moreover, the enhancement of mitochondrial biogenesis, modulation of mitochondrial dynamics, or administration of cardioprotective agents (e.g.: dexrazoxane), could be possible targets to reduce long-term cardiotoxic effects of doxorubicin.

## 6. Zusammenfassung

Anthrazykline wie Doxorubicin finden sowohl bei Erwachsenen als auch Kindern breite Anwendung als Chemotherapeutikum zur Behandlung solider Tumoren und hämatologisch maligner Erkrankungen. Trotz ihrer hohen Effizienz ist die Anwendung durch Nebenwirkungen auf somatisches Gewebe, insbesondere auf das Herz, eingeschränkt. Eine Behandlung mit Doxorubicin kann zu irreversiblen kardiotoxischen Effekten führen, die sich in Form von Arrhythmien, langfristige kardiovaskulären Komplikationen oder Herzinsuffizienz manifestieren können. An der Entstehung kardiotoxischer Effekte sind vermutlich mehrere Mechanismen beteiligt, darunter die Induktion von DNA Schäden, die Beteiligung an der Entstehung von oxidativem Stress, sowie die Schädigung von Organellen, insbesondere der Mitochondrien. Frühere Studien konnten bereits eine mitochondriale Dysfunktion feststellen, allerdings meist unter vergleichsweise hohen Behandlungskonzentrationen oder längerer Expositionsdauern. Dies wirft die Frage auf, ob die beobachteten Auswirkungen auf die mitochondriale Funktion jedeglich Folgeerscheinungen der genotoxischen Effekte von Doxorubicin auf die nukleäre DNA darstellen. Um den Einfluss der Mitochondrien auf die Vermittlung der Doxorubicin induzierten Toxizität näher zu untersuchen, wurde ein Behandlungsschema gewählt, das sich an klinisch relevanten Bedingungen orientiert. Eine weitere Herausforderung stellte die Verfügbarkeit humaner Kardiomyozyten dar. Zu diesem Zweck wurden humane induzierte pluripotente Stammzellen (iPSCs) etabliert, aus denen Herzvorläuferzellen (CP) und Kardiomyzyten (iCMs) generiert wurden. Diese dienten als experimentelle Plattform, um in einem klinisch relevanten Kontext zelltyp- oder differenzierungsabhängige Effekte der Doxorubizinbehandlung zu untersuchen. Die hier vorliegende Studie untersuchte die Auswirkungen einer akuten Exposition gegenüber niedrigen Doxorubicin-Konzentrationen auf iPSCs und iCMs, wobei der Schwerpunkt auf DNA Schadensantwort, mitochondrialer Funktion, Genexpression, sowie zellulärer Funktion lag. Durch den Vergleich von iPSCs und iCMs sollten Erkenntnisse über die differenzierungsabhängigen Suszeptibilität gegenüber Doxorubicin und die Induktion transkriptioneller Programme gewonnen werden, die möglicherweise eine Rolle bei der Entwicklung langfristiger kardiotoxischer Effekte spielen. Darüber hinaus wurde im Rahmen der Idee eines Hormesis-Effekts untersucht, ob eine Vorbehandlung von iPSCs mit Doxorubicin vor der kardialen Differenzierung die Suszeptibilität von iCMs gegenüber einer zweiten Exposition verändert und ob diese Vorbehandlung mit einer Hochregulierung von Genen assoziiert mit zellulären Stressantworten einhergeht.

Im Rahmen dieser Studie wurden die Auswirkungen von niedrigen und akuten Doxorubicin-Expositionen induziert-pluripotente Stammzellen (iPSCs) auf und iPSC-generierte Kardiomyozyten (iCMs) untersucht. Hierbei lag der Schwerpunkt auf Untersuchung der mitochondrialen Funktion, der DNA-Schadensreaktion und transkriptionellen Veränderungen. Die Ergebnisse lieferten mehrere wichtige Erkenntnisse über die zellulären Auswirkungen von Doxorubicin bei klinisch relevanten Konzentrationen und Expositionszeiten. Die Ergebnisse deuten darauf hin, dass selbst eine kurze Exposition gegenüber niedrigen Doxorubicin-Konzentrationen eine erhebliche mitochondriale Dysfunktion und Inhibierung des Metabolismus auslöst, die mit Transkriptionsveränderungen einhergehen und zur langfristigen Kardiotoxizität beitragen.

Zu Beginn hat die vorliegende Studie hat gezeigt, dass iPSCs selbst gegenüber einer kurzzeitigen Exposition mit niedrigen Konzentrationen eine hohe Sensitvität aufweisen. Darüber hinaus wiesen Mitochondrien eine verstärkte Fragmentierung, einen Verlust des mitochondrialen Membranpotenzials und eine Verringerung des mtDNA:gDNA Verhältnis auf. Die beobachteten Effekte traten unabhängig von der Bildung von DNA-Doppelstrangbrüchen (DSB) und der Aktivierung der DNA-Schadensreaktion auf, was darauf hindeutet, dass die Beeinträchtigung der Mitochondrien ein direktes und primäres Ziel von Doxorubicin ist und nicht eine sekundäre Folge der nuklearen Genotoxizität. Die vorliegenden Ergebnisse unterstreichen, dass die Störung der mitochondrialen Dynamik und Funktion eine entscheidende Rolle beim Fortschreiten der Doxorubicin-induzierten Kardiotoxizität spielen könnte, auch wenn weitere Ansätze erforderlich sind, um die beobachteten Auswirkungen zu validieren.

Zudem gab es Hinweise auf differenzierungsabhängige Unterschiede in der Anfälligkeit von iPSCs und iCMs für Doxorubicin. Im Gegensatz zu terminal differenzierten Kardiomyozyten aktivieren iPSCs vorwiegend die Apoptose als Schutzmechanismus gegen genomische Instabilität. Tatsächlich zeigten iPSCs im Vergleich zu differenzierten iCMs eine höhere Empfindlichkeit gegenüber Doxorubicin-induzierter Apoptose, ein Ergebnis, das mit der hohen Proliferationsfähigkeit von iPSCs und der allgemein niedrigeren Schwelle von iPSCs, Apoptose zu durchlaufen, korreliert. Die erhöhte Anfälligkeit von iPSCs könnte auf mitochondrialen Stress zurückzuführen sein, der aus dem Verlust des mitochondrialen Membranpotenzials, Stoffwechselstörungen und Veränderungen im mitochondrialen Genom besteht. Letzteres steht im Einklang mit der bekannten genotoxischen Rolle von Doxorubicin durch die Hemmung der mitochondrial lokalisierten Topoisomerase IIβ.

Darüber hinaus offenbarte die Analyse des Transkriptoms tiefgreifende Auswirkungen der Doxorubicin-Behandlung auf den zellulären Stoffwechsel und die Herzfunktion. In iPSCs führte die Doxorubicin-Exposition zu einer Herunterregulierung von Genen des glykolytischen Stoffwechsels. Energiestoffwechsel was auf einen gestörten schließen Doxorubicin-Behandlung Interessanterweise konnten wir bei iPSCs nach einer kompensatorische Mechanismen in Form von vermehrten mitochondrialen DNA-kodierten OXPHOS-Genen beobachten. Im Gegensatz dazu kam es bei iCMs zu einem Rückgang von Genen, die mit einer normalen Herzfunktion in Verbindung stehen (z.B. Kontraktilität, Kalziumhomöostase und Sarkomerorganisation). Dies zeigt, dass Doxorubicin die

Herzfunktion selbst bei niedrigen Konzentrationen beeinträchtigen kann. Weitergehend deutet die Aktivierung von Genen, die die extrazelluläre Matrix modifizieren, auf die Förderung von Fibrose unter Doxorubicin-Behandlungsschemata hin.

Die vorliegenden Daten zeigen, dass die Vorbehandlung von Zellen im pluripotenten Zustand mit einer transkriptionellen Umprogrammierung einhergeht, so dass die Differenzierung in Kardiomyozyten zwar nicht *per se* beeinträchtigt wird, jedoch die Herzfunktion verändert wird. Darüber hinaus wollten wir herausfinden, ob eine Vorbehandlung von iPSCs vor der Herzdifferenzierung mit Doxorubicin bei zweiter Exposition mit Doxorubicin im iCM-Stadium, schützende Anpassungen dieser Zellen hervorruft. Entgegen den Erwartungen verschlimmerte dieser Ansatz die mitochondriale Dysfunktion und erhöhte die Anfälligkeit für eine nachfolgende Doxorubicin-Exposition. Hier zeigten doppelt behandelte iCMs eine stärkere Herabregulierung mitochondrialer und kontraktilitätsbezogener Gene sowie eine verstärkte Expression von Apoptosemarkern. Diese Erkenntnisse untermauern, dass eine wiederholte Doxorubicin-Exposition kumulative und anhaltende schädliche Auswirkungen hat, selbst bei Anwendung niedriger Konzentrationen.

Insgesamt unterstreichen die vorliegenden Ergebnisse die Potenz von Doxorubicin, da bereits eine akute Exposition gegenüber niedrigen Doxorubicin-Konzentrationen zu mitochondrialer Dysfunktion, metabolischer Dysregulation und transkriptionellen Veränderungen führt, die möglicherweise kardiotoxische Effekte vermitteln. Es sind weitere Untersuchungen erforderlich, um die Beziehung zwischen kardialer Fehlfunktion und dem Beitrag des kardialen Stammzellpools zur Manifestation der bei Patienten beobachteten Kardiotoxizität besser zu verstehen. Mit dem iPSC-basierten Modell konnten wir jedoch die häufigsten Nebenwirkungen von Doxorubicin, nämlich die Induktion von Fibrose und die kontraktile Dysfunktion von iCMs, bei vergleichsweise niedrigen Doxorubicin-Konzentrationen eindeutig reproduzieren, was die Anfälligkeit von Stammzellen gegenüber Doxorubicin verdeutlicht. Künftige experimentelle Ansätze sollten daher die Anwendung niedriger Doxorubicin-Konzentrationen umfassen, um die zugrundeliegenden Mechanismen der Doxorubicin-induzierten Schädigungsreaktion zu untersuchen und die mögliche Rolle kardialer Stammzellen bei der Manifestation der Kardiotoxizität zu ermitteln.

Darüber hinaus sollte der Schutz der mitochondrialen Funktion implementiert werden, um die zelluläre Resistenz gegen metabolischen Stress zu verbessern. Weitergehend könnten Modulationen der mitochondrialen Biogenese, der mitochondrialen Dynamik oder die Verabreichung von kardioprotektiven Wirkstoffen (z.B.: Dexrazoxane) mögliche Ziele sein, um die langfristigen toxischen Auswirkungen von Doxorubicin auf das Herz zu reduzieren.

.

### 7. References

- Abdullah, C. S., Alam, S., Aishwarya, R., Miriyala, S., Bhuiyan, M. A. N., Panchatcharam, M., Pattillo, C. B., Orr, A. W., Sadoshima, J., Hill, J. A., & Bhuiyan, M. S. (2019). Doxorubicin-induced cardiomyopathy associated with inhibition of autophagic degradation process and defects in mitochondrial respiration. *Scientific Reports*, 9(1), 1–20. https://doi.org/10.1038/s41598-018-37862-3
- Abe, K., Ikeda, M., Ide, T., Tadokoro, T., Miyamoto, H. D., Furusawa, S., Tsutsui, Y., Miyake, R., Ishimaru, K., Watanabe, M., Matsushima, S., Koumura, T., Yamada, K. I., Imai, H., & Tsutsui, H. (2022). Doxorubicin causes ferroptosis and cardiotoxicity by intercalating into mitochondrial DNA and disrupting Alas1-dependent heme synthesis. *Science Signaling*, *15*(758). https://doi.org/10.1126/SCISIGNAL.ABN8017/SUPPL\_FILE/SCISIGNAL.ABN8017\_MD AR REPRODUCIBILITY CHECKLIST.PDF
- Ahmad, F., Banerjee, S. K., Lage, M. L., Huang, X. N., Smith, S. H., Saba, S., Rager, J., Conner, D. A., Janczewski, A. M., Tobita, K., Tinney, J. P., Moskowitz, I. P., Perez-Atayde, A. R., Keller, B. B., Mathier, M. A., Shroff, S. G., Seidman, C. E., & Seidman, J. G. (2008). The Role of Cardiac Troponin T Quantity and Function in Cardiac Development and Dilated Cardiomyopathy. *PLoS ONE*, *3*(7), e2642. https://doi.org/10.1371/journal.pone.0002642
- Althoff, T., Mills, D. J., Popot, J. L., & Kühlbrandt, W. (2011). Arrangement of electron transport chain components in bovine mitochondrial supercomplex I 1 III 2 IV 1. *EMBO Journal*, 30(22), 4652–4664. https://doi.org/10.1038/emboj.2011.324
- Alvarez, I. M. H., Kulkarni, S. S., Joffraud, M., Boutant, M., Ratajczak, J., Gao, A. W., Maclachlan, C., Raymond, F., Metairon, S., Descombes, P., Houtkooper, R. H., Zorzano, A., & Cantó, C. (2016). Mfn1 deficiency in the liver protects against dietinduced insulin resistance and enhances the hypoglycemic effect of metformin. *Diabetes*, 65(12), 3552–3560. https://doi.org/10.2337/db15-1725
- Anand, R., Wai, T., Baker, M. J., Kladt, N., Schauss, A. C., Rugarli, E., & Langer, T. (2014). The i-AAA protease YME1L and OMA1 cleave OPA1 to balance mitochondrial fusion and fission. *Journal of Cell Biology*, 204(6), 919–929. https://doi.org/10.1083/jcb.201308006
- Anders, S., Pyl, P. T., & Huber, W. (2015). HTSeq—a Python framework to work with high-throughput sequencing data. *Bioinformatics*, *31*(2), 166–169. https://doi.org/10.1093/bioinformatics/btu638
- Anderson, S., Bankier, A. T., Barrell, B. G., De Bruijn, M. H. L., Coulson, A. R., Drouin, J., Eperon, I. C., Nierlich, D. P., Roe, B. A., Sanger, F., Schreier, P. H., Smith, A. J. H., Staden, R., & Young, I. G. (1981). Sequence and organization of the human mitochondrial genome. *Nature*, *290*(5806), 457–465. https://doi.org/10.1038/290457a0
- Ang, Y. S., Rivas, R. N., Ribeiro, A. J. S., Srivas, R., Rivera, J., Stone, N. R., Pratt, K., Mohamed, T. M. A., Fu, J. D., Spencer, C. I., Tippens, N. D., Li, M., Narasimha, A., Radzinsky, E., Moon-Grady, A. J., Yu, H., Pruitt, B. L., Snyder, M. P., & Srivastava, D. (2016). Disease Model of GATA4 Mutation Reveals Transcription Factor Cooperativity in Human Cardiogenesis. *Cell*, *167*(7), 1734-1749.e22. https://doi.org/10.1016/j.cell.2016.11.033
- Arcamone, F., Cassinelli, G., Fantini, G., Grein, A., Orezzi, P., Pol, C., & Spalla, C. (1969). Adriamycin, 14-hydroxydaimomycin, a new antitumor antibiotic from *S. Peucetius* var. caesius. Biotechnology and Bioengineering, 11(6), 1101–1110. https://doi.org/10.1002/bit.260110607

- Árnadóttir, E. R., Moore, K. H. S., Guðmundsdóttir, V. B., Ebenesersdóttir, S. S., Guity, K., Jónsson, H., Stefánsson, K., & Helgason, A. (2024). The rate and nature of mitochondrial DNA mutations in human pedigrees. *Cell*, *187*(15), 3904-3918.e8. https://doi.org/10.1016/J.CELL.2024.05.022
- Arruebo, M., Vilaboa, N., Sáez-Gutierrez, B., Lambea, J., Tres, A., Valladares, M., & González-Fernández, Á. (2011). Assessment of the Evolution of Cancer Treatment Therapies. *Cancers 2011, Vol. 3, Pages 3279-3330*, *3*(3), 3279–3330. https://doi.org/10.3390/CANCERS3033279
- Ashley, N., & Poulton, J. (2009). Anticancer DNA intercalators cause p53-dependent mitochondrial DNA nucleoid re-modelling. *Oncogene 2009 28:44*, *28*(44), 3880–3891. https://doi.org/10.1038/onc.2009.242
- Avagimyan, A., Pogosova, N., Kakturskiy, L., Sheibani, M., Challa, A., Kogan, E., Fogacci, F., Mikhaleva, L., Vandysheva, R., Yakubovskaya, M., Faggiano, A., Carugo, S., Urazova, O., Jahanbin, B., Lesovaya, E., Polana, S., Kirsanov, K., Sattar, Y., Trofimenko, A., ... Sarrafzadegan, N. (2024). Doxorubicin-related cardiotoxicity: review of fundamental pathways of cardiovascular system injury. In *Cardiovascular Pathology* (Vol. 73, p. 107683). Elsevier Inc. https://doi.org/10.1016/j.carpath.2024.107683
- Bacakova, L., Zarubova, J., Travnickova, M., Musilkova, J., Pajorova, J., Slepicka, P., Kasalkova, N. S., Svorcik, V., Kolska, Z., Motarjemi, H., & Molitor, M. (2018). Stem cells: their source, potency and use in regenerative therapies with focus on adipose-derived stem cells a review. In *Biotechnology Advances* (Vol. 36, Issue 4, pp. 1111–1126). Elsevier Inc. https://doi.org/10.1016/j.biotechadv.2018.03.011
- Baker, M. J., Lampe, P. A., Stojanovski, D., Korwitz, A., Anand, R., Tatsuta, T., & Langer, T. (2014). Stress-induced OMA1 activation and autocatalytic turnover regulate OPA1-dependent mitochondrial dynamics. *EMBO Journal*, *33*(6), 578–593. https://doi.org/10.1002/embj.201386474
- Bakkenist, C. J., & Kastan, M. B. (2003). DNA damage activates ATM through intermolecular autophosphorylation and dimer dissociation. *Nature 2003 421:6922*, *421*(6922), 499–506. https://doi.org/10.1038/nature01368
- Balafkan, N., Mostafavi, S., Schubert, M., Siller, R., Liang, K. X., Sullivan, G., & Bindoff, L. A. (2020). A method for differentiating human induced pluripotent stem cells toward functional cardiomyocytes in 96-well microplates. *Scientific Reports*, *10*(1), 18498. https://doi.org/10.1038/s41598-020-73656-2
- Bartlett, K., & Eaton, S. (2004). Mitochondrial β-oxidation. *European Journal of Biochemistry*, 271(3), 462–469. https://doi.org/10.1046/j.1432-1033.2003.03947.x
- Belger, C., Abrahams, C., Imamdin, A., & Lecour, S. (2024). Doxorubicin-induced cardiotoxicity and risk factors. *IJC Heart and Vasculature*, *50*, 101332. https://doi.org/10.1016/j.ijcha.2023.101332
- Bellin, M., Marchetto, M. C., Gage, F. H., & Mummery, C. L. (2012). Induced pluripotent stem cells: The new patient? In *Nature Reviews Molecular Cell Biology* (Vol. 13, Issue 11, pp. 713–726). Nature Publishing Group. https://doi.org/10.1038/nrm3448
- Benincá, C., Zanette, V., Brischigliaro, M., Johnson, M., Reyes, A., Valle, D. A. Do, Robinson, A. J., Degiorgi, A., Yeates, A., Telles, B. A., Prudent, J., Baruffini, E., Santos, M. L. S. F., De Souza, R. L., Fernandez-Vizarra, E., Whitworth, A. J., & Zeviani, M. (2021). Mutation in the MICOS subunit gene APOO (MIC26) associated with an X-linked recessive mitochondrial myopathy, lactic acidosis, cognitive impairment and autistic features. *Journal of Medical Genetics*, *58*(3), 155–167. https://doi.org/10.1136/jmedgenet-2020-106861

- Bergmann, O., Bhardwaj, R. D., Bernard, S., Zdunek, S., Barnabé-Heide, F., Walsh, S., Zupicich, J., Alkass, K., Buchholz, B. A., Druid, H., Jovinge, S., & Frisén, J. (2009). Evidence for cardiomyocyte renewal in humans. *Science*, *324*(5923), 98–102. https://doi.org/10.1126/SCIENCE.1164680/SUPPL FILE/BERGMANN.SOM.PDF
- Bergmann, O., Zdunek, S., Felker, A., Salehpour, M., Alkass, K., Bernard, S., Sjostrom, S. L., Szewczykowska, M., Jackowska, T., Dos Remedios, C., Malm, T., Andrä, M., Jashari, R., Nyengaard, J. R., Possnert, G., Jovinge, S., Druid, H., & Frisén, J. (2015). Dynamics of Cell Generation and Turnover in the Human Heart. *Cell*, *161*(7), 1566–1575. https://doi.org/10.1016/j.cell.2015.05.026
- Bers, D. M. (2000). Calcium fluxes involved in control of cardiac myocyte contraction. In *Circulation Research* (Vol. 87, Issue 4, pp. 275–281). Lippincott Williams and Wilkins. https://doi.org/10.1161/01.RES.87.4.275
- Bers, D. M. (2002). Cardiac excitation-contraction coupling. In *Nature* (Vol. 415, Issue 6868, pp. 198–205). Nature Publishing Group. https://doi.org/10.1038/415198a
- Birky, C. W. (1995). Uniparental inheritance of mitochondrial and chloroplast genes: Mechanisms and evolution. In *Proceedings of the National Academy of Sciences of the United States of America* (Vol. 92, Issue 25, pp. 11331–11338). Proceedings of the National Academy of Sciences. https://doi.org/10.1073/pnas.92.25.11331
- Bishop, S. P., Zhou, Y., Nakada, Y., & Zhang, J. (2021). Changes in cardiomyocyte cell cycle and hypertrophic growth during fetal to adult in mammals. *Journal of the American Heart Association*, 10(2), 1–12. https://doi.org/10.1161/JAHA.120.017839/ASSET/80282B72-EA27-4ACE-BFEE-0E1BD94E9B62/ASSETS/GRAPHIC/JAH35829-FIG-0001.PNG
- Bobowski-Gerard, M., Boulet, C., Zummo, F. P., Dubois-Chevalier, J., Gheeraert, C., Bou Saleh, M., Strub, J. M., Farce, A., Ploton, M., Guille, L., Vandel, J., Bongiovanni, A., Very, N., Woitrain, E., Deprince, A., Lalloyer, F., Bauge, E., Ferri, L., Ntandja-Wandji, L. C., ... Eeckhoute, J. (2022). Functional genomics uncovers the transcription factor BNC2 as required for myofibroblastic activation in fibrosis. *Nature Communications*, 13(1), 1–20. https://doi.org/10.1038/s41467-022-33063-9
- Bogenhagen, D. F., Rousseau, D., & Burke, S. (2008). The layered structure of human mitochondrial DNA nucleoids. *Journal of Biological Chemistry*, 283(6), 3665–3675. https://doi.org/10.1074/jbc.M708444200
- Bradski, G. (2000). *The OpenCV Library*. Avilable Online: Https://Www.Drdobbs.Com/Open-Source/the-Opencv-Library/184404319. https://www.drdobbs.com/open-source/the-opencv-library/184404319
- Bratic, A., & Larsson, N. G. (2013). The role of mitochondria in aging. In *Journal of Clinical Investigation* (Vol. 123, Issue 3, pp. 951–957). American Society for Clinical Investigation. https://doi.org/10.1172/JCl64125
- Bray, F., Laversanne, M., Weiderpass, E., & Soerjomataram, I. (2021). The ever-increasing importance of cancer as a leading cause of premature death worldwide. *Cancer*, 127(16), 3029–3030. https://doi.org/10.1002/CNCR.33587
- Bremer, S., & Hartung, T. (2005). The Use of Embryonic Stem Cells for Regulatory Developmental Toxicity Testing In Vitro The Current Status of Test Development. *Current Pharmaceutical Design*, *10*(22), 2733–2747. https://doi.org/10.2174/1381612043383700
- Brown, W. M., Prager, E. M., Wang, A., & Wilson, A. C. (1982). Mitochondrial DNA sequences of primates: Tempo and mode of evolution. *Journal of Molecular Evolution*, *18*(4), 225–239. https://doi.org/10.1007/BF01734101/METRICS
- Brüser, C., Keller-Findeisen, J., & Jakobs, S. (2021). The TFAM-to-mtDNA ratio defines

- inner-cellular nucleoid populations with distinct activity levels. *Cell Reports*, 37(8), 110000. https://doi.org/10.1016/j.celrep.2021.110000
- Bu, L., Jiang, X., Martin-Puig, S., Caron, L., Zhu, S., Shao, Y., Roberts, D. J., Huang, P. L., Domian, I. J., & Chien, K. R. (2009). Human ISL1 heart progenitors generate diverse multipotent cardiovascular cell lineages. *Nature*, 460(7251), 113–117. https://doi.org/10.1038/nature08191
- Budowle, B., Allard, M. W., Wilson, M. R., & Chakraborty, R. (2003). Forensics and Mitochondrial DNA: Applications, Debates, and Foundations. In *Annual Review of Genomics and Human Genetics* (Vol. 4, Issue Volume 4, 2003, pp. 119–141). Annual Reviews. https://doi.org/10.1146/annurev.genom.4.070802.110352
- Burbaum, L., Schneider, J., Scholze, S., Böttcher, R. T., Baumeister, W., Schwille, P., Plitzko, J. M., & Jasnin, M. (2021). Molecular-scale visualization of sarcomere contraction within native cardiomyocytes. *Nature Communications*, *12*(1), 1–12. https://doi.org/10.1038/s41467-021-24049-0
- Burkhalter, M. D., Rudolph, K. L., & Sperka, T. (2015). Genome instability of ageing stem cells-Induction and defence mechanisms. In *Ageing Research Reviews* (Vol. 23, Issue PA, pp. 29–36). Elsevier Ireland Ltd. https://doi.org/10.1016/j.arr.2015.01.004
- Burma, S., Chen, B. P., Murphy, M., Kurimasa, A., & Chen, D. J. (2001). ATM Phosphorylates Histone H2AX in Response to DNA Double-strand Breaks. *Journal of Biological Chemistry*, 276(45), 42462–42467. https://doi.org/10.1074/jbc.C100466200
- Burridge, P. W., Keller, G., Gold, J. D., & Wu, J. C. (2012). Production of de novo cardiomyocytes: Human pluripotent stem cell differentiation and direct reprogramming. In *Cell Stem Cell* (Vol. 10, Issue 1, pp. 16–28). Cell Stem Cell. https://doi.org/10.1016/j.stem.2011.12.013
- Burridge, P. W., Li, Y. F., Matsa, E., Wu, H., Ong, S. G., Sharma, A., Holmström, A., Chang, A. C., Coronado, M. J., Ebert, A. D., Knowles, J. W., Telli, M. L., Witteles, R. M., Blau, H. M., Bernstein, D., Altman, R. B., & Wu, J. C. (2016). Human induced pluripotent stem cell-derived cardiomyocytes recapitulate the predilection of breast cancer patients to doxorubicin-induced cardiotoxicity. *Nature Medicine*, *22*(5), 547–556. https://doi.org/10.1038/nm.4087
- Burridge, P. W., Matsa, E., Shukla, P., Lin, Z. C., Churko, J. M., Ebert, A. D., Lan, F., Diecke, S., Huber, B., Mordwinkin, N. M., Plews, J. R., Abilez, O. J., Cui, B., Gold, J. D., & Wu, J. C. (2014). Chemically defined generation of human cardiomyocytes. *Nature Methods*, 11(8), 855–860. https://doi.org/10.1038/NMETH.2999
- Cai, C. L., Liang, X., Shi, Y., Chu, P. H., Pfaff, S. L., Chen, J., & Evans, S. (2003). Isl1 identifies a cardiac progenitor population that proliferates prior to differentiation and contributes a majority of cells to the heart. *Developmental Cell*, *5*(6), 877–889. https://doi.org/10.1016/S1534-5807(03)00363-0
- Cao, Y. P., & Zheng, M. (2019). Mitochondrial dynamics and inter-mitochondrial communication in the heart. *Archives of Biochemistry and Biophysics*, *663*, 214–219. https://doi.org/10.1016/J.ABB.2019.01.017
- Carbognin, E., Betto, R. M., Soriano, M. E., Smith, A. G., & Martello, G. (2016). Stat3 promotes mitochondrial transcription and oxidative respiration during maintenance and induction of naive pluripotency. *The EMBO Journal*, *35*(6), 618–634. https://doi.org/10.15252/embj.201592629
- Carvalho, C., Santos, R. X., Cardoso, S., Correia, S., Oliveira, P. J., Santos, M. S., & Moreira, P. I. (2009). Doxorubicin: The Good, the Bad and the Ugly Effect. *Current Medicinal Chemistry*, *16*(25), 3267–3285. https://doi.org/10.2174/092986709788803312

- Chambers, I., & Smith, A. (2004). Self-renewal of teratocarcinoma and embryonic stem cells. In *Oncogene* (Vol. 23, Issue 43 REV. ISS. 6, pp. 7150–7160). Nature Publishing Group. https://doi.org/10.1038/sj.onc.1207930
- Champoux, J. J. (2001). DNA topoisomerases: Structure, function, and mechanism. In *Annual Review of Biochemistry* (Vol. 70, Issue Volume 70, 2001, pp. 369–413). Annual Reviews. https://doi.org/10.1146/annurev.biochem.70.1.369
- Chen, B., Dodge, M. E., Tang, W., Lu, J., Ma, Z., Fan, C.-W., Wei, S., Hao, W., Kilgore, J., Williams, N. S., Roth, M. G., Amatruda, J. F., Chen, C., & Lum, L. (2009). Small molecule—mediated disruption of Wnt-dependent signaling in tissue regeneration and cancer. *Nature Chemical Biology*, *5*(2), 100–107. https://doi.org/10.1038/nchembio.137
- Chen, H., & Chan, D. C. (2005). Emerging functions of mammalian mitochondrial fusion and fission. In *Human Molecular Genetics* (Vol. 14, Issue SUPPL. 2, pp. R283–R289). Oxford Academic. https://doi.org/10.1093/hmg/ddi270
- Chen, H., Chomyn, A., & Chan, D. C. (2005). Disruption of fusion results in mitochondrial heterogeneity and dysfunction. *Journal of Biological Chemistry*, *280*(28), 26185–26192. https://doi.org/10.1074/jbc.M503062200
- Chen, Q., Liu, L. Y., Tian, Z., Fang, Z., Wang, K. N., Shao, X., Zhang, C., Zou, W., Rowan, F., Qiu, K., Ji, B., Guan, J. L., Li, D., Mao, Z. W., & Diao, J. (2023). Mitochondrial nucleoid condensates drive peripheral fission through high membrane curvature. *Cell Reports*, *42*(12). https://doi.org/10.1016/j.celrep.2023.113472
- Ching, Y. H., Ghosh, T. K., Cross, S. J., Packham, E. A., Honeyman, L., Loughna, S., Robinson, T. E., Dearlove, A. M., Ribas, G., Bonser, A. J., Thomas, N. R., Scotter, A. J., Caves, L. S. D., Tyrrell, G. P., Newbury-Ecob, R. A., Munnich, A., Bonnet, D., & Brook, J. D. (2005). Mutation in myosin heavy chain 6 causes atrial septal defect. *Nature Genetics*, *37*(4), 423–428. https://doi.org/10.1038/ng1526
- Cho, Y. M., Kwon, S., Pak, Y. K., Seol, H. W., Choi, Y. M., Park, D. J., Park, K. S., & Lee, H. K. (2006). Dynamic changes in mitochondrial biogenesis and antioxidant enzymes during the spontaneous differentiation of human embryonic stem cells. *Biochemical and Biophysical Research Communications*, *348*(4), 1472–1478. https://doi.org/10.1016/j.bbrc.2006.08.020
- Choi, W.-G., Kim, D. K., Shin, Y., Park, R., Cho, Y.-Y., Lee, J. Y., Kang, H. C., Lee, H. S., Yoon, S., & Cho, H.-J. (2020). molecules Liquid Chromatography-Tandem Mass Spectrometry for the Simultaneous Determination of Doxorubicin and its Metabolites Doxorubicinol, Doxorubicinone, Doxorubicinolone, and 7-Deoxydoxorubicinone in Mouse Plasma. https://doi.org/10.3390/molecules25051254
- Christoffels, V. M., Smits, G. J., Kispert, A., & Moorman, A. F. M. (2010). Development of the pacemaker tissues of the heart. In *Circulation Research* (Vol. 106, Issue 2, pp. 240–254). Lippincott Williams & Wilkins. https://doi.org/10.1161/CIRCRESAHA.109.205419
- Corrie, P. G. (2008). Cytotoxic chemotherapy: clinical aspects. *Medicine*, *36*(1), 24–28. https://doi.org/10.1016/J.MPMED.2007.10.012
- Cruet-Hennequart, S., Prendergast, Á. M., Shaw, G., Barry, F. P., & Carty, M. P. (2012). Doxorubicin induces the DNA damage response in cultured human mesenchymal stem cells. *International Journal of Hematology*, *96*(5), 649–656. https://doi.org/10.1007/s12185-012-1196-5
- Cunningham, J. J., Ulbright, T. M., Pera, M. F., & Looijenga, L. H. J. (2012). Lessons from human teratomas to guide development of safe stem cell therapies. In *Nature Biotechnology* (Vol. 30, Issue 9, pp. 849–857). Nature Publishing Group. https://doi.org/10.1038/nbt.2329

- Das, B. B., Ghosh, A., Bhattacharjee, S., & Bhattacharyya, A. (2021). Trapped topoisomerase-DNA covalent complexes in the mitochondria and their role in human diseases. *Mitochondrion*, *60*, 234–244. https://doi.org/10.1016/j.mito.2021.08.017
- Davies, K. J. A., & Doroshow, J. H. (1986). Redox cycling of anthracyclines by cardiac mitochondria. I. Anthracycline radical formation by NADH dehydrogenase. *Journal of Biological Chemistry*, 261(7), 3060–3067. https://doi.org/10.1016/S0021-9258(17)35746-0
- de Sena-Tomás, C., Aleman, A. G., Ford, C., Varshney, A., Yao, D., Harrington, J. K., Saúde, L., Ramialison, M., & Targoff, K. L. (2022). Activation of Nkx2.5 transcriptional program is required for adult myocardial repair. *Nature Communications*, *13*(1), 1–16. https://doi.org/10.1038/s41467-022-30468-4
- Degli Esposti, M. (2014). Bioenergetic Evolution in Proteobacteria and Mitochondria. *Genome Biology and Evolution*, 6(12), 3238–3251. https://doi.org/10.1093/gbe/evu257
- Dhingra, R., Margulets, V., Chowdhury, S. R., Thliveris, J., Jassal, D., Fernyhough, P., Dorn, G. W., & Kirshenbaum, L. A. (2014). Bnip3 mediates doxorubicin-induced cardiac myocyte necrosis and mortality through changes in mitochondrial signaling. Proceedings of the National Academy of Sciences of the United States of America, 111(51), E5537–E5544. https://doi.org/10.1073/PNAS.1414665111/SUPPL\_FILE/PNAS.201414665SI.PDF
- Díaz del Moral, S., Benaouicha, M., Villa del Campo, C., Torres, M., Wagner, N., Wagner, K. D., Muñoz-Chápuli, R., & Carmona, R. (2023). Cardiomyocyte-Specific Wt1 Is Involved in Cardiac Metabolism and Response to Damage. *Journal of Cardiovascular Development and Disease*, *10*(5), 211. https://doi.org/10.3390/jcdd10050211
- Dimroth, P., Kaim, G., & Matthey, U. (2000). Crucial role of the membrane potential for ATP synthesis by F1F(o) ATP synthases. *Journal of Experimental Biology*, *203*(1), 51–59. https://doi.org/10.1242/jeb.203.1.51
- Duvezin-Caubet, S., Jagasia, R., Wagener, J., Hofmann, S., Trifunovic, A., Hansson, A., Chomyn, A., Bauer, M. F., Attardi, G., Larsson, N. G., Neupert, W., & Reichert, A. S. (2006). Proteolytic processing of OPA1 links mitochondrial dysfunction to alterations in mitochondrial morphology. *Journal of Biological Chemistry*, 281(49), 37972–37979. https://doi.org/10.1074/jbc.M606059200
- Elisa Martin. (2024). MuRF1 and MuRF3 coordinately regulate the energy homeostasis of heart and skeletal muscle by regulation of mitochondrial function Doctoral thesis. (Accessed: February 2025 [University of Greifswald]. https://nbn-resolving.org/urn:nbn:de:gbv:9-opus-109094
- Elstner, A., Damaschun, A., Kurtz, A., Stacey, G., Arán, B., Veiga, A., & Borstlap, J. (2009). The changing landscape of European and international regulation on embryonic stem cell research. *Stem Cell Research*, *2*(2), 101–107. https://doi.org/10.1016/j.scr.2008.10.003
- Evans, M. J., & Kaufman, M. H. (1981). Establishment in culture of pluripotential cells from mouse embryos. *Nature*, *292*(5819), 154–156. https://doi.org/10.1038/292154a0
- Falzone, L., Salomone, S., & Libra, M. (2018). Evolution of cancer pharmacological treatments at the turn of the third millennium. *Frontiers in Pharmacology*, 9(NOV), 421926. https://doi.org/10.3389/FPHAR.2018.01300/BIBTEX
- Feher, J. (2012). The Heart as a Pump. In J. Feher (Ed.), *Quantitative Human Physiology* (pp. 446–454). Elsevier. https://doi.org/10.1016/b978-0-12-382163-8.00047-5
- Feng, Y., Huang, W., Paul, C., Liu, X., Sadayappan, S., Wang, Y., & Pauklin, S. (2021). Mitochondrial nucleoid in cardiac homeostasis: bidirectional signaling of mitochondria

- and nucleus in cardiac diseases. *Basic Research in Cardiology*, *116*(1). https://doi.org/10.1007/S00395-021-00889-1
- Feric, M., Demarest, T. G., Tian, J., Croteau, D. L., Bohr, V. A., & Misteli, T. (2021). Self-assembly of multi-component mitochondrial nucleoids via phase separation. *The EMBO Journal*, *40*(6). https://doi.org/10.15252/embj.2020107165
- Ferlay, J., Steliarova-Foucher, E., Lortet-Tieulent, J., Rosso, S., Coebergh, J. W. W., Comber, H., Forman, D., & Bray, F. (2013). Cancer incidence and mortality patterns in Europe: Estimates for 40 countries in 2012. *European Journal of Cancer*, *49*(6), 1374–1403. https://doi.org/10.1016/J.EJCA.2012.12.027
- Fernández-Vizarra, E., Enríquez, J. A., Pérez-Martos, A., Montoya, J., & Fernández-Silva, P. (2011). Tissue-specific differences in mitochondrial activity and biogenesis. *Mitochondrion*, *11*(1), 207–213. https://doi.org/10.1016/j.mito.2010.09.011
- Ficara, F., Murphy, M. J., Lin, M., & Cleary, M. L. (2008). Pbx1 Regulates Self-Renewal of Long-Term Hematopoietic Stem Cells by Maintaining Their Quiescence. *Cell Stem Cell*, 2(5), 484–496. https://doi.org/10.1016/j.stem.2008.03.004
- Finkel, T., Menazza, S., Holmström, K. M., Parks, R. J., Liu, J., Sun, J., Liu, J., Pan, X., & Murphy, E. (2015). The ins and outs of mitochondrial calcium. In *Circulation Research* (Vol. 116, Issue 11, pp. 1810–1819). Lippincott Williams and Wilkins. https://doi.org/10.1161/CIRCRESAHA.116.305484
- Folmes, C. D. L., Nelson, T. J., Martinez-Fernandez, A., Arrell, D. K., Lindor, J. Z., Dzeja, P. P., Ikeda, Y., Perez-Terzic, C., & Terzic, A. (2011). Somatic oxidative bioenergetics transitions into pluripotency-dependent glycolysis to facilitate nuclear reprogramming. *Cell Metabolism*, *14*(2), 264–271. https://doi.org/10.1016/j.cmet.2011.06.011
- Fonseca, T. B., Sánchez-Guerrero, Á., Milosevic, I., & Raimundo, N. (2019). Mitochondrial fission requires DRP1 but not dynamins. In *Nature* (Vol. 570, Issue 7761, pp. E34–E42). Nature Publishing Group. https://doi.org/10.1038/s41586-019-1296-y
- Frey, T. G., & Mannella, C. A. (2000). The internal structure of mitochondria. *Trends in Biochemical Sciences*, *25*(7), 319–324. https://doi.org/10.1016/S0968-0004(00)01609-1
- Friedman, J. R., & Nunnari, J. (2014). Mitochondrial form and function. In *Nature* (Vol. 505, Issue 7483, pp. 335–343). Nature Publishing Group. https://doi.org/10.1038/nature12985
- Fuchs, E., & Chen, T. (2013). A matter of life and death: Self-renewal in stem cells. In *EMBO Reports* (Vol. 14, Issue 1, pp. 39–48). John Wiley & Sons, LtdChichester, UK. https://doi.org/10.1038/embor.2012.197
- Galanjuk, S., Zühr, E., Dönmez, A., Bartsch, D., Kurian, L., Tigges, J., & Fritsche, E. (2022). The Human Induced Pluripotent Stem Cell Test as an Alternative Method for Embryotoxicity Testing. *International Journal of Molecular Sciences*, 23(6), 3295. https://doi.org/10.3390/IJMS23063295/S1
- Gao, Q., Tian, R., Han, H., Slone, J., Wang, C., Ke, X., Zhang, T., Li, X., He, Y., Liao, P., Wang, F., Chen, Y., Fu, S., Zhang, K., Zeng, F., Yang, Y., Li, Z., Tan, J., Li, J., ... Zhang, Z. (2022). PINK1-mediated Drp1S616 phosphorylation modulates synaptic development and plasticity via promoting mitochondrial fission. *Signal Transduction and Targeted Therapy*, 7(1), 1–16. https://doi.org/10.1038/s41392-022-00933-z
- Gewirtz, D. A. (1999). A critical evaluation of the mechanisms of action proposed for the antitumor effects of the anthracycline antibiotics adriamycin and daunorubicin. *Biochemical Pharmacology*, *57*(7), 727–741. https://doi.org/10.1016/S0006-2952(98)00307-4

- Gherghiceanu, M., Barad, L., Novak, A., Reiter, I., Itskovitz-Eldor, J., Binah, O., & Popescu, L. M. (2011). Cardiomyocytes derived from human embryonic and induced pluripotent stem cells: comparative ultrastructure. *Journal of Cellular and Molecular Medicine*, 15(11), 2539–2551. https://doi.org/10.1111/j.1582-4934.2011.01417.x
- Giacomello, M., Pyakurel, A., Glytsou, C., & Scorrano, L. (2020). The cell biology of mitochondrial membrane dynamics. *Nature Reviews Molecular Cell Biology 2020 21:4*, 21(4), 204–224. https://doi.org/10.1038/s41580-020-0210-7
- Gogvadze, V., Orrenius, S., & Zhivotovsky, B. (2009). Mitochondria as targets for chemotherapy. In *Apoptosis* (Vol. 14, Issue 4, pp. 624–640). Springer. https://doi.org/10.1007/s10495-009-0323-0
- González-Alonso, J. (2012). Human thermoregulation and the cardiovascular system. *Experimental Physiology*, 97(3), 340–346. https://doi.org/10.1113/expphysiol.2011.058701
- Goto, Y. I., Nonaka, I., & Horai, S. (1990). A mutation in the tRNALeu(UUR) gene associated with the MELAS subgroup of mitochondrial encephalomyopathies. *Nature*, *348*(6302), 651–653. https://doi.org/10.1038/348651a0
- Goversen, B., van der Heyden, M. A. G., van Veen, T. A. B., & de Boer, T. P. (2018). The immature electrophysiological phenotype of iPSC-CMs still hampers in vitro drug screening: Special focus on IK1. In *Pharmacology and Therapeutics* (Vol. 183, pp. 127–136). Elsevier Inc. https://doi.org/10.1016/j.pharmthera.2017.10.001
- Govindaraj, P., Rani, B., Sundaravadivel, P., Vanniarajan, A., Indumathi, K. P., Khan, N. A., Dhandapany, P. S., Rani, D. S., Tamang, R., Bahl, A., Narasimhan, C., Rakshak, D., Rathinavel, A., Premkumar, K., Khullar, M., & Thangaraj, K. (2019). Mitochondrial genome variations in idiopathic dilated cardiomyopathy. *Mitochondrion*, *48*, 51–59. https://doi.org/10.1016/j.mito.2019.03.003
- Green, D. R. (2005). Apoptotic pathways: Ten minutes to dead. In *Cell* (Vol. 121, Issue 5, pp. 671–674). Elsevier B.V. https://doi.org/10.1016/j.cell.2005.05.019
- Green, D. R., & Kroemer, G. (2004). The Pathophysiology of Mitochondrial Cell Death. *Science*, 305(5684), 626–629. https://doi.org/10.1126/science.1099320
- Gu, Z. (2022). Complex heatmap visualization. *IMeta*, 1(3), e43. https://doi.org/10.1002/IMT2.43
- Gu, Z., Eils, R., & Schlesner, M. (2016). Complex heatmaps reveal patterns and correlations in multidimensional genomic data. *Bioinformatics*, *32*(18), 2847–2849. https://doi.org/10.1093/BIOINFORMATICS/BTW313
- Guo, C., Sun, Y., Zhou, B., Adam, R. M., Li, X. K., Pu, W. T., Morrow, B. E., Moon, A., & Li, X. (2011). A Tbx1-Six1/Eya1-Fgf8 genetic pathway controls mammalian cardiovascular and craniofacial morphogenesis. *Journal of Clinical Investigation*, *121*(4), 1585–1595. https://doi.org/10.1172/JCI44630
- Halim, V. A., García-Santisteban, I., Warmerdam, D. O., Van Den Broek, B., Heck, A. J. R., Mohammed, S., & Medema, R. H. (2018). Doxorubicin-induced DNA damage causes extensive ubiquitination of ribosomal proteins associated with a decrease in protein translation. *Molecular and Cellular Proteomics*, 17(12), 2297–2308. https://doi.org/10.1074/mcp.RA118.000652
- Hanson, J., & Huxley, H. E. (1953). Structural basis of the cross-striations in muscle. *Nature*, 172(4377), 530–532. https://doi.org/10.1038/172530b0
- Harner, M., Körner, C., Walther, D., Mokranjac, D., Kaesmacher, J., Welsch, U., Griffith, J., Mann, M., Reggiori, F., & Neupert, W. (2011). The mitochondrial contact site complex, a

- determinant of mitochondrial architecture. *EMBO Journal*, *30*(21), 4356–4370. https://doi.org/10.1038/emboj.2011.379
- Harris, I. S., & Black, B. L. (2010). Development of the endocardium. *Pediatric Cardiology*, *31*(3), 391–399. https://doi.org/10.1007/s00246-010-9642-8
- Harvey, A. J., Rathjen, J., & Gardner, D. K. (2016). Metaboloepigenetic regulation of pluripotent stem cells. In *Stem Cells International* (Vol. 2016). Hindawi Publishing Corporation. https://doi.org/10.1155/2016/1816525
- He, L., Nguyen, N. B., Ardehali, R., & Zhou, B. (2020). Heart regeneration by endogenous stem cells and cardiomyocyte proliferation: Controversy, fallacy, and progress. *Circulation*, 142(3), 275–291. https://doi.org/10.1161/CIRCULATIONAHA.119.045566/ASSET/520A7548-2B38-4ED8-93C5-03167C07868F/ASSETS/GRAPHIC/CIRCULATIONAHA.119.045566.FIG05.JPG
- He, S., Nakada, D., & Morrison, S. J. (2009). Mechanisms of stem cell self-renewal. In *Annual Review of Cell and Developmental Biology* (Vol. 25, Issue Volume 25, 2009, pp. 377–406). Annual Reviews Inc. https://doi.org/10.1146/annurev.cellbio.042308.113248
- He, W., He, W., Chen, X., Zeng, L., Zeng, L., Liu, Y., He, P., & Sun, Z. (2024). Mitochondrial elongation confers protection against doxorubicin-induced cardiotoxicity. *Biochemical Pharmacology*, 229, 116495. https://doi.org/10.1016/j.bcp.2024.116495
- Helal, M., Alcorn, J., & Bandy, B. (2021). Doxorubicin Cytotoxicity in Differentiated H9c2 Cardiomyocytes: Evidence for Acute Mitochondrial Superoxide Generation. *Cardiovascular Toxicology*, *21*(2), 152–161. https://doi.org/10.1007/s12012-020-09606-1
- Henderson, I. C., & Frei, E. I. (1979). Adriamycin and the Heart. *New England Journal of Medicine*, 300(6), 310–312. https://doi.org/10.1056/NEJM197902083000610
- Hengartner, M. O. (2000). The biochemistry of apoptosis. *Nature 2000 407:6805*, *407*(6805), 770–776. https://doi.org/10.1038/35037710
- Herrgård, M. J., Fong, S. S., & Palsson, B. Ø. (2006). Identification of Genome-Scale Metabolic Network Models Using Experimentally Measured Flux Profiles. *PLoS Computational Biology*, 2(7), e72. https://doi.org/10.1371/journal.pcbi.0020072
- Hinken, A. C., & Solaro, R. J. (2007). A Dominant Role of Cardiac Molecular Motors in the Intrinsic Regulation of Ventricular Ejection and Relaxation. *Physiology*, *22*(2), 73–80. https://doi.org/10.1152/physiol.00043.2006
- Holmgren, G., Sartipy, P., Andersson, C. X., Lindahl, A., & Synnergren, J. (2018). Expression Profiling of Human Pluripotent Stem Cell-Derived Cardiomyocytes Exposed to Doxorubicin—Integration and Visualization of Multi-Omics Data. *Toxicological Sciences*, 163(1), 182–195. https://doi.org/10.1093/toxsci/kfy012
- Hoppins, S., Collins, S. R., Cassidy-Stone, A., Hummel, E., DeVay, R. M., Lackner, L. L., Westermann, B., Schuldiner, M., Weissman, J. S., & Nunnari, J. (2011). A mitochondrial-focused genetic interaction map reveals a scaffold-like complex required for inner membrane organization in mitochondria. *Journal of Cell Biology*, 195(2), 323–340. https://doi.org/10.1083/jcb.201107053
- Hoque, A., Sivakumaran, P., Bond, S. T., Ling, N. X. Y., Kong, A. M., Scott, J. W., Bandara, N., Hernández, D., Liu, G. S., Wong, R. C. B., Ryan, M. T., Hausenloy, D. J., Kemp, B. E., Oakhill, J. S., Drew, B. G., Pébay, A., & Lim, S. Y. (2018). Mitochondrial fission protein Drp1 inhibition promotes cardiac mesodermal differentiation of human pluripotent stem cells. *Cell Death Discovery*, 4(1), 1–13. https://doi.org/10.1038/s41420-018-0042-9

- Hoshijima, M. (2006). Mechanical stress-strain sensors embedded in cardiac cytoskeleton: Z disk, titin, and associated structures. American Journal of Physiology Heart and Circulatory Physiology, 290(4), 1313–1325. https://doi.org/10.1152/AJPHEART.00816.2005/ASSET/IMAGES/LARGE/ZH400406658 70005.JPEG
- Hu, Y. P., Moraes, C. T., Savaraj, N., Priebe, W., & Lampidis, T. J. (2000). p0 Tumor cells: A model for studying whether mitochondria are targets for rhodamine 123, doxorubicin, and other drugs. *Biochemical Pharmacology*, 60(12), 1897–1905. https://doi.org/10.1016/S0006-2952(00)00513-X
- Huelsenbeck, S. C., Schorr, A., Roos, W. P., Huelsenbeck, J., Henninger, C., Kaina, B., & Fritz, G. (2012). Rac1 protein signaling is required for DNA damage response stimulated by topoisomerase II poisons. *Journal of Biological Chemistry*, 287(46), 38590–38599. https://doi.org/10.1074/jbc.M112.377903
- Ingman, M., Kaessmann, H., Pääbo, S., & Gyllensten, U. (2000). Mitochondrial genome variation and the origin of modern humans. *Nature 2000 408:6813*, 408(6813), 708–713. https://doi.org/10.1038/35047064
- Ishihara, N., Fujita, Y., Oka, T., & Mihara, K. (2006). Regulation of mitochondrial morphology through proteolytic cleavage of OPA1. *EMBO Journal*, *25*(13), 2966–2977. https://doi.org/10.1038/sj.emboj.7601184
- Iyama, T., & Wilson, D. M. (2013). DNA repair mechanisms in dividing and non-dividing cells. *DNA Repair*, *12*(8), 620–636. https://doi.org/10.1016/j.dnarep.2013.04.015
- Jahn, S. K., Hennicke, T., Kassack, M. U., Drews, L., Reichert, A. S., & Fritz, G. (2020). Distinct influence of the anthracycline derivative doxorubicin on the differentiation efficacy of mESC-derived endothelial progenitor cells. *Biochimica et Biophysica Acta* (BBA) - Molecular Cell Research, 1867(7), 118711. https://doi.org/10.1016/j.bbamcr.2020.118711
- Jawad, B., Poudel, L., Podgornik, R., Steinmetz, N. F., & Ching, W. Y. (2019). Molecular mechanism and binding free energy of doxorubicin intercalation in DNA. *Physical Chemistry Chemical Physics*, 21(7), 3877–3893. https://doi.org/10.1039/c8cp06776g
- John, G. B., Shang, Y., Li, L., Renken, C., Mannella, C. A., Selker, J. M. L., Rangell, L., Bennett, M. J., & Zha, J. (2005). The mitochondrial inner membrane protein mitofilin controls cristae morphology. *Molecular Biology of the Cell*, *16*(3), 1543–1554. https://doi.org/10.1091/mbc.E04-08-0697
- John, J. C. S., Ramalho-Santos, J., Gray, H. L., Petrosko, P., Rawe, V. Y., Navara, C. S., Simerly, C. R., & Schatten, G. P. (2005). The Expression of Mitochondrial DNA Transcription Factors during Early Cardiomyocyte In Vitro Differentiation from Human Embryonic Stem Cells. In *CLONING AND STEM CELLS* (Vol. 7). www.liebertpub.com
- Johnson, W., Loskutoff, N., Plante, Y., & Betteridge, K. (1995). Production of four identical calves by the separation of blastomeres from an in vitro derived four-cell embryo. *Veterinary Record*, *137*(1), 15–16. https://doi.org/10.1136/vr.137.1.15
- Kadenbach, B. (2021). Complex IV The regulatory center of mitochondrial oxidative phosphorylation. In *Mitochondrion* (Vol. 58, pp. 296–302). Elsevier B.V. https://doi.org/10.1016/j.mito.2020.10.004

- Karsner, H. T., Saphir, O., & Todd, T. W. (1925). The State of the Cardiac Muscle in Hypertrophy and Atrophy. *The American Journal of Pathology*, *1*(4), 351. https://doi.org/10.1016/s0002-8703(25)90020-8
- Kashifa Fathima, J., Lavanya, V., Jamal, S., & Ahmed, N. (2022). The Effectiveness of Various Chemotherapeutic Agents in Cancer Treatment. In *Current Pharmacology Reports* (Vol. 8, Issue 4, pp. 236–252). Springer Science and Business Media Deutschland GmbH. https://doi.org/10.1007/s40495-022-00289-6
- Kelly, O. G., Pinson, K. I., & Skarnes, W. C. (2004). The Wnt co-receptors Lrp5 and Lrp6 are essential for gastrulation in mice. *Development*, 131(12), 2803–2815. https://doi.org/10.1242/DEV.01137
- Khacho, M., Clark, A., Svoboda, D. S., Azzi, J., MacLaurin, J. G., Meghaizel, C., Sesaki, H., Lagace, D. C., Germain, M., Harper, M. E., Park, D. S., & Slack, R. S. (2016). Mitochondrial Dynamics Impacts Stem Cell Identity and Fate Decisions by Regulating a Nuclear Transcriptional Program. *Cell Stem Cell*, 19(2), 232–247. https://doi.org/10.1016/j.stem.2016.04.015
- Khiati, S., Rosa, I. D., Sourbier, C., Ma, X., Rao, V. A., Neckers, L. M., Zhang, H., & Pommier, Y. (2014). Mitochondrial topoisomerase i (Top1mt) is a novel limiting factor of doxorubicin cardiotoxicity. *Clinical Cancer Research*, 20(18), 4873–4881. https://doi.org/10.1158/1078-0432.CCR-13-3373
- Kim, D., Paggi, J. M., Park, C., Bennett, C., & Salzberg, S. L. (2019). Graph-based genome alignment and genotyping with HISAT2 and HISAT-genotype. *Nature Biotechnology*, 37(8), 907–915. https://doi.org/10.1038/s41587-019-0201-4
- Kim, S. Y., Kim, S. J., Kim, B. J., Rah, S. Y., Sung, M. C., Im, M. J., & Kim, U. H. (2006). Doxorubicin-induced reactive oxygen species generation and intracellular Ca2+increase are reciprocally modulated in rat cardiomyocytes. *Experimental & Molecular Medicine* 2006 38:5, 38(5), 535–545. https://doi.org/10.1038/emm.2006.63
- King, N. M. P., & Perrin, J. (2014). Ethical issues in stem cell research and therapy. In *Stem Cell Research and Therapy* (Vol. 5, Issue 4, pp. 1–6). BioMed Central Ltd. https://doi.org/10.1186/scrt474
- Kishita, Y., Shimura, M., Kohda, M., Akita, M., Imai-Okazaki, A., Yatsuka, Y., Nakajima, Y., Ito, T., Ohtake, A., Murayama, K., & Okazaki, Y. (2020). A novel homozygous variant in *MICOS13 / QIL1* causes hepato-encephalopathy with mitochondrial DNA depletion syndrome. *Molecular Genetics & Genomic Medicine*, 8(10), e1427. https://doi.org/10.1002/mgg3.1427
- Kleele, T., Rey, T., Winter, J., Zaganelli, S., Mahecic, D., Perreten Lambert, H., Ruberto, F. P., Nemir, M., Wai, T., Pedrazzini, T., & Manley, S. (2021). Distinct fission signatures predict mitochondrial degradation or biogenesis. *Nature*, *593*(7859), 435–439. https://doi.org/10.1038/s41586-021-03510-6
- Knight, R. A., & Melino, G. (2011). Cell death in disease: From 2010 onwards. In *Cell Death and Disease* (Vol. 2, Issue 9, pp. e202–e202). Nature Publishing Group. https://doi.org/10.1038/cddis.2011.89
- Knott, A. B., Perkins, G., Schwarzenbacher, R., & Bossy-Wetzel, E. (2008). Mitochondrial fragmentation in neurodegeneration. In *Nature Reviews Neuroscience* (Vol. 9, Issue 7, pp. 505–518). https://doi.org/10.1038/nrn2417
- Korga, A., Ostrowska, M., Iwan, M., Herbet, M., & Dudka, J. (2019). Inhibition of glycolysis disrupts cellular antioxidant defense and sensitizes HepG2 cells to doxorubicin treatment. *FEBS Open Bio*, *9*(5), 959–972. https://doi.org/10.1002/2211-5463.12628
- Koshiba, T., Detmer, S. A., Kaiser, J. T., Chen, H., McCaffery, J. M., & Chan, D. C. (2004).

- Structural basis of mitochondrial tethering by mitofusin complexes. *Science*, *305*(5685), 858–862. https://doi.org/10.1126/science.1099793
- Kovács, N., Shahin, B., Andrade, C. A. S., Mahrouseh, N., & Varga, O. (2024). Lifestyle and metabolic risk factors, and diabetes mellitus prevalence in European countries from three waves of the European Health Interview Survey. *Scientific Reports*, *14*(1), 1–10. https://doi.org/10.1038/s41598-024-62122-y
- Krantz, S., Kim, Y. M., Srivastava, S., Leasure, J. W., Toth, P. T., Marsboom, G., & Rehman, J. (2021). Mitophagy mediates metabolic reprogramming of induced pluripotent stem cells undergoing endothelial differentiation. *Journal of Biological Chemistry*, 297(6). https://doi.org/10.1016/j.jbc.2021.101410
- Kukat, C., Wurm, C. A., Spåhr, H., Falkenberg, M., Larsson, N. G., & Jakobs, S. (2011). Super-resolution microscopy reveals that mammalian mitochondrial nucleoids have a uniform size and frequently contain a single copy of mtDNA. *Proceedings of the National Academy of Sciences of the United States of America*, 108(33), 13534–13539. https://doi.org/10.1073/pnas.1109263108
- Kumarapeli, A. R. K., Horak, K. M., Glasford, J. W., Li, J., Chen, Q., Liu, J., Zheng, H., & Wang, X. (2005). A novel transgenic mouse model reveals deregulation of the ubiquitin-proteasome system in the heart by doxorubicin. *The FASEB Journal*, *19*(14), 2051–2053. https://doi.org/10.1096/FJ.05-3973FJE
- Kuznetsov, A. V., Hermann, M., Saks, V., Hengster, P., & Margreiter, R. (2009). The cell-type specificity of mitochondrial dynamics. In *International Journal of Biochemistry and Cell Biology* (Vol. 41, Issue 10, pp. 1928–1939). Pergamon. https://doi.org/10.1016/j.biocel.2009.03.007
- Lagoa, R., Gañán, C., López-Sánchez, C., García-Martínez, V., & Gutierrez-Merino, C. (2014). The decrease of NAD(P)H:quinone oxidoreductase 1 activity and increase of ROS production by NADPH oxidases are early biomarkers in doxorubicin cardiotoxicity. *Biomarkers*, *19*(2), 142–153. https://doi.org/10.3109/1354750X.2014.885084
- Laker, R. C., Xu, P., Ryall, K. A., Sujkowski, A., Kenwood, B. M., Chain, K. H., Zhang, M., Royal, M. A., Hoehn, K. L., Driscoll, M., Adler, P. N., Wessells, R. J., Saucerman, J. J., & Yan, Z. (2014). A novel mitotimer reporter gene for mitochondrial content, structure, stress, and damage in vivo. *Journal of Biological Chemistry*, 289(17), 12005–12015. https://doi.org/10.1074/jbc.M113.530527
- Lang, B. F., Burger, G., O'Kelly, C. J., Cedergren, R., Golding, G. B., Lemieux, C., Sankoff, D., Turmel, M., & Gray, M. W. (1997). An ancestral mitochondrial DNA resembling a eubacterial genome in miniature. *Nature*, *387*(6632), 493–497. https://doi.org/10.1038/387493a0
- Larsen, R. L., Jakacki, R. I., Vetter, V. L., Meadows, A. T., Silber, J. H., & Barber, G. (1992). Electrocardiographic changes and arrhythmias after cancer therapy in children and young adults. *The American Journal of Cardiology*, *70*(1), 73–77. https://doi.org/10.1016/0002-9149(92)91393-I
- Law, C. W., Chen, Y., Shi, W., & Smyth, G. K. (2014). Voom: Precision weights unlock linear model analysis tools for RNA-seq read counts. *Genome Biology*, *15*(2), R29. https://doi.org/10.1186/gb-2014-15-2-r29
- Leboucher, G. P., Tsai, Y. C., Yang, M., Shaw, K. C., Zhou, M., Veenstra, T. D., Glickman, M. H., & Weissman, A. M. (2012). Stress-Induced Phosphorylation and Proteasomal Degradation of Mitofusin 2 Facilitates Mitochondrial Fragmentation and Apoptosis. *Molecular Cell*, 47(4), 547–557. https://doi.org/10.1016/J.MOLCEL.2012.05.041
- Lebrecht, D., Setzer, B., Ketelsen, U. P., Haberstroh, J., & Walker, U. A. (2003). Time-

- Dependent and Tissue-Specific Accumulation of mtDNA and Respiratory Chain Defects in Chronic Doxorubicin Cardiomyopathy. *Circulation*, *108*(19), 2423–2429. https://doi.org/10.1161/01.CIR.0000093196.59829.DF
- Lee, M. S., Finch, W., & Mahmud, E. (2013). Cardiovascular complications of radiotherapy. In *American Journal of Cardiology* (Vol. 112, Issue 10, pp. 1688–1696). Excerpta Medica. https://doi.org/10.1016/j.amjcard.2013.07.031
- Legros, F., Malka, F., Frachon, P., Lombès, A., & Rojo, M. (2004). Organization and dynamics of human mitochondrial DNA. *Journal of Cell Science*, *117*(13), 2653–2662. https://doi.org/10.1242/JCS.01134
- Li, H., Handsaker, B., Wysoker, A., Fennell, T., Ruan, J., Homer, N., Marth, G., Abecasis, G., & Durbin, R. (2009). The Sequence Alignment/Map format and SAMtools. *Bioinformatics*, *25*(16), 2078–2079. https://doi.org/10.1093/bioinformatics/btp352
- Li, L., Wan, Z., Wang, R., Zhao, Y., Ye, Y., Yang, P., Qi, Y., Jiang, W., Cai, L., & Zhang, D. (2022). Generation of high-performance human cardiomyocytes and engineered heart tissues from extended pluripotent stem cells. *Cell Discovery 2022 8:1*, 8(1), 1–5. https://doi.org/10.1038/s41421-022-00446-7
- Lian, X., Zhang, J., Azarin, S. M., Zhu, K., Hazeltine, L. B., Bao, X., Hsiao, C., Kamp, T. J., & Palecek, S. P. (2012). Directed cardiomyocyte differentiation from human pluripotent stem cells by modulating Wnt/β-catenin signaling under fully defined conditions. *Nature Protocols 2013 8:1*, *8*(1), 162–175. https://doi.org/10.1038/nprot.2012.150
- Lian, X., Zhang, J., Azarin, S. M., Zhu, K., Hazeltine, L. B., Bao, X., Hsiao, C., Kamp, T. J., & Palecek, S. P. (2013). Directed cardiomyocyte differentiation from human pluripotent stem cells by modulating Wnt/β-catenin signaling under fully defined conditions. *Nature Protocols*, *8*(1), 162–175. https://doi.org/10.1038/nprot.2012.150
- Liao, C., Ashley, N., Diot, A., Morten, K., Phadwal, K., Williams, A., Fearnley, I., Rosser, L., Lowndes, J., Fratter, C., Ferguson, D. J. P., Vay, L., Quaghebeur, G., Moroni, I., Bianchi, S., Lamperti, C., Downes, S. M., Sitarz, K. S., Flannery, P. J., ... Poulton, J. (2017). Dysregulated mitophagy and mitochondrial organization in optic atrophy due to OPA1 mutations. *Neurology*, *88*(2), 131–142. https://doi.org/10.1212/WNL.00000000000003491
- Lin, R. W., Ho, C. J., Chen, H. W., Pao, Y. H., Chen, L. E., Yang, M. C., Huang, S. B., Wang, S., Chen, C. H., & Wang, C. (2018). P53 enhances apoptosis induced by doxorubicin only under conditions of severe DNA damage. *Cell Cycle*, *17*(17), 2175–2186. https://doi.org/10.1080/15384101.2018.1520565
- Linders, A. N., Dias, I. B., López Fernández, T., Tocchetti, C. G., Bomer, N., & Van der Meer, P. (2024). A review of the pathophysiological mechanisms of doxorubicin-induced cardiotoxicity and aging. *Npj Aging 2024 10:1*, *10*(1), 1–9. https://doi.org/10.1038/s41514-024-00135-7
- Lisowski, P., Kannan, P., Mlody, B., & Prigione, A. (2018). Mitochondria and the dynamic control of stem cell homeostasis. *EMBO Reports*, *19*(5), 1–12. https://doi.org/10.15252/embr.201745432
- Litviňuková, M., Talavera-López, C., Maatz, H., Reichart, D., Worth, C. L., Lindberg, E. L., Kanda, M., Polanski, K., Heinig, M., Lee, M., Nadelmann, E. R., Roberts, K., Tuck, L., Fasouli, E. S., DeLaughter, D. M., McDonough, B., Wakimoto, H., Gorham, J. M., Samari, S., ... Teichmann, S. A. (2020). Cells of the adult human heart. *Nature*, *588*(7838), 466–472. https://doi.org/10.1038/s41586-020-2797-4
- Liu, P., Wakamiya, M., Shea, M. J., Albrecht, U., Behringer, R. R., & Bradley, A. (1999). Requirement for Wnt3 in vertebrate axis formation. *Nature Genetics* 1999 22:4, 22(4),

- 361-365. https://doi.org/10.1038/11932
- Löser, P., Schirm, J., Guhr, A., Wobus, A. M., & Kurtz, A. (2010). Human Embryonic Stem Cell Lines and Their Use in International Research. *Stem Cells*, *28*(2), 240–246. https://doi.org/10.1002/stem.286
- Lowell, B. B., & Shulman, G. I. (2005). Mitochondrial dysfunction and type 2 diabetes. Science, 307(5708), 384–387. https://doi.org/10.1126/SCIENCE.1104343/ASSET/9AB92F2B-F27C-4F4B-9E2E-35D6928CC6FB/ASSETS/GRAPHIC/307\_384\_F2B.JPEG
- Lu, F., & Zhang, Y. (2015). Cell totipotency: molecular features, induction, and maintenance. *National Science Review*, *2*(2), 217–225. https://doi.org/10.1093/nsr/nwv009
- Lucas, B. D., & Kanade, T. (1981). *An Iterative Image Registration Technique with an Application to Stereo Vision*. 2, 674–679. https://doi.org/10.34894/VQ1DJA
- Lundy, S. D., Zhu, W. Z., Regnier, M., & Laflamme, M. A. (2013). Structural and functional maturation of cardiomyocytes derived from human pluripotent stem cells. *Stem Cells and Development*, 22(14), 1991–2002. https://doi.org/10.1089/scd.2012.0490
- Luo, W., & Brouwer, C. (2013). Pathview: An R/Bioconductor package for pathway-based data integration and visualization. *Bioinformatics*, *29*(14), 1830–1831. https://doi.org/10.1093/bioinformatics/btt285
- Mahdavi, V., Chambers, A. P., & Nadal-Ginard, B. (1984). Cardiac α- and β-myosin heavy chain genes are organized in tandem. *Proceedings of the National Academy of Sciences of the United States of America*, *81*(9 I), 2626–2630. https://doi.org/10.1073/pnas.81.9.2626
- Maillet, A., Tan, K., Chai, X., Sadananda, S. N., Mehta, A., Ooi, J., Hayden, M. R., Pouladi, M. A., Ghosh, S., Shim, W., & Brunham, L. R. (2016). Modeling Doxorubicin-Induced Cardiotoxicity in Human Pluripotent Stem Cell Derived-Cardiomyocytes. *Scientific Reports*, 6. https://doi.org/10.1038/SREP25333
- Mandal, S., Lindgren, A. G., Srivastava, A. S., Clark, A. T., & Banerjee, U. (2011a). Mitochondrial function controls proliferation and early differentiation potential of embryonic stem cells. Stem Cells, 29(3), 486–495. https://doi.org/10.1002/stem.590
- Mandal, S., Lindgren, A. G., Srivastava, A. S., Clark, A. T., & Banerjee, U. (2011b).
  Mitochondrial Function Controls Proliferation and Early Differentiation Potential of
  Embryonic Stem Cells. Stem Cells, 29(3), 486–495. https://doi.org/10.1002/stem.590
- Mannella, C. A. (2006). Structure and dynamics of the mitochondrial inner membrane cristae. In *Biochimica et Biophysica Acta Molecular Cell Research* (Vol. 1763, Issues 5–6, pp. 542–548). Elsevier. https://doi.org/10.1016/j.bbamcr.2006.04.006
- Männer, J., Pérez-Pomares, J. M., Macías, D., & Muñoz-Chápuli, R. (2001). The origin, formation and developmental significance of the epicardium: A review. In *Cells Tissues Organs* (Vol. 169, Issue 2, pp. 89–103). S. Karger AG. https://doi.org/10.1159/000047867
- Mannino, G., Russo, C., Maugeri, G., Musumeci, G., Vicario, N., Tibullo, D., Giuffrida, R., Parenti, R., & Lo Furno, D. (2022). Adult stem cell niches for tissue homeostasis. In *Journal of Cellular Physiology* (Vol. 237, Issue 1, pp. 239–257). John Wiley and Sons Inc. https://doi.org/10.1002/jcp.30562
- Mansilla, N., Racca, S., Gras, D., Gonzalez, D., & Welchen, E. (2018). The Complexity of Mitochondrial Complex IV: An Update of Cytochrome c Oxidase Biogenesis in Plants. *International Journal of Molecular Sciences*, 19(3), 662. https://doi.org/10.3390/ijms19030662

- Martínez-Diez, M., Santamaría, G., Ortega, Á. D., & Cuezva, J. M. (2006). Biogenesis and Dynamics of Mitochondria during the Cell Cycle: Significance of 3'UTRs. *PLoS ONE*, 1(1), e107. https://doi.org/10.1371/journal.pone.0000107
- Martínez-Reyes, I., & Chandel, N. S. (2020). Mitochondrial TCA cycle metabolites control physiology and disease. In *Nature Communications* (Vol. 11, Issue 1, pp. 1–11). Nature Research. https://doi.org/10.1038/s41467-019-13668-3
- Marvin, M. J., Di Rocco, G., Gardiner, A., Bush, S. M., & Lassar, A. B. (2001). Inhibition of Wnt activity induces heart formation from posterior mesoderm. *Genes and Development*, *15*(3), 316–327. https://doi.org/10.1101/gad.855501
- Mathieu, J., Zhou, W., Xing, Y., Sperber, H., Ferreccio, A., Agoston, Z., Kuppusamy, K. T., Moon, R. T., & Ruohola-Baker, H. (2014). Hypoxia-inducible factors have distinct and stage-specific roles during reprogramming of human cells to pluripotency. *Cell Stem Cell*, *14*(5), 592–605. https://doi.org/10.1016/j.stem.2014.02.012
- Menzies, R. A., & Golds, P. H. (1971). The Turnover of Mitochondria in a Variety of Tissues of Young Adult and Aged Rats\*. *THE JOURNAL OF BIoLoGrCaL CHEMISTRY*, 246(8), 2425–2429. https://doi.org/10.1016/S0021-9258(18)62305-1
- Minotti, G., Menna, P., Salvatorelli, E., Cairo, G., & Gianni, L. (2004). Anthracyclines: Molecular advances and pharmacologie developments in antitumor activity and cardiotoxicity. In *Pharmacological Reviews* (Vol. 56, Issue 2, pp. 185–229). American Society for Pharmacology and Experimental Therapeutics. https://doi.org/10.1124/pr.56.2.6
- Mishra, P., Carelli, V., Manfredi, G., & Chan, D. C. (2014). Proteolytic cleavage of Opa1 stimulates mitochondrial inner membrane fusion and couples fusion to oxidative phosphorylation. *Cell Metabolism*, *19*(4), 630–641. https://doi.org/10.1016/j.cmet.2014.03.011
- Mollova, M., Bersell, K., Walsh, S., Savla, J., Das, L. T., Park, S. Y., Silberstein, L. E., Dos Remedios, C. G., Graham, D., Colan, S., & Kühn, B. (2013). Cardiomyocyte proliferation contributes to heart growth in young humans. *Proceedings of the National Academy of Sciences of the United States of America*, *110*(4), 1446–1451. https://doi.org/10.1073/PNAS.1214608110/SUPPL\_FILE/SM06.MOV
- Morris, S., Molina-Riquelme, I., Barrientos, G., Bravo, F., Aedo, G., Gómez, W., Lagos, D., Verdejo, H., Peischard, S., Seebohm, G., Psathaki, O. E., Eisner, V., & Busch, K. B. (2023). Inner mitochondrial membrane structure and fusion dynamics are altered in senescent human iPSC-derived and primary rat cardiomyocytes. *Biochimica et Biophysica Acta (BBA) Bioenergetics*, *1864*(2), 148949. https://doi.org/10.1016/J.BBABIO.2022.148949
- Morrison, S. J., & Kimble, J. (2006). Asymmetric and symmetric stem-cell divisions in development and cancer. In *Nature* (Vol. 441, Issue 7097, pp. 1068–1074). Nature Publishing Group. https://doi.org/10.1038/nature04956
- Mortensen, S. A., Olsen, H. S., & Baandrup, U. (1986). Chronic anthracycline cardiotoxicity: Haemodynamic and histopathological manifestations suggesting a restrictive endomyocardial disease. *British Heart Journal*, *55*(3), 274–282. https://doi.org/10.1136/hrt.55.3.274
- Mozaffarian, D., Wilson, P. W. F., & Kannel, W. B. (2008). Beyond established and novel risk factors lifestyle risk factors for cardiovascular disease. In *Circulation* (Vol. 117, Issue 23, pp. 3031–3038). Lippincott Williams & Wilkins. https://doi.org/10.1161/CIRCULATIONAHA.107.738732
- Mujoo, K., Pandita, R. K., Tiwari, A., Charaka, V., Chakraborty, S., Singh, D. K., Hambarde,

- S., Hittelman, W. N., Horikoshi, N., Hunt, C. R., Khanna, K. K., Kots, A. Y., Butler, E. B., Murad, F., & Pandita, T. K. (2017). Differentiation of Human Induced Pluripotent or Embryonic Stem Cells Decreases the DNA Damage Repair by Homologous Recombination. *Stem Cell Reports*, *9*(5), 1660–1674. https://doi.org/10.1016/j.stemcr.2017.10.002
- Mulrooney, D. A., Yeazel, M. W., Kawashima, T., Mertens, A. C., Mitby, P., Stovall, M., Donaldson, S. S., Green, D. M., Sklar, C. A., Robison, L. L., & Leisenring, W. M. (2009). Cardiac outcomes in a cohort of adult survivors of childhood and adolescent cancer: retrospective analysis of the Childhood Cancer Survivor Study cohort. *BMJ*, 339(7736), 34. https://doi.org/10.1136/BMJ.B4606
- Nakamura, T., Sano, M., Songyang, Z., & Schneider, M. D. (2003). A Wnt- and β-catenin-dependent pathway for mammalian cardiac myogenesis. *Proceedings of the National Academy of Sciences of the United States of America*, *100*(10), 5834–5839. https://doi.org/10.1073/pnas.0935626100
- Naon, D., & Scorrano, L. (2014). At the right distance: ER-mitochondria juxtaposition in cell life and death. In *Biochimica et Biophysica Acta Molecular Cell Research* (Vol. 1843, Issue 10, pp. 2184–2194). Elsevier B.V. https://doi.org/10.1016/j.bbamcr.2014.05.011
- Natarajan, K. N., Teichmann, S. A., & Kolodziejczyk, A. A. (2017). Single cell transcriptomics of pluripotent stem cells: reprogramming and differentiation. In *Current Opinion in Genetics and Development* (Vol. 46, pp. 66–76). Elsevier Ltd. https://doi.org/10.1016/j.gde.2017.06.003
- Nicholls, T. J., Nadalutti, C. A., Motori, E., Sommerville, E. W., Gorman, G. S., Basu, S., Hoberg, E., Turnbull, D. M., Chinnery, P. F., Larsson, N. G., Larsson, E., Falkenberg, M., Taylor, R. W., Griffith, J. D., & Gustafsson, C. M. (2018). Topoisomerase 3α Is Required for Decatenation and Segregation of Human mtDNA. *Molecular Cell*, *69*(1), 9-23.e6. https://doi.org/10.1016/j.molcel.2017.11.033
- Nishikawa, S. I., Goldstein, R. A., & Nierras, C. R. (2008). The promise of human induced pluripotent stem cells for research and therapy. In *Nature Reviews Molecular Cell Biology* (Vol. 9, Issue 9, pp. 725–729). Nature Publishing Group. https://doi.org/10.1038/nrm2466
- Nitiss, J. L. (2009). Targeting DNA topoisomerase II in cancer chemotherapy. In *Nature Reviews Cancer* (Vol. 9, Issue 5, pp. 338–350). Nature Publishing Group. https://doi.org/10.1038/nrc2607
- Nussbaumer, S., Bonnabry, P., Veuthey, J. L., & Fleury-Souverain, S. (2011). Analysis of anticancer drugs: A review. In *Talanta* (Vol. 85, Issue 5, pp. 2265–2289). Elsevier B.V. https://doi.org/10.1016/j.talanta.2011.08.034
- Nysom, K., Holm, K., Lipsitz, S. R., Mone, S. M., Colan, S. D., Orav, E. J., Sallan, S. E., Olsen, J. H., Hertz, H., Jacobsen, J. R., & Lipshultz, S. E. (1998). Relationship between cumulative anthracycline dose and late cardiotoxicity in childhood acute lymphoblastic leukemia. *Journal of Clinical Oncology*, *16*(2), 545–550. https://doi.org/10.1200/JCO.1998.16.2.545
- Okita, K., Nakagawa, M., Hyenjong, H., Ichisaka, T., & Yamanaka, S. (2008). Generation of Mouse Induced Pluripotent Stem Cells Without Viral Vectors. *Science*, *322*(5903), 949–953. https://doi.org/10.1126/science.1164270
- Pääbo, S. (1999). Human evolution. In *Trends in Cell Biology* (Vol. 9, Issue 12, pp. M13–M16). Elsevier. https://doi.org/10.1016/S0962-8924(99)01688-8
- Pedron, S., van Lierop, S., Horstman, P., Penterman, R., Broer, D. J., & Peeters, E. (2011). Stimuli Responsive Delivery Vehicles for Cardiac Microtissue Transplantation.

- Advanced Functional Materials, 21(9), 1624–1630. https://doi.org/10.1002/adfm.201002708
- Peng, S., Chen, L.-L., Lei, X.-X., Yang, L., Lin, H., Carmichael, G. G., & Huang, Y. (2011). Genome-Wide Studies Reveal That Lin28 Enhances the Translation of Genes Important for Growth and Survival of Human Embryonic Stem Cells. *Stem Cells*, *29*(3), 496–504. https://doi.org/10.1002/stem.591
- Pereira, S. L., Grãos, M., Rodrigues, A. S., Anjo, S. I., Carvalho, R. A., Oliveira, P. J., Arenas, E., & Ramalho-Santos, J. (2013). Inhibition of Mitochondrial Complex III Blocks Neuronal Differentiation and Maintains Embryonic Stem Cell Pluripotency. *PLoS ONE*, 8(12), e82095. https://doi.org/10.1371/journal.pone.0082095
- Peris-Moreno, D., Taillandier, D., & Polge, C. (2020). MuRF1/TRIM63, Master Regulator of Muscle Mass. *International Journal of Molecular Sciences 2020, Vol. 21, Page 6663*, 21(18), 6663. https://doi.org/10.3390/IJMS21186663
- Pinto, A. R., Ilinykh, A., Ivey, M. J., Kuwabara, J. T., D'antoni, M. L., Debuque, R., Chandran, A., Wang, L., Arora, K., Rosenthal, N. A., & Tallquist, M. D. (2016). Revisiting cardiac cellular composition. *Circulation Research*, *118*(3), 400–409. https://doi.org/10.1161/CIRCRESAHA.115.307778
- Prigione, A., Fauler, B., Lurz, R., Lehrach, H., & Adjaye, J. (2010). The Senescence-Related Mitochondrial/Oxidative Stress Pathway is Repressed in Human Induced Pluripotent Stem Cells. *Stem Cells*, *28*(4), 721–733. https://doi.org/10.1002/stem.404
- Prigione, A., Hossini, A. M., Lichtner, B., Serin, A., Fauler, B., Megges, M., Lurz, R., Lehrach, H., Makrantonaki, E., Zouboulis, C. C., & Adjaye, J. (2011). Mitochondrial-Associated Cell Death Mechanisms Are Reset to an Embryonic-Like State in Aged Donor-Derived iPS Cells Harboring Chromosomal Aberrations. *PLoS ONE*, *6*(11), e27352. https://doi.org/10.1371/journal.pone.0027352
- Prondzynski, M., Berkson, P., Trembley, M. A., Tharani, Y., Shani, K., Bortolin, R. H., Sweat, M. E., Mayourian, J., Yucel, D., Cordoves, A. M., Gabbin, B., Hou, C., Anyanwu, N. J., Nawar, F., Cotton, J., Milosh, J., Walker, D., Zhang, Y., Lu, F., ... Pu, W. T. (2024). Efficient and reproducible generation of human iPSC-derived cardiomyocytes and cardiac organoids in stirred suspension systems. *Nature Communications*, *15*(1), 1–17. https://doi.org/10.1038/s41467-024-50224-0
- Rabl, R., Soubannier, V., Scholz, R., Vogel, F., Mendl, N., Vasiljev-Neumeyer, A., Körner, C., Jagasia, R., Keil, T., Baumeister, W., Cyrklaff, M., Neupert, W., & Reichert, A. S. (2009). Formation of cristae and crista junctions in mitochondria depends on antagonism between Fcj1 and Su e/g. *Journal of Cell Biology*, *185*(6), 1047–1063. https://doi.org/10.1083/jcb.200811099
- Ranieri, M., Brajkovic, S., Riboldi, G., Ronchi, D., Rizzo, F., Bresolin, N., Corti, S., & Comi, G. P. (2013). Mitochondrial Fusion Proteins and Human Diseases. *Neurology Research International*, 2013(1), 1–11. https://doi.org/10.1155/2013/293893
- Ranjbarvaziri, S., Kooiker, K. B., Ellenberger, M., Fajardo, G., Zhao, M., Vander Roest, A. S., Woldeyes, R. A., Koyano, T. T., Fong, R., Ma, N., Tian, L., Traber, G. M., Chan, F., Perrino, J., Reddy, S., Chiu, W., Wu, J. C., Woo, J. Y., Ruppel, K. M., ... Bernstein, D. (2021). Altered Cardiac Energetics and Mitochondrial Dysfunction in Hypertrophic Cardiomyopathy. *Circulation*, 144(21), 1714–1731. https://doi.org/10.1161/CIRCULATIONAHA.121.053575
- Ritchie, M. E., Phipson, B., Wu, D., Hu, Y., Law, C. W., Shi, W., & Smyth, G. K. (2015). Limma powers differential expression analyses for RNA-sequencing and microarray studies. *Nucleic Acids Research*, *43*(7), e47. https://doi.org/10.1093/nar/gkv007

- Rizwan, M., Rasheed, H. Al, & Tarjan, G. (2018). Succinate dehydrogenase complex: An updated review. *Archives of Pathology and Laboratory Medicine*, *142*(12), 1564–1570. https://doi.org/10.5858/arpa.2017-0285-RS
- Rizzuto, R., De Stefani, D., Raffaello, A., & Mammucari, C. (2012). Mitochondria as sensors and regulators of calcium signalling. In *Nature Reviews Molecular Cell Biology* (Vol. 13, Issue 9, pp. 566–578). Nature Publishing Group. https://doi.org/10.1038/nrm3412
- Robinson, M. D., McCarthy, D. J., & Smyth, G. K. (2009). edgeR: A Bioconductor package for differential expression analysis of digital gene expression data. *Bioinformatics*, *26*(1), 139–140. https://doi.org/10.1093/bioinformatics/btp616
- Robinson, M. D., & Oshlack, A. (2010). A scaling normalization method for differential expression analysis of RNA-seq data. *Genome Biology*, *11*(3). https://doi.org/10.1186/gb-2010-11-3-r25
- Rocha, A. G., Franco, A., Krezel, A. M., Rumsey, J. M., Alberti, J. M., Knight, W. C., Biris, N., Zacharioudakis, E., Janetka, J. W., Baloh, R. H., Kitsis, R. N., Mochly-Rosen, D., Townsend, R. R., Gavathiotis, E., & Dorn, G. W. (2018). MFN2 agonists reverse mitochondrial defects in preclinical models of Charcot-Marie-Tooth disease type 2A. *Science*, *360*(6386), 336–341. https://doi.org/10.1126/science.aao1785
- Rochais, F., Mesbah, K., & Kelly, R. G. (2009). Signaling pathways controlling second heart field development. In *Circulation Research* (Vol. 104, Issue 8, pp. 933–942). Lippincott Williams & Wilkins. https://doi.org/10.1161/CIRCRESAHA.109.194464
- Rogakou, E. P., Pilch, D. R., Orr, A. H., Ivanova, V. S., & Bonner, W. M. (1998). DNA double-stranded breaks induce histone H2AX phosphorylation on serine 139. *Journal of Biological Chemistry*, 273(10), 5858–5868. https://doi.org/10.1074/JBC.273.10.5858/ASSET/FCF77A15-48E9-40D3-90C2-7C668B006F59/MAIN.ASSETS/GR13.JPG
- Rosencrans, W. M., Rajendran, M., Bezrukov, S. M., & Rostovtseva, T. K. (2021). VDAC regulation of mitochondrial calcium flux: From channel biophysics to disease. *Cell Calcium*, *94*, 102356. https://doi.org/10.1016/j.ceca.2021.102356
- Rouillard, A. D., Gundersen, G. W., Fernandez, N. F., Wang, Z., Monteiro, C. D., McDermott, M. G., & Ma'ayan, A. (2016). The harmonizome: a collection of processed datasets gathered to serve and mine knowledge about genes and proteins. *Database*, *2016*, baw100. https://doi.org/10.1093/database/baw100
- Rowe, R. G., & Daley, G. Q. (2019). Induced pluripotent stem cells in disease modelling and drug discovery. In *Nature Reviews Genetics* (Vol. 20, Issue 7, pp. 377–388). Nature Publishing Group. https://doi.org/10.1038/s41576-019-0100-z
- Ryall, J. G., Cliff, T., Dalton, S., & Sartorelli, V. (2015). Metabolic Reprogramming of Stem Cell Epigenetics. In *Cell Stem Cell* (Vol. 17, Issue 6, pp. 651–662). Cell Press. https://doi.org/10.1016/j.stem.2015.11.012
- Sacks, M. S., David Merryman, W., & Schmidt, D. E. (2009). On the biomechanics of heart valve function. In *Journal of Biomechanics* (Vol. 42, Issue 12, pp. 1804–1824). Elsevier. https://doi.org/10.1016/j.jbiomech.2009.05.015
- Sainero-Alcolado, L., Liaño-Pons, J., Ruiz-Pérez, M. V., & Arsenian-Henriksson, M. (2022). Targeting mitochondrial metabolism for precision medicine in cancer. *Cell Death & Differentiation 2022 29:7*, *29*(7), 1304–1317. https://doi.org/10.1038/s41418-022-01022-y
- Sakai, H., Sagara, A., Arakawa, K., Sugiyama, R., Hirosaki, A., Takase, K., Jo, A., Sato, K., Chiba, Y., Yamazaki, M., Matoba, M., & Narita, M. (2014). Mechanisms of cisplatin-induced muscle atrophy. *Toxicology and Applied Pharmacology*, *278*(2), 190–199.

- https://doi.org/10.1016/J.TAAP.2014.05.001
- Santo-Domingo, J., & Demaurex, N. (2010). Calcium uptake mechanisms of mitochondria. In *Biochimica et Biophysica Acta Bioenergetics* (Vol. 1797, Issues 6–7, pp. 907–912). Elsevier. https://doi.org/10.1016/j.bbabio.2010.01.005
- Sardão, V. A., Oliveira, P. J., Holy, J., Oliveira, C. R., & Wallace, K. B. (2009). Morphological alterations induced by doxorubicin on H9c2 myoblasts: Nuclear, mitochondrial, and cytoskeletal targets. *Cell Biology and Toxicology*, *25*(3), 227–243. https://doi.org/10.1007/s10565-008-9070-1
- Sarosiek, K. A., Ni Chonghaile, T., & Letai, A. (2013). Mitochondria: Gatekeepers of response to chemotherapy. In *Trends in Cell Biology* (Vol. 23, Issue 12, pp. 612–619). Elsevier. https://doi.org/10.1016/j.tcb.2013.08.003
- Savitzky, A., & Golay, M. J. E. (1964). Smoothing and Differentiation of Data by Simplified Least Squares Procedures. *Analytical Chemistry*, *36*(8), 1627–1639. https://doi.org/10.1021/ac60214a047
- Schägger, H., & Pfeiffer, K. (2000). Supercomplexes in the respiratory chains of yeast and mammalian mitochondria. *EMBO Journal*, *19*(8), 1777–1783. https://doi.org/10.1093/emboj/19.8.1777
- Schmidt, M., Zeevaert, K., Elsafi Mabrouk, M. H., Goetzke, R., & Wagner, W. (2023). Epigenetic biomarkers to track differentiation of pluripotent stem cells. *Stem Cell Reports*, *18*(1), 145–158. https://doi.org/10.1016/j.stemcr.2022.11.001
- Schofield, R. (1978). The relationship between the spleen colony-forming cell and the haemopoietic stem cell. A hypothesis. *Blood Cells*, *4*(1–2), 7–25.
- Seo, B. J., Yoon, S. H., & Do, J. T. (2018). Mitochondrial dynamics in stem cells and differentiation. In *International Journal of Molecular Sciences* (Vol. 19, Issue 12, p. 3893). MDPI AG. https://doi.org/10.3390/ijms19123893
- Sheng, B., Wang, X., Su, B., Lee, H., Casadesus, G., Perry, G., & Zhu, X. (2012). Impaired mitochondrial biogenesis contributes to mitochondrial dysfunction in Alzheimer's disease. *Journal of Neurochemistry*, *120*(3), 419–429. https://doi.org/10.1111/j.1471-4159.2011.07581.x
- Sies, H., & Jones, D. P. (2020). Reactive oxygen species (ROS) as pleiotropic physiological signalling agents. In *Nature Reviews Molecular Cell Biology* (Vol. 21, Issue 7, pp. 363–383). Nature Research. https://doi.org/10.1038/s41580-020-0230-3
- Simon, H. U., Haj-Yehia, A., & Levi-Schaffer, F. (2000). Role of reactive oxygen species (ROS) in apoptosis induction. *Apoptosis*, *5*(5), 415–418. https://doi.org/10.1023/A:1009616228304
- Smirnova, E., Griparic, L., Shurland, D. L., & Van der Bliek, A. M. (2001). Dynamin-related protein Drp1 is required for mitochondrial division in mammalian cells. *Molecular Biology of the Cell*, 12(8), 2245–2256. https://doi.org/10.1091/mbc.12.8.2245
- Smits, A. M., van Vliet, P., Metz, C. H., Korfage, T., Sluijter, J. P. G., Doevendans, P. A., & Goumans, M. J. (2009). Human cardiomyocyte progenitor cells differentiate into functional mature cardiomyocytes: an in vitro model for studying human cardiac physiology and pathophysiology. *Nature Protocols* 2009 4:2, 4(2), 232–243. https://doi.org/10.1038/nprot.2008.229
- Sobecki, M., Mrouj, K., Colinge, J., Gerbe, F., Jay, P., Krasinska, L., Dulic, V., & Fisher, D. (2017). Cell-cycle regulation accounts for variability in Ki-67 expression levels. *Cancer Research*, 77(10), 2722–2734. https://doi.org/10.1158/0008-5472.CAN-16-0707

- Sousa, J. S., Mills, D. J., Vonck, J., & Kühlbrandt, W. (2016). Functional asymmetry and electron flow in the bovine respirasome. *ELife*, *5*(NOVEMBER2016). https://doi.org/10.7554/eLife.21290
- Sritharan, S., & Sivalingam, N. (2021). A comprehensive review on time-tested anticancer drug doxorubicin. In *Life Sciences* (Vol. 278, p. 119527). Elsevier Inc. https://doi.org/10.1016/j.lfs.2021.119527
- Steinberg, J. S., Cohen, A. J., Wasserman, A. G., Cohen, P., & Ross, A. M. (1987a). Acute arrhythmogenicity of doxorubicin administration. *Cancer*, *60*(6), 1213–1218. https://doi.org/10.1002/1097-0142(19870915)60:6<1213::AID-CNCR2820600609>3.0.CO;2-V
- Steinberg, J. S., Cohen, A. J., Wasserman, A. G., Cohen, P., & Ross, A. M. (1987b). Acute arrhythmogenicity of doxorubicin administration. *Cancer*, *60*(6), 1213–1218. https://doi.org/10.1002/1097-0142(19870915)60:6<1213::AID-CNCR2820600609>3.0.CO;2-V
- Stephan, T., Brüser, C., Deckers, M., Steyer, A. M., Balzarotti, F., Barbot, M., Behr, T. S., Heim, G., Hübner, W., Ilgen, P., Lange, F., Pacheu-Grau, D., Pape, J. K., Stoldt, S., Huser, T., Hell, S. W., Möbius, W., Rehling, P., Riedel, D., & Jakobs, S. (2020). MICOS assembly controls mitochondrial inner membrane remodeling and crista junction redistribution to mediate cristae formation. *The EMBO Journal*, 39(14). https://doi.org/10.15252/embj.2019104105
- Stewart, J. B., & Chinnery, P. F. (2015). The dynamics of mitochondrial DNA heteroplasmy: implications for human health and disease. *Nature Reviews Genetics* 2015 16:9, 16(9), 530–542. https://doi.org/10.1038/nrg3966
- Strauss, M., Hofhaus, G., Schröder, R. R., & Kühlbrandt, W. (2008). Dimer ribbons of ATP synthase shape the inner mitochondrial membrane. *EMBO Journal*, *27*(7), 1154–1160. https://doi.org/10.1038/emboj.2008.35
- Sturtzel, C. (2017). Endothelial cells. In *Advances in Experimental Medicine and Biology* (Vol. 1003, pp. 71–91). Springer New York LLC. https://doi.org/10.1007/978-3-319-57613-8\_4
- Suhr, S. T., Chang, E. A., Tjong, J., Alcasid, N., Perkins, G. A., Goissis, M. D., Ellisman, M. H., Perez, G. I., & Cibelli, J. B. (2010). Mitochondrial Rejuvenation After Induced Pluripotency. *PLoS ONE*, *5*(11), e14095. https://doi.org/10.1371/journal.pone.0014095
- Sunter, N. J., Cowell, I. G., Willmore, E., Watters, G. P., & Austin, C. A. (2010). Role of Topoisomerase IIβ in DNA Damage Response following IR and Etoposide. *Journal of Nucleic Acids*, *2010*, 710589. https://doi.org/10.4061/2010/710589
- Supino, R. (1995). MTT assays. *Methods in Molecular Biology (Clifton, N.J.)*, *43*, 137–149. https://doi.org/10.1385/0-89603-282-5:137
- Swain, S. M., Whaley, F. S., & Ewer, M. S. (2003). Congestive heart failure in patients treated with doxorubicin. *Cancer*, 97(11), 2869–2879. https://doi.org/10.1002/cncr.11407
- Szendroedi, J., Phielix, E., & Roden, M. (2012). The role of mitochondria in insulin resistance and type 2 diabetes mellitus. In *Nature Reviews Endocrinology* (Vol. 8, Issue 2, pp. 92–103). Nature Publishing Group. https://doi.org/10.1038/nrendo.2011.138
- Tábara, L. C., Segawa, M., & Prudent, J. (2024). Molecular mechanisms of mitochondrial dynamics. In *Nature Reviews Molecular Cell Biology*. Nature Research. https://doi.org/10.1038/s41580-024-00785-1
- Takahashi, K., Tanabe, K., Ohnuki, M., Narita, M., Ichisaka, T., Tomoda, K., & Yamanaka, S.

- (2007). Induction of Pluripotent Stem Cells from Adult Human Fibroblasts by Defined Factors. *Cell*, 131(5), 861–872. https://doi.org/10.1016/j.cell.2007.11.019
- Takahashi, K., & Yamanaka, S. (2006). Induction of Pluripotent Stem Cells from Mouse Embryonic and Adult Fibroblast Cultures by Defined Factors. *Cell*, *126*(4), 663–676. https://doi.org/10.1016/j.cell.2006.07.024
- Tallquist, M. D., & Molkentin, J. D. (2017). Redefining the identity of cardiac fibroblasts. In *Nature Reviews Cardiology* (Vol. 14, Issue 8, pp. 484–491). Nature Publishing Group. https://doi.org/10.1038/nrcardio.2017.57
- Tan, G., Lou, Z., Liao, W., Zhu, Z., Dong, X., Zhang, W., Li, W., & Chai, Y. (2011). Potential Biomarkers in Mouse Myocardium of Doxorubicin-Induced Cardiomyopathy: A Metabonomic Method and Its Application. *PLoS ONE*, *6*(11), e27683. https://doi.org/10.1371/journal.pone.0027683
- Tanaka, R., Umemura, M., Narikawa, M., Hikichi, M., Osaw, K., Fujita, T., Yokoyama, U., Ishigami, T., Tamura, K., & Ishikawa, Y. (2020). Reactive fibrosis precedes doxorubicin-induced heart failure through sterile inflammation. *ESC Heart Failure*, 7(2), 588–603. https://doi.org/10.1002/ehf2.12616
- Tang, H., Tao, A., Song, J., Liu, Q., Wang, H., & Rui, T. (2017). Doxorubicin-induced cardiomyocyte apoptosis: Role of mitofusin 2. *International Journal of Biochemistry and Cell Biology*, *88*, 55–59. https://doi.org/10.1016/j.biocel.2017.05.006
- Tewey, K. M., Rowe, T. C., Yang, L., Halligan, B. D., & Liu, L. F. (1984). Adriamycin-induced DNA damage mediated by mammalian DNA topoisomerase II. *Science*, 226(4673), 466–468. https://doi.org/10.1126/science.6093249
- Thomson, J. A. (1998). Embryonic stem cell lines derived from human blastocysts. *Science*, 282(5391), 1145–1147. https://doi.org/10.1126/science.282.5391.1145
- Tracy, R. E., & Sander, G. E. (2011). Histologically Measured Cardiomyocyte Hypertrophy Correlates with Body Height as Strongly as with Body Mass Index. *Cardiology Research and Practice*, 2011(1), 658958. https://doi.org/10.4061/2011/658958
- Trager, L. E., Lyons, M., Kuznetsov, A., Sheffield, C., Roh, K., Freeman, R., Rhee, J., Guseh, J. S., Li, H., & Rosenzweig, A. (2023). Beyond cardiomyocytes: Cellular diversity in the heart's response to exercise. *Journal of Sport and Health Science*, *12*(4), 423–437. https://doi.org/10.1016/J.JSHS.2022.12.011
- Valera-Alberni, M., Joffraud, M., Miro-Blanch, J., Capellades, J., Junza, A., Dayon, L., Núñez Galindo, A., Sanchez-Garcia, J. L., Valsesia, A., Cercillieux, A., Söllner, F., Ladurner, A. G., Yanes, O., & Cantó, C. (2021). Crosstalk between Drp1 phosphorylation sites during mitochondrial remodeling and their impact on metabolic adaptation. *Cell Reports*, 36(8), 109565. https://doi.org/10.1016/J.CELREP.2021.109565
- van Berlo, J. H., Kanisicak, O., Maillet, M., Vagnozzi, R. J., Karch, J., Lin, S.-C. J., Middleton, R. C., Marbán, E., & Molkentin, J. D. (2014). c-kit+ cells minimally contribute cardiomyocytes to the heart. *Nature*, *509*(7500), 337–341. https://doi.org/10.1038/nature13309
- van den Boogaard, W. M. C., Komninos, D. S. J., & Vermeij, W. P. (2022). Chemotherapy Side-Effects: Not All DNA Damage Is Equal. *Cancers 2022, Vol. 14, Page 627, 14*(3), 627. https://doi.org/10.3390/CANCERS14030627
- van der Velden, J., & Stienen, G. J. M. (2019). Cardiac disorders and pathophysiology of sarcomeric proteins. In *Physiological Reviews* (Vol. 99, Issue 1, pp. 381–426). American Physiological Society. https://doi.org/10.1152/physrev.00040.2017
- van der Zanden, S. Y., Qiao, X., & Neefjes, J. (2021). New insights into the activities and

- toxicities of the old anticancer drug doxorubicin. In *FEBS Journal* (Vol. 288, Issue 21, pp. 6095–6111). John Wiley and Sons Inc. https://doi.org/10.1111/febs.15583
- Van Laar, V. S., Berman, S. B., & Hastings, T. G. (2016). Mic60/mitofilin overexpression alters mitochondrial dynamics and attenuates vulnerability of dopaminergic cells to dopamine and rotenone. *Neurobiology of Disease*, *91*, 247–261. https://doi.org/10.1016/j.nbd.2016.03.015
- Varga, D., Hoegel, J., Maier, C., Jainta, S., Hoehne, M., Patino-Garcia, B., Michel, I., Schwarz-Boeger, U., Kiechle, M., Kreienberg, R., & Vogel, W. (2006). On the difference of micronucleus frequencies in peripheral blood lymphocytes between breast cancer patients and controls. *Mutagenesis*, 21(5), 313–320. https://doi.org/10.1093/mutage/gel035
- Varum, S., Rodrigues, A. S., Moura, M. B., Momcilovic, O., Easley, C. A., Ramalho-Santos, J., Van Houten, B., & Schatten, G. (2011). Energy Metabolism in Human Pluripotent Stem Cells and Their Differentiated Counterparts. *PLoS ONE*, *6*(6), e20914. https://doi.org/10.1371/journal.pone.0020914
- Vercellino, I., & Sazanov, L. A. (2021). The assembly, regulation and function of the mitochondrial respiratory chain. *Nature Reviews Molecular Cell Biology 2021 23:2*, 23(2), 141–161. https://doi.org/10.1038/s41580-021-00415-0
- Verfaillie, C. M. (2002). Adult stem cells: Assessing the case for pluripotency. In *Trends in Cell Biology* (Vol. 12, Issue 11, pp. 502–508). Elsevier. https://doi.org/10.1016/S0962-8924(02)02386-3
- Verkhusha, V. V., Chudakov, D. M., Gurskaya, N. G., Lukyanov, S., & Lukyanov, K. A. (2004). Common pathway for the red chromophore formation in fluorescent proteins and chromoproteins. *Chemistry and Biology*, *11*(6), 845–854. https://doi.org/10.1016/j.chembiol.2004.04.007
- Vinothkumar, K. R., Zhu, J., & Hirst, J. (2014). Architecture of mammalian respiratory complex I. *Nature*, *515*(7525), 80–84. https://doi.org/10.1038/nature13686
- von der Malsburg, K., Müller, J. M., Bohnert, M., Oeljeklaus, S., Kwiatkowska, P., Becker, T., Loniewska-Lwowska, A., Wiese, S., Rao, S., Milenkovic, D., Hutu, D. P., Zerbes, R. M., Schulze-Specking, A., Meyer, H. E., Martinou, J. C., Rospert, S., Rehling, P., Meisinger, C., Veenhuis, M., ... van der Laan, M. (2011). Dual Role of Mitofilin in Mitochondrial Membrane Organization and Protein Biogenesis. *Developmental Cell*, *21*(4), 694–707. https://doi.org/10.1016/j.devcel.2011.08.026
- Vučković, S., Dinani, R., Nollet, E. E., Kuster, D. W. D., Buikema, J. W., Houtkooper, R. H., Nabben, M., van der Velden, J., & Goversen, B. (2022). Characterization of cardiac metabolism in iPSC-derived cardiomyocytes: lessons from maturation and disease modeling. Stem Cell Research & Therapy, 13(1), 332. https://doi.org/10.1186/s13287-022-03021-9
- Wagers, A. J., & Weissman, I. L. (2004). Plasticity of adult stem cells. In *Cell* (Vol. 116, Issue 5, pp. 639–648). Elsevier B.V. https://doi.org/10.1016/S0092-8674(04)00208-9
- Wagner, N., Ninkov, M., Vukolic, A., Deniz, G. C., Rassoulzadegan, M., Michiels, J. F., & Wagner, K. D. (2021). Implications of the wilms' tumor suppressor wt1 in cardiomyocyte differentiation. *International Journal of Molecular Sciences*, 22(9), 4346. https://doi.org/10.3390/ijms22094346
- Wake, E., & Brack, K. (2016). Characterization of the intrinsic cardiac nervous system. In *Autonomic Neuroscience: Basic and Clinical* (Vol. 199, pp. 3–16). Elsevier B.V. https://doi.org/10.1016/j.autneu.2016.08.006
- Walker, J. E., & Dickson, V. K. (2006). The peripheral stalk of the mitochondrial ATP

- synthase. In *Biochimica et Biophysica Acta Bioenergetics* (Vol. 1757, Issues 5–6, pp. 286–296). Biochim Biophys Acta. https://doi.org/10.1016/j.bbabio.2006.01.001
- Wallace, D. C. (2018). Mitochondrial genetic medicine. *Nature Genetics*, *50*(12), 1642–1649. https://doi.org/10.1038/s41588-018-0264-z
- Wallace, D. C., Ye, J., Neckelmann, S. N., Singh, G., Webster, K. A., & Greenberg, B. D. (1987). Sequence analysis of cDNAs for the human and bovine ATP synthase β subunit: mitochondrial DNA genes sustain seventeen times more mutations. *Current Genetics*, *12*(2), 81–90. https://doi.org/10.1007/BF00434661
- Wang, Z., Grange, M., Pospich, S., Wagner, T., Kho, A. L., Gautel, M., & Raunser, S. (2022). Structures from intact myofibrils reveal mechanism of thin filament regulation through nebulin. *Science*, *375*(6582). https://doi.org/10.1126/science.abn1934
- Warburg, O., Wind, F., & Negelein, E. (1927). The metabolism of tumors in the body. *Journal of General Physiology*, *8*(6), 519–530. https://doi.org/10.1085/jgp.8.6.519
- Wu, T., Hu, E., Xu, S., Chen, M., Guo, P., Dai, Z., Feng, T., Zhou, L., Tang, W., Zhan, L., Fu, X., Liu, S., Bo, X., & Yu, G. (2021). clusterProfiler 4.0: A universal enrichment tool for interpreting omics data. *Innovation*, *2*(3). https://doi.org/10.1016/j.xinn.2021.100141
- Xu, H., Morishima, M., Wylie, J. N., Schwartz, R. J., Bruneau, B. G., Lindsay, E. A., & Baldini, A. (2004). Tbx1 has a dual role in the morphogenesis of the cardiac outflow tract. *Development*, 131(13), 3217–3227. https://doi.org/10.1242/dev.01174
- Xu, X., Jin, K., Bais, A. S., Zhu, W., Yagi, H., Feinstein, T. N., Nguyen, P. K., Criscione, J. D., Liu, X., Beutner, G., Karunakaran, K. B., Rao, K. S., He, H., Adams, P., Kuo, C. K., Kostka, D., Pryhuber, G. S., Shiva, S., Ganapathiraju, M. K., ... Lo, C. W. (2022). Uncompensated mitochondrial oxidative stress underlies heart failure in an iPSC-derived model of congenital heart disease. *Cell Stem Cell*, 29(5), 840-855.e7. https://doi.org/10.1016/j.stem.2022.03.003
- Yamamoto, T., Arita, M., Kuroda, H., Suzuki, T., & Kawamata, S. (2022). Improving the differentiation potential of pluripotent stem cells by optimizing culture conditions. *Scientific Reports* 2022 12:1, 12(1), 1–12. https://doi.org/10.1038/s41598-022-18400-8
- Yang, F., Chen, H., Liu, Y., Yin, K., Wang, Y., Li, X., Wang, G., Wang, S., Tan, X., Xu, C., Lu, Y., & Cai, B. (2013). Doxorubicin caused apoptosis of mesenchymal stem cells via p38, JNK and p53 Pathway. *Cellular Physiology and Biochemistry*, *32*(4), 1072–1082. https://doi.org/10.1159/000354507
- Yang, X., Rodriguez, M. L., Leonard, A., Sun, L., Fischer, K. A., Wang, Y., Ritterhoff, J., Zhao, L., Kolwicz, S. C., Pabon, L., Reinecke, H., Sniadecki, N. J., Tian, R., Ruohola-Baker, H., Xu, H., & Murry, C. E. (2019). Fatty Acids Enhance the Maturation of Cardiomyocytes Derived from Human Pluripotent Stem Cells. *Stem Cell Reports*, *13*(4), 657–668. https://doi.org/10.1016/j.stemcr.2019.08.013
- Yellon, D. M., & Downey, J. M. (2003). Preconditioning the myocardium: From cellular physiology to clinical cardiology. In *Physiological Reviews* (Vol. 83, Issue 4, pp. 1113–1151). American Physiological Society. https://doi.org/10.1152/physrev.00009.2003
- Yien, Y. Y., & Perfetto, M. (2022). Regulation of Heme Synthesis by Mitochondrial Homeostasis Proteins. In *Frontiers in Cell and Developmental Biology* (Vol. 10, p. 895521). Frontiers Media S.A. https://doi.org/10.3389/fcell.2022.895521
- Yin, J., Guo, J., Zhang, Q., Cui, L., Zhang, L., Zhang, T., Zhao, J., Li, J., Middleton, A., Carmichael, P. L., & Peng, S. (2018). Doxorubicin-induced mitophagy and mitochondrial damage is associated with dysregulation of the PINK1/parkin pathway. *Toxicology in Vitro*, *51*, 1–10. https://doi.org/10.1016/j.tiv.2018.05.001

- Yu, J., Vodyanik, M. A., Smuga-Otto, K., Antosiewicz-Bourget, J., Frane, J. L., Tian, S., Nie, J., Jonsdottir, G. A., Ruotti, V., Stewart, R., Slukvin, I. I., & Thomson, J. A. (2007). Induced pluripotent stem cell lines derived from human somatic cells. *Science*, *318*(5858), 1917–1920. https://doi.org/10.1126/science.1151526
- Yuan, H., Zhang, Q., Guo, J., Zhang, T., Zhao, J., Li, J., White, A., Carmichael, P. L., Westmoreland, C., & Peng, S. (2016). A PGC-1α-Mediated Transcriptional Network Maintains Mitochondrial Redox and Bioenergetic Homeostasis against Doxorubicin-Induced Toxicity in Human Cardiomyocytes: Implementation of TT21C. *Toxicological Sciences*, *150*(2), 400–417. https://doi.org/10.1093/toxsci/kfw006
- Zhang, D., Li, Y., Heims-Waldron, D., Bezzerides, V., Guatimosim, S., Guo, Y., Gu, F., Zhou, P., Lin, Z., Ma, Q., Liu, J., Wang, D. Z., & Pu, W. T. (2018). Mitochondrial Cardiomyopathy Caused by Elevated Reactive Oxygen Species and Impaired Cardiomyocyte Proliferation. *Circulation Research*, *122*(1), 74–87. https://doi.org/10.1161/CIRCRESAHA.117.311349
- Zhang, J., Khvorostov, I., Hong, J. S., Oktay, Y., Vergnes, L., Nuebel, E., Wahjudi, P. N., Setoguchi, K., Wang, G., Do, A., Jung, H. J., McCaffery, J. M., Kurland, I. J., Reue, K., Lee, W. N. P., Koehler, C. M., & Teitell, M. A. (2011). UCP2 regulates energy metabolism and differentiation potential of human pluripotent stem cells. *EMBO Journal*, 30(24), 4860–4873. https://doi.org/10.1038/emboj.2011.401
- Zhang, J., Ratanasirintrawoot, S., Chandrasekaran, S., Wu, Z., Ficarro, S. B., Yu, C., Ross, C. A., Cacchiarelli, D., Xia, Q., Seligson, M., Shinoda, G., Xie, W., Cahan, P., Wang, L., Ng, S. C., Tintara, S., Trapnell, C., Onder, T., Loh, Y. H., ... Daley, G. Q. (2016). LIN28 Regulates Stem Cell Metabolism and Conversion to Primed Pluripotency. *Cell Stem Cell*, 19(1), 66–80. https://doi.org/10.1016/j.stem.2016.05.009
- Zhang, S., Liu, X., Bawa-Khalfe, T., Lu, L. S., Lyu, Y. L., Liu, L. F., & Yeh, E. T. H. (2012). Identification of the molecular basis of doxorubicin-induced cardiotoxicity. *Nature Medicine*, *18*(11), 1639–1642. https://doi.org/10.1038/nm.2919
- Zhang, X., Agborbesong, E., & Li, X. (2021). The role of mitochondria in acute kidney injury and chronic kidney disease and its therapeutic potential. In *International Journal of Molecular Sciences* (Vol. 22, Issue 20, p. 11253). MDPI. https://doi.org/10.3390/ijms222011253
- Zhao, L., & Zhang, B. (2017). Doxorubicin induces cardiotoxicity through upregulation of death receptors mediated apoptosis in cardiomyocytes. *Scientific Reports* 2017 7:1, 7(1), 1–11. https://doi.org/10.1038/srep44735
- Zickermann, V., Kerscher, S., Zwicker, K., Tocilescu, M. A., Radermacher, M., & Brandt, U. (2009). Architecture of complex I and its implications for electron transfer and proton pumping. In *Biochimica et Biophysica Acta Bioenergetics* (Vol. 1787, Issue 6, pp. 574–583). Elsevier. https://doi.org/10.1016/j.bbabio.2009.01.012
- Zorova, L. D., Popkov, V. A., Plotnikov, E. Y., Silachev, D. N., Pevzner, I. B., Jankauskas, S. S., Babenko, V. A., Zorov, S. D., Balakireva, A. V., Juhaszova, M., Sollott, S. J., & Zorov, D. B. (2018). Mitochondrial membrane potential. *Analytical Biochemistry*, *552*, 50–59. https://doi.org/10.1016/j.ab.2017.07.009

#### 8. Publications

Nguyen, L., Thewes, L., <u>Westerhoff, M.</u>, Wruck, W., Reichert, A. S., Berndt, C., & Adjaye, J. (2023). JNK signalling regulates self-renewal of proliferative urine-derived renal progenitor cells via inhibition of ferroptosis. *Cells*, *12*(17), 2197.

**Westerhoff, M.**, Brocke-Ahmadinejad, N., Schaumkessel, Y., Köhrer, K., Dönmez, A., Ghodrat, R., Borchardt, A., Enjuanes-Ruiz, L., Tigges, J., Koch, K., Fritz, G., Kondadi, A., Reichert, A. (2025). Preconditioning of human iPSCs with doxorubicin causes genome-wide transcriptional reprogramming in iPSC-derived cardiomyocytes linked to mitochondrial dysfunction and impaired cardiac regeneration. *BioRxiv*, doi: 10.1101/2025.04.18.649376.

## 9. Acknowledgements

When I look back to the past years of my PhD, my heart is full of gratitude. So many people contributed to this thesis and I would like to acknowledge them.

First, I want to thank Prof. Dr. Andreas S. Reichert as my doctoral father who gave me the chance to work on my doctoral thesis in his institute, although I started in the mitochondrial and the stem cell field from the very beginning. I remember the hours of discussions with the ambition to move the project forward. I know I was usually very insistent and I really appreciate his calmness and his patience with me. I would not want to miss it. He formed my way of thinking and questioning. I am grateful for the influence he had on me, it helped me to develop to the scientist I am today. Thank you for being patient with me and listening to my thoughts and ideas.

Another important person, whom I want to thank, is Prof. Dr. Gerhard Fritz. I am thankful for his support as my second supervisor. During the time in the RTG2578, I learned a lot from him and I still have a lot to learn. He took the time to sit down with me to discuss and was always willing to help me out with questions. Thank you for taking your time and reminding me to call when I had questions.

Furthermore, I want to thank Prof. Dr. Peter Brenneisen for his support, readiness to discuss, and to help me out if I felt stuck. I am thankful for the time he spent with us telling us stories about his life. They were always little escapes from everyday life. Thank you for sharing them with us.

Furthermore, I want to thank Dr. Nahal-Brocke Ahmadinejad for her support during the times of writing the manuscript. Her positive energy and calmness helped me out a multiple times. I am glad for the discussions we had and I learned a lot from you. Thank you for being an inspiring role model of a strong, female scientist.

I also want to thank Dr. Arun Kumar Kondadi, who supported me with experimental ideas and helped me out when I felt lost. Thank you for your support.

I want to thank the technicians, Andrea Borchardt, Gisela Pansegrau, Tanja Portugall, and Sandra Schmidt. Thank you for being there when I had questions and for the amazing technical suport. Without you, I would have been lost in the lab. But most importantly, you filled this intisute with spirit and love making it nearly a homely place.

Especially, I want to thank Andrea who did an amazing job acquiring our EM images for the publication. Thank you for your willingness to support me with new things in the lab and being there, when I felt down.

Furthermore, I want to thank Gisela Pansegrau, our "Sonnenschein" of the institute. No day would have been the same without your motivational and inspiring words in the morning. I am thankful for our little talks and the support you gave me. Also; I want to thank Raja for her amazing job as therapy dog in this institute. You're simply the cutest dog ever.

Within my time at Bumbi1, I had the honor to work with many unique people. Especially, the PhDs in particular have formed a sworn community. In this short time, many wonderful moments have been created that I would not want to have missed. I would like to thank three people in the lab in particular, and I am honored to call them my friends: Alexander Becker, Deepti Pai Tonse and Chantal Wenzel.

Alex, my hessian brother in spirit, you always sweetened my Monday meetings. I really appreciated your direct and honest manner. Thank you for the interesting discussions, your open ear and your support.

Deepti, my brave sweet soul. I've never met anyone like you. Open, unbiased and selfless. I know you will make your way and you can be proud of what you have achieved so far. Thank you for your open ear and the support you have always given me. I would also like to thank you for the many culinary excursions and insights during this time, they have broadened my culinary spectrum.

Chantal, no words could ever describe what you are to me. You were the person I could go to at any time, who listened to me and stood by me with help and advice. I would never want to miss your laughter, your craziness, your spontaneity. I am infinitely grateful for the support and love you gave me. I still remember Peter's words, "Two people have found each other". And I really think we did.

Zum Schluss möchte ich noch meiner Familie, meinem Partner und meinen Freunden danken, die mich zu jeder Zeit untersützt haben. Danke für eure Geduld, euer Verständnis und auch eure Nachsicht. Ich bin unendlich dankbar euch zu haben.

Thank you.

# 10. Eidesstatliche Erklärung

Ich versichere an Eides Statt, dass die Dissertation von mir selbständig und ohne unzulässige fremde Hilfe unter Beachtung der Grundsätze zur Sicherung guter wissenschaftlicher Praxis an der Heinrich-Heine-Universität Düsseldorf erstellt worden ist. Die aus fremden Quellen übernommenen Gedanken sind als solche kenntlich gemacht. Die Dissertation wurde in der vorgelegten oder in ähnlicher Form noch bei keiner anderen Institution eingereicht. Ich habe bisher keine erfolglosen Promotionsversuche unternommen.

Michelle Westerhoff

Düsseldorf, den 23.04.2025

### 11. List of contribution to this publication

#### **Publication**

**Westerhoff, M.**, Brocke-Ahmadinejad, N., Schaumkessel, Y., Köhrer, K., Dönmez, A., Ghodrat, R., Borchardt, A., Enjuanes-Ruiz, L., Tigges, J., Koch, K., Fritz, G., Kondadi, A., Reichert, A. (2025). Preconditioning of human iPSCs with doxorubicin causes genome-wide transcriptional reprogramming in iPSC-derived cardiomyocytes linked to mitochondrial dysfunction and impaired cardiac regeneration. *BioRxiv*, doi: 10.1101/2025.04.18.649376.

#### Contribution of Michelle Westerhoff to the manuscript:

Writing of entire first draft of manuscript; completion with advice and help of A.S. Reichert and AK Kondadi. Preparation of all figures. Ideas for experiments together with A.S. Reichert. Planning of all experiments. Conduction of all experiments except for OPA1 blots and analysis of whole genome transcriptome analysis, which was conducted by R Ghodrat and N Brocke-Ahmadinejad, respectively. EM images were conducted by A Borchardt. Performance of data analysis and statistics.

Parts of the following paragraphs/figures of this thesis were adapted from the manuscript:

- 2.2.1. Cell culture methods (from p. 34)
- 2.2.3. Cell viability assays (from p. 35)
- 2.2.4.3 Western Blot (from p. 38)
- 2.2.5. Blue Native and Clear Native PAGE (from p. 40)
- 2.2.2.6.4. Quantitative real-time PCR (qRT-PCR) (from p. 44)
- 2.2.8. Immunofluorescence staining (from p. 46)
- 2.2.10. Electron microscopy (EM) (from p. 53)
- 2.2.11. Measurement of bioenergetics (from p. 54)
- 2.2.13. Beating characterization of iPSC-derived cardiomyocytes (from p. 56)
- 2.2.14. Whole genome transcriptome profiling (from p. 59)
- 3.1.1. Pulse-treatment of iPSCs with doxorubicin is not accompanied with loss of the pluripotent state (from p. 66-70, all figures), Exception: Fig. 17 CD
- 3.1.2. Pulse-treatment with low concentrations of doxorubicin is insufficient to initiate elevated apoptosis or activate canonical DNA damage response (from p. 71-75, all figures)

- 3.1.3. Influence of acute doxorubicin exposure on mitochondrial function in human iPSCs (from p. 76- 91), Exception: Fig. 21, Fig. 24, Fig. 27D
- 3.2.1. Establishment of iCMs as robust cardiac model system (p. 93,Fig. 31)
- 3.2.2. Stable cardiac differentiation even under exposure to doxorubicin at different stages of cardiac differentiation (p. 95, Fig. 33C)
- 3.3. Whole genome transcriptome profiling of iPSCs and iCMs upon exposure to low concentrations of doxorubicin (from p. 102-125 and all figures)
- 3.3.8. Suppression of contractility function of iCMs upon is directly associated with treatment in iPSC stage prior to cardiac differentiation (p. 127, Fig. 52)